FABAD

JOURNAL of PHARMACEUTICAL SCIENCES

ISSN 1300-4182
e-ISSN: 2651-4648
www.fabad.org.tr

Volume: 48 • Issue: 1 • March 2023

An Official Journal of The Society of Pharmaceutical Sciences of Ankara (FABAD)

The Society of Pharmaceutical Sciences of Ankara (FABAD)
FABAD Journal of Pharmaceutical Sciences
Volume: 48 Issue: 1 March 2023

The FABAD Journal of Pharmaceutical Sciences is published three times a year by the
Society of Pharmaceutical Sciences of Ankara (FABAD)

The FABAD Journal of Pharmaceutical Sciences is indexed in Chemical Abstracts,
Analytical Abstracts, International Pharmaceutical Abstracts, Excerpta Medica (EMBASE), Scopus and TR Index
All manuscripts and editorial correspondences should be sent via e-mail to Nesrin GÖKHAN KELEKÇİ
(Editor-in-Chief): fabadankara@gmail.com

CONTENTS

Research Articles

Review Article

FABAD J. Pharm. Sci., 48, 1, 1-10, 2023
Doi: 10.55262/fabadeczacilik.1095369
RESEARCH ARTICLE

Carbon Monoxide and Their Donor (CORM-2) Change the Healing Rate of Skin Wound Healing in Mice Through Reduced Expression of Aquaporin-3

Serhii BESCHASNYI[*°], Olena HASIUK[**]

Carbon Monoxide and Their Donor (CORM-2) Change the Healing Rate of Skin Wound Healing in Mice Through Reduced Expression of Aquaporin-3

SUMMARY

Carbon monoxide (CO) is a toxic gas, has a beneficial effect on cells in low doses. Low concentrations of this gas are produced in the body during the decay of heme-containing proteins and have pro-apoptotic, anti-inflammatory, anti-allergic and vasodilator effects, stimulating angiogenesis. Danger of using this gas is the difficulty of its dosage. CO donors control the amount and gradual release of carbon monoxide. Main aim – studied the effect of treatment with CO and donor tricarbonyldichlororuthenium (II) dimer (CORM-2) on wound healing processes in laboratory mice. Most significant delay in healing was observed in animals whose wounds were treated with CO. In this group, aquaporin-3 (AQP3) mRNA expression was decreased to the most minor degree among all other animals. Most likely it caused the appearance of crusts. CORM-2 treatment also led to a decrease in AQP3 mRNA expression, but no crusts have appeared. Received data can be explained by the fact that CO is released slowly. Dry crust on the wound increases the healing time. Formation of a dry crust is helpful in healing of burns, because with a dry scab, pus cannot appear. With some degrees of burns it prevents suppuration and creates a protective barrier. Study confirmed the hypothesis that CO and CORM-2 reduce AQP3 expression after treatment of damaged skin.

Key Words: *Aquaporin-3, CO-releasing molecule, CORM-2, carbon monoxide, skin wound*

Karbon Monoksit ve Donörünün (CORM-2), Aquaporin-3'ün Ekspresyonunu Azaltarak Farelerde Cilt Yara İyileşmesinin İyileşme Hızını Değiştirmesi

ÖZ

Karbon monoksit (CO) düşük dozlarda hücreler üzerinde yararlı bir etkiye sahip toksik bir gazdır. Bu gazın düşük konsantrasyonları, hem-içeren proteinlerin çürümesi sırasında vücutta üretilir ve anjiyogenezi uyaran pro-apoptotik, anti-enflamatuar, anti-alerjik ve vazodilatör etkilere sahiptir. Bu gazı kullanmanın tehlikesi, dozajını ayarlamanın zorluğudur. CO donörleri, karbon monoksitin miktarını ve kademeli olarak salınımını kontrol eder. Ana amaç - CO ve donör trikarbonildiklororutenyum (II) dimer (CORM-2) ile tedavinin laboratuvar farelerinde yara iyileşme süreçleri üzerindeki etkisini incelemektir. İyileşmede en önemli gecikme, yaraları CO ile tedavi edilen hayvanlarda gözlenmiştir. Bu grupta, aquaporin-3 (AQP3) mRNA ekspresyonu diğer tüm hayvanlar arasında en az seviyeye kadar kadar azalmıştır. Büyük olasılıkla skar dokusunun ortaya çıkmasına neden olmuştur. CORM-2 tedavisi ayrıca AQP3 mRNA ekspresyonunda bir azalmaya yol açmıştır, ancak skar dokusu ortaya çıkmamıştır. Alınan veriler, CO'nun yavaş yavaş serbest bırakılması gerçeğiyle açıklanabilir. Yara üzerindeki skar dokusu iyileşme süresini arttırır. Skar dokusunun oluşumu yanıkların iyileşmesinde yardımcı olur, skar dokusu ile inflamasyon oluşumu engellenebilir ve irin görünemez. Bazı yanıklarda inflamasyonu önler ve koruyucu bir bariyer oluşturur. Çalışma, CO ve CORM-2'nin hasarlı cildin tedavisinden sonra AQP3 ekspresyonunu azalttığı hipotezini doğrulamaktadır.

Anahtar Kelimeler: *Aquaporin-3, CO salan molekül, CORM-2, karbon monoksit, cilt yarası*

Received: 29.03.2022
Revised: 08.07.2022
Accepted: 10.07.2022

[*] ORCID: 0000-0002-7423-4112, Department of Human Biology and Immunology, Kherson State University, Ukraine
[**] ORCID: 0000-0003-1055-2848, Department of Human Biology and Immunology, Kherson State University, Ukraine

[°] Corresponding Author; Serhii BESCHASNYI
Tel. +380954188384, e-Mail: beschasnyis@gmail.com

INTRODUCTION

Skin is the outer protective shell of the body, which supports the integrity of the organism. Skin damage can lead to pathological conditions and death. Once a wound is formed, complex processes associated with death of the damaged cells begin.

The repair of the defect is carried out through reparative regeneration and is completed by the scarring process. Continuing high level of domestic and industrial injuries, growth of purulent and inflammatory diseases determine the relevance of finding new means to ensure the effectiveness of treatment of this pathology. There are many known regional therapies (Chang, 2019; Kirsner, 2019; Patel, 2019; Jones, 2020), that can significantly improve treatment effectiveness. On the other hand, studies show that each of these methods has certain shortcomings, and it is very essential to make a differentiated choice without causing increased tissue injury (Jones, 2020).

Depending on the localization of the wound, the issue of not only closing wound defect but also cosmetic result is relevant. Restoration of the structure of intact skin does not occur in the case of full-layer wounds; only tissue regeneration is possible. A zone of tissue replenishment in the area of the wound defect, the changed variant of tissues forming the skin is determined (Singer, 1999). The following groups of drugs are mainly used: vitamins, steroid and non-steroidal anabolic and biogenic stimulants. Among them, there are no gases or gaseous drugs whose effects are less harmful to the body.

Recently, much attention has been paid to the studying of gases that are formed endogenously. These gases are called gas transmitters because they can influence the functions of cells and tissues in picomolar quantities (Wang, 2004; Kolupaev, 2019). Carbon monoxide (CO) is singled out among these gas transmitters. CO is a toxic gas that binds to hemoglobin and forms methemoglobin, enters the mitochondria, and blocks the respiratory chain (Hermann, 2012). At the same time, CO has been shown to form in the body as a result of the breakdown of heme in the spleen and liver, as well as other organs. The formation of CO is regulated by the enzyme heme oxygenase-1 (HO-1), which has anti-inflammatory properties (Olszanecki, 2007).

There are known cases of experimental use of CO or CO drugs-donors (CO-releasing molecules, CORMs) to treat colitis and stomach ulcers (Magierowski, 2017). At the same time, the authors noted the difficulty of using gaseous CO. All studies of regenerative and anti-inflammatory properties of CO were aimed at studying the production of pro-inflammatory cytokines, calcium-dependent ion channels and transcription factors (Brouard, 2002; Abdel-Magied, 2019).

Among donors of carbon monoxide are tricarbonyldichlororuthenium (II) dimer or CORM-2 (Magierowska, 2019). CORM-2 is commonly used in experiments to control the production of small quantities of CO without significant changes in carboxyhemoglobin levels in the blood (Motterlini, 2003). CORM-2 also showed anti-inflammatory action (Qureshi, 2016; Liu, 2019). The drug suppresses lipopolysaccharide-induced inflammation of the respiratory tract (Lin, 2019), enhances plasma coagulation, and weakens fibrinolysis in plasma *in vitro* (Johnson, 2019). Preliminary studies revealed that CORM-2 affects the Ca^{2+}-activated K^{+}-channels and aquaporin 3 transmembrane channels (AQP3) of red blood cells (Beschasnyi, 2020).

Attempts to use CO for experimental wound healing have shown positive results. Hemin was used to enhance the expression of HO-1, which promotes CO release. The iron-containing porphyrin significantly increases cytokine interleukin 10 and decreases tumour necrosis factor alpha in the granulation tissue (Ahanger, 2021). Recent studies have shown that carbon monoxide accelerates wound healing gastrointestinal trauma (Takagi, 2021). CORM-2 after intravenous injection was a promoter for precision wound

healing and stimulated enhanced vascular growth in a chick chorion-allantoic envelope model (Ahanger, 2011).

However, an essential role in the healing process is played by the relatively recently discovered water and glycerin-aquaporin transporters. These are important channels that take part in the transport of water and glycerol into cells, in processes of embryogenesis, angiogenesis and oncogenesis (Ma, 2002; Ikarashi, 2019). Aquaporin transporters are present in the membrane of almost all cells (Verkman, 2014). More recently, AQP3 has been singled out among the aquaporin channels, which, besides water, is responsible for transporting glycerin and hydrogen peroxide (Bollag, 2020). How aquaporins respond to CO remains unknown.

The purpose of the study is to determines how CO and CORM-2 affect the expression of aquaporin-3 in the dermis and the wound healing rate in laboratory mice.

MATERIALS AND METHODS

The experiment was carried out on 30 white non-breeding male mice weighing 17-19 g. Conditions of the animals were per the standard conditions of the vivarium. Temperatures to be maintained within the range 20-24°C, humidity – 45-65%, light mode – 12 h light/12 h darkness.

Mice were in individual cells with free access to food and water. Animal experiments were carried out in full compliance with the European Council Directive on ethical principles in the management of laboratory animals (The European Council Directive (86/609/EEC)) and Directive 2010/63/EU of the European Parliament and the Council of the European Union. Study protocol was reviewed and approved by the Kherson State University Ethical Committee (ethical committee no: 2020/6).

The induction of pathology (surgical intervention to inflict skin wounds) was performed under anesthesia. "Zoletil 100" (Virbac, France) (30 mg/kg of body weight, intramuscular) was used as an anesthetic and anesthetic substance. Before inflicting a full-skin wound on the animal, the fur on its back was cut with scissors. Remains of the hair were removed with the help of depilation cream (Eveline Cosmetics, Poland). Operating field was then sequentially treated with 70° ethyl alcohol once. Using of a sterile dermo-punch skin biopsy stylet (5 mm in diameter, Sterylab, Italy), mice have applied two full-layer skin wounds through the pulled-back skin fold between the shoulder blades as deep as the surface muscle fascia (Galiano, 2004). The presence of the wound did not affect the motor activity and appetite of the animals.

Two experimental groups of mouse were formed. The case of the members of the first group, after developing skin wounds, two sterile polyethylene bladders (unrelated) were glued to the wound with medical adhesive (BF-6 Lubnypharm, Ukraine). Pure CO (Sciencegases, Ukraine) was injected into the cavity of the left polyethylene bubble, and atmospheric air was injected into the cavity of the right one. Indices obtained during wound healing in the right bubble were taken as control ones.

In the case of the second group (wounds were completely open, without polyethylene bubbles), one injury treated with a solution containing carbon monoxide donor CORM-2 (50 μm/l, Sigma-Aldrich) dissolved in saline. To improve the dissolution of CORM-2 in saline, it was initially dissolved in dimethylsulfoxide (DMSO), the resulting solution had a DMSO concentration not exceeding 0.1%, and this concentration didn't affect the experiment's performance. DMSO was added to saline to treat the control wound (Figure 1).

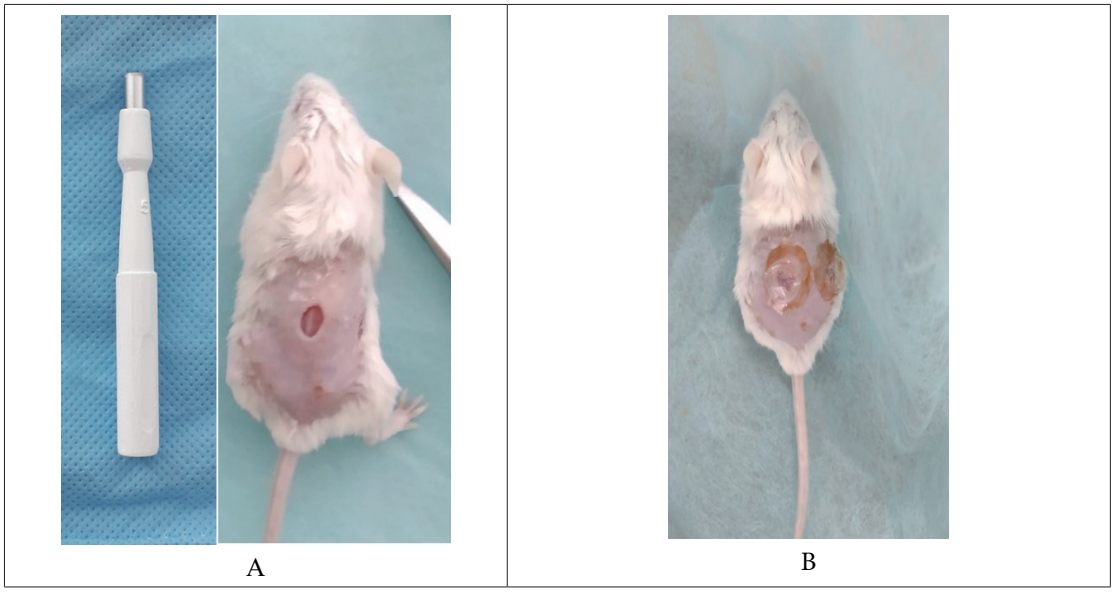

Figure 1. Mouse with a wound made with Dermo Punch (left) (A) and with polyethylene bubbles glued into which CO and atmospheric air were injected (B)

Throughout the experiment, the wounds were photographed daily. The area of wound injury was calibrated and measured using the Image J software (USA). Results were expressed in % of the original size. Every animal was weighed prior to the experiment and the following days.

At the end of the experiment, a skin biopsy was taken for further histological examination. Collected skin samples of mice were fixed in 10% formalin and placed in paraffin. The 4 μm thick skin incisions were cut using a Leica RM 2125 RTS microtome (Wetzlar, Germany) and stained with hematoxylin and eosin (Sigma-Aldrich); the Van Gieson's trichrome stain (Diagnostic Biosystems, Pleasanton, USA) was used to identify collagen fibers.

On the 5th and 21st days, a skin biopsy was taken from animals for further PCR research into the quantitative expression of mRNA AQP-3. RNA was extracted, and complementary DNA was obtained by reverse transcription. Expression levels of AQP3 mRNA were measured by quantitative PCR using specific primers, (Forward: 5'- GTCAACCCTGCCCGTGACTTTG, Reverse: 5'-CGAAGACACCAGCGATGGAACC, GenBank ID NM_016689.2) (Metabion, Germany). PCR reactions were performed using 30 μl reaction mixtures containing 1.0 μl of PrimeScript enzymes, 1.0 μl of each primer (30 μM), 4.0 μl 5 × buffer 2 PrimerScript, 14 μl of sterile distilled water, and 10 μl of DNA matrix (100 ng / μl). Each sample was analyzed in three repeats, and the average Ct value was determined based on three experiments. Relative expression of mRNA was expressed as ΔCt = Ct (target gene) – Ct (calibrator). Expression of mRNA β-actin was used as internal control, and the relative expression of mRNA was calculated as ΔΔCt = ΔCt (treatment) - ΔCt (control). Relative levels of gene expression were transformed and expressed as a multiple of the difference (2-ΔΔCt).

Statistical analysis

All data of measurements are presented as means ± standard error of the mean (SEM). Comparison between independent samples was made using Mann-Whitney U-test and Wilcoxon Signed Ranks Test. Significance was considered at $P < 0.05$. Statistical analysis was performed using SPSS (SPSS-17, Chicago, IL, USA).

RESULTS

The general condition of mice with control and experimental wounds was satisfactory. The animals had a good appetite and high motor activity. No complications such as a wound infection or fluid collection occurred. During the experiment, the weight of the mice did not differ significantly from the baseline.

In the group of animals with wounds treated with CO and air, observed the healing process of the wound from the 5th day in case of air treatment. Injuries treated by CO on the same animals began to heal after the 15th day. It is necessary to indicate that a massive crust was formed which covered the wound. From the 19th day on, the injuries treated with CO began to decrease sharply in size (by 45 ± 2.25%) (Figure 2, 3).

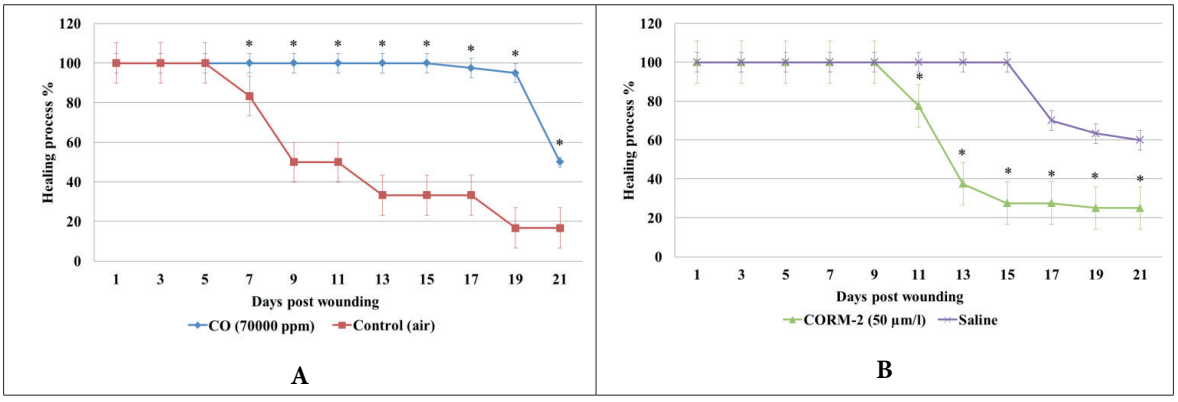

Figure 2. Diagram of the kinetics of wound closure in mice treated with different conditions. Each point represents the mean percentage of reducing the size of a wound. Data are expressed as mean ± SEM. A - CORM-2 & saline (n=15), B - CO & control (n=15).

** - significant difference, p ≤ 0,05 (U-test)*

In the animal group (one wound was washed with CORM-2 and the second with saline) we found a positive effect of CORM-2 on wound healing.

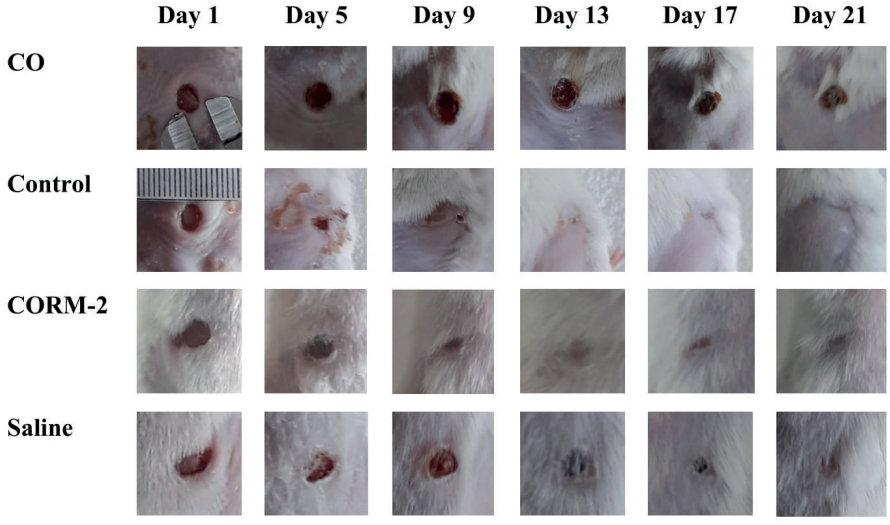

Figure 3. Representative photographs showing wound closure of wounds treated with CORM-2 (50 µm/l), CO (70,000 ppm), and saline immediately after an injury is inflicted (compared to the control).

Wounds washed with saline began to heal after the 15th day, and were treated with CORM-2 – from the 9th. In this case, from the 9th to the 11th day, the wound decreased by 22.5 ± 1.1%. Then the healing rate decreased – the size of the injury decreased by 40 ± 1.25% from day 11 to day 13, from day 13 to day 15 by 10 ± 1.25%, from day 15 to 17 it didn't change, and from day 17 to day 19 it decreased by 2 ± 0.1%. No complications, such as a wound infection or fluid collection, occurred in either group (Figure 4).

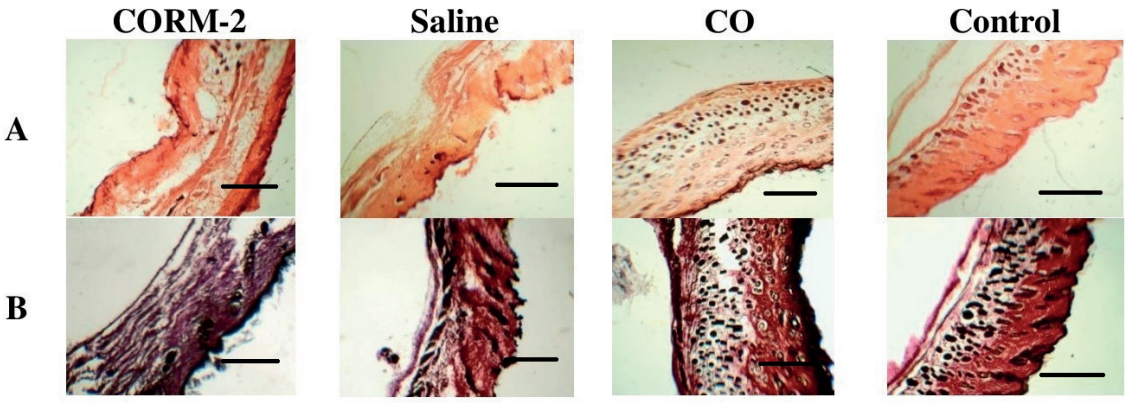

Figure 4. Histological sections of skin with hematoxylin-eosin (A) and Van-Gieson's stain (B), original magnification ×100 (overview photo). Skin samples were taken on the 21st day of the experiment, 500μm scale bar.

The expression of AQP3 in epidermis cells differed in different groups. Compared with control, AQP3 expression in the epidermis of the group treated with CORM-2 decreased on the 5th day and increased on the 21st day (Figure 5).

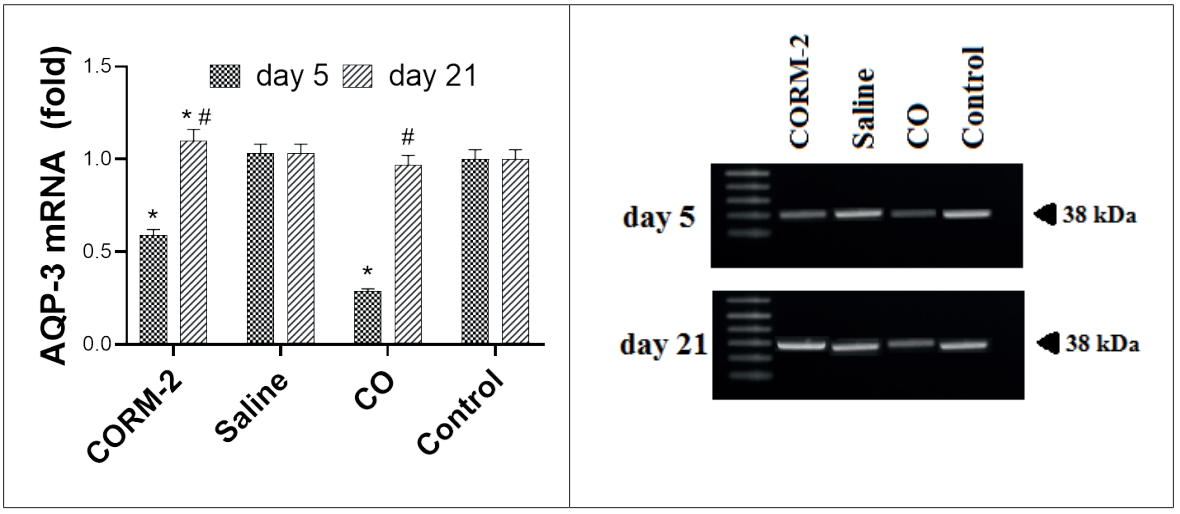

Figure 5. Effect of CORM-2, saline, CO on AQP3 mRNA expression level in the mouse skin
** - significant difference compared with control, p ≤ 0,05 (U-test)*
 # - significant difference in comparison with the initial indicator, p ≤ 0,05 (Wilcoxon Test)
CORM-2 (50 μm/l) & saline (n=15), CO (70000 ppm) & control (air) (n=15)

After CO treatment, AQP3 (and protein) expression was also maximally reduced and increased at the end of healing. In wounds treated with saline, AQP3 expression, to the contrary, was raised, at the end of the experiment - decreased, but was at the level of the control group. The control group, the expression was initially increased but slightly reduced at the end of healing.

DISCUSSION

It is known that AQP3 transports water, glycerin, and hydrogen peroxide (Verkman, 2008; Hara-Chikuma, 2015), which in the epidermis promotes the proliferation and differentiation of keratinocytes (Bollag, 2007). Studies of AQP3 knockout mice suggest that this aquaglyceroporin is also necessary for normal skin hydration, barrier restoration, wound healing, and elasticity (Choudhary, 2015). Activity of AQP3 has also been associated with various human skin diseases (Boury-Jamot, 2006; Olsson, 2006; Qin, 2011; Ikarashi, 2012). Some AQP3 studies indicate that excessive AQP3 expression is associated with skin flat cell carcinoma (Hara-Chikuma, 2008).

CO was previously considered only in terms of toxicity. But after it was found that CO is produced in the body under normal conditions (when heme-containing proteins decompose), it was added to the group of gas transmitters (Wu, 2005). In addition, CO is a signal molecule with a potential therapeutic effect (Wang, 2020).

One of the effects on cells is the activation or inactivation of ion channels, due to which CO is involved in the regulation of the cardiovascular system: it relaxes the smooth muscles of blood vessels and stimulates angiogenesis (Kapetanaki, 2018), regulates apoptosis (Olas, 2014). However, the problem is that the therapeutic use of gas-like CO is very complicated. Therapy with CO is complex because this substance is very tough to dose. Promising way is to use carbon monoxide donor substances (Motterlini, 2017).

The findings confirm that CO (or donor of CO) can influence the healing process of the wound. Results showed that all effects (compared to control) reduced the rate of wound healing. Most significant healing delay was observed in animals whose injuries were treated with CO. In animals of this group, the expression of aquaporins mRNA was the least reduced among all others. That was probably the source of the scabs. CORM-2 treatment also resulted in a decrease in AQP3 mRNA expression, but not a crust has been formed. It can be attributed to the fact that the CO from CORM-2 was released slowly.

According to modern views, the presence of dry crust on the injury worsens its healing: the time and traces of the wound increase. But, at the same time, the formation of a dry crust is helpful in healing burns (under a dry scab, the construction of pus is impossible, this is achieved in available treatment). Question is debatable, whether healing under a scab should be classified as a primary or secondary type of healing. Usually, the opinion is that it occupies an intermediate position and represents a particular type of healing of surface wounds. However, the importance of the scab in the open treatment of burn disease cannot be underestimated: at some degrees of burn, it prevents festering and creates a protective barrier. The study confirmed the hypothesis that CO (like CORM-2) after treatment of injured skin reduces AQP3 expression. Promising thing is that reducing AQP3 expression with CO or CORM can reduce cancer cell invasiveness, which is increased in malignant cells.

CONCLUSION

Wound treatment with CO results in the dry crust. Treatment with CORM-2 did not lead to the formation of a crust. Acting on wounds with CO or CORM-2 resulted in a decrease in AQP-3 mRNA expression early in the wound healing process. At the end of healing, expression increased in a compensatory way. After treatment with CORM-2 on the 11th day, we observed a sharp increase in the wound healing rate (compared with the saline-treated wounds). Changes in the wound healing rate are associated with changes in AQP-3 mRNA expression under the influence of CO.

ACKNOWLEDGMENT

We would like to thank grad student Lebid Anton for technical assistance.

CONFLICT OF INTEREST

The authors declare that no conflict of interest exists

AUTHOR CONTRIBUTION STATEMENT

Idea (BS, HO), manuscript design (BS), performing experiments (BS, HO), data analysis (HO), data interpretation (BS, HO), literature review (BS), writing article (BS).

REFERENCES

Abdel-Magied, N., & Shedid, S. M. (2019). The effect of naringenin on the role of nuclear factor (erythroid-derived 2)-like2 (Nrf2) and haem oxygenase 1 (HO-1) in reducing the risk of oxidative stress-related radiotoxicity in the spleen of rats. *Environmental Toxicology, 34*(7), 788-795. doi: 10.1002/tox.22745

Ahanger, A. A., Prawez, S., Kumar, D., Prasad, R., Tandan, S. K., Kumar, D. (2011). Wound healing activity of carbon monoxide liberated from CO-releasing molecule (CO-RM). *Naunyn-Schmiedeberg's Archives of Pharmacology, 384*(1), 93-102. doi: 10.1007/s00210-011-0653-7

Ahanger, A. A., Prawez, S., Shakoor, A., Ahmad, W., Khan, A. M., Kumar, D. (2021). Topical application of 'Hemin'promotes wound healing in Streptozotocin-induced diabetic rats. *Veterinarski Arhiv, 91*(3), 287-296. doi: 10.24099/vet.arhiv.1117

Beschasnyi, S. P., & Hasiuk, O. M. (2020). CO-Releasing Molecule (CORM-2) in the regulation of Ca^{2+} dependent K^{+} permeability of erythrocyte. *Ukrainian Journal of Medicine, Biology and Sport, 5*(2), 166-171. doi: 10.26693/jmbs05.02.166

Bollag, W. B., Aitkens, L., White, J., Hyndman, K. A. (2020). Aquaporin-3 in the epidermis: more than skin deep. *American Journal of Physiology-Cell Physiology, 318*(6), C1144-C1153. doi: 10.1152/ajpcell.00075.2020

Bollag, W. B., Xie, D., Zheng, X., Zhong, X. (2007). A potential role for the phospholipase D2-aquaporin-3 signaling module in early keratinocyte differentiation: production of a phosphatidylglycerol signaling lipid. *Journal of Investigative Dermatology, 127*(12), 2823-2831. doi: 10.1038/sj.jid.5700921

Boury-Jamot, M., Sougrat, R., Tailhardat, M., Le Varlet, B., Bonté, F., Dumas, M., Verbavatz, J. M. (2006). Expression and function of aquaporins in human skin: Is aquaporin-3 just a glycerol transporter? *Biochimica et Biophysica Acta (BBA)-Biomembranes, 1758*(8), 1034-1042. doi: 10.1016/j.bbamem.2006.06.013

Brouard, S., Berberat, P. O., Tobiasch, E., Seldon, M. P., Bach, F. H., Soares, M. P. (2002). Heme oxygenase-1-derived carbon monoxide requires the activation of transcription factor NF-κB to protect endothelial cells from tumor necrosis factor-α-mediated apoptosis. *Journal of Biological Chemistry, 277*(20), 17950-17961. doi: 10.1074/jbc.M108317200

Chang, R. Y. K., Das, T., Manos, J., Kutter, E., Morales, S., Chan, H. K. (2019). Bacteriophage PEV20 and ciprofloxacin combination treatment enhances removal of Pseudomonas aeruginosa biofilm isolated from cystic fibrosis and wound patients. *The AAPS Journal, 21*(3), 1-8. doi: 10.1208/s12248-019-0315-0

Choudhary, V., Olala, L. O., Qin, H., Helwa, I., Pan, Z. Q., Tsai, Y. Y., ... Bollag, W. B. (2015). Aquaporin-3 re-expression induces differentiation in a phospholipase D2-dependent manner in aquaporin-3-knockout mouse keratinocytes. *Journal of Investigative Dermatology, 135*(2), 499-507. doi: 10.1038/jid.2014.412

Galiano, R. D., Michaels, V, J., Dobryansky, M., Levine, J. P., Gurtner, G. C. (2004). Quantitative and reproducible murine model of excisional wound healing. *Wound Repair and Regeneration, 12*(4), 485-492. doi: 10.1111/j.1067-1927.2004.12404.x

Hara-Chikuma, M., Satooka, H., Watanabe, S., Honda, T., Miyachi, Y., Watanabe, T., Verkman, A. S. (2015). Aquaporin-3-mediated hydrogen peroxide transport is required for NF-κB signalling in keratinocytes and development of psoriasis. *Nature Communications, 6*(1), 1-14. doi: 10.1038/ncomms8454

Hara-Chikuma, M., & Verkman, A. S. (2008). Prevention of skin tumorigenesis and impairment of epidermal cell proliferation by targeted aquaporin-3 gene disruption. *Molecular and Cellular Biology, 28*(1), 326-332. doi: 10.1128/MCB.01482-07

Hermann, A., Sitdikova, G. F., Weiger, T. M. (2012). *Gasotransmitters: Physiology and Pathophysiology*. Berlin; Heidelberg: Springer. Available online at: http://www.springer.com/biomed/human+physiology/book/978-3-642-30337-1

Ikarashi, N., Aburada, T., Kon, R., Sugiyama, K. (2019). Water control mechanism of byakkokaninjinto and its active components via aquaporins. *Traditional & Kampo Medicine, 6*(2), 57-61. doi: 10.1002/tkm2.1213

Ikarashi, N., Ogiue, N., Toyoda, E., Kon, R., Ishii, M., Toda, T., ... Sugiyama, K. (2012). Gypsum fibrosum and its major component $CaSO_4$ increase cutaneous aquaporin-3 expression levels. *Journal of Ethnopharmacology, 139*(2), 409-413. doi: 10.1016/j.jep.2011.11.025

Johnson, T. E., Wells, R. J., Bell, A., Nielsen, V. G., Olver, C. S. (2019). Carbon monoxide releasing molecule enhances coagulation and decreases fibrinolysis in canine plasma exposed to Crotalus viridis venom in vitro and in vivo. *Basic & Clinical Pharmacology & Toxicology, 125*(4), 328-336. doi: 10.1111/bcpt.13242

Jones, M., Kujundzic, M., John, S., Bismarck, A. (2020). Crab vs. Mushroom: A review of crustacean and fungal chitin in wound treatment. *Marine Drugs, 18*(1), 64. doi: 10.3390/md18010064

Kapetanaki, S. M., Burton, M. J., Basran, J., Uragami, C., Moody, P. C., Mitcheson, J. S., ... Raven, E. (2018). A mechanism for CO regulation of ion channels. *Nature Communications, 9*(1), 1-10. doi: 10.1038/s41467-018-03291-z

Kirsner, R., Dove, C., Reyzelman, A., Vayser, D., Jaimes, H. (2019). A prospective, randomized, controlled clinical trial on the efficacy of a single-use negative pressure wound therapy system, compared to traditional negative pressure wound therapy in the treatment of chronic ulcers of the lower extremities. *Wound Repair and Regeneration, 27*(5), 519-529. doi: 10.1111/wrr.12727

Kolupaev, Y. E., Karpets, Y. V., Beschasniy, S. P., Dmitriev, A. P. (2019). Gasotransmitters and their role in adaptive reactions of plant cells. *Cytology and Genetics, 53*(5), 392-406. doi: 10.3103/S0095452719050098

Lin, C. C., Hsiao, L. D., Cho, R. L., Yang, C. M. (2019). Carbon monoxide releasing molecule-2-upregulated ROS-dependent heme oxygenase-1 axis suppresses lipopolysaccharide-induced airway inflammation. *International Journal of Molecular Sciences, 20*(13), 3157. doi: 10.3390/ijms20133157

Liu, Y., Wang, X., Xu, X., Qin, W., Sun, B. (2019). Protective effects of carbon monoxide releasing molecule-2 on pancreatic function in septic mice. *Molecular Medicine Reports, 19*(5), 3449-3458. doi: 10.3892/mmr.2019.10049

Ma, T., Hara, M., Sougrat, R., Verbavatz, J. M., Verkman, A. S. (2002). Impaired stratum corneum hydration in mice lacking epidermal water channel aquaporin-3. *Journal of Biological Chemistry, 277*(19), 17147-17153. doi: 10.1074/jbc.M200925200

Magierowska, K., Korbut, E., Hubalewska-Mazgaj, M., Surmiak, M., Chmura, A., Bakalarz, D., ... Magierowski, M. (2019). Oxidative gastric mucosal damage induced by ischemia/reperfusion and the mechanisms of its prevention by carbon monoxide-releasing tricarbonyldichlororuthenium (II) dimer. *Free Radical Biology and Medicine, 145*, 198-208. doi: 10.1016/j.freeradbiomed.2019.09.032

Magierowski, M., Magierowska, K., Hubalewska-Mazgaj, M., Sliwowski, Z., Ginter, G., Pajdo, R., ... Brzozowski, T. (2017). Carbon monoxide released from its pharmacological donor, tricarbonyldichlororuthenium (II) dimer, accelerates the healing of pre-existing gastric ulcers. *British Journal of Pharmacology, 174*(20), 3654-3668. doi: 10.1111/bph.13968

Motterlini, R., Foresti, R. (2017). Biological signaling by carbon monoxide and carbon monoxide-releasing molecules. *American Journal of Physiology-Cell Physiology, 312*(3), C302-C313. doi: 10.1152/ajpcell.00360.2016

Motterlini, R., Mann, B. E., Johnson, T. R., Clark, J. E., Foresti, R., Green, C. J. (2003). Bioactivity and pharmacological actions of carbon monoxide-releasing molecules. *Current Pharmaceutical Design, 9*(30), 2525-2539. doi: 10.2174/1381612033453785

Olas, B. (2014). Carbon monoxide is not always a poison gas for human organism: Physiological and pharmacological features of CO. *Chemico-biological Interactions, 222*, 37-43. doi: 10.1016/j.cbi.2014.08.005

Olsson, M., Broberg, A., Jernås, M., Carlsson, L., Rudemo, M., Suurküla, M., ... Benson, M. (2006). Increased expression of aquaporin 3 in atopic eczema. *Allergy, 61*(9), 1132-1137. doi: 10.1111/j.1398-9995.2006.01151.x

Olszanecki, R., Gebska, A., Korbut, R. (2007). The role of haem oxygenase-1 in the decrease of endothelial intercellular adhesion molecule-1 expression by curcumin. *Basic & Clinical Pharmacology & Toxicology, 101*(6), 411-415. doi: 10.1111/j.1742-7843.2007.00151.x

Patel, S., Srivastava, S., Singh, M. R., Singh, D. (2019). Mechanistic insight into diabetic wounds: Pathogenesis, molecular targets and treatment strategies to pace wound healing. *Biomedicine & Pharmacotherapy, 112*, 108615. doi: 10.1016/j.biopha.2019.108615

Takagi, T., Naito, Y., Higashimura, Y., Uchiyama, K., Okayama, T., Mizushima, K., Katada, K., Kamada, K., Ishikawa, T., Itoh, Y. (2021). Rectal administration of carbon monoxide inhibits the development of intestinal inflammation and promotes intestinal wound healing via the activation of the Rho-kinase pathway in rats. *Nitric Oxide, 107*, 19-30. https://doi.org/10.1016/j.niox.2020.12.006).

Qin, H., Zheng, X., Zhong, X., Shetty, A. K., Elias, P. M., Bollag, W. B. (2011). Aquaporin-3 in keratinocytes and skin: Its role and interaction with phospholipase D2. *Archives of Biochemistry and Biophysics, 508*(2), 138-143. doi: 10.1016/j.abb.2011.01.014

Qureshi, O. S., Zeb, A., Akram, M., Kim, M. S., Kang, J. H., Kim, H. S., ... Kim, J. K. (2016). Enhanced acute anti-inflammatory effects of CORM-2-loaded nanoparticles via sustained carbon monoxide delivery. *European Journal of Pharmaceutics and Biopharmaceutics, 108*, 187-195. doi: 10.1016/j.ejpb.2016.09.008

Singer, A. J., & Clark, R. A. (1999). Cutaneous wound healing. *New England Journal of Medicine, 341*(10), 738-746. doi: 10.1056/NEJM199909023411006

Verkman, A. S. (2008). A cautionary note on cosmetics containing ingredients that increase aquaporin-3 expression. *Experimental Dermatology, 17*(10), 871-872. doi: 10.1111/j.1600-0625.2008.00698.x

Verkman, A. S., Anderson, M. O., & Papadopoulos, M. C. (2014). Aquaporins: important but elusive drug targets. *Nature Reviews Drug Discovery, 13*(4), 259-277. doi: 10.1038/nrd4226

Wang, M., Yang, X., Pan, Z., Wang, Y., De La Cruz, L. K., Wang, B., Tan, C. (2020). Towards "CO in a pill": Pharmacokinetic studies of carbon monoxide prodrugs in mice. *Journal of Controlled Release, 327*, 174-185. doi: 10.1016/j.jconrel.2020.07.040

Wang, R. (Ed.). (2004). *Signal Transduction and the Gasotransmitters: NO, CO, and H_2S in Biology and Medicine*. Springer Science & Business Media.

Wu, L., & Wang, R. (2005). Carbon monoxide: endogenous production, physiological functions, and pharmacological applications. *Pharmacological Reviews, 57*(4), 585-630. doi: 10.1124/pr.57.4.3

FABAD J. Pharm. Sci., 48, 1, 11-24, 2023
Doi: 10.55262/fabadeczacilik.1083066
RESEARCH ARTICLE

Glycosides Isolated from Leaf Extract of *Phyllanthus muellerianus* (Kuntze) Excell (Phyllanthaceae) Upregulated Cell-mediated Innate Immunity

Martha. N. OFOKANSI[*], Ogechukwu N. ISIOGUGU[**], Ikechukwu E PETER[***], Matthias O. AGBO[****°], Festus B.C. OKOYE[*****], Peter A. AKAH[******]

Glycosides Isolated from Leaf Extract of Phyllanthus muellerianus (Kuntze) Excell (Phyllanthaceae) Upregulated Cell-mediated Innate Immunity

SUMMARY

Intracellular pathogens are mainly eliminated by cell-mediated immunity from phagocytic cells like neutrophils, macrophages, and monocytes. Tannin glycosides, 1-O-galloyl-6-O-luteoyl-α-D-glucopyranoside (1) and 3-O-methylellagic acid 3'-O-α-rhamnopyranoside (2) were isolated from the ethyl acetate fraction (EF) of the methanol leaf extract of Phyllanthus muellerianus. Structures of the isolated compounds were elucidated by 1H-NMR and by mass spectroscopy. Effects of the isolated compounds on the phagocytic competence of macrophages and neutrophils using in vitro models were evaluated. Tannin glycosides 1 and 2 significantly ($p<0.05$) increased both phagocytic ability and intracellular killing capacity of neutrophils. Present study established that tannin glycosides stimulated cell-mediated innate immunity by increasing the phagocytic function of neutrophils and thus may be helpful to both the clinical and prophylactic treatment of intracellular microbial infections.

Key Words: *Glycosides, cell-mediated immunity, phagocytosis, neutrophils, macrophages.*

Phyllanthus muellerianus (Kuntze) Excell (Phyllanthaceae) Yaprak Ekstresinden İzole Edilen Glikozitlerin Hücre-Aracılı Doğuştan Bağışıklığı Yukarı Regüle Etmesi

ÖZ

Hücre içi patojenler esas olarak nötrofiller, makrofajlar ve monositler gibi fagositik hücreler tarafından sunulan hücre aracılı bağışıklık tarafından elimine edilir. İki adet tanen glikozit, 1-O-galloil-6-O-luteoil-α-D-glukopiranozit (1) ve 3-O-metilelajik asit 3'-O-α-ramnopiranozit (2) Phyllanthus muellerianus yaprak metanol ekstresinin etil asetat fraksiyonundan (EF) izole edilmiştir. İzole edilen bileşiklerin yapıları, 1H-NMR ve kütle spektroskopisi ile aydınlatılmıştır. İzole edilen bileşiklerin makrofajların ve nötrofillerin fagositik yeterliliği üzerindeki etkileri in vitro modeller kullanılarak değerlendirilmiştir. Bileşik 1 ve 2, nötrofillerin hem fagositik kabiliyetini hem de hücre içi öldürme kapasitesini önemli ölçüde ($p<0.05$) arttırmıştır. Bu çalışma, tanen glikozitlerin, nötrofillerin fagositik fonksiyonunu artırarak hücre aracılı doğuştan gelen bağışıklığı uyardığını ve bu nedenle hücre içi mikrobiyal enfeksiyonların hem klinik hem de profilaktik tedavisinde yararlı olabileceğini ortaya koymuştur.

Anahtar Kelimeler: *Glikozitler, hücre-aracılı bağışıklık, fagositoz, nötrofiller, makrofajlar.*

Received: 07.03.2022
Revised: 29.07.2022
Accepted: 01.08.2022

[*] ORCID: 0000-0001-7660-6800, Department of Pharmacology and Toxicology, Faculty of Pharmaceutical Sciences, University of Nigeria, Nsukka, 410001, Enugu State Nigeria.
[**] ORCID: 0000-0003-4285-9860, Department of Pharmacology and Toxicology, Faculty of Pharmaceutical Sciences, University of Nigeria, Nsukka, 410001, Enugu State Nigeria.
[***] ORCID: 0000-0003-1223-582X, Department of Pharmacology and Toxicology, Faculty of Pharmaceutical Sciences, University of Nigeria, Nsukka, 410001, Enugu State Nigeria.
[****] ORCID: 0000-0001-8210-306X, Natural Products Chemistry Unit, Department of Pharmaceutical and Medicinal Chemistry, Faculty of Pharmaceutical Sciences, University of Nigeria, Nsukka, 410001, Enugu State Nigeria.
[*****] ORCID: 0000-0001-8414-2329, Department of Pharmaceutical and Medicinal Chemistry, Faculty of Pharmaceutical Sciences, Nnamdi Azikiwe University, PMB 2025 Awka, Anambra State Nigeria.
[******] ORCID: 0000-0002-5064-1522, Department of Pharmacology and Toxicology, Faculty of Pharmaceutical Sciences, University of Nigeria, Nsukka, 410001, Enugu State Nigeria.

[°] Corresponding Author; Matthias Onyebuchi Agbo
Phone: +234 8162661991; e.mail: matthias.agbo@unn.edu.ng

INTRODUCTION

The immune system is the body's natural defense against foreign substances. It is composed of biological structures, a network of cells and processes within the body that works to protect it against myriads of pathogens (Froy et al. 2007). An immune system must detect various agents, including viruses, bacteria, fungi, parasitic worms and particulate materials, and distinguish them from the body's healthy tissues. The body then mounts a counter-attack against these infectious agents and thus wards off their harmful effects. Main line of defense in the innate immune response is the recruitment of phagocytic cells (neutrophils, monocytes, macrophages, etc.) to the site of infection (cell-mediated innate immunity). Immune system dysfunction is responsible for various diseases like arthritis, ulcerative colitis, asthma, allergy, parasitic diseases, cancer, and infectious diseases (Patwardhan et al. 1991). Degree to which a patient becomes abnormally susceptible to infections by microbial agents depends on the extent of immunosuppression. Suppression of the immune system is characterized by impairment of phagocytosis. This results from a reduction in the number and phagocytic function of the neutrophils and macrophages, as well as impairment of the intracellular killing capacity of these cells.

Immunosuppression predisposes to attack by infectious agents and allows opportunistic pathogens to overwhelm the host to cause secondary infections (Rao et al. 1994). Phagocytosis is the primary defense mechanism against foreign body invasion, and it is offered by neutrophils and macrophages. Compounds with immunomodulatory activities are replete with many adverse effects. Microbial resistance to almost all the available chemotherapeutic agents has shifted research interest to explore the enhancement of immune response against infectious agents using natural products. *In vitro* and *in vivo* tests are available for screening of phagocytic competence of immune cells. Medicinal plants derived compounds have been reported to modulate phagocytic functions (Fujinaga et al, 2000; Byrd-Leifer et al. 2001; Gertsch et al. 2004; Schepetkin et al. 2009).

Phyllanthus muellerianus (Kuntze) Exell (Phyllanthaceae) is an evergreen shrub with numerous stems, distributed in tropical and subtropical regions of West Africa (Boakye-Gyasi et al. 2016). Different parts of *P. muellerianus* are used in folkloric medicine to treat dysmenorrhea, fevers, convulsions, toothache, anemia, dysentery, diarrhea, and constipation (Ben-Bala, 2008; Nisar et al, 2018). Immunomodulatory effects of *P. muellerianus* on humoral and cellular adaptive immunity have been reported (Ofokansi et al. 2018). The present study aimed to investigate the cell-mediated innate immunity potentials of *Phyllanthus muellerianus* by evaluating the phagocytic competence of the isolated compounds using *in vitro* models.

MATERIAL AND METHODS

Instrumentation

^{1}H-NMR spectra were recorded using Bruker ARX 300 NMR spectrometer with chemical shifts given in ppm (δ) using CD_3OD and coupling constants (J) in Hz. HPLC-ESIMS measurements were recorded on a Thermo Finnigan LCQ DECA mass spectrometer coupled to an Agilent 1100 HPLC system that included an online photodiode array detector. Analytical HPLC analysis was performed with a Dionex HPLC system (Column: 125 *x* 4 mm, adsorbent: 5 µm Eurosphere 100 C18) with a photodiode array detector, employing a gradient of methanol in acidic water (pH = 2, 0.1% formic acid) from 5% to 100% in 35 min (Table 1). Detection was set at wavelengths 235, 254, 280 and 340 nm. semi-preparative HPLC separation was performed on a C18 column (300 *x* 8 mm, Eurosphere 100–10) on a Hitachi system equipped with a UV Detector and Flatbed Recorder and a flow rate of 5.0 mL/min. Vacuum liquid chromatography (VLC) purification was done in a glass column (30 *x* 3 cm, ID) using silica gel (230–400 mesh) as the adsorbent.

Table 1. Gradient for standard HPLC Analysis

Time (minutes)	Acidic water (%)	MeOH (%)
0	90	10
5	90	10
35	0	100
45	0	100
50	0	10
60	0	10

Chemicals and reagents

Methanol, *n*-hexane, ethyl acetate, lipopolysaccharide (LPS), and nitroblue tetrazolium (NBT) were purchased from Sigma-Aldrich (Germany). Also used are Tween 80 (Janssen, Belgium), phosphate buffer saline, (PBS 8 g NaCl, 0.2 g KC1, 1.44 g Na_2PO_4, 0.24 g $KHPO_4$ in 1L distilled water, pH=7.4). Ethylenediaminetetraacetic acid (EDTA), silica gel 60, 70-230 mesh (Merck, Germany), Leishman, and carbofushsin stains (Hopskin and William, England). Nylon fibers were locally sourced. Neubauer counter (Gallenkamp), Indian ink were used. McFarland point five turbidity standards were prepared from barium chloride, tetraoxosulphate (VI) acid, and water.

Plant Material

Fresh leaves of *P. muellerianus* were collected in November 2018 from Uzo-Uwani Local Government Area of Enugu State, Nigeria. They were identified and authenticated by Mr. A. O. Ozioko of the International Centre for Ethnomedicine and Drug Development (InterCEDD) with a voucher specimen with number INTERCEDD062014. Leaves were air-dried for fourteen days and pulverized.

Extraction and Isolation Procedure

Powdered leaves (1.0 kg) were extracted with methanol using a Soxhlet apparatus. Methanol extract was concentrated *in vacuo* to obtain the dry extract (ME, 170 g). Extract (10.0 g) was fractionated using a glass column (150 *x* 1.5 cm, ID) on silica gel (70-230 mm mesh) and eluted successfully with *n*-hexane, ethyl acetate, and methanol to obtain the solvent fractions *n*-hexane fraction (HF: 0.25 g), ethyl acetate fraction (EF, 3.22 g) and methanol fraction (MF, 5.7 g). EF (3.0 g) was further purified by vacuum liquid chromatography using silica gel (230–400 mesh) as the stationary phase with a glass column (30 *x* 3 cm, ID) and eluted with a gradient of *n*-hexane in ethyl acetate (10:0, 8:2, 6:4, 4:6, 2:8, 0:10 each 500 mL) and of dichloromethane in methanol (9:1, 7:3, 5:5, 3:7,1:9, 0:10 each 1000 mL) to afford eleven sub-fractions (EF1-EF11) (Agbo et al. 2017). EF6 (135.6 mg) and EF7 (261.7 mg) were purified using semi-preparative HPLC with methanol-water as the mobile phase to yield compounds **1** (45.0 mg) and **2** (120 mg), respectively.

In vitro phagocytosis of killed Candida albicans

Preparation of Candida albicans Suspension

Candida albicans culture was incubated in Sabouraud dextrose broth overnight and centrifuged to form a cell button. Supernatant was discarded, and the cell button was washed 3-4 times with sterile PBS and then centrifuged. The washed cell button was resuspended in a mixture of PBS and rat serum (4:1). The *C. albicans* count was adjusted to 10^8 cells/mL using a 0.5 McFarland standard.

Slide preparation

A suspension of leukocytes was prepared from the buffy coat after centrifugation of rat blood collected in an EDTA container. Leukocyte suspension was adjusted to a concentration of 6.5 *x* 10^3 µL by diluting with PBS, and 0.2 mL of the rest was introduced into four sets of six test tubes arranged serially. Two-fold serial dilution of compounds 1 and 2 (100, 50, 25, and 12.5 µg/mL) was made. 0.1 mL of each concentration was introduced into the first four test tubes. The fifth and the sixth tubes contained PBS (0.1 mL) and a suspension of 100 µg LPS (0.1 mL) and served as negative and positive controls, respectively. Lines were incubated for 15 mins and, a 0.2 mL aliquot of the prepared *C. albicans* suspension was added into the test tubes. Lines were incubated for one hour, centrifuged at 500 rpm for 5 mins, and supernatant discarded. The cells were resuspended in 0.1 mL of PBS and a thin

film made with a drop on a clean glass slide. Smeared glass slide was dipped in methanol and stained with Giemsa thrice (Ganachari et al. 2004).

Phagocytosis evaluation

The number of *C. albicans* cells phagocytosed by Polymorphonuclear leucocytes (PMNs) on the slide was determined microscopically for 100 granulocytes using morphological criteria. Number of cells phagocytosed was taken as Phagocytic Index (PI) and compared with the basal PI of the control. Immunostimulant percentage (%) is calculated using the following equation (Ganachari et al. 2004):

$$Stimlation(\%) = \frac{PI_{test} - PI_{comtrol}}{PI_{control}} \times 100$$

Intracellular killing capacity of neutrophils

A suspension of leukocytes was prepared from the buffy coat after centrifugation of sheep blood collected in an EDTA container. Leukocyte suspensions were pooled and adjusted to a concentration of 17.0 *x* 10^3/μL by diluting with PBS. 0.5 mL of the rest was introduced into four sets of six test tubes arranged serially. Twofold serial dilution (100, 50, 25, and 12.5 μg/mL) of compounds **1** and **2** were made, and 0.1 mL of each concentration was introduced into the first four test tubes. The fifth and the sixth tubes contained PBS (0.1 mL) and a suspension of LPS (0.1 mL) and served as negative and positive controls, respectively. 0.2 mL aliquot of a freshly made 0.2% Nitroblue tetrazolium (NBT) solution was added to each tube and incubated at 37°C for 20 min. Lines were centrifuged at 500 rpm for 5 min and the supernatant was discarded. Cells were resuspended in 0.1 mL of PBS and, a thin film made. Film was dried, fixed by heating, and counterstained with dilute carbol-fuchsin for 15 sec. Slide was washed under tap water, dried, and viewed (100 *x*) under oil immersion. Two hundred neutrophils were counted, and proportion of NBT-positive cells containing blue granules determined. Procedure was repeated three times (Wilkinson 1981, Ganachari et al. 2004).

Statistical analysis

Results are expressed as mean ± SEM (n=3). Data obtained were analyzed using a one-way analysis of variance followed post hoc test (LSD) for multiple comparisons. Differences between mean observations were considered significant at $p<0.05$.

RESULTS AND DISCUSSION

The isolated compounds (Figure 1)

Properties of 1-O-galloyl-6-O-luteoyl-α-D-glucopyranoside (**1**)

Pale brown powder; retention time (t_R) of 18.023 mins; UV (MeOH) λ_{max} 222.0, 268.0 nm; ^{1}H (500 MHz CD_3OD) NMR data: See Table 2; Figures 2a & 2b; 3a & 3b. HPLC-MS *m/z* 657.0 $[M + Na]^+$ ($C_{27}H_{22}O_{18}$ + Na), 465 $[M-170]^+$ (loss of gallic acid), 303 $[M-170-162]^+$ (loss of hexose sugar).

Table 2. ^{1}H-NMR Data of Compound 1

	Compound **1**	
Position	δ_H^* (J in Hz)	$\delta_H^{a,**}$ (J in Hz)
1	6.36, d (2.16)	6.37, d (3.7)
2	3.98, d (2.0)	3.99, m
3	4.80, d (3.1)	4.81, m
4	4.46, m	4.47
5	4.51, t (9.4)	4.53, ddd (2.1, 5.0, 11.4)
6	4.96, m	4.99, dd (2.1, 11.1)
	4.16, dd (8.0, 11.0)	4.15, dd (5.0, 11.1)
2′	7.05, s	7.06, s
6′	7.05, s	7.06, s
5′′	6.66, s	6.66, s
5′′′	6.69, s	6.69
*Measured in (500 MHz), **Measured in MeOH-d_4 (500 MHz), a) (Okoye *et al.*, 2015)		

Properties of 3-O-methylellagic acid 3'-O-α-L-rhamnopyronoside (**2**)

Pale yellow powder; retention time (t_R) of 26.170 mins; UV (MeOH) λ_{max} 250.0, 364.0 nm. HPLC-MS *m/z* 484.9 $[M + Na]^+$ ($C_{21}H_{17}O_{12}$ + Na), 317.2 $[M-145]^+$ (loss of rhamnose) and 315 $[M-1-146]^-$ (loss of aglycone).

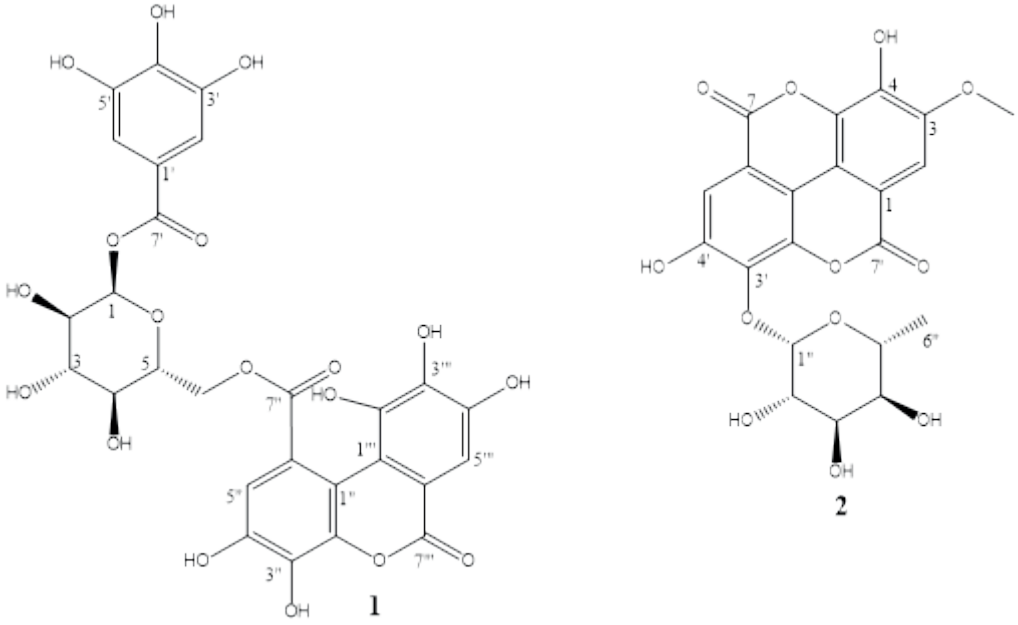

Figure 1: Structures of the Isolated Flavonoid glycosides

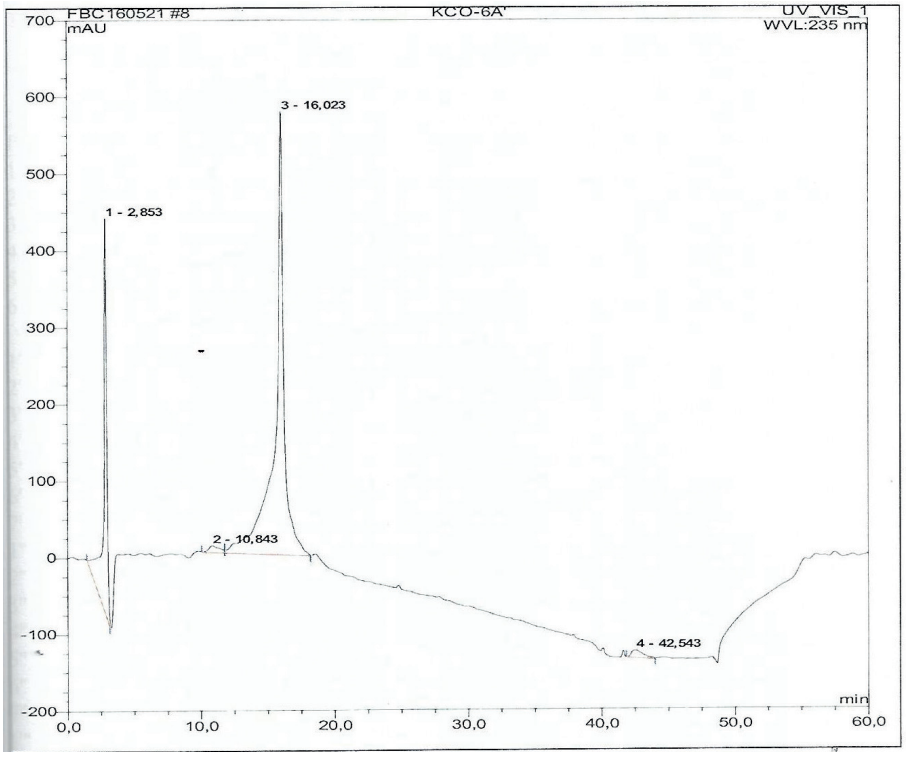

Figure 2a: HPLC Chromatogram of Compound 1

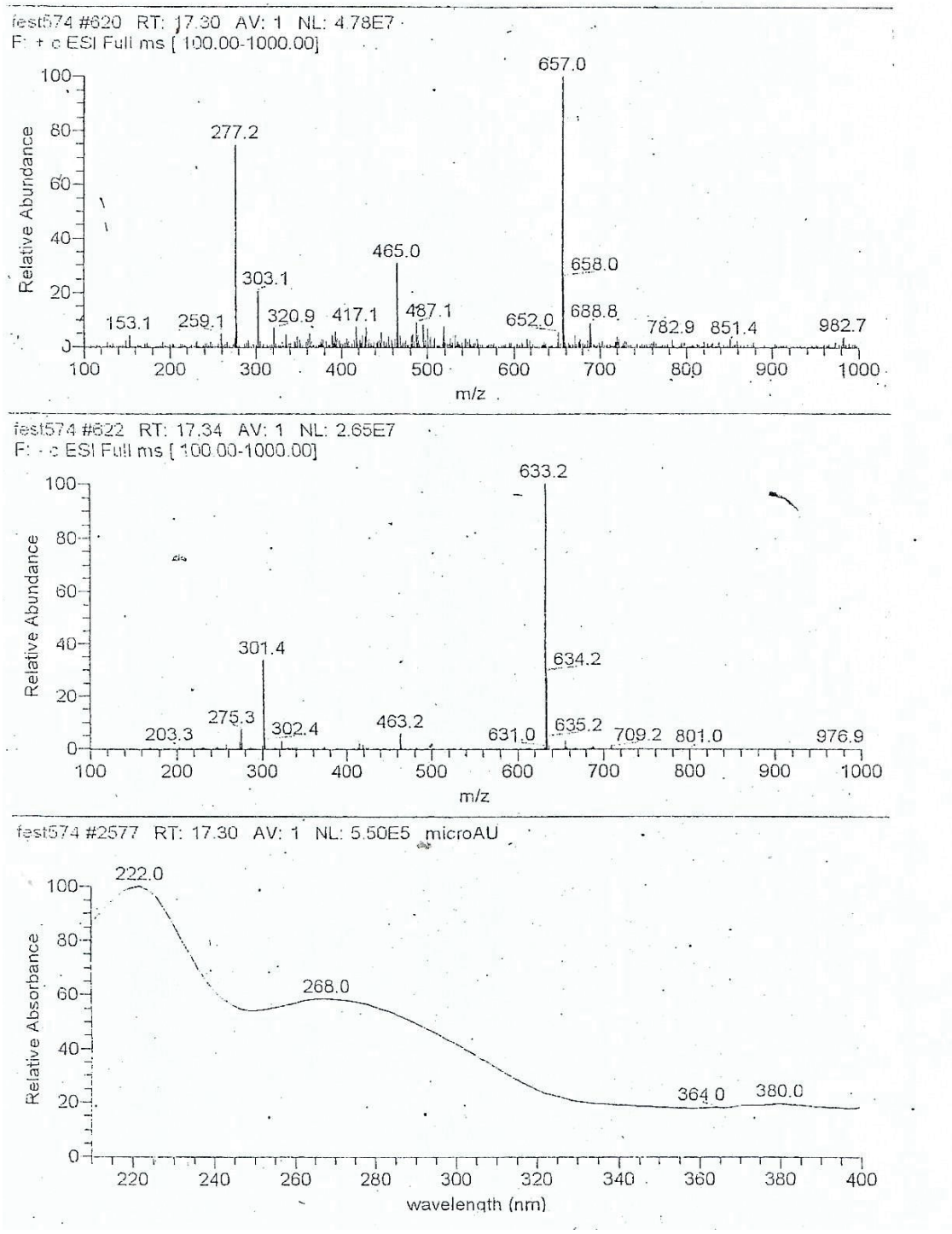

Figure 2b: HPLC-MS Spectrum (Positive mode) of Compound 1; HPLC-MS Spectrum (Negative mode) of Compound 1; UV Spectrum of Compound 1.

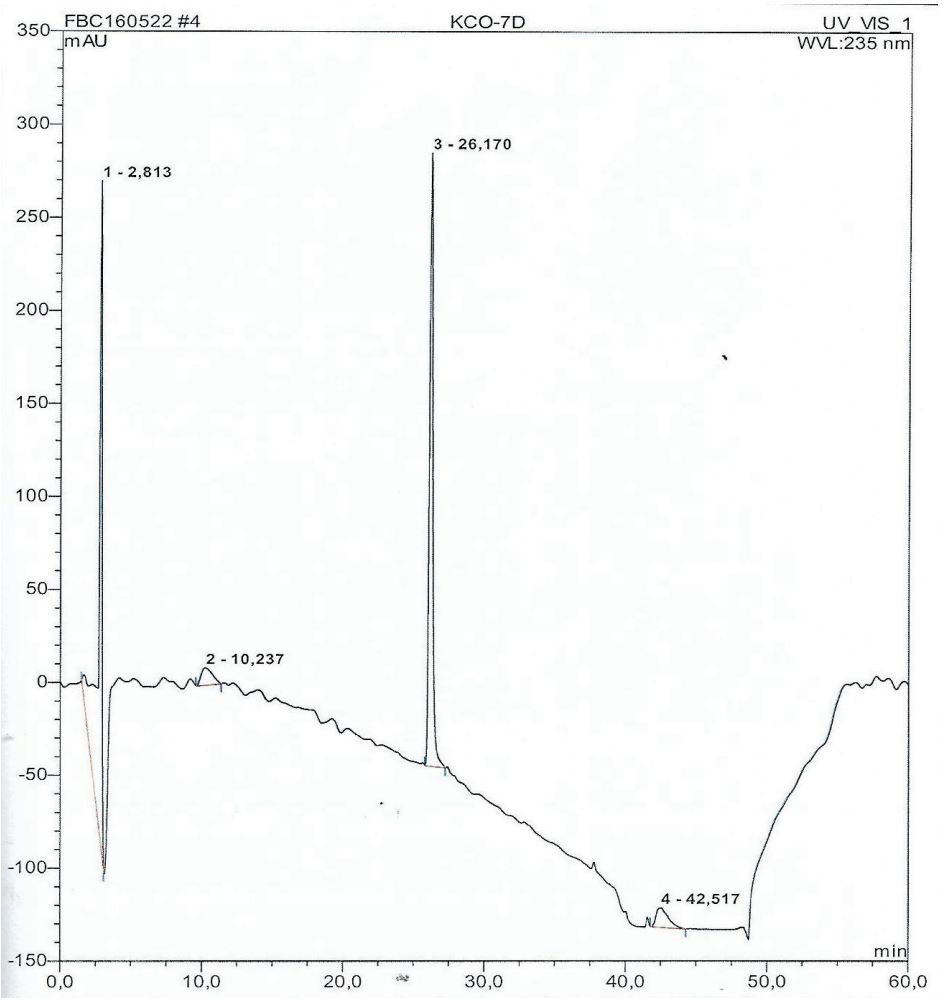

Figure 3a: HPLC Chromatogram of Compound 2

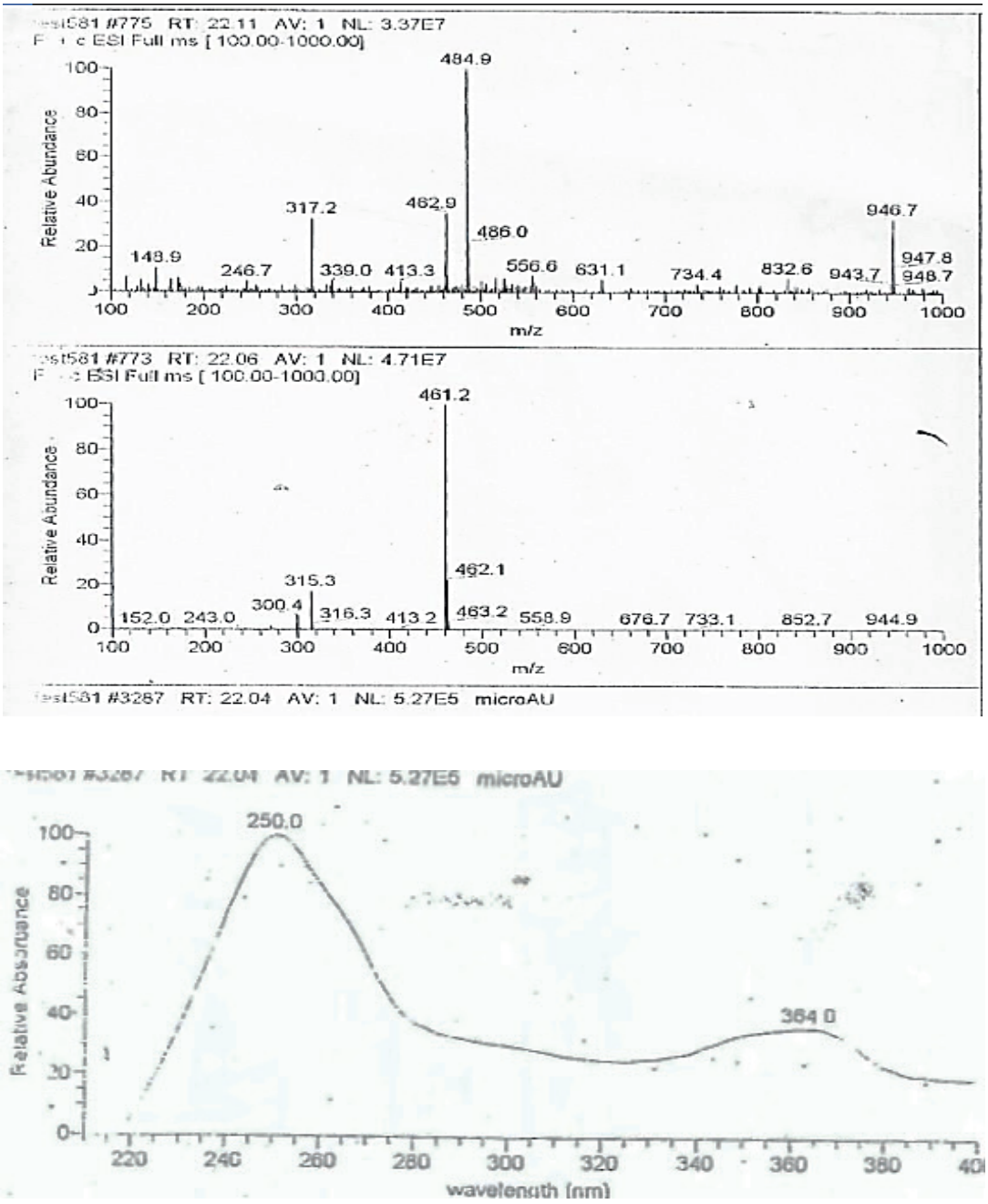

Figure 3b: HPLC-MS Spectrum (Positive mode) of Compound 2; HPLC-MS Spectrum (Negative mode) of Compound 2; UV Spectrum of Compound 2.

Effect of isolated compounds on in vitro Phagocytic ability of Neutrophils

There was a dose-dependent increase in the number of *Candida* cells phagocytosed by neutrophils compared to the control. At the dose of 100 µg/mL, compounds **1** and **2** elicited significant increase ($p < 0.01$) in phagocytic index (Figures 4a & 4b).

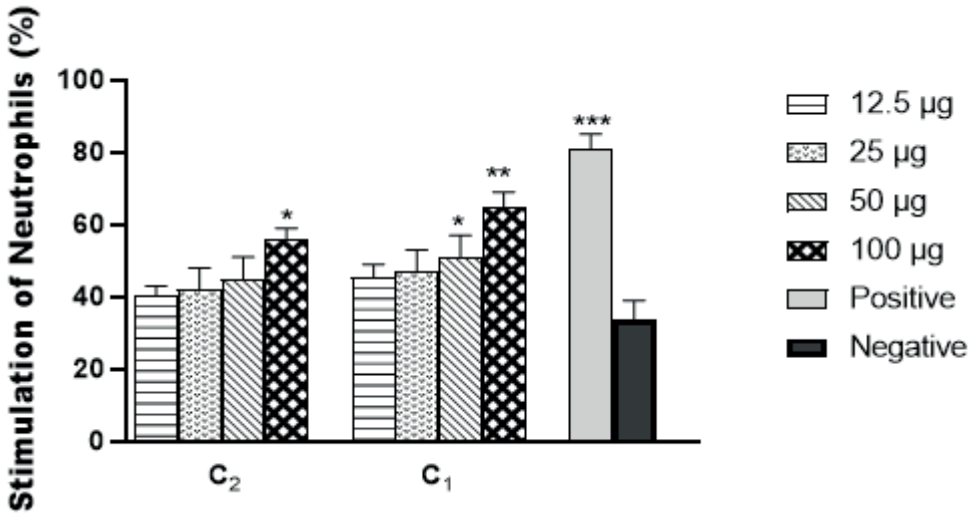

Figure 4a: Effects of the isolated compounds on *in vitro* Phagocytic ability of neutrophils, n= 5, **P<0.05*, *** P< 0.01, *** P< 0.001*. C_2 = compound 2, C_1 = compound 1, LPS= Lipopolysaccharide, PBS= Phosphate buffered solution

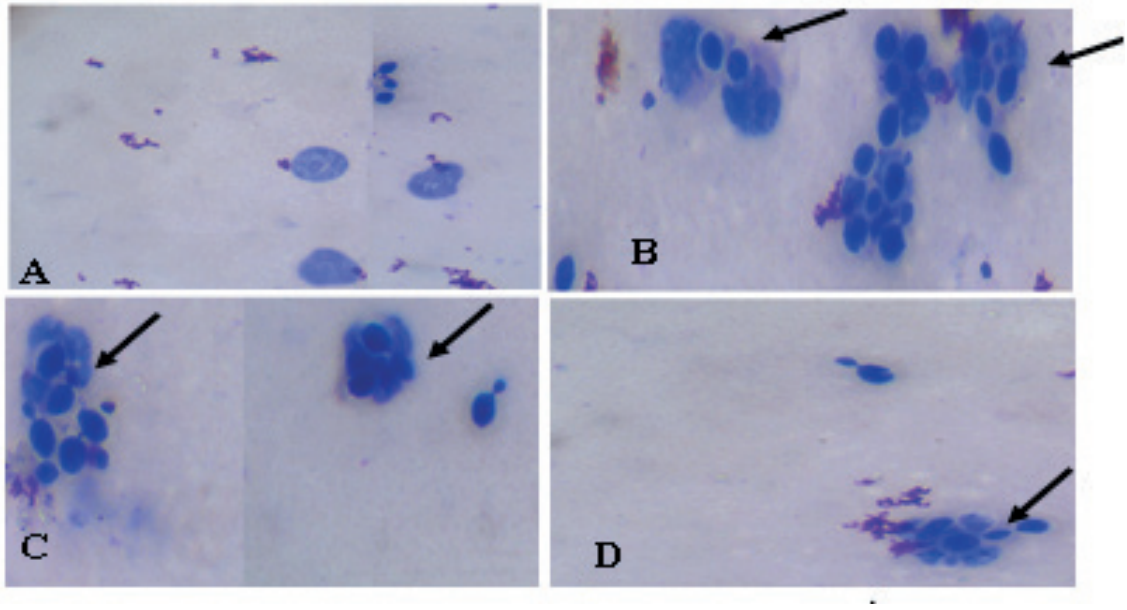

Figure 4b: Photomicrograph Phagocytosis of the isolated compounds. A = negative control. B = positive control (LPS), C = compound 1 and D = compound 2. Arrows reveal the neutrophils (multi-lobed) extending pseudopods to engulf *Candida* cells (spherical shape).

Effects of isolated compounds on Intracellular Killing Capacity of Neutrophils

All the treatment groups elicited a dose-dependent and significant increase in the number of NBT-positive cells relative to the control (Figures 5a & 5b).

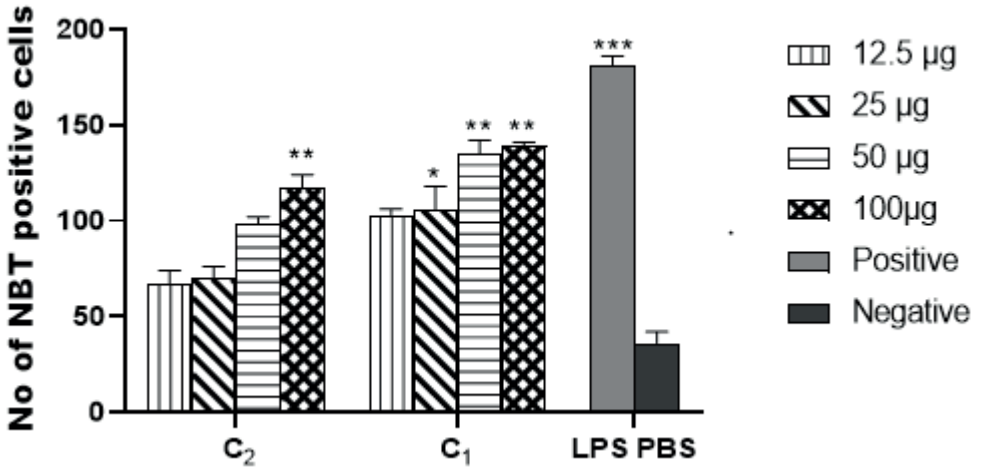

Figure 5a: Effects of the compounds on Intracellular killing capacity of neutrophils, n= 5, **P<0.05*, *** P< 0.01, *** P< 0.001*. C_2 = compound 2, C_1 = compound 1, LPS= Lipopolysaccharide, PBS= Phosphate buffered solution

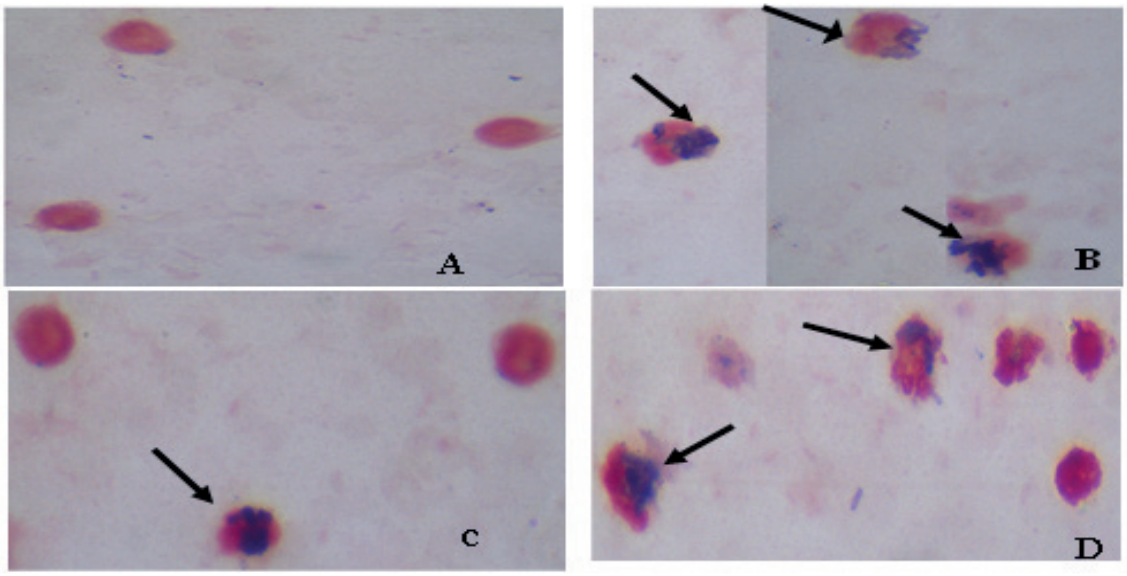

Figure 5b: Photomicrograph of NBT Positive Cells. A = negative control, B = positive control (LPS), C = compound 2 and D = compound 1. Arrows show the neutrophils (red) containing the red

Compound **1** was obtained as pale brown powder exhibiting a molecular ion peak at *m/z* 657.0 $[M+Na]^+$ in the positive mode and *m/z* 633 $[M-H]^-$ in the negative mode corresponding to a molecular formula of $C_{27}H_{22}O_{18}$. UV spectrum showed a characteristic band at λ_{max} of 222.0 and 268.0 nm suggesting the presence of a benzoic ring and C=O chromophore (Figure 1). HPLC-MS showed loss of gallic acid *m/z*

465 $[M-170]^+$ and subsequent loss of a hexose sugar *m/z* 303 $[M-170-162]^+$ (Figure 2). Galloyl moiety was further confirmed by the proton signal at δ_H 7.05 (s, 2H) assigned to H-2'/6' of gallic acid. Presence of the hexose unit was confirmed by the signals at δ_H 6.36 (d, J=2.16, 1H) assignable to the anomeric proton (H-1) (Table 1). ^{1}H NMR of the sugar moiety agrees with reported NMR data suggesting that the sugar was glucose, and the coupling constant of the anomeric proton supported the equatorial orientation of the anomeric proton, which is consistent with an α-D glucopyranoside configuration (Okoye et al. 2015; Jantan et al. 2014). Signals at δ_H 6.66 s (1H) and 6.69 s (1H) assignable to H-5" and H-5"" respectively suggested the presence of luteoyl moiety. Tannin glycoside (**1**) was thus deduced as 1-*O*-galloyl-6-*O*-luteoyl-α-D-glucopyranoside (Figure 1), which was previously reported (Subeki et al. 2005; Okoye et al. 2015).

Compound **2** was obtained as a pale brown powder. Structure of tannin glycoside (**2**) was deduced based on the HPLC-MS and UV spectra. UV spectrum showed two maxima at 250.0 and 364.0 nm, which is consistent with ellagic acid derivatives (Figure 3). HPLC-MS spectrum showed prominent peaks at *m/z* 484.9 $[M+Na]^+$ in the positive mode and 461.2 $[M-H]^-$ in the negative mode, which is consistent with a molar mass of 462 g/mol. Fragment ion at *m/z* 317.2 $[M-145]^+$ in the positive mode corresponds with a loss of deoxyhexose (rhamnose) with a corresponding 315.3 $[M-1-146]^-$ in the negative mode suggests the loss of aglycone moiety. α-rhamnose is the most abundant naturally occurring deoxyhexose, and we propose the presence of rhamnose and methyl ellagic acid derivatives. Tannin glycoside (**2**) is thus presented as 3-*O*-methylellagic acid 3'-*O*-α-rhamnopyranoside (Figure 1), which has been previously reported (Kim et al. 2001).

Phagocytosis and intracellular killing of invading microorganisms by macrophages and polymorphonuclear neutrophils constitute the body's primary line of defense. Phagocytes are powerful defense tools against invading microbes that threaten the life or functional integrity of the host (Splettstoesser and Schuff-Werner, 2002).

Phagocytes like neutrophils normally circulate with blood to migrate to the infection site (extravasation) and engulf any antigen. They first adhere firmly to the vascular endothelium so that they are not swept away by the sheer force of the flowing blood. Neutrophils bind firmly to the endothelium because the cell adhesion molecule on the neutrophil cell membrane called integrin is usually activated by chemoattractants secreted during infection to increase its affinity for the adhesion molecules on the vascular endothelium (Haddad, 2009). Bound neutrophils are afterward guided to the site of infection to cause phagocytosis by chemokines secreted by local macrophages at the injection site. Accumulation of neutrophils at the infection site leads to phagocytosis and, in addition to other mechanisms, leads to inflammation.

In this study, the adhesion of neutrophils to nylon fibers demonstrates a neutrophil attachment to the vascular endothelium and the number of neutrophils reaching the site of infection. Next step in phagocytosis after adhesion and migration of phagocytes to the infection site is the ingestion of the ingesting invader. Reticuloendothelial system (RES) is usually assessed by the rate at which carbon particles injected intravenously are cleared from the system. Overall phagocytic competence of neutrophils can be evaluated using the *in vitro* slide method, giving a reliable, quick, and easy assessment (Ganachari et al. 2004). *In vitro* evaluation of tannin glycoside **1** and **2** revealed a direct relationship between the concentration of the tannin glycoside and the phagocytic ability of neutrophils (Figures 4a & 5a). This is evident by the significant increase ($p < 0.01$) in the number of *C. albicans* cells engulfed by the treated neutrophils on the increasing dose. A comparison of the groups across various treatments showed a stepwise increase in phagocytic index, with **1** eliciting the highest phagocytic index, therefore revealing that its activity increases with pu-

rity. This suggests that some constituents might have antagonistic effects on the phagocytic pathway.

Final step in phagocytosis is ability of phagocytes to kill the engulfed pathogens intracellularly. It is one thing for phagocytosis to occur and another for the phagocyte to kill phagocytosed pathogens inside its cell. Competent phagocyte should be able to kill any engulfed pathogen. In some disease conditions like chronic granulomatous, phagocytes cannot kill some pathogens after engulfment because they cannot produce oxygen-dependent intracellular metabolites. These organisms remain inside the phagocytes and continue to grow and multiply, wreaking havoc on the body. Phagocytes kill pathogens using either toxic oxygen metabolites or lytic enzymes contained in their lysosomes. Present study showed that tannin glycoside **1** and **2** elicited a concentration-dependent and increase in the ability of neutrophils to kill within their cell the engulfed pathogens.

This experiment is based on the fact that during phagocytosis, a metabolic process known as respiratory burst activates a membrane-bound NADPH oxidase which catalyzes the generation of reactive oxygen radicals (O_2^-, OH, $^1O_2$, H_2O_2) that are microbicidal. We assayed for the generation of these toxic oxygen radicals by exposing our treated phagocytes (neutrophils) to nitroblue tetrazolium (NBT) dye – an oxidizing agent. This yellow dye gives a blue precipitate of formazan particles after a redox reaction with oxygen radicals. It was the presence of these blue deposits of reduced formazan in phagocyte solution that confirmed that our treated phagocytes became activated and generated oxygen radicals that reduced the NBT dye. Ability to produce and release within the cell large amounts of toxic oxygen radicals is an exceptional quality of activated mononuclear and polymorphonuclear phagocytes (Splettstoesser and Schuff-Werner, 2002). Therefore, compounds **1** and **2** not only increased phagocytosis as seen in the preceding model but also significantly stimulated the capacity to kill pathogens intracellularly in the treated neutrophils.

The varying degree of reduction of NBT by **1** and **2** confirms neutrophil's intracellular killing property and thus indicates immune-boosting effects. Intracellular infections cannot be killed by humoral immunity but by cell-mediated immunity, affected mainly by activated phagocytic and T cells. Cellular immunity also contributes significantly to the elimination of extracellular pathogens. Tannin glycosides isolated from *Phyllanthus* species have previously been reported to modulate various aspects of the immune system (Singh et al, 2017; Jantan et al, 2014; Jantan et al, 2019).

CONCLUSION

It is evident from these results that the tannin glycosides isolated from the leaves of *Phyllanthus muellerianus* not only have significant positive effects on phagocytosis via activation of neutrophils but also enhance their capacity to kill phagocytized pathogens. These compounds may be helpful '*leads*' in the development of agents for immune-deficiency diseases, antimicrobial agents, and vaccine adjuvants where they can enhance phagocytosis following opsonization by antibodies.

ACKNOWLEDGEMENTS

The authors are grateful to Mr. A. O. Ozioko of the International Centre for Ethnomedicine and Drug Development (InterCEDD) for the collection and authentication of the plant material. Prof John Ihedioha for granting us a bench space in his laboratory. Dr. W. Peters of the Institute of Organic Chemistry, Heinrich-Heine University Dusseldorf, is appreciated for assisting with the NMR measurements.

CONFLICT OF INTEREST

The authors declare that there is no conflict of interest.

AUTHOR CONTRIBUTION STATEMENT

MNO: Conceptualization, Methodology, Investigation, Original draft preparation. **MOA**: Extraction of plant material, Investigation. **ONI**: Visualization, Investigation, Original draft preparation. **IP***:* Original draft preparation, Formal analysis. **FBCO**: Investigation, Formal analysis Validation. **PAA:** Supervision

REFERENCES

Agbo M.O., Odimegwu D.C., Okoye F.B.C., Osadebe P.O. (2017). Antiviral activity of salidroside from the leaves of Nigerian mistletoe (*Loranthus micranthus* Linn) parasitic on *Hevea brasiliensis* against respiratory syncytial virus. *Pakistan Journal of Pharmaceutical Sciences*, 30(4):1251-1256.

Ben-Bala, K.D. *Phyllanthus muellerianus* (Kuntze) Exell. Record from PROTA4U.Schmelzer, G.H. & Gurib-Fakim, A. (Editors). PROTA (Plant Resources of Tropical), Wageningen, Netherlands. Published on the Internet, http://www.prota4u.org/search.asp. (2008).

Boakye-Gyasi E, Kasanga E.A., Biney R.P., Mensah K.B., Agyare C., Woode E. (2016). Anti-Nociceptive effects of geraniin and an aqueous extract of the aerial parts of *Phyllanthus muellerianus* (Kuntze) Exell. in murine models of chemical nociception. *Iranian Journal of Pharmaceutical Sciences*, 12(3):17-30.

Byrd-Leifer C.A., Block E.F., Takeda K., Akira S., Ding A. (2001). The role of MyD88 and TLR4 in the LPS-mimetic activity of Taxol. *European Journal of Immunology*, 31:2448-2457.

Froy O, Hananel A., Chapnik N., Madar Z. (2007). Differential effect of insulin treatment on decreased levels of beta-defensins and toll-like receptors in diabetic rats. *Molecular Immunology*, 44(5):796-802.

Fujinaga Y, Inoue K., Nomura T., Sasaki J., Marvaud J.C., Popoff M.R., Kozaki S., Oguma K. (2000). Identification and characterization of functional subunits of *Clostridium botulinum* type a progenitor toxin involved in binding to intestinal microvilli and erythrocytes. *FEBS Letters*, 467(2-3):179-183.

Ganachari M.S., Kumar S., Bhat K.G. (2004). Effects of *Ziziphus jujuba* leaves extract on phagocytosis by human neutrophils. *Journal of Natural Remedies*, 4:47–51.

Gertsch J, Schoop R., Kuenzle U., Suter A. (2004). Echinacea alkylamides modulate TNF-alpha gene expression *via* cannabinoid receptor CB2 and multiple signal transduction pathways. *FEBS Letters*, 577(3):563-569.

Haddad J.J. (2009). Leucocyte migration and inflammation, In Immunology, Chapter 15. An e-book. Published on the Internet, http://johnjhaddad.weebly.com/uploads/2/5/2/0/2520519/.pdf.

Jantan I., Haque M.A., Ilangkovan M., Arshad L. (2019). An insight into the modulatory effects and mechanisms of action of *Phyllanthus* species and their bioactive metabolites on the immune system. *Frontiers in Pharmacology*, 10:878.

Jantan I., Ilangkovan M., Mohamad H.F. (2014). Correlation between the major components of *Phyllanthus amarus* and *Phyllanthus urinaria* and their inhibitory effects on phagocytic activity of human neutrophils. *BMC Complementary and Alternative Medicine*, 14:429.

Kim J.P., Lee I.K., Yun B.S., Chung S.H., Shim G.S., Koshino H., Yoo I.D. (2001). Ellagic acid rhamnosides from the stem bark of Eucalyptus globulus. *Phytochemistry*, 57(4):587-591.

Nisar M.F., He J., Ahmed A., Yang Y., Li M., Wan C. (2018). Chemical components and biological activities of the genus Phyllanthus: A review of the recent literature. *Molecules*, 23(10):2567.

Ofokansi M.N., Nworu C.S., Akunne T.C., Agbo M.O., Akah P.A. (2018). Immunomodulatory effects of *Phyllanthus muellerianus*: A mechanistic approach. *Journal of Clinical and Cellular Immunology*, 9:5.

Okoye F.B.C., Sawadogo W.R., Sendker J., Aly A.H., Quandt B., Wray V., Hensel A., Esimone C.O., Debbab A., Diederich M., Proksch P. (2015). Flavonoid glycosides from *Olax mannii*: Structure elucidation and effect on the nuclear factor kappa B pathway. *Journal of Ethnopharmacology*, 176:27-34.

Patwardhan B, Kalbag D., Patki P. S., Nagasampagi B. A. (1991). Search of immunomodulatory agents - a review. *Indian Drugs*, 28:249-254.

Rao C.S., Raju C., Gopumadhavan S., Chauhan B.L., Kulkarni R.D., Mitra S.K. (1994). Immunotherapeutic modification by an ayurvedic formulation septilin. *Indian Journal of Experimental Biology*, 32(8):553-558.

Schepetkin I.A., Kirpotina L.N., Jakiw L., Khlebnikov A.I., Blaskovich C.L., Jutila M.A., Quinn M.T. (2009). Immunomodulatory activity of oenothein B isolated from *Epilobium angustifolium*. *Journal of Immunology*, 183(10):6754.

Singh N., Tailang M., Mehta S.C. (2017). Phytochemical screening and immunomodulatory activity of different extract of *Spinacia oleracia* leaves. *International Journal of Pharmaceutical Sciences and Research*, 8(2):878-882.

Splettstoesser W.D, Schuff-Werner P. (2002). Oxidative stress in phagocytes: "The enemy within". *Microscopy Research and Technique*, 57:441-445.

Subeki S., Matsuura H., Takahashi K., Yamasaki M., Yamato O., Maede Y., Katakura K., Kobayashi S., Trimurningsih T., Chairul C., Yoshihara T. (2005). Anti-babesial and anti-plasmodial compounds from *Phyllanthus niruri*. *Journal of Natural Products*, 68:537-539.

Wilkinson PC. (1981) In: Thomson RA (Ed). Technique in Clinical Immunology, Blackwell Scientific Publication: London; 273-293.

FABAD J. Pharm. Sci., 48, 1, 25-36, 2023
Doi: 10.55262/fabadeczacilik.1103532
RESEARCH ARTICLE

The Relative Bioavailability Study of Two Cefdinir Formulations in Healthy Males Under Fasting Conditions

Fırat YERLİKAYA[*°], Aslıhan ARSLAN[**], Özlem ATİK[***], Seda KOZAN[****], Ahmet PARLAK[*****], Meltem ÖZEL KARATAŞ[******], Onursal SAĞLAM[*******], Peri AYTAÇ[********]

The Relative Bioavailability Study of Two Cefdinir Formulations in Healthy Males Under Fasting Conditions

SUMMARY

A new oral formulation of cefdinir, Cefdinir 600 mg tablets has been developed and, in this study, its relative bioavailability has been compared with another oral solid dosage form, Cefdinir 300 mg Capsules, which is already on the market. An open-label, randomized, two-period, cross-over relative bioavailability study has been conducted with healthy males under fasting conditions in compliance with Good Clinical Practice (GCP) principles. A single dose of the novel tablet formulation of 600 mg cefdinir has been compared to two doses of Cefdinir 300 mg Capsules (two capsules at once) regarding pharmacokinetic properties. The comparison study was performed as a single-center clinical study, and blood samples of the participants were withdrawn at specified time points, before and after dosing. The plasma concentrations and pharmacokinetic properties of two cefdinir formulations were assessed from the collected samples by using a validated LC-MS/MS analytical method. The relative bioavailability of the new formulation has been shown, and both products were introduced as safe.

Keywords: *Bioavailability, cefdinir, cephalosporin, GCP*

İki Sefdinir Formülasyonunun Sağlıklı Erkeklerde Açlık Koşulları Altında Bağıl Biyoyararlanım Çalışması

ÖZ

600 mg sefdinir içeren yeni bir oral tablet formülasyonu geliştirilmiş ve bu çalışmada bu formülasyonun bağıl biyoyararlanımı halihazırda piyasada bulunan başka bir oral katı dozaj formu olan Sefdinir 300 mg kapsül ile karşılaştırılmıştır. Sağlıklı erkeklerde, açlık koşulları altında açık etiketli, randomize, iki periyotlu, çapraz geçişli bir bağıl biyoyararlanım çalışması İyi Klinik Uygulamaları (İKU) ilkelerine uygun olarak yürütülmüştür. Tek doz uygulanan 600 mg Sefdinir Tablet formülasyonunun farmakokinetik özellikleri, iki doz (tek seferde iki kapsül) olarak uygulanan Sefdinir 300 mg Kapsül ile karşılaştırılmıştır. Bu karşılaştırma çalışması, tek merkezli bir klinik çalışma olarak gerçekleştirilmiştir ve katılımcıların kan örnekleri, dozlamadan önce ve sonra belirtilen zaman noktalarında alınmıştır. Sefdinir formülasyonlarının plazma konsantrasyonları ve farmakokinetik özellikleri, valide edilmiş bir LC-MS/MS analitik yöntemi ile toplanan örnekler kullanılarak değerlendirilmiştir. Çalışmada yeni formülasyonun bağıl biyoyararlanımı gösterilmiş ve her iki ürünün de güvenli olduğu bildirilmiştir.

Anahtar Kelimeler: *Biyoyararlanım, sefdinir, sefalosporin, İKU*

Received: 19.04.2022
Revised: 09.08.2022
Accepted: 26.09.2022

[*] ORCID: 0000-0003-4648-3258, Elixir İlaç Araştırma ve Geliştirme AŞ, Ankara, Turkey, Department of Pharmaceutical Technology, Faculty of Pharmacy, Lokman Hekim University, Ankara, Turkey
[**] ORCID: 0000-0002-3520-608X, Elixir İlaç Araştırma ve Geliştirme AŞ, Ankara, Turkey
[***] ORCID: 0000-0001-7867-6316, İ.E. Ulagay İlaç Sanayii Türk A.Ş. (Istanbul, Turkey)
[****] ORCID: 0000-0003-3925-0317, İ.E. Ulagay İlaç Sanayii Türk A.Ş. (Istanbul, Turkey)
[*****] ORCID: 0000-0002-4921-0004, İ.E. Ulagay İlaç Sanayii Türk A.Ş. (Istanbul, Turkey)
[******] ORCID: 0000-0001-9226-2603, İ.E. Ulagay İlaç Sanayii Türk A.Ş. (Istanbul, Turkey)
[*******] ORCID: 0000-0002-1421-6633, Novagenix Biyoanalitik İlaç Ar-Ge Merkezi San. ve Tic. AŞ, Ankara, Turkey
[********] ORCID: 0000-0002-9985-3382, Novagenix Biyoanalitik İlaç Ar-Ge Merkezi San. ve Tic. AŞ, Ankara, Turkey

[°] Corresponding Author; Fırat YERLİKAYA
Telephone: +90532609463; E-mail: firat.yerlikaya@elixirlabs.com.tr;

INTRODUCTION

Cefdinir is a semi-synthetic cephalosporin that exhibits its antimicrobial effects against a broad spectrum of bacteria, both gram-negative and gram-positive (Cabri, 2006). It is used for the treatment of mild to moderate infections caused by various conditions in pediatric, adolescent, and adult patients (Richer, 1995, Cefdinir Capsules USP 300 mg Label, 2020), and its capsule formulation is generally prescribed as either 300 mg twice a day or 600 mg once a day via oral administration (Perry, 2004). However, cefdinir exerts low oral bioavailability and dose-disproportionality. Previous studies showed that in adults, while a single oral dose of 300 mg capsule showed 21% bioavailability, the bioavailability of a single oral dose of 600 mg capsule was 16% (Perry, 2004). For the 300 mg single dose capsule, some pharmacokinetic properties are as follows: the time to reach the peak concentration (t_{max}) is 2 – 4 hours, the maximum plasma concentration (C_{max}) is 1.60 µg/mL, the volume of distribution is 0.35 L/kg, and the terminal half-life ($t_{½}$) is 1.7 ± 0.6 hours. It is eliminated principally via renal excretion without significant metabolization (Cefdinir Capsules USP 300 mg Label, 2020).

To improve drug compliance of patients who needs to take 600 mg of cefdinir at once, a novel 600 mg tablet formulation has been developed by Elixir İlaç Araştırma ve Geliştirme AŞ for İ.E. Ulagay İlaç Sanayii Türk A.Ş. (Istanbul, Turkey). Together with this, to assess the impact on the bioavailability of the new formulation, a pharmacokinetics study on healthy males has been designed in accordance with the regulations of the International Council on Harmonization (ICH), European Medicines Agency (EMA), and Food and Drug Administration (FDA).

Therefore, the aim of this study is to evaluate the pharmacokinetic properties and bioavailability of the single oral dose of novel Cefdinir 600 mg Tablets (Test Drug) formulation compared to Cefdinir 300 mg Capsules (Reference Drug), which was administered as two capsules in healthy males under fasting conditions.

MATERIALS AND METHODS

In Vitro Characterization of the Test and Reference Drugs

The test drug product was developed by Elixir İlaç Araştırma ve Geliştirme AŞ (Ankara, Turkey), with a formulation comprising cefdinir, microcrystalline cellulose, calcium carboxymethyl cellulose, polyoxyl 40 stearate, colloidal silicon dioxide, magnesium stearate and Opadry® Y-1-7000 White as the film-coating. Dissolution profiles of the test and reference drugs were studied in physiological media.

Clinical Study

Twenty-four healthy adult males aged 18 – 55 years with a body mass index of 18.5 – 30 kg/m^2 were enrolled in this study. The participants voluntarily involved in the clinical study have read, understood, and signed the written informed consent form of their free will.

The volunteers who have atopic constitution or asthma and/or known allergy to cefdinir and, or other cephalosporin group antibiotics and, or penicillin or any excipients of the study products were excluded from the study. The volunteers who have the following conditions were also excluded from the study: (*i*) who have any history or presence of clinical relevance to cardiovascular, neurological, musculoskeletal, hematological, hepatic, gastrointestinal, renal, pulmonary, endocrinological, metabolism disorders; (*ii*) who have a history of malabsorption or other conditions that might affect the pharmacokinetics of study drugs; (*iii*) who donated blood more than 400 mL within the last two months before the first administration or were included in another clinical trial; (*iv*) who took depot injectable solutions within six months and, or enzyme-inducing, organotoxic or long half-life drugs within four weeks before the start of the study.

The volunteers who have been consuming beverages or food containing methylxanthines over a certain amount, taking any grapefruit, or grapefruit juice for seven days before drug administration, during the

study, or during the washout periods, who had a history of drug or alcohol abuse and, or had a positive alcohol breath test result were excluded, as well. The eligible volunteers who gave their written informed consents and understood that they could withdraw from the study anytime without specifying any reason were enrolled.

This study was designed as an open-label, randomized, single oral dose, cross-over, two-period study, under fasting conditions. It was conducted at FARMAGEN Good Clinical Practice Center (Gaziantep, Turkey), enrolling 24 healthy adult males. Erciyes University Ethical Committee of Bioequivalence/Bioavailability Studies (2019/78; 19.06.2019) and the Turkish Medicines and Medical Devices Agency (28.06.2019) reviewed and approved this study in compliance with the Declaration of Helsinki and Good Clinical Principles (GCP) (The Ministry of Health of Turkey, 2015).

The duration of the clinical study period was approximately four weeks, including pre-study screening (Day -14 to -1), a wash-out period (7 days), and a final examination (2 – 8 days after the last blood sampling). The individuals who voluntarily attended the study were screened for their eligibility with the standard clinical and biochemical examinations of blood and urine samples. The standard clinical screening included brief anamnestic and demographic data, physical analysis, body temperature determination, weight, and height, standard electrocardiogram (12 lead), blood pressure (BP), and pulse rate (PR) measurements. All laboratory tests were carried out in a certified local laboratory. The volunteers were checked for the presence of Hepatitis B surface antigen (HBsAg), hepatitis C virus antibodies (HCV-Ab) and human immunodeficiency virus antibody (HIV-Ab) in serum to avoid possible infections. They were requested to provide urine samples for drug screening for amphetamines, cannabinoids, benzodiazepines, cocaine, opioids, and barbiturates. Their alcohol breath tests were also applied on entry visits and hospitalization days in both periods of the study.

Twenty-four volunteers were hospitalized and randomized on the day before the dosing day at the GCP clinic. An evening meal was provided on hospitalization days (total caloric value of approximately 1200 kcal) in each period.

After staying ten h fasted, they received their study drugs and were not allowed to drink water from one h before until one h after the administration of study products, except while dosing. On medication days, a standard lunch (total caloric value is approximately 1200 kcal) was provided four h after dosing, and a standard dinner (total caloric value is approximately 1200 kcal) was provided ten h after dosing in each period. Immediately after pre-dose sampling, one tablet of the test drug (600 mg cefdinir) or two capsules of the reference drug (2 x 300 mg cefdinir) was administered to the volunteers with 240 mL water. Blood samplings were done just before dosing and following 16-time points after administration: at 0.33, 0.66, 1.00, 1.33, 1.66, 2.00, 2.33, 2.66, 3.00, 3.50, 4.00, 5.00, 6.00, 8.00, 10.00, 14.00 h and the samples were collected into polypropylene tubes using K_2EDTA as an anti-coagulating agent. After sampling, the samples were immediately refrigerated at approximately +4 °C not more than 30 min. Following the centrifugation (3.000 rpm, 4 – 6°C, 10 min), the separated plasma from each sample was transferred into two 3 mL transparent, polypropylene tubes, transferred to a deep freezer, and stored at -70 °C until the clinical study ended. Later, they were transported to the bioanalytical center for the analysis.

Following the washout period, in Period II, the volunteers took the other product they did not take in Period I. The same procedures were applied in each period.

Bioanalytical Study

The bioanalytical studies have been run using a validated chromatographic in-house method at Novagenix Bioanalytical R&D Center (Ankara, Turkey). To be in compliance with GCP rules and avoid bias, the analytical studies were done analytically blinded.

The analytical reference standard of cefdinir was

supplied by Covalent Laboratories Private Limited (India) and the internal standard (IS), cefaclor, was supplied from Alsachim (France). Solvents: methanol, acetonitrile, dichloromethane, and formic acid were supplied from Merck (Darmstadt, Germany). Ultrapure (Type 1) water was supplied from Millipore MilliQ water purification system; K_2EDTA blank human plasma was supplied from Gaziantep University Farmagen GCP Centre (Turkey).

A Shimadzu Liquid Chromatograph Mass Spectrometer LCMS-8040 was used as the high-performance liquid chromatography with mass spectrometry (LC-MS/MS) system. Atlantis dC18, 3 µm (4.6 × 75 mm) column was chosen with a mobile phase consisting of 0.2% formic acid and acetonitrile/methanol (1:1) (80/20, *v*/*v*) with a column oven temperature maintained at 30 °C. The flow rate was 0.9 mL/min. Electrospray ionization was performed in MRM mode to detect *m*/*z* 396.00 > 126.05 (cefdinir) and *m*/*z* 368.00 > 118.05 (cefaclor) ions, simultaneously. The total run time for the method was 5.5 min.

Stock standard solutions of cefdinir were prepared at a concentration of 1 mg/mL. Working solutions were prepared in the concentration range of 0.4 – 180 µg/mL. The working IS was prepared at a concentration of 1 mg/mL. Stock solutions of cefdinir and IS were stored at -70 °C. Calibration standards were prepared by spiking the appropriate amounts of standard solutions into the blank plasma to obtain final concentration levels between 20 – 9,000 ng/mL. The quality control samples were prepared similarly, at concentrations between 20 – 6,750 ng/mL. The lower limit of quantification (LLOQ) was 20 ng/mL. Calibration standards and quality control (QC) samples were stored at -70 °C freezer until analyses.

Protein precipitation followed by liquid-liquid extraction was selected to extract cefdinir, and the sample preparation has done according to the bioanalytical center sample preparation standard operation procedures.

The method was validated for selectivity, specificity, carry-over, linearity, precision and accuracy, recovery, dilution integrity, the influence of hemolyzed and hyperlipidemic plasma, drug-drug interaction, matrix effect, and stabilities, and the validation was performed with K_2EDTA human plasma according to EMA Guideline on Bioanalytical Method Validation (EMA, 2011).

The analytical curves were constructed from a plasma sample processed without IS (blank), a plasma sample processed with IS (zero), and eight concentrations of cefdinir, including the LLOQ, ranging from 20 to 9,000 ng/mL. The concentrations were calculated using peak area ratios and the linearity of the calibration curve was determined using least squares regression analysis. The acceptance criteria for each calculated standard concentration were not more than 15% deviation from the nominal value, except for the LLOQ, which was set at 20%. The within-batch precision and accuracy were evaluated by analyzing QC samples at four different concentration levels between 20 – 6,750 ng/mL. The matrix effects of cefdinir were evaluated by comparing the peak areas of post-extraction blank plasma that were spiked at certain concentrations of QC samples with the areas obtained by the direct injection of the corresponding standard solutions.

An in-house LC-MS/MS was developed and validated to quantify cefdinir in plasma. The plasma samples were maintained at -70 °C during the assay.

Pharmacokinetic and Statistical Analyses

1. To assess relative bioavailability, 24 volunteers were included in the study. The C_{max} and area under the curve from time 0 to the last sampling time ($AUC_{0\text{-}tlast}$) were considered the primary target variables; the area under the curve from time 0 to the infinite time ($AUC_{0\text{-}\infty}$), t_{max} and $t_{½}$ are secondary target variables. The terminal rate constant (λ_z) and mean residence time (*MRT*) were determined, as well. Relative bioavailability (*F*) was calculated using $AUC_{0\text{-tlast}}$ values of the test and reference products. Since this study was designed as a relative bioavailability study, demonstration of the acceptance intervals was not applicable.

C_{max} and t_{max} for cefdinir were obtained directly by plasma concentration-time curves. $AUC_{0\text{-}tlast}$ was calculated using the trapezoidal rule. $AUC_{0\text{-}\infty}$ was calculated by summing $AUC_{0\text{-}tlast}$ and extrapolated area (residual area). The latter was determined by dividing the last measured concentration by λ_z, which was estimated by regression of the terminal log-linear plasma concentration-time points.

C_{max} and $AUC_{0\text{-}tlast}$ were tested for statistically significant differences by means of the analysis of variance (ANOVA) test procedure after logarithmic transformation (ln). The effects of ANOVA were treatment, period, sequence, and volunteer within the sequence and tested at 5% level of significance. 90% confidence interval for the ratio of mean values of C_{max} and $AUC_{0\text{-}tlast}$ which are indicatives of the rate and extent of absorption, respectively, were calculated using ln-transformed.

All statistical analyses were done using Phoenix WinNonlin (Version 8.1, Certara L.P.).

RESULTS AND DISCUSSION

In Vitro Characterization of the Test and Reference Drugs

In vitro dissolution data and similarity factors are given in Table 1 – 6. All tests were conducted with 900 mL media volume with a temperature set at 37 ± 0.5 °C using a paddle apparatus with 50 rpm agitation.

Table 1. *In vitro* dissolution data of the Reference Product (2 x 300 mg capsules) in 0.1 N HCl medium (%) (n = 12).

No.	Time Point (min)							
	0	5	10	15	20	30	45	60
1	0	62.2	82.9	84.9	86.8	89.3	90.7	91.3
2	0	40.6	64.1	76.3	80.0	84.5	87.9	89.2
3	0	59.1	82.9	84.6	85.6	87.0	88.6	89.7
4	0	56.8	78.9	81.2	84.9	87.7	90.1	91.8
5	0	49.6	76.9	79.9	84.3	86.8	90.6	93.2
6	0	46.9	72.6	75.7	78.5	81.8	86.6	89.3
7	0	54.6	87.4	82.1	83.8	87.3	90.6	92.2
8	0	48.9	85.5	86.5	88.1	89.7	91.0	91.8
9	0	53.2	84.5	85.9	86.8	88.2	88.7	90.9
10	0	54.0	80.8	83.2	84.4	86.5	88.8	90.4
11	0	42.4	76.0	79.7	82.8	87.4	89.4	90.7
12	0	51.0	77.3	80.0	82.1	85.6	88.0	89.5
Average	0	51.6	79.1	81.7	84.0	86.8	89.3	90.8
Standard Deviation	-	6.4	6.4	3.5	2.8	2.1	1.4	1.3
Relative Standard Deviation	-	12.4	8.1	4.3	3.4	2.5	1.5	1.4

Table 2. *In vitro* dissolution data of the Test Product (600 mg film-coated tablets) in 0.1 N HCl medium (%) (n = 12).

No.	Time Point (min)							
	0	5	10	15	20	30	45	60
1	0	55.6	75.7	81.6	84.5	87.2	88.2	88.9
2	0	47.6	69.5	76.8	80.6	85.2	87.3	88.1
3	0	43.5	70.9	78.5	82.4	85.4	86.6	87.3
4	0	47.0	75.1	81.4	83.6	86.4	88.4	88.5
5	0	46.5	68.2	75.1	79.5	82.9	85.0	85.4
6	0	52.1	78.5	84.3	86.9	89.2	89.8	89.8
7	0	65.1	81.4	86.0	87.2	88.8	89.0	90.1
8	0	42.3	68.5	81.9	84.4	87.3	88.3	88.4
9	0	61.8	82.0	86.2	88.1	89.7	90.1	90.2
10	0	54.2	78.6	83.0	85.1	86.7	87.5	87.6
11	0	48.0	70.1	76.2	79.3	83.4	85.1	85.9
12	0	43.5	70.1	76.8	79.9	83.8	85.9	86.3
Average	0	50.6	74.1	80.7	83.5	86.3	87.6	88.1
Standard Deviation	-	7.3	5.1	3.9	3.1	2.3	1.7	1.6
Relative Standard Deviation	-	14.5	6.9	4.8	3.7	2.6	1.9	1.8

The similarity factor between the test and reference products was found to be 79.3 in the 0.1 N HCl medium.

Table 3. *In vitro* dissolution data of the Reference Product (2 x 300 mg capsules) in pH 4.5 acetate buffer medium (%) (n = 12).

No.	Time Point (min)							
	0	5	10	15	20	30	45	60
1	0	44.8	83.3	87.1	88.6	89.7	91.4	92.0
2	0	42.9	85.1	89.3	90.8	92.5	94.1	95.0
3	0	35.2	86.2	89.0	90.3	91.1	91.8	92.4
4	0	39.6	83.0	84.4	85.8	87.2	89.0	90.0
5	0	34.4	78.9	86.5	88.6	90.1	91.3	92.4
6	0	42.8	85.0	89.0	90.3	92.0	93.7	94.6
7	0	52.8	82.6	84.6	85.3	87.6	89.0	90.0
8	0	39.5	85.2	88.2	89.1	88.9	92.0	93.6
9	0	43.8	75.7	79.6	81.9	84.6	87.2	88.7
10	0	43.3	74.8	83.1	85.7	88.4	90.0	91.0
11	0	54.9	87.6	89.2	90.2	91.2	91.8	92.8
12	0	55.2	88.1	89.8	90.8	91.8	92.4	93.4
Average	0	44.1	82.9	86.6	88.1	89.6	91.1	92.2
Standard Deviation	-	7.0	4.4	3.1	2.8	2.4	2.0	1.9
Relative Standard Deviation	-	15.9	5.3	3.6	3.2	2.6	2.2	2.1

Table 4. *In vitro* dissolution data of the Test Product (600 mg film-coated tablets) in pH 4.5 acetate buffer medium (%) (n = 12).

No.	Time Point (min)							
	0	5	10	15	20	30	45	60
1	0	33.8	73.6	81.3	85.4	89.9	91.3	91.8
2	0	39.2	77.0	84.8	88.4	90.4	91.2	92.1
3	0	43.6	79.2	88.4	91.1	92.7	93.7	93.9
4	0	45.8	76.0	84.7	88.6	91.6	93.1	93.6
5	0	38.4	73.9	81.7	85.3	89.0	90.7	91.9
6	0	34.0	77.0	85.1	88.2	90.3	91.2	91.9
7	0	52.0	81.4	88.0	88.5	92.2	92.8	92.0
8	0	40.6	79.2	85.0	88.0	89.8	90.6	91.0
9	0	49.9	80.2	86.9	89.2	91.5	92.6	93.5
10	0	49.3	89.4	91.8	93.2	93.0	93.5	93.8
11	0	34.5	83.4	89.3	91.5	92.5	93.1	93.5
12	0	51.9	82.4	87.4	90.1	92.0	92.7	93.0
Average	0	42.8	79.4	86.2	89.0	91.3	92.2	92.7
Standard Deviation	-	6.9	4.5	3.0	2.3	1.3	1.1	1.0
Relative Standard Deviation	-	16.2	5.6	3.5	2.6	1.4	1.2	1.1

Since both the test and reference products were dissolved more than 85%, the similarity factor was not calculated in pH 4.5 acetate buffer medium.

Table 5. *In vitro* dissolution data of the Reference Product (2 x 300 mg capsules) in pH 6.8 phosphate buffer medium (%) (n = 12).

No.	Time Point (min)							
	0	5	10	15	20	30	45	60
1	0	56.1	87.3	93.3	94.2	94.9	96.9	96.9
2	0	36.4	79.5	90.4	91.7	93.7	96.0	97.1
3	0	46.3	84.3	93.4	94.0	94.3	95.6	96.8
4	0	38.6	72.2	83.2	85.0	88.7	92.1	94.2
5	0	44.9	81.3	90.2	89.8	95.3	97.5	98.8
6	0	43.9	78.6	87.2	89.5	92.2	93.9	95.3
7	0	62.6	88.2	90.3	91.8	93.2	94.9	95.0
8	0	54.9	87.4	90.0	91.3	93.2	95.2	96.8
9	0	57.8	91.0	93.1	93.8	95.1	97.0	97.6
10	0	51.2	87.1	91.0	92.9	95.0	97.0	97.3
11	0	55.3	86.5	88.9	90.5	93.1	95.4	96.6
12	0	67.6	91.5	92.6	93.1	94.2	95.9	96.1
Average	0	51.3	84.6	90.3	91.5	93.6	95.6	96.5
Standard Deviation	-	9.5	5.7	2.9	2.6	1.8	1.5	1.2
Relative Standard Deviation	-	18.5	6.7	3.2	2.8	1.9	1.6	1.3

Table 6. *In vitro* dissolution data of the Test Product (600 mg film-coated tablets) in pH 6.8 phosphate buffer medium (%) (n = 12).

No.	Time Point (min)							
	0	5	10	15	20	30	45	60
1	0	52.3	86.2	90.2	92.1	94.0	94.8	95.0
2	0	58.8	84.2	89.6	91.3	93.5	94.2	95.0
3	0	50.0	82.7	88.6	91.5	93.7	94.5	95.3
4	0	47.5	82.1	86.0	88.3	89.8	90.8	91.3
5	0	50.6	83.5	88.6	90.3	92.1	93.0	93.3
6	0	51.4	80.8	86.5	88.6	91.0	91.6	92.2
7	0	49.9	84.9	91.0	92.8	94.6	95.3	95.9
8	0	54.5	88.8	91.5	92.9	93.6	94.1	94.3
9	0	49.9	85.0	90.9	93.2	94.6	95.4	95.6
10	0	42.4	86.2	90.6	92.2	93.1	93.9	94.3
11	0	47.3	79.8	84.8	87.1	90.0	93.5	92.2
12	0	45.5	79.0	85.5	87.7	90.4	91.7	92.1
Average	0	50.0	83.6	88.6	90.7	92.5	93.6	93.9
Standard Deviation	-	4.2	2.9	2.4	2.2	1.8	1.5	1.6
Relative Standard Deviation	-	8.4	3.4	2.7	2.4	2.0	1.6	1.7

Since both the test and reference products were dissolved more than 85%, the similarity factor was not calculated in pH 6.8 phosphate buffer medium.

Based on the *in vitro* dissolution tests that are conducted in three different media, the test and reference drug products' release profiles were found to be similar.

Clinical Study

To enroll in this study, 46 volunteers were screened; 24 of them were included and randomized into two groups and completed the clinical study. All the volunteers were Caucasian. The mean ± SD age of volunteers is 24.17 ± 6.48 years, and the mean ± SD body mass index (BMI) was 25.01 ± 2.34. The demographic data of volunteers are presented in Table 7. There was no protocol deviation throughout the clinical period.

Table 7. Demographic data of the volunteers.

n = 24	Age	Weight (kg)	Height (cm)	BMI
Mean	24.17	78.88	177.38	25.01
SD	6.48	9.89	5.64	2.34
Minimum	19	62	165	20.6
Maximum	50	98	186	29.7

To estimate the pharmacokinetic parameters, the actual time of sampling was used. The wash-out duration was sufficient since no pre-dose concentration of cefdinir was detected in t_0 samples of the second period. As primary variables, the mean ± SD of C_{max} were found to be 3,098.30 ± 1,102.72 ng/mL and 3,461.70 ± 1,013.93 ng/mL, and the mean ± SD of $AUC_{0\text{-tlast}}$ were found to be 14,287.11 ± 5,146.29 h.ng/mL and 15,244.83 ± 4,406.45 h.ng/mL for test and reference products, respectively (Table 8).

Table 8. The arithmetic means ± SD of pharmacokinetic parameters of a single oral dose of 600 mg cefdinir in test drug and the reference drug in healthy adult male volunteers under fasting conditions (Arithmetic Mean ± SD) (n = 24).

Parameters (Units)	Test (T)	Reference (R)
C_{max} (ng/mL)	3098.30 ± 1102.72	3461.70 ± 1013.93
$AUC_{0\text{-tlast}}$ (ng.h/mL)	14287.11 ± 5146.29	15244.83 ± 4406.45
$AUC_{0\text{-}\infty}$ (ng.h/mL)	14458.54 ± 5218.76	15397.98 ± 4457.30
t_{max} (h)*	3.10 ± 0.79	3.04 ± 0.66
$t_{½}$ (h)	1.75 ± 0.13	1.74 ± 0.15
λ_z (1/h)	0.40 ± 0.03	0.40 ± 0.03
MRT (h)	4.71 ± 0.68	4.48 ± 0.52

* t_{max} values are presented as median with range (minimum – maximum) in parentheses.

In Table 8, the pharmacokinetic parameters of the study drugs; in Table 3, the geometric least-square means, ratios and 90% Confidence Intervals (CI)s are shown. The 90% CIs for the geometric mean ratios of C_{max} and $AUC_{0\text{-tlast}}$ have been found as 80.67 – 96.37% and 86.23 – 98.17%, respectively (Table 9).

Table 9. Geometric Least Square Means, Ratio and 90% Confidence Intervals of the test drug and the reference drug in healthy adult male volunteers under fasting conditions.

Parameter	Difference	DiffSE	TESTLSM	REFLSM	Ratio%	90% CI	ISCV%	Power%
ln(C_{max})	-0.1259	0.0518	7.9793	8.1052	0.8817	0.8067 – 0.9637	18.09	56.92
ln($AUC_{0\text{-tlast}}$)	-0.0833	0.0377	9.5093	9.5926	0.9201	0.8623 – 0.9817	13.13	97.40
ln($AUC_{0\text{-}\infty}$)	-0.0814	0.0378	9.5211	9.6025	0.9218	0.8639 – 0.9836	13.14	97.66
t_{max} (h)	0.0563	0.1802	3.0958	3.0396	1.0185	0.9167 – 1.1203		
$t_{½}$ (h)	0.0054	0.0199	1.7453	1.7399	1.0031	0.9835 – 1.0227		
λz (1/h)	-0.0016	0.0045	0.3994	0.4009	0.9961	0.9770 – 1.0151		
MRT (h)	0.2264	0.1140	4.7062	4.4798	1.0505	1.0068 – 1.0942		

The average plasma concentration-time curves and the average ln plasma concentration-time curves of study drugs are displayed in Figures 1 and 2, respectively.

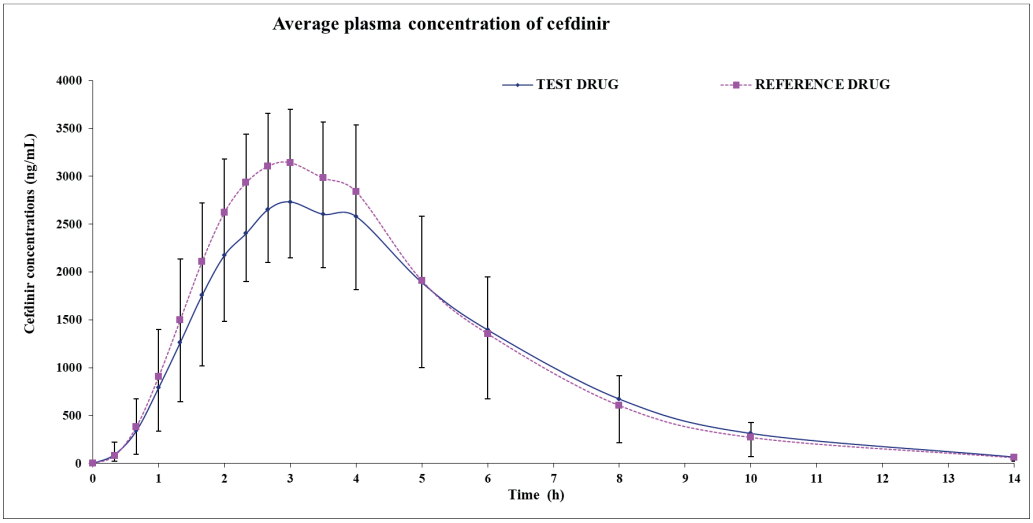

Figure 1. Mean plasma concentration-time curves of cefdinir after a single dose of the test drug and the reference drug of oral cefdinir in healthy adult male volunteers (n = 24) under fasting conditions.

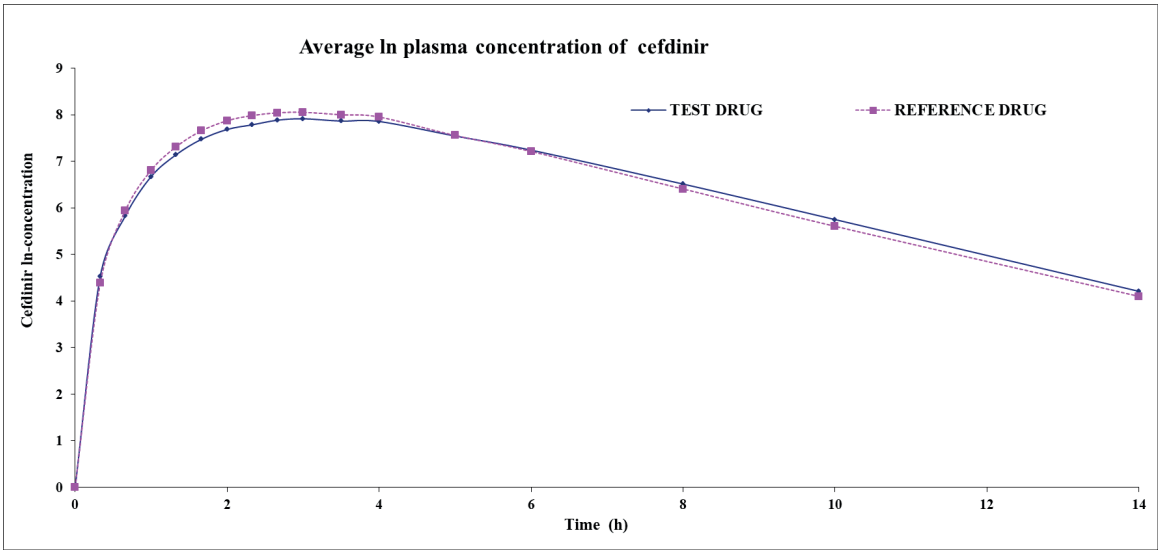

Figure 2. Average ln plasma concentration curves of cefdinir after a single dose of the test drug and the reference drug of oral cefdinir in healthy adult male volunteers (n = 24) under fasting conditions.

As the secondary variables, the median of t_{max} for study drugs was found to be three h and ranged from 2.0 to 5.0 h for the test, and from 2.0 to 4.0 h, for the reference drug. In addition, the mean ± SD of $t_{1/2}$ for the test and reference products were found similar: 1.75 ± 0.13 h and 1.74 ± 0.14 h, respectively (Table 8).

Three adverse events occurred during the study, and one of them was defined as "probable" and the other two were assessed as "possible" drug-related adverse events that occurred in all two periods. Two of those three have fully recovered. One volunteer received concomitant medication (paracetamol, an analgesic agent known to have no interaction with cefdinir as stated in the study protocol) due to a headache. The overall tolerability of the products was considered as good. There were no serious adverse events or adverse reactions reported throughout the study.

There are no pharmacokinetic studies in the literature with 600 mg cefdinir doses, yet, we have identified some recent studies conducted with various doses and formulations of cefdinir (Table 10) (Abdel, 2011, Zhang, 2011, Chen, 2012).

Table 10. Recent pharmacokinetic studies conducted with various doses of cefdinir.

Author	Dose	C_{max} (μg/mL)	t_{max} (h)	$t_{1/2}$ (h)	AUC_{0-t} (μg.h/mL)
Abdel	125 mg/5 mL	T*: 2.49 ± 1.15	T: 2.81 ± 0.55	T: 4.92 ± 1.58	T: 15.09 ± 5.00
		R*: 2.41 ± 1.04	R: 3.02 ± 0.85	R: 5.07 ± 1.66	R: 14.74 ± 5.68
Chen	100 mg	T: 0.95 ± 0.24	T: 2.68 ± 0.77	T: 1.99 ± 0.71	T: 4.34 ± 0.94
		R: 0.88 ± 0.16	R: 3.68 ± 0.99	R: 1.78 ± 0.42	R: 4.21 ± 0.74
Zhang	200 mg	T: 1.52 ± 0.48	T: 3.08 ± 0.73	T: 2.04 ± 0.53	T: 7.12 ± 1.85
		R: 1.42 ± 0.39	R: 3.22 ± 0.81	R: 1.87 ± 0.29	R: 6.86 ± 1.60

*T: Test Drug, R: Reference Drug

Cefdinir is a preferred antibiotic in mild and moderate infections due to its extensive spectrum against bacteria, despite its low oral bioavailability. Together with this, the non-linear pharmacokinetics of cefdinir gives rise to the risk of limiting the adequacy of treatment. Therefore, a 600 mg tablet formulation of cefdinir was developed, which is aimed to improve compliance of patients in need of 600 mg/day taken

as a single dose, and a relative bioavailability study has been designed and conducted over the current regulations. In this single-dose study, the subjects received either one tablet of 600 mg cefdinir or two capsules of 300 mg cefdinir in a randomized order, and plasma cefdinir concentrations of study drugs were evaluated relatively.

CONCLUSIONS

The overall objective of this study is to assess the oral relative bioavailability of two formulations of cefdinir on 24 healthy volunteers. Concluding the results, the *F* value was found as 93.52%. Moreover, both study drugs were well-tolerated and considered to be safe.

ACKNOWLEDGMENT

This study was sponsored by İ.E. Ulagay İlaç Sanayii Türk A.Ş. (Istanbul, Turkey). The test drug product was developed by Elixir İlaç Araştırma ve Geliştirme AŞ (Ankara, Turkey) and the biobatch of the test drug product was manufactured by Nobel İlaç San. ve Tic. AŞ (Düzce, Turkey) under current Good Manufacturing Practices. The clinical study was carried out by FARMAGEN Good Clinical Practice and Research Center (Gaziantep, Turkey) and the bioanalyses and statistical analyses were carried out by Novagenix Bioanalytical Drugs R&D (Ankara, Turkey).

CONFLICT OF INTEREST

The authors declare that there is no conflict of interest.

AUTHOR CONTRIBUTION STATEMENT

FY: Writing, Design, Review; AA: Experimenting, Interpretation, Review; ÖA: Design, Interpretation, Review; SK: Design, Interpretation, Review; AP: Design, Interpretation, Review; MÖK: Design, Interpretation, Review; OS: Statistics, Design, Interpretation, Review; SPA: Writing, Review.

REFERENCES

Abdel, Z., Franco, A., Jamal, K., & Waleed, S. (2011). Comparative Bioavailability of Two Cefdinir Suspension Formulations in Middle Eastern Healthy Volunteers after Single Oral Administration. Arzneimittelforschung, 58(03), 149–153.

Cabri, W., Ghetti, P., Alpegiani, M., Pozzi, G., Justoerbez, A., Perezmartinez, J., Munozruiz, A. (2006). Cefdinir: A comparative study of anhydrous vs. monohydrate form Microstructure and tabletting behaviour. European Journal of Pharmaceutics and Biopharmaceutics, 64(2), 212–221.

Chen, J., Jiang, B., Lou, H., Yu, L., & Ruan, Z. (2012). Bioequivalence Evaluation of Cefdinir in Healthy Fasting Subjects. Arzneimittelforschung, 62(01), 9–13.

EMA, (2011), Guideline on Bioanalytical Method Validation, EMEA/CHMP/EWP/192217/2009 Rev.1 Corr.2, London, 21 July 2011. https://www.ema.europa.eu/en/documents/scientific-guideline/guideline-bioanalytical-method-validation_en.pdf, Access Date: 12.04.2022.

FDA, (2020), Cefdinir 300 mg Capsules Label, https://dailymed.nlm.nih.gov/dailymed/fda/fdaDrugXsl.cfm?setid=38f6adf7-e26c-4764-8ec9-360813874dd4&type=display, Access Date: 12.04.2022.

Perry, C. M., & Scott, L. J. (2004). Cefdinir. Drugs, 64(13), 1433–1464.

Republic of Turkey Ministry of Health, (2015), The Guidance for GCP. https://titck.gov.tr/storage/Archive/2020/legislation/KADKLVZ01IKU13.11.2015Rev08_13ac0133-274b-44dc-98cd-33998758cc72.pdf, Access Date: 12.04.2022.

Richer, M., Allard, S., Manseau, L., Vallée, F., Pak, R., & LeBel, M. (1995). Suction-induced blister fluid penetration of cefdinir in healthy volunteers following ascending oral doses. Antimicrobial Agents and Chemotherapy, 39(5), 1082–1086. https://doi.org/10.1128/AAC.39.5.1082.

Zhang, C. L., Jiao, J. J., Wu, Y. N., Song, J. Q., Gao, W. Z., Ma, W. D. L., and Lou J. S. (2011). Study on Pharmacokinetics and Bioequivalence of Cefdinir Dispersible Tablet in Healthy Chinese Volunteers. Journal of Bioequivalence & Bioavailability, 3(6), 114-117.

FABAD J. Pharm. Sci., 48, 1, 37-52, 2023
Doi: 10.55262/fabadeczacilik.1145208
RESEARCH ARTICLE

Ifosfamide-Loaded Cubosomes: An Approach to Potentiate Cytotoxicity against MDA-MB-231 Breast Cancer Cells

Popat S. KUMBHAR[*°] , Vishvajit M. KHADE[**], Varsha S. KHADAKE[***], Pradnya S. MARALE[****], Arehalli S. MANJAPPA[*****], Sameer J. NADAF[******], Vijay M. KUMBAR[*******], Durgacharan A. BHAGWAT[********], Ravindra A. MARATHE[*********], John I. DISOUZA[**********°]

Ifosfamide-Loaded Cubosomes: An Approach to Potentiate Cytotoxicity against MDA-MB-231 Breast Cancer Cells

SUMMARY

Ifosfamide (IFS) is proven efficacious against breast cancer, an enormously diagnosed cancer across the globe. However, the clinical efficacy of IFS is limited owing to its hydrophilicity, less stability, and dose-dependent toxicities. Therefore, the primary goal of the present research was to develop IFS-loaded cubosomes with improved anticancer efficacy and reduced dose-dependent toxicities. The IFS-cubosomes were optimized using a 32factorial design based on IFS content and zeta potential. The optimized cubosomal dispersion was further assessed for particle size, in vitro IFS release, hemolysis, cytotoxicity, cellular uptake, and physical stability. The optimized IFS-cubosomal dispersion exhibited maximum IFS content (89.75±4.3%) and better zeta potential value (-40.0±1.6 mV), and size in nanometer. Moreover, IFS-cubosomes retarded IFS release (about 91 %) 12 h than plain IFS solution (>99 % within 2 h). The IFS-cubosomes displayed lower hemolysis (3.7±0.79%) towards human RBCs. Besides, the in vitro cytotoxicity of IFS-cubosomes was noticed to be substantially higher (IC50: 0.64±0.08 µM) than plain IFS solution (IC50: 1.46±0.21 µM) against multi-drug resistant (MDR) breast cancer (MDA-MB-231) cells. The 4',6-diamidino-2-phenylindole (DAPI) staining revealed the death of IFS-cubosomes treated cells mainly by apoptosis. The cubosomes showed increased uptake by cancer cells. Furthermore, IFS-cubosomes were found to be more stable at refrigeration temperature than at room temperature. Thus, IFS-cubosomes could be a novel avenue in the treatment of breast cancer with improved anticancer efficacy and reduced toxicity. However, further in vivo investigations are desired to validate these claims.

Key Words: *Breast cancer, ifosfamide, cubosomes, haemolysis, cytotoxicity, cellular uptake.*

İfosfamid Yüklü Kübozomlar: MDA-MB-231 Meme Kanseri Hücrelerine Karşı Sitotoksisiteyi Güçlendirmeye Yönelik Bir Yaklaşım

ÖZ

İfosfamidin (IFS), dünya çapında çok fazla teşhis edilen bir kanser olan meme kanserine karşı etkili olduğu kanıtlanmıştır. Bununla birlikte, hidrofilikliği, daha az stabilitesi ve doza bağlı toksisiteleri nedeniyle IFS'nin klinik etkinliği sınırlıdır. Bu nedenle, mevcut araştırmanın birincil amacı, gelişmiş antikanser etkinliği ve doza bağlı toksisiteleri azaltılmış IFS yüklü kübozomlar geliştirmektir. IFS-kübozomları, IFS içeriğine ve zeta potansiyeline dayalı 32 faktörlü bir tasarım kullanılarak optimize edildi. Optimize edilmiş kübozomal dispersiyon ayrıca partikül boyutu, in vitro IFS salımı, hemoliz, sitotoksisite, hücresel alım ve fiziksel stabilite açısından da değerlendirildi. Optimize edilmiş IFS-kübozomal dispersiyonu, maksimum IFS içeriği (%89.75±4.3) ve daha iyi zeta potansiyel değeri (-40.0±1.6 mV) ve nanometre cinsinden boyut sergiledi. Ayrıca , IFS-kübozomlar, IFS salımını (yaklaşık %91) düz- IFS solüsyonuna (2 saat içinde >%99) göre 12 saat geciktirmiştir. IFS-kübozomları, insan RBC'lerine karşı daha düşük hemoliz (%3.7±0.79) gösterdi. Ayrıca, IFS-kübozomların in vitro sitotoksisitesinin, çoklu ilaca dirençli (MDR) meme kanserine (MDA-MB--231 hücreler) karşı düz IFS solüsyonundan (IC50: 1.46±0.21 µM) önemli ölçüde daha yüksek (IC50: 0.64±0.08 µM) olduğu fark edildi. 4',6-diamidino-2-phenylindole(DAPI) boyaması, IFS-kübozomlarla tedavi edilen hücrelerin başlıca apoptoz yoluyla ölümünü ortaya çıkardı. Kübozomların kanser hücrelerine alımları yüksek düzeyde gerçekleşti. Ayrıca, IFS-kübozomlarının buzdolabı sıcaklığında oda sıcaklığından daha kararlı olduğu bulundu. Bu nedenlerle IFS-kübozomlar, gelişmiş antikanser etkinliği ve azaltılmış toksisitesi ile meme kanseri tedavisinde yeni bir yol olabilir. Bununla birlikte, bu iddiaları doğrulamak için daha fazla in vivo araştırma istenmektedir.

Anahtar Kelimeler: *Meme kanseri, ifosfamid, kübozomlar, hemoliz, sitotoksisite, hücresel alım.*

Received: 18.07.2022 *Revised: 01.10.2022* *Accepted: 17.10.2022*

[*] ORCID: 0000-0002-6753-239X, Tatyasaheb Kore College of Pharmacy, Warananagar, Tal: Panhala, Dist: Kolhapur Maharashtra, India, 416113
[**] ORCID: 0000-0002-7522-8400, Tatyasaheb Kore College of Pharmacy, Warananagar, Tal: Panhala, Dist: Kolhapur Maharashtra, India, 416113
[***] ORCID: 0000-0003-3623-6595, Tatyasaheb Kore College of Pharmacy, Warananagar, Tal: Panhala, Dist: Kolhapur Maharashtra, India, 416113
[****] ORCID: 0000-0003-2633-5928, Tatyasaheb Kore College of Pharmacy, Warananagar, Tal: Panhala, Dist: Kolhapur Maharashtra, India, 416113
[*****] ORCID: 0000-0002-8576-6608, Tatyasaheb Kore College of Pharmacy, Warananagar, Tal: Panhala, Dist: Kolhapur Maharashtra, India, 416113
[******] ORCID: 0000-0002-7132-1886, Sant Gajanan Maharaj College of Pharmacy, Mahagaon, Gadhinglaj, Maharashtra, India
[*******] ORCID: 0000-0001-6261-1665, Dr. Prabhakar Kore Basic Science Research Centre, KLE Academy of Higher Education & Research, Belagavi, India
[********] ORCID: 0000-0002-3993-8851, Bharati Vidyapeeth College of Pharmacy, Kolhapur 416013, Maharashtra, India
[*********] ORCID: 0000-0002-9807-7932, Tatyasaheb Kore College of Pharmacy, Warananagar, Tal: Panhala, Dist: Kolhapur Maharashtra, India, 416113
[**********] ORCID: 0000-0002-0180-7266, Bharati Vidyapeeth (Deemed to be University), Yashwantrao Mohite Institute of Management, Karad

[°] Corresponding Author;
1. Dr. John I. Disouza
Phone: 02328 223526, Fax: 02328 223501
Email: jidisouza@tkcpwarana.ac.in

2. Mr. Popat S. Kumbhar
Phone: 02328 223526, Fax: 02328 223501
Email: pskumbhar@tkcpwarana.ac.in

INTRODUCTION

Cancer is the second most common cause of mortality globally. Amongst the various cancers, female breast cancer is the most prevalent cancer with a diagnosis rate of 11.7% followed by lung cancer (11.4%). Breast cancer is conceivably the single most important medical condition women face at present. It is an unrestrained growth of epithelial cells in the ducts or breast lobules (Elakkad, 2021). Breast cancer, from etiology to cure, is a complex disease that needs multidisciplinary management including a customized therapy plan based on severity and histologic subtype (Rick, 2021).

So far, surgery and chemotherapy are preferred procedures for the treatment of breast cancer either alone or in combination (Almotwaa, 2021). However, chemotherapy is associated with numerous side effects including myelosuppression, neurotoxicity, gastrointestinal dysfunctions, and damage to enteric neurons (Carr, 2008; McQuade, 2016; Escalante, 2017), *etc*. Furthermore, adverse effects of chemotherapy are identified to disturb the psychological health of patients and thereby impact their quality of life and social interactions (Suwankhong, 2018).

Ifosfamide (IFS) is a DNA alkylating therapeutic employed in the treatment of diverse cancers including lung, ovary, cervix, breast, and endometrium cancer (Wang, 2018; Almotwaa, 2021).It mainly acts *via* inhibition of DNA replication and thereby causes cell apoptosis. Nevertheless, the clinical efficacy of IFS is limited owing to its hydrophilic characteristics and dose-related toxicities such as encephalopathy, neurotoxicity, nephrotoxicity, and cardiotoxicity (Almotwaa, 2021).Hemorrhagic cystitis is a dose-limiting toxicity of IFS (Saito, 2016). Further, pH-dependent solubility profiling (Wang, 2018), multi-drug resistance (MDR) (Zhang, 2010; Noujaim, 2018),*etc.* are the other parameters that limit its therapeutic efficacy. Thus, to overcome the above issues, there is an utmost need to develop a suitable nanocarrier to deliver IFS with increased bioavailability, selectivity and stability with decreased side effects and MDR.

Lipid-based nanosized systems, for example, solid-lipid nanoparticles, nanostructured-lipid carriers, liposomes, cubosomes, hexosomes, *etc*., have revolutionized cancer management *via* improving anti-cancer effects of ample therapeutic actives (Garcia-Pinel, 2019). Cubosomes are cubic liquid crystalline particles that are a surfactant of self-assembled liquid crystalline particles with the right microstructure/nanostructure and water ratio. Cubosomes offer numerous formulation benefits including high encapsulation capacity, delivery of hydrophilic, hydrophobic, and amphiphilic drugs, biodegradability, biocompatibility, and increased physical and chemical stabilization of drugs (Lakshmi, 2014). In addition, cubosomes can be administered *via* various routes (oral, topical, and intravenous) of administration.

Both cubosomes and liposomes were reported to exhibit an increase in pharmacokinetic and pharmacodynamic results to intravenous administration that can broaden the therapeutic window and results in the enhancement of therapeutic efficacy. Besides, they were found to be promising in the reduction of neurotoxicity, cardiotoxicity, nephrotoxicity, ototoxicity, hepatotoxicity, and hematological toxicities (Alavi, 2020). For instance, the delivery of doxorubicin *via* liposomes caused a reduction of cardiotoxicity and other types of toxicities associated with doxorubicin (Addeo, 2008). Furthermore, cubosomes were reported to minimize the MDR in the treatment of cancer (Alavi, 2020). Cubosomes can also selectively target cancer cells *via* the enhanced permeation and retention (EPR) effect.

Glycerol monooleate (GMO) is a commonly employed lipid in the fabrication of cubosomes. GMO in the presence of excess water form liquid crystalline cubic phases that can control the release of the drug molecules. Moreover, it can deliver therapeutics of varying molecular sizes and solubilities (Nasr, 2015).

The main intend of the present research was to develop IFS-loaded cubosomes with improved cytotoxicity towards cancer cells, increased stability and reduced toxicities. The cubosomes were optimized using an experimental design approach and the optimized formulation was subjected to different *in vitro* analysis.

MATERIALS AND METHODS

MATERIALS

Ifosfamide was purchased from Believe Pharma, Gujarat. Glyceryl monooleate and Poloxamer-188 (P-188) were procured from Sigma Aldrich, Mumbai. Methanol and chloroform were obtained from Molychem, Mumbai. All the analytical grade chemicals were used in the experiments.

METHODS

Preparation of IFS-loaded cubosomes

Briefly, GMO and P-188 have melted at 70±2°Cin a water bath. The weighed quantity of IFS was then dissolved into double-distilled water maintained at 70±2°C with stirring. Then the melted mixture was gradually added to the double-distilled with the aid of stirring. The obtained dispersion was then subjected to probe sonication for 10 min employing an energy input (400 W) and a pulse mode (9-second pulses interrupted by 18-second breaks) under cooling in a 20°C water bath.

Optimization of IFS-loaded cubosomes

The IFS-loaded cubosomes formulation was optimized using 3^2 (2-factor, 3-levels) factorial design *via* Design-Expert software Version 13.0 (Stat-Ease Inc., Minneapolis, USA). Total of 09 runs (F1-F9) were generated using software and the consequence of independent variables was investigated on response variables at three levels. GMO concentration (X_1) and P-188 concentration (X_2) were selected as independent variables, whereas drug content (Y_1), and zeta potential (Y_2) as dependent variables. All independent and response variables with their coded and actual levels are shown in Table 1. Experimental runs were prepared according to the software-generated experimental design matrix (Table 2) and evaluated for results. The statistical significance of obtained results was evaluated by analysis of variance (ANOVA). 3-D response surface and 2-D contour plots were also obtained *via* design expert software and the consequence of independent variables on dependent variables were investigated further.

Table 1. Independent and dependent variables used with their coded and actual levels

Variables	Levels		
	Low (-1)	Medium (0)	High (+1)
Independent variables			
X_1: GMO concentration (mg)	0.25	0.5	1
X_2: Poloxamer concentration (mg)	0.5	1	1.5
Dependent (response) variables	**Goal**		
Y_1: Drug content (%)	Maximize		
Y_2: Zeta potential (mV)	Maximize		

Characterization of IFS-loaded cubosomes

% Entrapment efficiency (%EE)

Cubosome formulation was centrifuged at 10000 rpm for 1hand the clear supernatant was collected. The free IFS content in the supernatant was estimated *via* a UV-visible spectrophotometer at 249 nm after suitable dilution with methanol (Zhang, 2010; Siddiqui, 2019). The maximum wavelength of IFS obtained in methanol is depicted in Figure 1. The %EE of cubosome formulation was determined using the following formula (1);

$$\%EE = \frac{Tp - Tf}{Tp} \times 100 \quad (1)$$

Where Tp is the total IFS used to prepare the cubosomes and Tf is the free IFS in the supernatant.

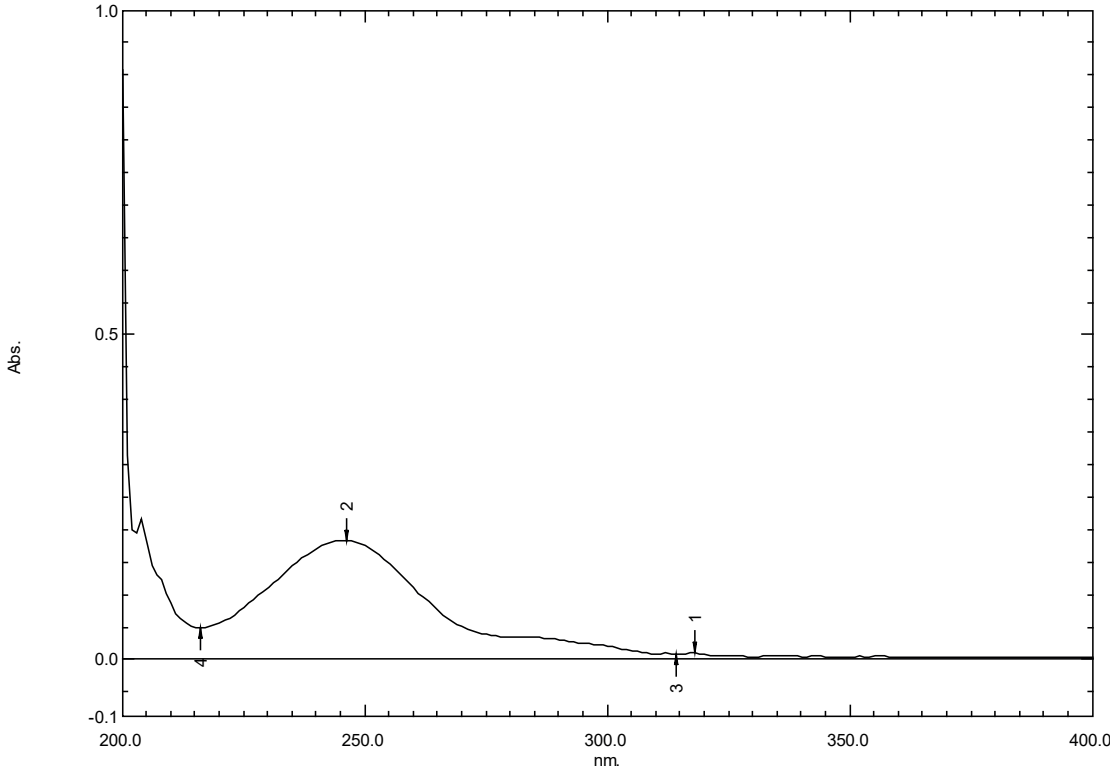

Figure 1. UV-spectra of ifosfamide in methanol

Vesicle size and Zeta potential

The particle size of the optimized batch and blank cubosomes, and zeta potential of all the formulated batches of IFS-loaded cubosomes were investigated using a Zeta sizer (Nano ZS, Malvern, UK).The samples (1 mL) were analyzed in triplicate at 25 ± 0.5°C following dilution with deionized water (29 mL) (Noujaim, 2018).

***In vitro* release**

The dialysis bag technique was employed to assess *in vitro* release behaviour of IFS from cubosomes and was compared with plain IFS solution. Briefly, both optimized IFS cubosomes (equivalent to 2 mg IFS) and plain IFS (2 mg) solution were filled in a separate dialysis bag (Molecular weight cut-off 12000). The dialysis bag was then immersed in 50 mL of release medium (phosphate buffer saline; PBS pH 6.8.) controlled at 37±2°C and 150 rpm. The release medium (2 mL) was collected following a determined time interval and the equivalent volume was substituted with fresh PBS pH 6.8. The collected solutions were assessed by UV-visible spectrophotometer at 249 nm. The experiment was repeated three times and the% cumulative IFS release from cubosomes and the plain solution was calculated (Nasr, 2015; Nasri, 2020).

***In vitro* hemolysis**

In vitro hemolysis of optimized IFS-cubosomes was carried out using human blood to investigate its safety and compatibility for intravenous use. The defibrinogeneted blood (3 mL) was diluted using 0.9% sodium chloride solution (10mL) and allowed to centrifuge at 1000rpm for 10 minutes to obtain erythrocyte pellets. The resultant pellet was washed repeatedly (3-4 times) using 0.9% NaCl solution and subsequently diluted with the same solution to obtain 3% erythrocyte dispersion which was set aside at 4°C until further use. The IFS-cubosomes were introduced into flasks holding 1mL of 3% erythrocyte dispersion and

the ultimate volume was attuned to 5mL with 0.9% NaCl solution to achieve a final concentration of 50 **µg/mL** respectively. A similar experiment was carried out with a plain IFS solution to achieve a concentration of 50 µg/mL respectively. 1mL of erythrocyte dispersion with 4mL 0.9% NaCl solution was considered a negative control whereas 1mL dispersion containing 4mL of deionized water was a positive control. All the aforementioned dispersions were incubated for 2h at 37±2°C. Following incubation, the dispersions were centrifuged (5000rpm) for 10 minutes. Resultant pellets were collected, re-dispersed in deionized water, and sonicated for 5 minutes. Next, the system was centrifuged (10000rpm) for 10 minutes and the absorbance of the supernatant was recorded at 420nm with a UV-visible spectrophotometer against deionized water as blank. The % hemolysis was computed *via* the following formula (Sambamoorthy, 2021).

$$\%Hemolysis = \frac{Test\ sample\ absorbance - Negative\ control\ absorbance}{Positive\ control\ absorbance - Negative\ control\ absorbance} \quad (2)$$

***In vitro* cytotoxicity**

The consequence of plain IFS and optimized IFS-cubosomes on the viability of breast cancer-resistant (MDA-MB 231) cells was investigated *via* a3-(4,5-dimethylthiazol-2-yl)-2,5-diphenyl-2H-tetrazolium bromide (MTT) dye reduction assay. Briefly, the cells were introduced to a 96-well plate and incubated overnight at 37°C and 5% CO_2. The cells were treated with the sample at diverse concentrations and plates were kept for another 48 h. Then 100µL of MTT (6 mg/10mL of MTT in PBS) was added to the plates by removing test solutions and the plates were further incubated for 4 h in an analogous environment. Eventually, the supernatant was eliminated and formazan crystals assembled in viable cells were solubilized by dimethyl sulphoxide (DMSO; 100µL). The absorbance of the ensuing solution was recorded at 570 nm employing a microplate. The IC_{50} values were then computed *via* dose-response curves (Kumbhar, 2020).

Apoptosis by (4', 6-diamidino-2-phenylindole) DAPI staining

The cells were seeded in a 24-well flat-bottom microplate containing a coverslip and controlled at 37°C in a CO_2incubator overnight. Next, cells were treated with IFS and IFS cubosomes at corresponding IC_{50} values and incubated for another 24 h. After the incubation, cells were washed with PBS and firmed with paraformaldehyde (4%) for 30 min. Finally, cells were contacted with DAPI (20 µL) for 5 minutes at room temperature in the dark and noticed under a fluorescent microscope (Bhat, 2018).

Cellular uptake study

Cells were introduced in 24 well plate holding coverslips and incubated overnight. Cells were then incubated with cubosomes (Rhodamine G-loaded) and incubated for 5 h, were firmed with paraformaldehyde (4%), and washed twice with PBS. Further, the nucleus cells were stained with DAPI. The cover slip containing the specimen was observed under the fluorescence microscope (Olympus BX41) (Andrgie, 2019).

***In vitro* stability**

The *in vitro* physical stability of cubosomes was assessed based on %EE and % cumulative drug release (%CDR) at different time intervals for three months of storage at refrigerator (2-8°C) and room temperature (25°C).

Statistical analysis

The statistical analysis was carried out *via* GraphPad Prism software version 8 (GraphPad Software, Inc., La Jolla, CA, USA). Data are depicted in terms of mean ± standard deviation independent experiments carried out in triplicate. The findings obtained were assessed through one-way and two-way ANOVA and statistically significant differences in the findings were expressed by considering $P<0.05$.

RESULTS AND DISCUSSION

Preparation of IFS-loaded cubosomes

The IFS-loaded cubosomal dispersions were prepared *via* rupturing a cubic gel phase composed of GMO and water withP-188 (stabilizer) by mechanical stirring. The formed cubosomal dispersions were uniform opaque white mixtures with an absence of aggregate.

Optimization of IFS-loaded cubosomes

Fitting of data to the model

The consequence of independent variables on dependent variables was thoroughly investigated using 3^2 factorial design. Total of 09 runs were generated and evaluated and results are reported in Table 2. All responses fitted to different models i.e. linear, two-factor interaction (2FI), and quadratic models. The best fit model was decided based on a high R^2 value and low predicted residual error sum of squares (PRESS). Best-fitted model for responses Y_1 and Y_2 was two-factor interactions (R^2: 0.9996 and PRESS: 2.35) and quadratic model (R^2: 0.9924 and PRESS: 5.05) respectively. This corroborates that suggested models can significantly predict the >99% variations in responses studied. The significance and efficacy of models were assessed by ANOVA. The Prob (p) value < 0.05 affirms the model term was significant. Model F- value for response variables Y_1 and Y_2 was found to be 4717.73 and 78.47 respectively, which indicates the significance of the model. For response Y_1, X_1, X_2, and X_1X_2 were significant model terms while, for Y_2, two factor terms [X_1 and X_2] and one quadratic term [X_1^2] were significant. For both responses, the predicted R^2 values of 0.9976 (Y_1) and 0.9456 (Y_2) were in agreement with adjusted R^2 of 0.9994 (Y_1) and 0.9798 (Y_2) respectively. Adequate precision values were found to be 202.90(Y_1) and 24.16 (Y_2). In general, a value greater than 4 is desired. Additionally, the multicollinearity of the formulation variables was evaluated based on the variance inflation factor (VIF). A VIF value of 1 reflected the absence of multicollinearity among the independent variables in the model.

The polynomial equation explaining the relationship between independent and dependent variables can be given as follows,

$$Y_1 \text{ (Drug content)} = +70.29 +7.36\, X_1 +10.49\, X_2 +1.45\, X_1 X_2 \quad (1)$$

$$Y_2 \text{ (Zeta potential)} = -42.38 +3.77\, X_1 +1.01 X_2 -0.0214 X_1 X_2 -2.09 X_1^2 -0.2500 X_2^2 \quad (2)$$

Factor coefficients from the polynomial equations were compared and the relative impact of the factors was assessed. In the case of both responses, the positive coefficient of X_1 and X_2 represents their synergistic effect on drug content and zeta potential. This means that drug content and zeta potential increased with an increase in the concentration of X_1 and X_2. The interaction term X_1X_2 showed a positive impact on drug content and a negative impact on zeta potential. Further, the F value of individual variables was compared to determine their impact on response. The F-value of 9308.94 confirmed the prominent effect of X_2 on drug content whereas, the F value of 362.36 indicated the prominent effect of X_1 on zeta potential. The 2-D contour (Figure 2A and 2C), and 3-D response surface plots (Figure 2B and 2D) confirmed the positive effects of independent variables on the response studied. Furthermore, the perturbation plots, where the response is determined by changing a single independent variable solely along its range, are helpful for interpreting the influence of independent factors on the response variables. The perturbation plots have also supported the same results (positive effects of independent variables on the response variables) obtained with 2-D and 3-D response surface plots. The steep slope for factor X_2 (Figure 3A) and curvature for X_1 (Figure 3B) confirmed their prominent effects on drug content and zeta potential respectively. The plots of predicted vs actual values for Y_1 and Y_2 are shown in Figure 3C and 3D. The

ANOVA results for both responses are summarized in Table 3 and model fit summary is presented in Table 4. Amongst the all batches prepared, batch F8 showing %EE of 89.75±4.3% and zeta potential of -40.0±1.6 mV (Figure 4A) was selected as an optimized batch. This optimized batch was further characterized for different parameters.

Table 2. Randomized experimental runs generated using 3^2 factorial design

Std	Run	X_1: GMO conc. (mg)	X_2: Poloxamer conc. (mg)	Y_1: Drug content (%)	Y_2: Zeta potential (mV)
6	1	1	1	77.25	-40.7
7	2	0.25	1.5	71.96	-47.3
3	3	1	0.5	65.96	-41.9
5	4	0.5	1	67.88	-43.4
2	5	0.5	0.5	57.67	-45.5
8	6	0.5	1.5	77.95	-43.2
1	7	0.25	0.5	54.07	-49.2
9	8	1	1.5	89.75	-40.0
4	9	0.25	1	62.76	-48.7

Table 3. ANOVA results for response Y_1 and Y_2

Source	Sum of Squares	Coeff	F-value	p-value
Response Y_1				
Model	985.84	70.29[a]	4717.73	< 0.0001[b]
A-GMO Conc.	337.25	7.36	4841.74	< 0.0001
B-Poloxamer Conc.	648.41	10.49	9308.94	< 0.0001
AB	8.75	1.45	125.61	< 0.0001
Residual	0.3483			
Cor Total	986.19			
Response Y_2				
Model	92.18	-42.38[a]	78.47	0.0022[b]
A-GMO Conc.	85.13	3.77	362.36	0.0003
B-Poloxamer Conc.	6.06	1.01	25.81	0.0147
AB	0.0019	-0.0214	0.0081	0.9339
A^2	6.64	-2.09	28.27	0.0130
B^2	0.1250	-0.2500	0.5321	0.5185
Residual	0.7048			
Cor Total	92.88			

[a]Intercept and [b] significant

Table 4. Model fit summary

Source	Sequential p-value	Lack of Fit p-value	Adjusted R^2	Predicted R^2	
Response Y_1					
Linear	< 0.0001		0.9877	0.9700	
2FI	**< 0.0001**		**0.9994**	**0.9976**	**Suggested**
Quadratic	0.4667		0.9994	0.9975	
Cubic	0.6316		0.9993	0.9782	**Aliased**
Response Y_2					
Linear	0.0005		0.8927	0.8531	
2FI	0.9729		0.8713	0.7422	
Quadratic	**0.0290**		**0.9798**	**0.9456**	**Suggested**
Cubic	0.9098		0.9498	-0.6157	**Aliased**

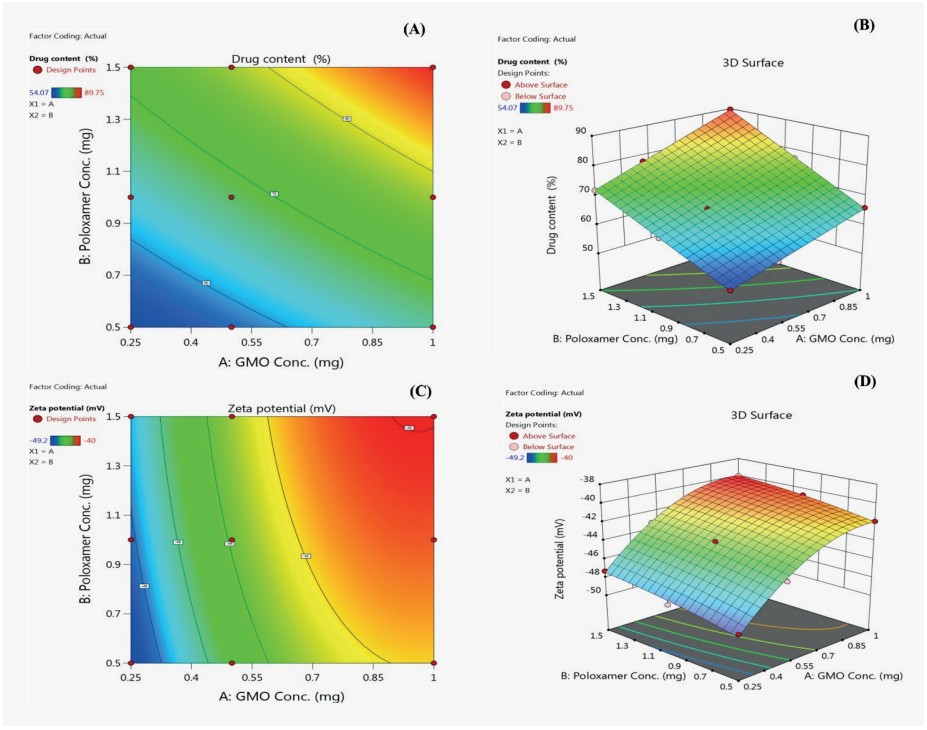

Figure 2. 2-D contour plots (2A and 2C) and 3-D response surface plots (2B and 2D) of independent variables showing effect on drug content and zeta potential

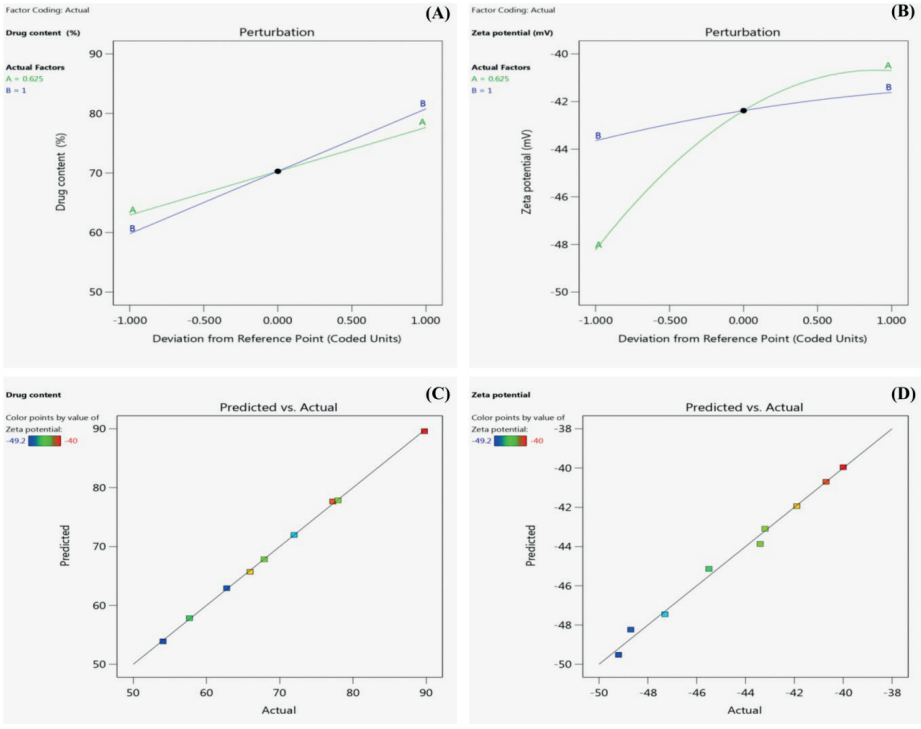

Figure 3. Perturbation plots **(A)** for factor X2 and **(B)** for factor X1, **(C & D)** predicted vs actual plot for Y1 and Y2

Particle size

The mean particle size of the optimized IFS-loaded cubosomes and blank cubosomes were found to be 192±7 nm (polydispersity index (PDI: 0.2±0.04) and 160±5 nm (PDI: 0.5±0.1) respectively (Figure 4B and 4C). This slight increase in the particle size of IFS-cubosomes is attributed to the loading of IFS in the cubosomes. The P-188 at high concentration might have contributed to form smaller and vesicular particles of cubosomes. These vesicular structures might be due to the development of bilayers amid mixed monoolein and poloxamer that cause sterically stabilization of the particles by evading their fusion into the cubic state (Gustafsson, 1996). Thus, the particle size of cubosomal dispersion was observed to be less than 200 nm which is essential to achieve targeting of IFS at the tumor *via* the EPR effect.

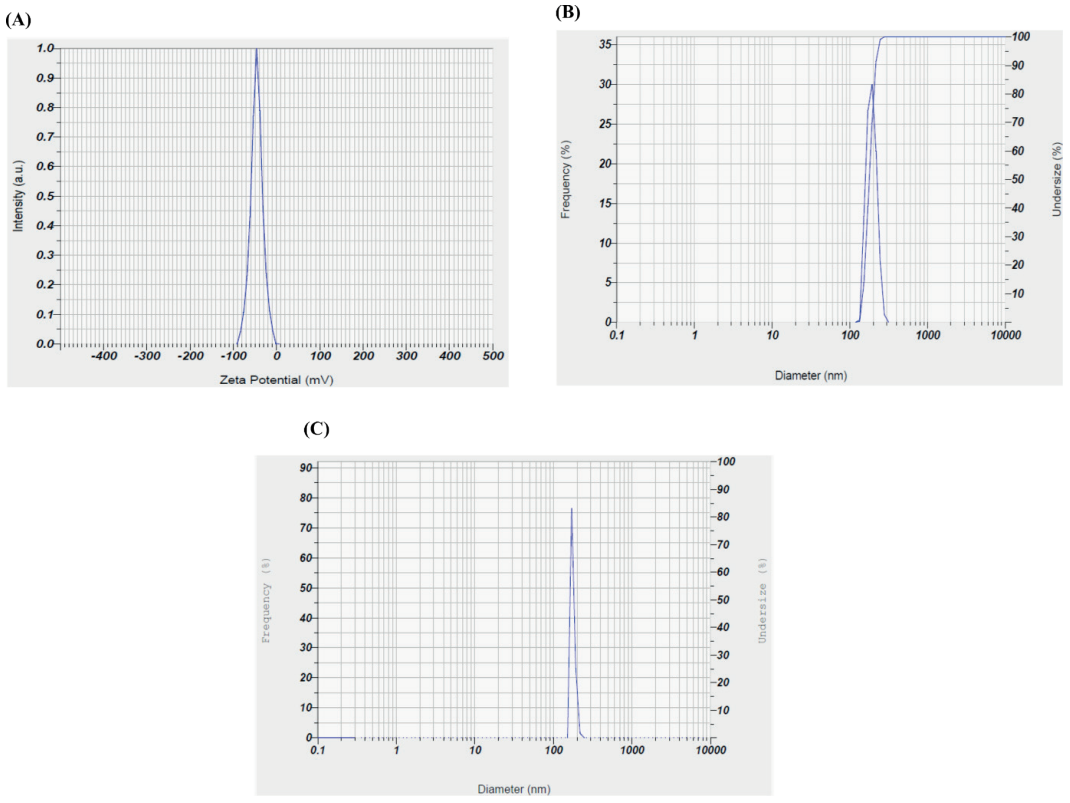

Figure 4. (A) Zeta potential of optimized cubosomes, **(B)** Mean particle size of optimized IFS-cubosomes, and **(C)** Blank cubosomes

***In vitro* drug release study**

The *in vitro* release of IFS from optimized cubosome was investigated *via* dialysis bag technique using PBS pH 6.8 and compared with plain IFS aqueous solution (Figure 5). IFS has displayed rapid and almost complete (99.54±7.5%) release from plain IFS (aqueous) solution within 2 h. In contrast, cubosomes have demonstrated a sustained release of IFS (91.12±7.22%) after 12 h. This remarkably slower release of IFS from the cubosomes could be due to the limited diffusion of IFS molecules entrapped in the aqueous channels of cubosomes where diffusion normally occurs *via* aqueous channels of narrow pore size. Thus, sustained release of IFS from cubosomes may retain the IFS in circulation for a longer time could cause better accumulation of drugs in the tumor *via* the EPR effect and, meet the criteria for an effective drug delivery carrier for cancer treatment (Nasr, 2015).

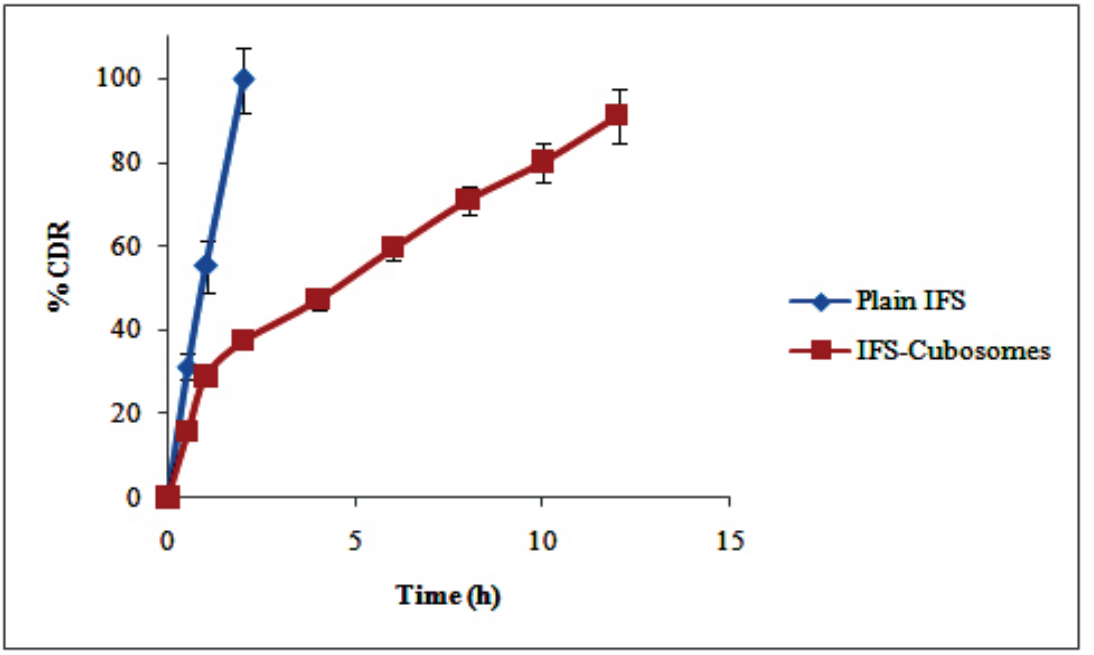

Figure 5. *In vitro* IFS release from plain IFS solution and IFS-cubosomes

***In vitro* hemolysis**

The compatibility of IFS and IFS cubosomal dispersion with the components of blood was assessed by *in vitro* hemolysis study. Herein, no hemoglobin was directly estimated to evade the interference of formulations that may alter the colour of hemoglobin. In the present research, the RBCs which remain intact following treatment with formulations were separated from the buoyant. The separated intact RBCs were lysed with deionized water and estimated for hemoglobin by subtracting its absorbance from the absorbance of positive control.

The plain IFS solution, blank cubosomes, and IFS-cubosomes have displayed % hemolysis of 2.6±0.23, 3.1±0.45, and 3.7±0.79%, respectively after 2 h of incubation. The slight increase in the hemolysis with cubosomes could be due to their interactions with blood components. However, no significant difference was observed in the % hemolysis with all three formulations. Thus, the lower hemolysis with IFS cubosomal dispersion indicates safety and appropriateness for intravenous injection (Sambamoorthy, 2021).

***In vitro* cytotoxicity**

The cytotoxic potential of plain IFS, blank cubosomes, and optimized IFS-cubosomes were investigated against breast cancer-resistant (MDA-MB-231) cells using an MTT dye reduction assay. Both plain IFS solution and IFS-cubosomes demonstrated cytotoxicity with respect to dose. The IFS-cubosomes have displayed substantially higher cytotoxicity (low IC_{50}: 0.64±0.08 µM) than plain IFS solution (IC_{50}: 1.46±0.21 µM) after 48 h of incubation. The blank cubosomes have shown very less cytotoxicity (11-23% inhibition of growth) after 48 h therefore IC_{50} value was not calculated.

The remarkable cytotoxicity of IFS-cubosomes could be due to the endocytosis-mediated cellular uptake in the tumor cell. In addition, the sustained release of IFS from the cubosomes may also be responsible for high cytotoxicity. Furthermore, poloxamer may cause an increase in the sensitivity of IFS toward MDR cells (Singh-Joy, 2008). Thus, obtained cytotoxicity results revealed that IFS was very efficient at a very low dose against cancer following its entrapment into the cubosomes. This reduction in

the dose of IFS can help to reduce the dose-dependent toxicities (neurotoxicity and nephrotoxicity and hemorrhagic cystitis) associated with IFS. Moreover, it can help to reduce MDR in the cancer cells especially breast cancer cell lines (Wang, 2018).

Apoptosis by DAPI staining

The alterations in the apoptotic nuclear morphology in MDA-MB-231 breast cancer cells were noticed after the treatment with IFS and IFS-cubosomes *via* DAPI staining. The normal intact nuclei with weak homogenous blue stains (Figure 6A) were noticed in the cells with no treatment. The IFS and IFS-cubosomes (Figure 6B and 6C) treated cells displayed small nuclei amidst blebbing, bright chromatin condensation, nuclear fragmentation, and generation of apoptotic bodies as shown in the picture. It was noticed that MDA-MB-231 cells treated with IFS-cubosomes demonstrated extreme fragmentation of the cell nuclei when compared to plain IFS. This extreme fragmentation of cell nuclei by IFS-cubosomes might be due to the increased cell accumulation and thereby higher cytotoxicity.

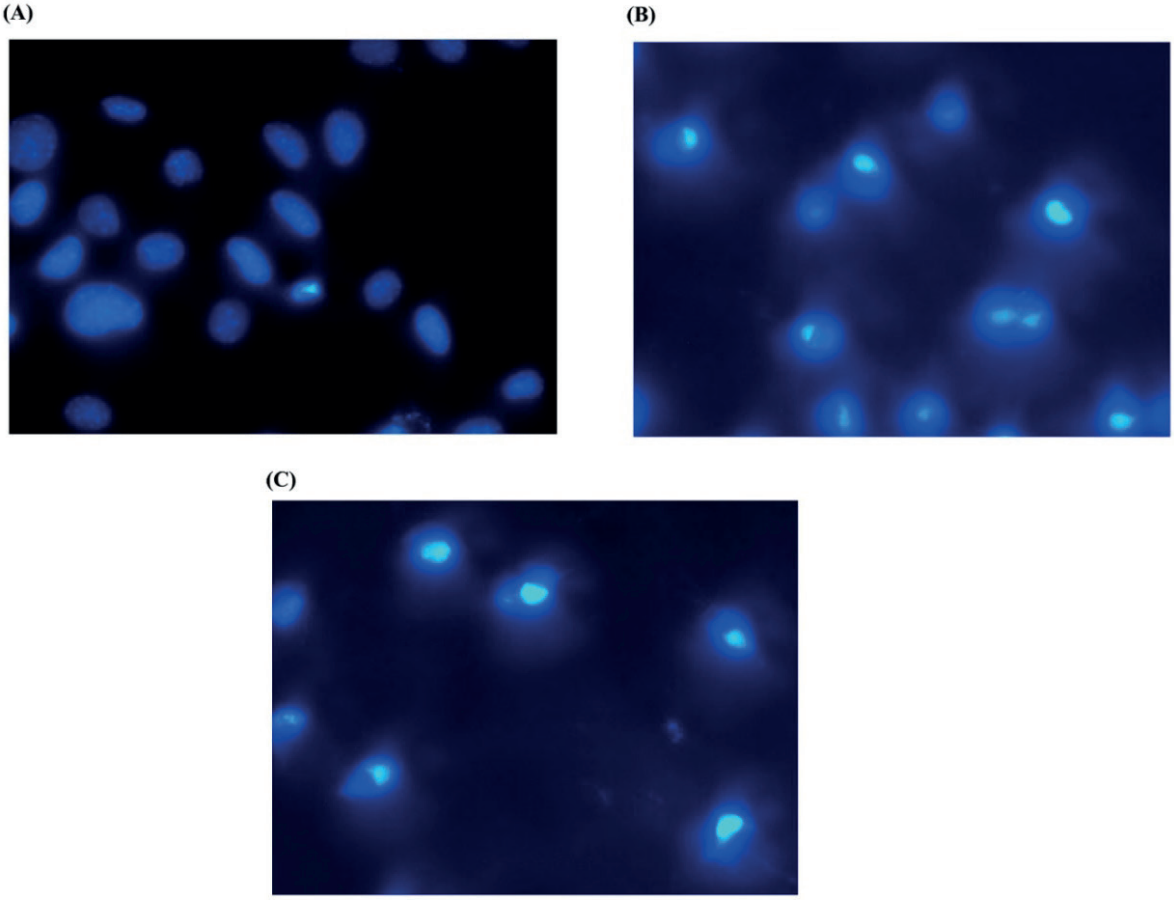

Figure 6. DAPI Apoptosis **(A)** Normal control, **(B)** Plain IFS treated and **(C)** IFS-cubosomes treated

Cellular uptake study

The cellular uptake potential of cubosomes was investigated using MDA-MB-231 cells. The cubosomes containing rhodamine G dye displayed intense red fluorescence indicating significant uptake of the cubosomes by the MDA-MB-231 cells (Figure 7A). Moreover, the nuclei of the cell were noticed to be blue owing to the DAPI stain (Figure 7B). The merged image showed blue stain nuclei of the cell and the presence of

rhodamine G-loaded cubosomes (Figure 7C). These obtained results confirmed the substantial uptake of IFS-cubosomes by the MDA-MB-231 cells. This increased uptake could be attributed to the nanosizing of prepared cubosomes that might have facilitated the physical interaction between the cubosomes and the cell membrane and thereby clustering of cubosomes on the cell surface and generation of cell membrane responses including disruption of permeability and integrity of cell membrane (Behzadi, 2017).

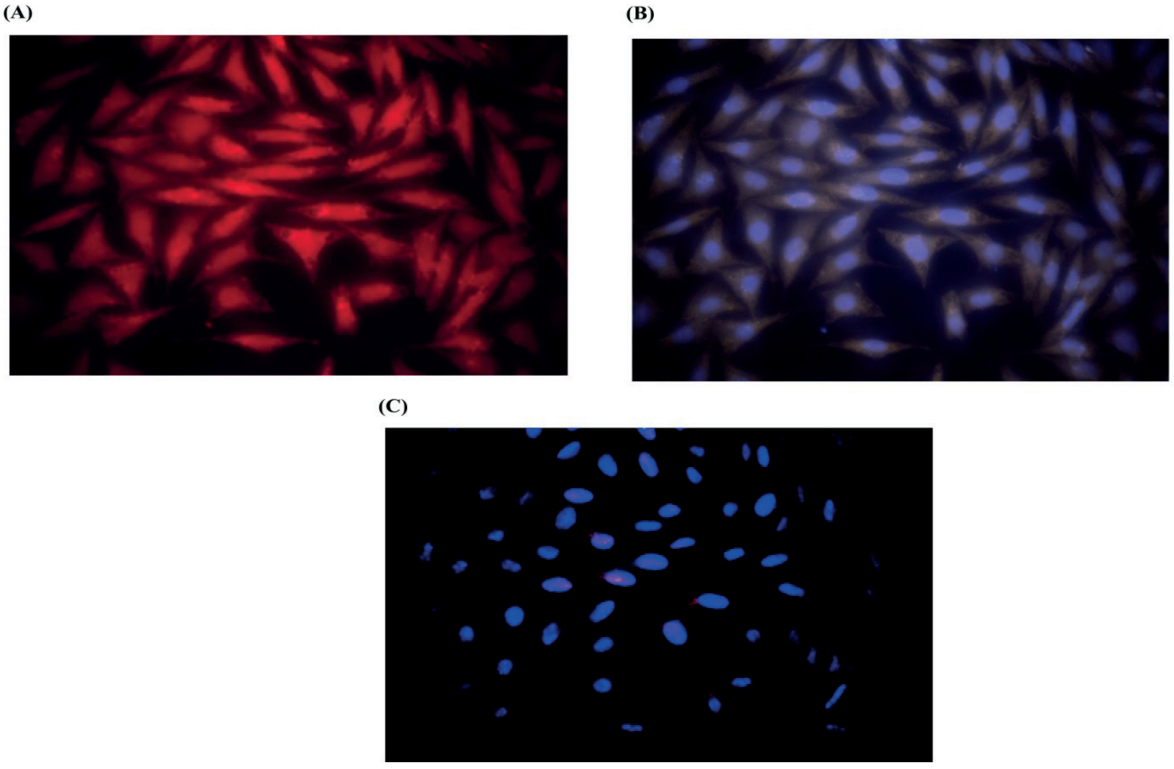

Figure 7. Cellular uptake **(A)** Rhodamine G-loaded cubosomes **(B)** DAPI stain in the nuclei of cell **(C)** Merged image of rhodamine G-loaded cubosomes and DAPI stained cell nuclei

Stability study

The *in vitro* (physical) stability of IFS-cubosomes was assessed based on the % EE and % CDR after storage at room temperature (25-30°C) and refrigerator (2-8°C) for three months (Table 5). No significant difference in the % EE and % CDR was observed following storage of cubosomes at refrigeration conditions indicating better stability of the IFS-cubosomes at refrigeration. In addition, no sign of phase separation was noticed. In contrast, during the storage at room temperature, % EE was reduced from 89 to 77% and % CDR from 91 to 70%. This could be attributed to the leakage of IFS from the cubosomes over time. This corroborates the poor storage stability of IFS-cubosomes at room temperature. Therefore, IFS-cubosomes could be stored safely in refrigeration conditions (Andrgie, 2019).

Table 5. Stability study optimized IFS-cubosomes at refrigerator condition and room temperature

Formulation	Storage condition	% EE				% CDR			
		Fresh	1 Month	2 Months	3 Months	Fresh	1 Month	2 Months	3 Months
IFS-cubosomes	Refrigerator temperature (2-8°C)	89.75±4.3	89.02±4.1	88.75±5.7	86.56±4.8	91.12±7.2	90.47±7.8	88.27±6.9	85.97±8.2
	Room temperature (25-30°C)	89.75±4.3	84.11±5.6	81.58±4.3	77.53±5.1	91.12±7.2	86.04±6.3	79.86±7.7	70.10±6.4

CONCLUSIONS

In the present research, the hydrophilic IFS-loaded cubosomes were successfully fabricated and optimized *via* factorial design. The IFS entrapment and zeta potential were found to be significantly dependent on the concentration of GMO and P-188. The optimized IFS-cubosomes displayed a size of less than 200 nm indicating their targeting potential at the site of the tumor *via* the EPR effect. Moreover, the release of IFS from IFS-cubosomes was noticed to be sustained, suggesting improved circulation and accumulation of IFS at the tumor. The IFS-cubosomes displayed lower hemolytic behavior revealing their biocompatibility and safety for intravenous injection. Furthermore, the remarkable cytotoxic potential of IFS-cubosomes at low dosage corroborates its enhanced anticancer effect without dose-dependent toxicities. In summary, cubosomes could serve as a carrier system to improve the anticancer potential of IFS at low doses and reduce toxicities. Nevertheless, *in vivo* testing's involving animal models are recommended to further ensure the formulation efficacy.

ACKNOWLEDGMENTS

We are greatly thankful to our Head of Institute and Institute Management for supporting this research project.

CONFLICT OF INTEREST

The authors declare that there is no conflict of interest.

AUTHOR CONTRIBUTION RATE STATEMENT

PK, VMK, VSK & PM: Performed all above research activities. PK & JD: Designed, monitored and coordinated the research activities. JD: Participated in statistical analysis and data interpretation. PK, SN, AM, VK, DB & RM: Involved in the preparation and drafting of the manuscript.

REFERENCES

Addeo, R., Faiola, V., Guarrasi, R., Montella, L., Vincenzi, B., Capasso, E., Cennamo, G., Rotundo, M. S., Tagliaferri, P., Caraglia, M., Del Prete, S. (2008). Liposomal pegylated doxorubicin plus vinorelbine combination as first-line chemotherapy for metastatic breast cancer in elderly women > or =65 years of age. *Cancer chemotherapy and pharmacology*, *62*(2), 285–292. https://doi.org/10.1007/s00280-007-0605-6.

Alavi, M., Webster, T. J. (2020). Nano liposomal and cubosomal formulations with platinum-based anticancer agents: therapeutic advances and challenges. *Nanomedicine (London, England)*, *15*(24), 2399–2410. https://doi.org/10.2217/nnm-2020-0199.

Almotwaa, Sahar. (2021). Coupling Ifosfamide to nanoemulsion-based clove oil enhances its toxicity on malignant breast cancer and cervical cancer cells. *Pharmacia*, 68. 779-787. http://dx.doi.org/10.3897/pharmacia.68.e68291

Andrgie, A. T., Birhan, Y. S., Mekonnen, T. W., Hanurry, E. Y., Darge, H. F., Lee, R. H., Chou, H. Y., Tsai, H. C. (2019). Redox-Responsive Heparin-Chlorambucil Conjugate Polymeric Prodrug for Improved Anti-Tumor Activity. *Polymers*, *12*(1), 43. https://doi.org/10.3390/polym12010043.

Behzadi, S., Serpooshan, V., Tao, W., Hamaly, M. A., Alkawareek, M. Y., Dreaden, E. C., Brown, D., Alkilany, A. M., Farokhzad, O. C., Mahmoudi, M. (2017). Cellular uptake of nanoparticles: journey inside the cell. *Chemical Society Reviews*, *46*(14), 4218–4244. https://doi.org/10.1039/c6cs00636a.

Bhat, S. S., Revankar, V. K., Kumbar, V., Bhat, K., Kawade, V. A. (2018). Synthesis, crystal structure and biological properties of a cis-dichloridobis(diimine)copper(II) complex. *Acta Crystallographica. Section C, Structural Chemistry*, *74*(Pt 2), 146–151. https://doi.org/10.1107/S2053229617018551.

Carr, C., Ng, J., Wigmore, T. (2008).The side effects of chemotherapeutic agents. *Current Anaesthesia Critical Care*, 19(2), 70–79.

Elakkad, Y. E., Mohamed, S., Abuelezz, N. Z. (2021). Potentiating the cytotoxic activity of a novel simvastatin-loaded cubosome against breast cancer cells: Insights on dual cell death via ferroptosis and apoptosis. *Breast Cancer (Dove Medical Press)*, *13*, 675–689. https://doi.org/10.2147/BCTT.S336712.

Escalante, J., McQuade, R. M., Stojanovska, V., Nurgali, K. (2017). Impact of chemotherapy on gastrointestinal functions and the enteric nervous system. *Maturitas*, *105*, 23–29. https://doi.org/10.1016/j.maturitas.2017.04.021

García-Pinel, B., Porras-Alcalá, C., Ortega-Rodríguez, A., Sarabia, F., Prados, J., Melguizo, C., López-Romero, J. M. (2019). Lipid-based nanoparticles: Application and recent advances in cancer treatment. *Nanomaterials (Basel, Switzerland)*, *9*(4), 638. https://doi.org/10.3390/nano9040638.

Gustafsson, J., Ljusberg-Wahren, H., Almgren, M., Larsson, K. (1996). Cubic lipid-water phase dispersed into submicron particles. *Langmuir*, 12, 4611–3.https://doi.org/10.1021/LA960318Y

Nasri, S., Ebrahimi-Hosseinzadeh, B., Rahaie, M., Sahraeian, R. (2020). Thymoquinone-loaded ethosome with breast cancer potential: Optimization, in vitro and biological assessment. *Journal Nanostructure Chemistry*, *10*, 19–31.

Kumbhar, P.S., Sakate, A.M., Patil, O.B., Manjappa, A. S., Disouza, J. I. (2020). Podophyllotoxin-polyacrylic acid conjugate micelles: improved anticancer efficacy against multidrug-resistant breast cancer. *Journal of Egyptian National Cancer Institute,* 32, 42, 1-8. https://doi.org/10.1186/s43046-020-00053-1.

Lakshmi, N. M., Yalavarthi, P. R., Vadlamudi, H. C., Thanniru, J., Yaga, G., K, H. (2014). Cubosomes as targeted drug delivery systems - a biopharmaceutical approach. *Current Drug Discovery Technologies*, *11*(3), 181–188. https://doi.org/10.2174/1570163811666140505125923.

McQuade, R. M., Stojanovska, V., Donald, E., Abalo, R., Bornstein, J. C., Nurgali, K. (2016). Gastrointestinal dysfunction and enteric neurotoxicity following treatment with anticancer chemotherapeutic agent 5-fluorouracil. *Neurogastroenterology and Motility: The Official Journal of the European Gastrointestinal Motility Society*, *28*(12), 1861–1875. https://doi.org/10.1111/nmo.12890

Nasr, M., Ghorab, M., Abdelazem, A. (2015). In vitro and in vivo evaluation of cubosomes containing 5-fluorouracil for liver targeting. *Acta Pharmaceutica B*, 5(1), 79–88.http://dx.doi.org/10.22159/ijap.2019v11i2.30582.

Noujaim, J., Constantinidou, A., Messiou, C., Thway, K., Miah, A., Benson, C., Judson, I.,Jones, R. L. (2018). Successful ifosfamide rechallenge in soft-tissue sarcoma. *American Journal of Clinical Oncology*, *41*(2), 147–151. https://doi.org/10.1097/COC.0000000000000243.

Rick D, Kellerman MD. (2021). In conn's current therapy. Elsevier, 1165-1168.

Saito, Y., Kumamoto, T., Makino, Y., Tamai, I., Ogawa, C., Terakado, H. (2016). A retrospective study of treatment and prophylaxis of ifosfamide-induced hemorrhagic cystitis in pediatric and adolescent and young adult (AYA) patients with solid tumors. *Japanese Journal of Clinical Oncology*, 46 (9), 856–861. https://doi.org/10.1093/jjco/hyw093.

Sambamoorthy, U., Manjappa, A. S., Eswara, B., Sanapala, A. K., Nagadeepthi, N. (2021). Vitamin E Oil Incorporated Liposomal Melphalan and Simvastatin: approach to obtain improved physicochemical characteristics of hydrolysable melphalan and anticancer activity in combination with simvastatin against multiple myeloma. *AAPS PharmSciTech*, *23*(1), 23. https://doi.org/10.1208/s12249-021-02177-6.

Siddiqui, J. F., Rizwana, I. (2019). UV-visible spectrophotometric method development and validation for the estimation of ifosfamide in bulk drug and pharmaceutical dosage form. *International Journal of Pharmaceutical Sciences Review and Research*, 59(1), 102-105.

Singh-Joy, S. D., McLain, V. C. (2008). Safety assessment of poloxamers 101, 105, 108, 122, 123, 124, 181, 182, 183, 184, 185, 188, 212, 215, 217, 231, 234, 235, 237, 238, 282, 284, 288, 331, 333, 334, 335, 338, 401, 402, 403, and 407, poloxamer 105 benzoate, and poloxamer 182 dibenzoate as used in cosmetics. *International Journal of Toxicology*, *27 Suppl 2*, 93–128. https://doi.org/10.1080/10915810802244595.

Suwankhong, D., Liamputtong, P. (2018). Physical and Emotional Experiences of Chemotherapy: A qualitative study among women with breast cancer in Southern Thailand. *Asian Pacific Journal of Cancer Prevention: APJCP*, *19*(2), 521–528. https://doi.org/10.22034/APJCP.2018.19.2.521

Wang, S. Q., Zhang, Q., Sun, C., Liu, G. Y. (2018). Ifosfamide-loaded lipid-core-nanocapsules to increase the anticancer efficacy in MG63 osteosarcoma cells. *Saudi Journal of Biological Sciences*, *25*(6), 1140–1145. https://doi.org/10.1016/j.sjbs.2016.12.001.

Zhang, J., Ng, K. Y., & Ho, P. C. (2010). Interaction of oxazaphosphorines with multidrug resistance-associated protein 4 (MRP4). *AAPS Journal*, *12*(3), 300–308. https://doi.org/10.1208/s12248-010-9189.

FABAD J. Pharm. Sci., 48, 1, 53-60, 2023
Doi: 10.55262/fabadeczacilik.1099539
RESEARCH ARTICLE

Assessment of Anxiety and Burden on Caregivers for Haemodialysis Patients in Southern Punjab, Pakistan

Hina RAZA[*], Memona NASIR[**], Zarmina RASHID[***], Rahat SHAMIM[****], Bushra ALAM[*****], Amjad KHAN[*****] , Shabnam NAZIR[******°]

Assessment of Anxiety and Burden on Caregivers for Haemodialysis Patients in Southern Punjab, Pakistan

SUMMARY

The aim of this work was to assess anxiety and depression experienced by unpaid caregivers of chronic hemodialysis patients suffering from end-stage renal failure (ESRF). The evaluation of factors influencing anxiety and depression and caregiving burden was performed. In the present study, non-paid primary caregivers (218 study participants) of patients with ESRF receiving hemodialysis, who were providing care (minimum 6 months and up to 5 years) were interviewed by using the Aga Khan University Anxiety and Depression Scale (AKUADS) and the carer's burden of peritoneal dialysis patients (CSCDP) questionnaire. According to the scoring of AKUADS, 90.4% of caregivers were found to be experiencing significant anxiety and depression. From the assessment of demographic factors collected using the AKUAD scale, it was found that the female was more in number (44%), wedded (72.01%), with a mean life span of 38.5 ± 2 (standard error) years, and have monthly income below average. The main relationships of caregivers with patients were life partners (38%) and parents (18.2%). The highest depression levels were found in mothers as attendants (67%), caregivers of age less than 30 years (22 %), and caregivers of elderly patients (87%). The outcome of this study has revealed a need to plan policies to support unpaid caregivers as well as patients.

Key Words: *Caregiver, anxiety, depression, hemodialysis, objective burden, subjective burden*

Pakistan, Güney Pencap'ta Hemodiyaliz Hastalarının Bakıcılarındaki Kaygı ve Yükün Değerlendirilmesi

ÖZ

Bu çalışmada, son dönem böbrek yetmezliğinden (SDBY) muzdarip kronik hemodiyaliz hastalarının ücretsiz bakıcılarının yaşadığı anksiyete ve depresyonu değerlendirmek amaçlanmıştır. Anksiyete, depresyon ve bakım verme yükünü etkileyen faktörlerin değerlendirilmesi yapıldı. Bu çalışmada, hemodiyaliz alan SDBY'li hastalara bakım veren (en az 6 ay ve 5 yıla kadar) ücretsiz birincil bakıcılarıyla (218 çalışma katılımcısı) Agha Khan Üniversitesi Anksiyete ve Depresyon Ölçeği (AKÜADÖ) ve periton diyalizi hastalarının bakıcılarının yükü (PDHBY) anketi kullanılarak görüşüldü. AKÜADÖ puanlamasına göre, bakım verenlerin %90.4'ünün önemli düzeyde anksiyete ve depresyon yaşadığı belirlendi. AKUAD ölçeği kullanılarak toplanan demografik faktörlerden, kadın cinsiyetin sayıca daha fazla olduğu (%44), %72.01'inin evli olduğu, ortalama ömrü 38.5 ± 2 (standart hata) yıl olduğu ve aylık gelirinin ortalamanın altında olduğu belirlendi. Bakım verenlerin hastalarla temel ilişkileri hayat arkadaşları (%38) ve ebeveynleri (%18.2) ile olmuştur. En yüksek depresyon düzeyi refakatçi annelerde (%67), 30 yaşından küçük bakım verenlerde (%22) ve yaşlı hasta bakıcılarında (%87) bulunmuştur. Bu çalışmanın sonucu, hastaların yanı sıra ücretsiz bakıcıları desteklemek için politikaların planlanması ihtiyacını ortaya çıkarmıştır.

Anahtar Kelimeler: *Bakıcı, anksiyete, depresyon, hemodiyaliz, nesnel yük, öznel yük*

Received: 18.05.2022
Revised: 25.10.2022
Accepted: 25.10.2022

[*] ORCID: 0000-0002-4733-4089, Bahauddin Zakariya University Faculty of Pharmacy Multan Pakistan
[**] ORCID: 0000-0003-3069-4990, Bahauddin Zakariya University Faculty of Pharmacy Multan Pakistan
[***] ORCID: 0000-0002-6537-6864, The Women University Department of Pharmacy Multan Pakistan
[****] ORCID: 0000-0003-3897-9421, University of Punjab Punjab University College of Pharmacy,Lahore Pakistan
[*****] ORCID: 0000-0002-1274-9233, Kohat University of Science and Technology Department of Pharmacy, Kohat Pakistan
[*****] ORCID: 0000-0002-4121-4400, Kohat University of Science and Technology Department of Pharmacy, Kohat Pakistan
[******] ORCID: 0000-0001-6543-0931, Kohat University of Science and Technology Department of Pharmacy, Kohat Pakistan

[°] Corresponding Author; Shabnam NAZIR
Email: Shabnammunirmalik@yahoo.com

INTRODUCTION

Prevalence of anxiety and depression among patients undergoing hemodialysis (HD) and their caregivers (CGs) are common psychiatric disorders (Bussotti and Sommaruga, 2018). Several factors contribute to triggering anxiety and depression in HD patients such as co-morbidities, frequent hospitalizations, chronic pain, sleep disturbances, chronic inflammation, increased fatigue, decreased sexual functioning, restrictions in diet and fluids, and dependency on health professionals are common psychiatric disorders their CGs (Zalai, et al., 2012).

A disease not only affects the patient but also affects the life of CGs in various aspects such as their social activities, professional activities, etc. (Zalai, et al., 2012). Dialysis therapy imposes several restrictions on caregivers' life such as decreased physical function, fatigue, social isolation, difficulties in relationships, and feelings of disappointment (Zalai, et al., 2012). Therefore, the prevalence of anxiety and depression among caregivers is reported by various previous studies (Heidari, et al. 2012, Loh, et al. 2017). Caregivers have to face versatile tasks and challenges while providing care to HD patients like patient transport-related issues and getting periodic appointments from doctors following the Medication regimen, coping with emergencies, dressing, symptomatic relief, and cooking customized food for patients as per recommendations.

To the best of our knowledge, research exploring the effects of anxiety and depression between patients and caregivers in Pakistan is limited. High prevalence of anxiety and depression among CGs of psychiatric patients showed 40.6%, 48 % of stroke patients and cancer patients reported 78% anxiety and depression in Pakistan (Khalid and Kausar 2008, Alvi, et al. 2014, Majeed, et al. 2018). To date, no data regarding any medical strategies adopted to reduce anxiety and depression in CGs were found in Pakistan. According to a study published, caregivers of patients use religious activity to manage stress (Kasi, et al. 2012). Only a few studies were found to assess the burden on HD CGs but no data was available to show both the anxiety and depression burden on HD CGs (Saeed, et al. 2012, Shah, et al. 2017). Thus, the present study aimed to explore the effect of anxiety and depression on CGs of HD patients.

However, the need for awareness and action to address this issue is necessary, requiring a further understanding of mental disorders to facilitate and aid in the development of policies to provide evidence-based support and guidance to unpaid caregivers.

METHODOLOGY

An analytical and descriptive cross-sectional research study was carried out from January 2020 to June 2020 in the dialysis unit of the district headquarters Hospital, in Muzaffargarh, Pakistan. Written legal consent was granted from the ethical committee (no#134P.Practice 2019 dated 26-11-19). All data was gathered through direct dialogues using the local language from the caregivers by one of the authors.

Inclusion Criteria:

Caregivers were enrolled in the study on the following basis:

1. Unpaid caregivers of age from 18 to 60 years
2. Caregivers of both genders were included.
3. Caregivers of patients on dialysis for the last 6 months
4. Caregivers of patients belonging to rural and urban areas were considered for the study.

Verbal consent was taken from caregivers individually Participants were provided with a verbal description of the study purpose and procedure.

Exclusion Criteria

CGs with any previous history of Psychiatry issues, suffering from any chronic disease, Reluctant to answer the questions, or unable to understand the sense of questions, were excluded from the study.

During the present study it was found that most CGs over 60 years were suffering from various chronic diseases such as cardiac diseases, hypertension, and diabetes so to avoid the impact of any anxiety and depression due to their diseases were excluded from the study.

Control Variables

Factors like gender specification of caregiver, life span, community and financial status, kinship with the patient, and duration of care.

Screening Tools

1. **AKUADS:** The Aga Khan University Anxiety and Depression Scale (AKUADS) is used in the present study to assess the prevalence of anxiety and depression among CGs of dialysis patients (Ali, et al. 1998). This scale consists of twenty-five contents which are further subdivided into thirteen contents representing and devoted towards mental and twelve contents representing physical health. These contents evaluate both sides to analyze anxiety and depression. With a cutoff score of 19 points, AKUADS has a specificity of 81%, a sensitivity of 74 %, and a positive predictive value of 63%.
2. **CSCDP:** To investigate the hardships which influence the life of the caregiver, the overload questionnaire for caregivers of patients on peritoneal dialysis (CSCDP) has been used which is developed by J. Teixido et al., particularly for HD patients CGs (Teixidó-Planas, et al. 2006). This screening tool comprises 3 dimensions: the patient's extent of dependence, the carer's subjective overload, and the carer's objective degree of overload. ***Objective*** overload indicates the patient's care requirements affiliated with noticeable caregiving activities. The presence of objective burden shows that the formal back inappropriately alternates with the informal back (Bayen, et al. 2015). ***Subjective*** overload indicates the emotional satisfaction related to the completion of caregiving tasks. The patient's degree of dependency, subjective burden, and objective burden were assessed according to Table 1.

Table 1. CSDP scoring scale to evaluate the degree of dependency, subjective and objective burden

Degree of overload	Patient's degree of dependency	Subjective overload	Objective overload
Slight or none	1-9	1-5	1-7
Mild to moderate	10-17	6-11	8-15
Moderate to severe	18 or more	12 or more	16 or more

Statistical Analysis

Statistical analysis was carried out by using Statistical Package for Social Sciences (SPSS, version 25). Descriptive statistics like mean, standard deviation, and frequencies were calculated for the analysis of collected data. The level of significance was $p < 0.05$.

RESULTS

In the present study, CGs' mean age was 38 years, and 50.5% & 49.5 % were men and women respectively. The most common relationship of CGs to the patient was spouse (36%) followed by daughters (12%). The highest frequency of CGs was between the age of 31-40 years (35.8%) followed by 20-30 years (33.3%), with 41-50 years (17.4%) and 51-60 years (13.3%) being the least. 57.3% of CGs provided full-time care to the patients as patients were fully dependent on them and no other CG was around.

By using **AKUADS**, anxiety and depression were classified into the categories of none, mild, moderate, and severe. To determine anxiety and depression according to the AKUADS scale cut-off score was 20. According to the responses of CGs, it was found that 9.6% had less than 20 scores and 90.4% scored 20 and above. Based on this it can be concluded among 218 CGs 90.4% suffered from anxiety and depression.

The highest levels of depression were found in CGs of age 51-60 years. Based on kinship, severe depression was seen in mothers (67%) and spouses 56.41% as compared to other relations. CGs of patients of age group 61-65 years showed a greater prevalence of anxiety and depression as compared to caregivers of patients of young age. Caregiving time is a prominent predictor of anxiety and depression with the full-time caregivers showing the highest prevalence. The *p*-value was less than 0.05 so it was a statistically significant difference (Table 3). Among 157 married CGs, 31% showed severe depression as compared to unmarried CGs (18%). According to the findings of the current research work, low socioeconomic status is one of the most contributing factors to producing high rates of anxiety and depression in CGs. CGs having a monthly income of $156 >$380 experienced higher levels of moderate to severe anxiety and depression in comparison to those earning greater than $500.

Table 2. Assessment of Anxiety and depression by *AKUADS on basis of CG's demographic characteristics*

Demographic factors	n	Prevalence of anxiety and depression				
		None	**Mild**	**Moderate**	**Severe**	***P*-value**
Kinship						
spouse	78	0	3.80%	39.74%	56.41%	>0.05
mother	18	0	0	33.34%	66.67%	>0.05
father	10	0	0	57.14%	42.85%	>0.05
daughter	27	3.70%	11.11%	48.14%	37.03%	>0.05
son	10	20%	30%	30%	20%	>0.05
other	75	20%	16%	24%	40%	>0.05
Caregiver's age						
21-30 yrs	73	4.10%	47.90%	26%	21.90%	< 0.05
31-40 yrs	78	3.84%	52.56%	30.76%	12.82%	> 0.05
41-50 yrs	38	21.05%	60.52%	15.70%	2.63%	> 0.05
51-60 yrs	29	24.14%	34.48%	17.24%	24.14%	> 0.05
Monthly income						
<$379	106	1.88%	31.13%	43.39%	23.58%	> 0.05
$380 ≥ $500	74	9.45%	35.14%	25.60%	29.72%	< 0.05
> $500	38	31.57%	26.31%	23.68%	18.42%	> 0.05
Patient age						
20-30 yrs	37	18.90%	45.90%	40.50%	0.00%	> 0.05
31-40 yrs	50	22.00%	44.00%	34.00%	0.00%	> 0.05
41-50 yrs	71	4.22%	49.20%	22.50%	23.90%	> 0.05
51-60 yrs	45	0.00%	31.10%	40.00%	28.80%	< 0.05
61-65 yrs	15	0.00%	0.00%	13.30%	86.00%	< 0.05
Marital status						
Married	157	2.90%	31.20%	35.00%	31.00%	< 0.05
unmarried	61	29.50%	26.20%	26.00%	18.00%	> 0.05
Caregiving time						
Full time (More than 8 hrs	125	4.90%	9.60%	53%	32%	< 0.05
Part-time (3-5 hrs.)	93	16.10%	24.70%	25.80%	33.90%	> 0.05

*$P < 0.05$ implies significance

Table 3. Level of significance of the impact of various variables on the level of depression

Caregiving time	**Part-time CGs n=93**	**Full-time CGs n=125**	***P*-value**
Below moderate and mild depression	73%	19%	$P < 0.05$*
Moderate and above depression	27%	81%	$P < 0.05$*
Patient's age	**CGs of younger age patients (20-50 years) n=158**	**Caregivers of elderly patients n=60**	***P-value***
Below moderate and mild depression	83%	13%	$P < 0.05$*
Moderate and above depression	28%	87%	$P < 0.05$*
Caregiver age	**21-30yrs**	**31-50yrs**	***P-value***
Below moderate and mild depression	21.9%	12.8%	$P < 0.05$*
Above moderate and mild depression	40.50%	56%	P < 0.05*

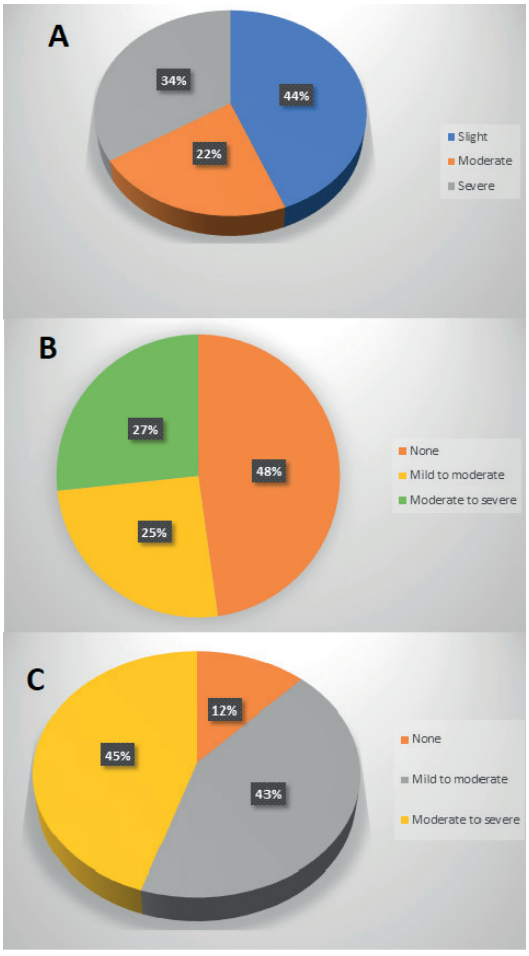

Figure 1. A, B & C represents the prevalence of anxiety and depression due to objective overload, subjective overload & physical dependency of the patient on CGs according to the CSCDP questionnaire respectively

CSCDP: Assessment of burden on CGs by application of the CSDP scale revealed that 80.9 % of them had severe anxiety due to dependence burden. 35.8% of patients showed severe dependency while 36.7% of patients had moderate dependence on their CGs. The dependency of patients on their CGs directly correlates with the health of the patient. In this study, 35.8% and 50% of CGs reported moderate and severe anxiety due to subjective overload, respectively. Mild objective burden was seen in 20.2% (n = 44), moderate objective burden was seen in 35.8% (n = 78) and severe objective burden was seen in 44% (n = 96) CGs. *CSCDP* interview results on different questions are given in Table 4.

In the present study, moderate anxiety, and depression in CGs due to dependence burden was 45%, subjective burden 24%, and objective burden 34%, while severe anxiety and depression in CGs due to dependence burden, subjective burden, and the objective burden was 43%, 24% & 22% respectively. Analysis of anxiety and depression on the base of different burdens is shown in Figures 1A, B & C.

DISCUSSION

A cross-sectional analysis of caregivers of HD patients was conducted and it was determined that a high degree of burden was experienced by CGs causing mental disorders such as clinical anxiety and depression. It must be acknowledged and discussed to

alleviate the undue burden and subjective burden on informal caregivers of dialysis patients especially in under progress countries like Pakistan. More studies are needed to develop policies that will support both the patients and their CGs. Caregiving can create enormous burdens on caregivers, causing a decline in their somatic and mental health.

The results of this study highlight the hardships of caregivers for patients with end-stage renal failure on hemodialysis treatment. Both the ailment and its cure have severe effects on the patient and their CGs. Providing long-term care for this chronic disease on daily basis badly influences the caregivers physical, and mental health due to bad standards of living and a reduction in earnings and savings.

In this study, more than 90% of caregivers had clinically significant anxiety and depression. The estimated burden of anxiety and depression is not indifferent from previous work, with rates varying from 27% to 66% (Jafar 2006, Alvi, et al. 2014).

The results of the present study unveil the various aspects of CGs and how their life had changed during these care-providing activities. It was found that CGS was obsessed and oversensitive to their caregiving activities resulting in their bad quality of health and ignorance of their self-care resulting in their mental health issues. Previous studies conducted to assess the burden on CGs also support this fact (Belasco, et al. 2006, Danial, et al. 2016).

The results of the percent study showed more time CGs spend with their patient, increased the degree of burden on CGs. These findings were also reported by Evans *et al.,* and Morton *et al.*(Evans, et al. 1985, Morton, et al. 2010).

Our study enlightens that CGs of bedridden patients and old age were suffering more depression as compared to patients who were not fully dependent on their CGs for common household activities.

This study revealed that the financial condition and marital status of CGs played a vital role in the development of anxiety and depression as lack of finances increased their stress level resulting in a lack of resources to facilitate that patient and CGs.

Further, patients under expectations from their care providers overwhelmed them, for being fully responsible for patient health and all tasks. These results are also consistent with the findings of the previous study (Ando, et al. 2015). The high prevalence of anxiety and depression among CGs in developing countries could be explained on basis of various contributing reasons such as underprivileged health facilities compared to other developed countries, lack of financial resources, and lack of training for CGs. Caregiving can create enormous burdens on caregivers, causing a decline in their somatic and mental health. Many interventions need to be considered to ease this overload like betterment in patient's condition and standards of living, caregivers' appreciation at community levels, coping plans, gratitude and appreciation of mutual relationship issues, and psychosocial backup.

CONCLUSION

It was determined that the high degree of anxiety and depression experienced by the CGs affected their physical and psychological health. There is an immense need to recognize and address this issue. Various strategies are needed to reduce this burden to enhance CGs' quality of life.

Limitations

The present study was carried out in one of the hospitals of southern Punjab. If multiple dialysis units were involved in the study, it would have been more interesting, and the results could have been more reliable as well as generalizable. The time-bound nature of the study prevented detailed exploration.

Table 4. Response of CGs according to the CSDSP questionnaire

Questions asked from CGs	CGs response			
	Never %	Sometimes %	Mostly %	Always %
1. Does the patient go out frequently?	29	44	19	8
2. Does the patient do any housekeeping tasks?	69.7	17.4	4.1	4.6
3. Does the patient need help with personal cleanliness?	61.9	18.3	11.9	3.2
4. Does the patient need help take his/her food?	52.3	41.3	2.8	3.7
5. Can the patient be left alone for 2-3 hrs. per day?	28.5	31.8	17.5	22.2
6. Can the patient be left alone all night long?	34.4	33	18.8	13.8
7. Does the patient seek help to solve problems associated with dialysis?				
8. CGs must give up all personal hobbies due to the patient's burden	0.9	13.8	75.2	10.1
9. CGs having sleeping troubles	10.5	15.6	32.6	41.3
10. CGs are tired day by day due to the patient burden	11.5	38.1	25.2	24.9
11. CGs feel depressed when thinking about peritoneal dialysis daily	2.8	27.9	31.2	38.1
12. CGs feel that life is not worth living	3.6	52.8	38.1	5.5
13. Do CGs react negatively to the stress and pressure of providing care to the patient?	27.1	68.0	3.2	1.7
14. CGs feel overwhelmed because they have the responsibility of the patient's dialysis appointments	5.0	74.0	17.9	3.1
15. I do not feel like going out or having fun	46	34	11	9
16. CGs do not look to the future with much hope	52	23	12	13
17. CGs get irritated when the patient does not do things correctly or makes mistakes	44	28	18	10
18. CGs are not able to show affection	82	12	5	1
19. CGs feel anguished having to face other problems	38	44	10	8
20. To what extent does helping with dialysis impact CGs working life	11	44	28	17
21. Do CGs have to modify their holidays due to caregiving activities?	9	42	34	15
22. Does care of the patient impact CGs family life?	15	38	18	14
23. To what extent has CGs social life been altered or affected?	16	44	23	17
24. To what extent have CGs had to modify or adapt their hobbies for helping with the care of the patients and hospital appointments?	16.5	21.1	45.0	17.4
25. Do you feel CGs health has been affected?	16.5	31.7	47.2	4.6
26. Are CGs family members being affected?	14.2	17.0	60.1	8.7
27. Do CGs feel completely responsible for the health and well-being of the patient?	25.2	43.6	12.9	18.3
28. To what extent have CGs readapted or modified their schedule to accommodate the caregiving duties?	8.7	20.2	49.1	22.0

CONFLICT OF INTEREST

The authors declare that there is no conflict of interest.

AUTHOR CONTRIBUTION STATEMENT

Research hypothesis (HR, MN). Experimentation and data collection (MN, ZR). Draft of the text (RS, BA) Interpretation of the data and use of software (HR), Text reviewed (AK). Statistical analysis (HR, MN). Writing, review & editing (HR, SN,)

REFERENCES

Ali, B. S., Reza, H., Khan, M. M., Jehan, I. (1998). Development of an indigenous screening instrument in Pakistan: the Aga Khan University Anxiety and Depression Scale. *Journal of Pakistan Medical Association*, *48*(9), 261-265. https://ecommons.aku.edu/pakistan_fhs_mc_chs_chs/430

Alvi, T., Hussain, S., Assad, F. (2021). Frequency of depression and anxiety among heart failure patients in a tertiary care hospital of Faisalabad, Pakistan. *Pakistan Bio Medical Journal, 11*(1), 18-20. http://doi.org/ 10.52229/pbmj

Ando, M., Ninosaka, Y., Okamura, K., & Ishi, Y. (2015). Difficulties in caring for a patient with cancer at the end of life at home and complicated grief. *American Journal of Hospice and Palliative Medicine, 32*(2), 173-177. https://doi.org/10.1177/1049909113514626.

Bayen, E., Papeix, C., Pradat, D. C., Lubetzki, C., & Joel, M. (2015). Patterns of the objective and subjective burden of informal caregivers in multiple sclerosis. *Behavioral neurology, 28*(6), 408–418. https://doi.org/10.1155/2015/648415.

Belasco, A., Barbosa, D., Bettencourt, B., Diccini, S., & Sesso, R. (2006). Quality of life of family caregivers of elderly patients on hemodialysis and peritoneal dialysis. *American Journal of Kidney Diseases, 48*(6), 955-963. https://doi.org/10.1053/j.ajkd.2006.08.017

Bussotti, M., & Sommaruga, M. (2018). Anxiety and depression in patients with pulmonary hypertension: impact and management challenges. *Vascular Health and Risk Management, 7*, 314-349. http://doi.org/ 10.2147/VHRM.S147173.

Danial, K., Khurram, K., & Ali, Z. (2016). Prevalence of Depression among the patients with end-stage renal disease and their caregivers, and its associated factors at a tertiary care hospital in Karachi. *Journal of Neurology and Stroke, 10*(4), 217-221. http://doi.org/ 10.15406/jnsk.2016.04.00138

Evans, R. W., Manninen, L. P., Garrison, L. G., Hart, C. R., Blagg, R., & Gutman, A. (1985). The quality of life of patients with end-stage renal disease. *New England Journal of Medicine, 312*(9), 1579-1580. http://doi.org/10.1056/nejm198506133122421

Heidari, M. A., Bouzar, M., Haghshenas, A., Kasaeeyan, M. R., & Ardebil, M. (2012). Quality of life and depression in caregivers of patients with breast cancer. *BMC Research Notes, 5*(1), 1-3. http//doi.org/ 10.1186/1756-0500-5-310

Jafar, T. H. (2006). The growing burden of chronic kidney disease in Pakistan. *New England Journal of Medicine, 354* (10), 995-997. http//doi.org/ 10.1056/nejmp058319

Kasi, P. M., Naqvi, A. K., Afghan, T., Khawar, F. H., Khan, U. Z., Khan, U. B., & Khan, H. M. (2012). Coping styles in patients with anxiety and depression. *International Scholarly Research Notices, 12*, 110-124, http//doi.org/: 10.5402/2012/128672

Khalid, T., & Kausar, R. (2017). Depression, anxiety, and quality of life in stroke survivors and their family caregivers: A pilot study using an actor/partner interdependence model. *An Electronic Physician, 19*(2), 103-110. http//doi.org/: 10.19082/4924

Loh, A. Z., Tan, J., Zhang, W., & Ho, R. (2017). The global prevalence of anxiety and depressive symptoms among caregivers of stroke survivors. *Journal of the American Medical Directors Association, 18*(2), 111-116. http//doi.org/: 10.1016/j.jamda.2016.08.014

Majeed, M. H., Khokhar, M., Abid, A., Raza, M. N., Qaisar, A., & Waqas, A. (2018). Frequency and correlates of symptoms of anxiety and depression among young caregivers of cancer patients: A pilot study. *BMC Research Notes, 11*(1), 1-6. http://doi.org/:10.1186/s13104-018-3740-8

Morton, R., A. Tong, K. Howard, P. Snelling & Webster, A. (2010). The views of patients and carers in treatment decision making for chronic kidney disease: systematic review and thematic synthesis of qualitative studies. *BMJ, 34*, 112-115. http://doi.org/:10.1136/bmj.c112

Saeed, Z., Ahmad, A., Shakoor, F., & Kanwal, S. (2012). Depression in patients on hemodialysis and their caregivers. *Saudi Journal of Kidney Diseases and Transplantation, 23*(5), 946-951. http://doi.org/10.4103/1319-2442.100869

Shah, H. B., Atif, F., Rashid, M., Babar, R., Arshad, F., & Qadir, M. (2017). Assessment of caregiver burden of patients receiving dialysis treatment in Rawalpindi. *Journal of Pakistan Medical Association, 67*(10), 1498-1501. https://doi.org/pubmed.ncbi.nlm.nih.gov/28955063

Teixido, P., Tarrats, J. L., Arias, N., & Cosculluela, A. (2006). Overload questionnaire for caregivers of patients on peritoneal dialysis. *Nefrología (English Edition), 26*(1), 74-83. http//doi.org/S2013251418301111

Zalai, D., Szeifert, L., & Novak, M. (2012). Psychological distress and depression in patients with chronic kidney disease. *Seminars in dialysis, Wiley Online Library, 22*(1), 111-115. http//doi.org/ 10.1111/j.1525-139x.2012. 01100.x

FABAD J. Pharm. Sci., 48, 1, 61-74, 2023
Doi: 10.55262/fabadeczacilik.1085351
RESEARCH ARTICLE

Central Composite Design for the Development of Trimetazidine Dihydrochloride-Loaded Fast Dissolving Film

Swapnil S. CHOPADE[*°], Mangesh A. PAWAR[**], Popat S. KUMBHAR[***], Arehalli S. MANJAPPA[****], John I. DISOUZA[*****], Santosh A. PAYGHAN[******°], Jagruti L. DESAI[*******]

Central Composite Design for the Development of Trimetazidine Dihydrochloride-Loaded Fast Dissolving Film

SUMMARY

A fast-dissolving dosage form is an approach used to improve therapeutic efficacy and bioavailability by avoiding the first-pass metabolism of the drug carrier. Besides, the approach causes rapid drug absorption from the pre-gastric area which may outcome in the quick inception of action. Trimetazidine dihydrochloride (TDC) is an anti-anginal drug, and there is a prerequisite to provide fast onset of action to treat angina. Therefore, the present work aimed to prepare and evaluate fast-dissolving oral films (FDOFs) of TDC to provide fast onset of action. The FDOF is prepared by using the solvent casting method, and it was optimized by employing a central composite statistical design (CCD). The two independent variables such as HPMC K4M (X1) and PEG 400 (X2) are the film-forming polymers that are evaluated at three levels. The dependent variables such as folding endurance (Y1), disintegration time (Y2), and % drug release (Y3). The formulation was prepared and optimized. The batch F-4 showed the least disintegration time (19 s) and the highest drug release (98.55±7.90%). Moreover, the ex-vivo mucus permeation study disclosed better permeation and satisfying physicochemical properties compared to plain drug solution. It was concluded that the prepared formulation could be a novel dosage form to improve drug delivery and patient compliance.

Key Words: *Anti-anginal, CCD, ex-vivo permeation, fast dissolving oral film, solvent casting method, trimetazidine dihydrochloride.*

Merkezi Kompozit Dizaynı ile Trimetazidin Dihidroklorit Yüklü Hızlı Çözünen Film Geliştirilmesi

ÖZ

Hızlı çözünen dozaj formu, ilk geçiş metabolizmasını elimine ederek ilaç taşıyıcı sistemin terapötik etkinliğini ve biyoyararlanımını geliştirmek amacıyla kullanılan bir yaklaşımdır. Ayrıca, bu yaklaşım etkinin hızlı bir şekilde başlamasıyla sonuçlanabilecek olan mide öncesi bölgeden hızlı ilaç emilimine neden olur. Trimetazidin dihidroklorür (TDC) anti-anjinal bir ilaçtır ve anjina tedavisi için hızlı etki başlangıcı sağlanması bir ön koşuldur. Bu nedenle, mevcut çalışmada hızlı etki başlangıcı sağlamak için TDC'nin hızlı çözünen oral filmlerinin (FDOFs) hazırlanması ve değerlendirilmesi amaçlanmıştır. FDOF, çözeltinin dökülmesi metodu ile hazırlanmıştır ve merkezi kompozit istatistiksel tasarım (CCD) uygulanarak optimize edilmiştir. HPMC (K4M) (X1) ve PEG 400 (X2) gibi iki bağımsız değişken, üç seviyede değerlendirilen film oluşturma polimerleridir. Katlanma sayısı (Y1), dağılma süresi (Y2) ve % ilaç salımı (Y3) bağımlı değişkenlerdir. Formülasyon hazırlanmış ve optimize edilmiştir. Seri F-4 en kısa dağılma süresini (19 s) ve en yüksek ilaç salımını (%98,55±7,90) göstermiştir. Ayrıca, ex-vivo mukus permeasyonu çalışması, boş ilaç çözeltisine kıyasla daha iyi permeasyon ve tatmin edici fizikokimyasal özellikler ortaya koymuştur. Hazırlanan formülasyonun ilaç taşınmasını ve hasta uyumunu geliştirmek için özgün bir dozaj formu olabileceği sonucuna varılmıştır.

Anahtar Kelimeler: *Anti-anjinal, CCD, ex-vivo permeasyon, hızlı çözünen oral film, solvan dökme metodu, trimetazidin dihidroklorür.*

Received: 14.03.2022
Revised: 06.10.2022
Accepted: 29.11.2022

[*] ORCID: 0000-0001-6173-6343 ,Tatyasaheb Kore College of Pharmacy, Warananagar (MS, India)
[**] ORCID: 0000-0002-0108-3149, Tatyasaheb Kore College of Pharmacy, Warananagar (MS, India)
[***] ORCID: 0000-0002-0108-3149, Tatyasaheb Kore College of Pharmacy, Warananagar (MS, India)
[****] ORCID: 0000-0002-8576-6608, Tatyasaheb Kore College of Pharmacy, Warananagar (MS, India)
[*****] ORCID: 0000-0002-8576-6608, Tatyasaheb Kore College of Pharmacy, Warananagar (MS, India)
[******] ORCID: 0000-0002-0653-6784, Vasantidevi Patil Institute of Pharmacy, Kodoli (MS, India).
[*******] ORCID: 0000-0001-7147-5861, Ramanbhai Patel College of Pharmacy, Gujarat (GJ, India)

[°] Corresponding Author;
1. Dr. Santosh A. Payghan, Email: santos14july@gmail.com
2. Mr. Swapnil S. Chopade, Phone: 02328 223526, Fax: 02328 223501, Email: swapnilchopade.tkcp@gmail.com

INTRODUCTION

Among the numerous routes of drug administration, the oral route is considered the most convenient, and preferred route of administration (Al-Ani, 2019). It contributes to 50-60% of total drug formulations. However, the administration of conventional dosage forms *via* the oral route is allied with various shortcomings like presystemic metabolism, poor absorption, bioavailability, non-localized action, and patient noncompliance etc (Masih A, 2017; Al-Mogheraha, 2020). In addition, the administration of dosage forms especially tablet through oral is challenging (dysphasia; difficulty in swallowing) and is a general problem in all age groups, particularly the elderly and pediatrics, because of physiological changes linked with these patients. Therefore, there is an unmet need to find out alternative oral dosage forms to overcome the aforementioned challenges (Logrippo, 2017; Bharti, 2018).

Fast dissolving oral film (FDOF) can be a suitable dosage form that would overcome the above challenges in oral delivery, and it is gaining more attention in the pharmaceutical industries. FDOF is a thin strip or film which is placed on the tongue where it gets disintegrates and dissolves quickly in the presence of saliva and undergoes rapid absorption through oral mucosa (Bose, 2013). FDOF offers various benefits including its suitability for bedridden, mentally disabled, and emetic patients. Besides, FDOF undergoes rapid dissolution or disintegration in the absence of water within a few seconds only and produces a fast onset of action (Binfeng, 2015; Bharti, 2018; Balaa, 2018). The system avoids degradation in the gastrointestinal tract and the first-pass effect as the drug is directly absorbed into the systemic circulation results in maximum bioavailability of the drug. In addition, another chief advantage of FDOF is in cancer chemotherapy patients immediately treat nausea and vomiting-related side effects of chemotherapy by eliciting rapid onset of action, and improving patient compliance towards therapy. Furthermore, it can produce a local effect in toothaches, oral ulcers, cold sores, or teething thereby reducing the side effects. Also, the FDOF increases patient compliance owing to the ease of administration (Ahn, 2015; Bharti, 2018).

Trimetazidine, also known as 1-[(2, 3, 4-trimethoxyphenyl) methyl] piperazine hydrochloride (TDC), is a medically active antiangiogenic agent used to prevent and treat angina pectoris, as well as ischemia of neuron sensory tissue in Meniere's disease (Chaudhary, 2016). Nevertheless, TDC undergoes rapid systemic metabolism after oral administration in the form of a tablet that causes a decrease in bioavailability. The conventional tablet formulations of TDC available in the market may have a slow onset of action and low bioavailability. As it is an anti-anginal drug therefore fast onset of action and better bioavailability is desired to treat angina efficiently. Previous research studies reported that TDC is given at a dosage of 40 to 60 mg per day, and it is rapidly absorbed and eliminated, with a plasma half-life of $t_{1/2}$ 6.0±1.4 hours and a T max of 1.80±7 hours. Because of the rapid absorption, the plasma level is very low at the time of the next dose, resulting in a large difference in peak and trough plasma levels at a steady state. To achieve this, a 20 mg preparation is given two or three times per day to maintain a relatively constant plasma level (Habib, 2014; Dezsi, 2016; Wang, 2016).

The range of hydrophilic polymers employed in the preparation of FDOF is cellulose derivatives (hydroxypropyl methylcellulose (HPMC), methylcellulose), polyethylene glycol (PEG), pullulan, polyvinylpyrrolidone (PVP), etc. The HPMC and PEG are enormously used polymers owing to their good film-forming properties. In addition, both polymers are widely accepted. Furthermore, they form highly transparent, tough, and flexible films with the aid of aqueous solutions (Zayed, 2019).

Nowadays, quality by design (QbD) is a widely used approach in the optimization of pharmaceutical formulation. The optimization of formulation using a design of experiment (DoE), a part QbD can help

in the reduction of batches, cost, and improvement of overall quality of the formulation (Nair, 2018). Thus, the objective of the present research was to develop and optimize the TDC-loaded FDOF for the treatment of angina pectoris effectively. Further, the main effects, interaction effects, and quadratic effects of the formulation excipients on dependent variables (responses) such as folding endurance, disintegration time, and % drug release were investigated using the design of the experiment (DoE).

MATERIALS AND METHODS

Materials

TDC was provided as a gift sample from, Cipla Pvt. Ltd. Verna, Goa, India. HPMC K4M, Sodium starch glycolate was obtained from S. D. Lab chemical center, Mumbai. Cross povidone, Citric acid, Polyethylene glycol (PEG) 400, Tween 80, and Peppermint oil were obtained from Molychem Industries, Mumbai. All other ingredients were used as film base materials in analytical grade without further modifications.

Methods

Drug-excipients compatibility study

Possible physicochemical interaction of the TDC with polymers and other excipients (1:1 ratios) used in the formulation was investigated to assess the compatibility between them in the FDOFs using Fourier Transform Infrared (FTIR) spectroscopy (Karki, 2016).

TDC-loaded FDOF

The solvent casting method was used to prepare the TDC-loaded FDOF. Briefly, the polymeric solution was prepared by dissolving a specific amount of HPMC K4M in 70% of distilled water with continuous stirring **(Solution A)**. Then the desired amount of TDC, PEG 400, and tween 80 was dissolved in 30% of distilled water **(Solution B)**. Next, solution A was added slowly to solution B with continuous stirring and set sideways for 30 min for defoaming. Finally, after defoamation, the solution was poured into petri plates and dried in a hot air oven at 45^0 C. Then the casted film was cut into a suitable size and shape and characterized (Table 1) (Binfeng, 2015; Balaa, 2018; Verma, 2018).

Table 1. Formulation batches of fast dissolving film of TDC

Ingredients	F1	F2	F3	F4	F5	F6	F7	F8	F9
TDC (mg)	20	20	20	20	20	20	20	20	20
HPMC K4M (mg)	10.0	10.5	11.0	11.5	12.0	12.5	13.0	13.5	14.0
PEG 400 (mL)	11	12	13	14	15	16	17	18	19
Crospovidone (mg)	3	3.5	4	4.5	5	5.5	6	6.5	7
Citric acid (mL)	2	2	2	2	2	2	2	2	2
Tween 80 (mL)	2	2	2	2	2	2	2	2	2
Peppermint oil (mL)	2	2	2	2	2	2	2	2	2

* All values in the table are expressed in mg and mL

Optimization of FDOFs by using DoE

Central composite design (CCD)

An experimental design is a concept of the careful balance between several variables affecting in the experiment. To decrease the number of trials and attain the highest amount of information, central composite design (CCD) is applied, for further optimization of design responses, and several batches were prepared by using Design-Expert software Version 12.0. A total of 9 runs were presented including centre points. CCD is a popular experimental design for optimizing process variables and determining regression model equations and operating conditions from eligible experiments. It is based on a multivariate nonlinear model. It can also be utilized to look at the inter-

play of the various parameters that affect the process (Khabade, 2017).

In this study, a 3^2 Central composite statistical design was used. Two independent variables are evaluated in this design, each at three levels. HPMC K4M (X_1) and PEG 400 (X_2) concentrations were chosen as factors (independent variables). As responses (dependent variables), folding endurance (Y_1), disintegration time (Y_2), and percent drug release (Y_3) were chosen. The data was processed with the trial software Design-Expert Version 12.0 and statistically analyzed with ANOVA (analysis of variance). The data was also subjected to a 3-D surface response methodology (RSM), which was used to evaluate the effects of HPMC K4M and PEG 400 on dependent variables. Further, the effects of factors on responses were analyzed using the 2FI statistical model developed by 3^2 CCD for optimization (Maheswari, 2014; Navamanisubramaniana, 2018).

$$\mathbf{Y= b_0 + b_1X_1 + b_2X_2 + b_3X_1X_2 + b_4X_{21} + b_5X_{22} + b_{12}X_1X_2 + b_{13}X_1X_3}$$

The dependent variable is Y, the intercept is b_0, and the regression coefficients are b_1, b_2, b_3, b_4, and b_5. Individual effects are X_1 and X_2, quadratic effects are X_{21} and X_{22}, and the interaction effect is X_1X_2. To determine the model's and individual response parameters' significance ($P< 0.05$), a one-way ANOVA was used. The effect of an independent variable on the measured responses was investigated using surface response plots (3-D) and contour plots (2-D) (Patel, 2014; Pethe, 2016).

Table 2. Variables used for the optimization of TDC-loaded FDOF

Factors	Name	Unit	Type	Low Actual	High Actual	Low Coded	Medium Coded	High Coded
X_1	HPMC K4M	Mg	Numeric	10	15	-1	0	1
X_2	PEG 400	Mg	Numeric	10	20	-1	0	1
Responses	**Name**	**Units**	**Remark**	**Analysis**		**Min.**	**Medium**	**Max**
Y_1	Folding Endurance	Numbers	9	Polynomial		77	102.5	128
Y_2	DT	Sec	9	Polynomial		19	34.5	50
Y_3	% Drug release	%	9	Polynomial		74	96.5	97

Evaluation of formulated FDOFs

Appearance

The morphological character was studied by the visual inspection of the film's appearance.

Thickness

A digital vernier caliper was used to measure the thickness of the film in five different locations. Finally, each fast-dissolving film formulation's average thickness and standard deviation were calculated (Balaa, 2018).

Weight variation test

The experiment was carried out on drug-loaded films with a diameter of 2×2 cm^2. The films were weighted individually on a digital balance, and the average weight for each batch was recorded (Patel, 2014; Khabade, 2017).

The pH of surface

The film was placed in a petri dish for examination. Briefly, the film was moistened with 0.5 mL of simulated saliva buffer (pH 6.8) and left for 30 seconds. After, the pH is measured with a digital pH meter by immersing the electrode in the formulation and allowing 1 minute for equilibration. The calculation was repeated three times, determining the average value (Khabade, 2017; Bharti, 2018).

Folding endurance

The film was evaluated for folding endurance. Briefly, the film was folded with a consistent cross-sectional area and thickness before breaking. The number

of times the film could be folded at the same location without breaking was calculated as the folding endurance value. This test ensures the film's tensile strength (Shimoda, 2009; Khabade, 2017; Bharti, 2018).

Drug content and content uniformity

The drug content and content uniformity were calculated by taking a (2×2 cm^2) diameter film from each formulation into a 100 mL volumetric flask and filling it with phosphate buffer at pH 6.6. It was left for 1-2 hours before the drug content was measured using a UV spectrophotometer at 269 nm wavelengths. The experiments were repeated three times, and the average results are shown in Table 3 (Singh, 2005).

Percent elongation (%), and tensile strength

The mechanical properties [% elongation at break (% EB) and tensile strength (TS)] of the film were determined by using the Santam testing machine (STM 20, Iran). The maximum deformation of the film without tearing is expressed in percent EB. The TS results indicated that, the film's optimum capacity to resist stress without tearing. This method involves clamping a film of a particular size (2×2 cm^2) between two clamp levers on the equipment and applying a 2 mm/min extension force to the film. At the time of tearing, the load at failure (F) and final length (L) were measured. The percent EB and TS were eventually determined using the following equations (Deswati, 2016):

% Elongation (cm %) = ((L – L0) * 100) / L0
Where, (L: length, L0: Initial length)
Tensile strength (N/cm^2) = (F * 100) / (t * w)
Where, (F: failure, t: thickness, w: width)

Disintegration time (DT)

The DT limit prescribed for orally disintegrating tablets as per CDERs is 30 seconds or less for FDOFs (fda.gov.2018), while no official rules are described for OFDFs. In this study, a Pharmacopoeial disintegrating test device will be used (Sadhukhan, 2016; Bharti, 2018).

In-vitro drug release study

The *in-vitro* drug release study was conducted in 900 mL simulated saliva (pH 6.8) held at 37 ±0.5^{0}C and stirred at 50 rpm using the USP dissolution test apparatus II (paddle apparatus). The film was cut into a 2 x 2 cm^2 patch and submerged into the dissolving apparatus. 1 mL of aliquot samples was withdrawn at 1, 2, 3, 4, and 5 min time intervals, filtered, and analyzed spectroscopically at 269 nm (Bharti, 2018; Zayed, 2019; Al-Mogheraha, 2020).

Ex-vivo permeation study

The goat buccal mucosa was used as a barrier membrane in this research. A local slaughterhouse provided the buccal pouch of a freshly slaughtered goat animal. The buccal mucosa was cut evenly and excised from the sides. Then, it was immediately washed in isotonic phosphate buffer (pH 6.6) and used.

The *ex-vivo* permeation study of a plain drug, optimized fast dissolving film of TDC and Quicobal® film through an excised layer of goat buccal mucosa was carried out using the Franz diffusion cell. The topside of each formulation's (2×2 cm^2) diameter film under analysis was coated with aluminum foil as a backing membrane and put in intimate contact with the excised goat buccal mucosa. The magnetic bead was mounted in a 30 mL pH 7.4 phosphate buffer-filled receptor compartment. A magnetic stirrer was used to stir the contents of the cells, and a temperature of 37±1°C was maintained during the experiment. The samples were taken at regular intervals, filtered, appropriately diluted, and then spectrophotometrically analyzed at 269 nm and, the percent drug permeated was calculated and plotted against time (Semalty, 2008; Tomar, 2012; Xin, 2014; Chonkar, 2016; Suryawanshi, 2021).

Stability study

Under various environmental conditions, the stability of the formulated FDOFs was investigated and the measurements were done by storing the film under controlled conditions at 40±2 °C and 75±5% RH for three months in a stability chamber according to the ICH guideline (Raza, 2019). During the storage period, various evaluating parameters like thickness; morphological properties, disintegration time,

drug content, surface pH, and dissolution behavior are checked (Dandagi, 2013;Izhar, 2015; Khan, 2016; Bharti, 2018).

RESULTS AND DISCUSSIONS

Drug excipients compatibility study

The FTIR spectra of TDC, HPMC K4, and their physical mixture are shown in Figure 1. In the FTIR spectra of pure TDC, characteristic peaks were observed at 3566 cm^{-1}, 2938 cm^{-1}, and 1500-1600 cm^{-1} which are attributed to O-H stretching, C-H stretching and C-O stretching vibrations respectively. The FTIR of HPMC K4 showed characteristic peaks at 1615, 1465, and 1452 cm^{-1} indicating C=C stretching, C-H bending in alkane and C-H bending in aldehyde respectively. The FTIR of the film displayed characteristic peaks at 3292 cm^{-1}, 1738 $cm^{-1}$and 1047 cm^{-1}, indicating–OH and C-O stretching vibrations of TDC. Besides, the peak at 2928 cm^{-1} indicates the C-H bond of alkane compounds. No significant broadening, loss, or presence of functional peaks was observed in the physical mixture of TDC and HPMC K4M, revealing no interactions (compatibility) between TDC and formulation excipients.

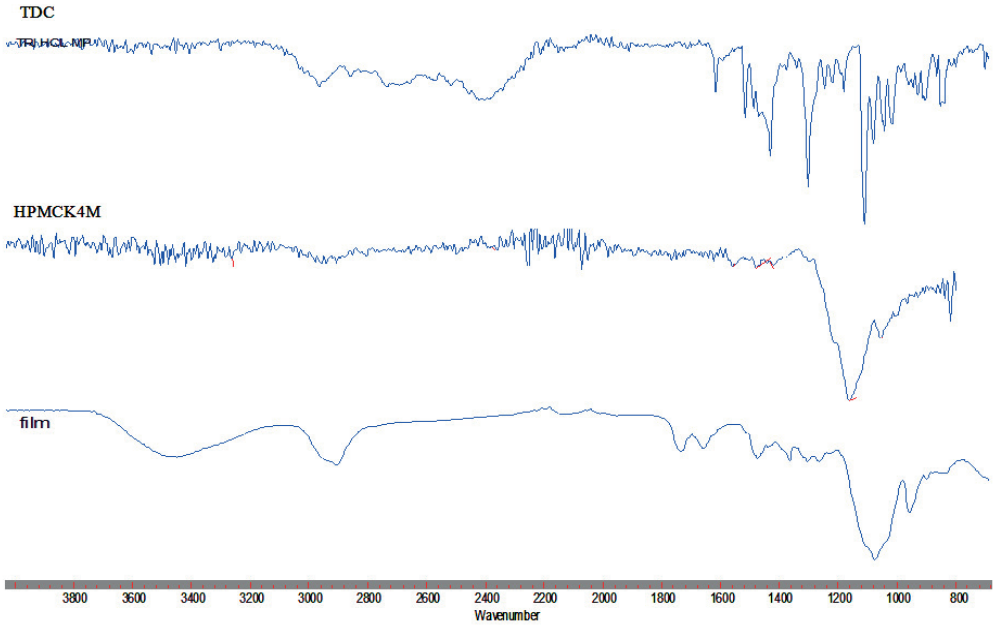

Figure 1. Comparative FTIR spectra of TDC, HPMC K4M, and TDC-loaded fast dissolving film

Optimization of independent variables (Factors)

We have selected the HPMC K4M and PEG 400 as polymers because they are hydrophilic and have good film formation ability. In addition, both polymers are reported to form a highly transparent film. Furthermore, low molecular weight (PEG 400) was selected due to its better dissolution and dispersion ability than high molecular weight PEG polymers. Preliminary study results suggested that 5-30% HPMC K4M and 20-30% PEG 400 cause stickiness in films. However, the concentration of HPMC K4M in prepared films was 10-15% and PEG 400 at 10-20% was non-sticky uniform, and transparent. Based on the results, polymers concentrations (10-15%) and plasticizer concentrations (10-20%) were selected for further formulations. It is also observed that the amount of polymer above 15% showed an increase in DT, below 10% the film did not show flexibility, and above 20% film became sticky.

Optimization of dependent variables (Response)

With the application of the CCD, the (2D contour and 3D RSM) plots were built based on the polynomial functions of the model to evaluate the change in the response surface. These plots can further help to understand the correlation between independent variables (factors) and dependent variables (response).

Response 1 (Y_1=Folding endurance)

ANOVA was employed to ascertain the model's and individual response parameters' significance ($p<0.05$). Contour plots and surface response plots were used to explore the consequence of independent variables on folding endurance (Figures 2 and 3). When the P-value is $p<0.007$, the F-value of 4.32 in the 2FI model suggests that the model is significant. The contour plots and response surface plots displayed the outcome of diverse factors on folding endurance. An increase in the concentration of polymer and plasticizer was found to increase the film's folding endurance.

Response 2 (Y_2= DT)

The ANOVA analysis of outcomes yielded the F-value of 6.34 for the 2FI model which implicates that the model is significant when the p-value is $p<0.03$. The consequence of several independent factors on DT was shown in the contour plots and response surface plots (Figures 2 and 3). As the amount of HPMC K4M in the film rose, the *in-vitro* DT was augmented, and the film became too sticky. Furthermore, augmenting the plasticizer concentration diminishes DT but makes the film brittle.

Response 3 (% Drug release =Y_3)

The ANOVA analysis of outcomes yielded a p-value of less than 0.04 ($p<0.04$) and an F-value of 4.02 which implicates that the model is significant. The contour plot and RSM plots displayed the consequence of diverse independent variables on drug release (Figures 2 and 3). As the amount of plasticizer and polymer in the film increased to 10-20% and 10-15%, respectively, the film's drug release increased. Drug release was reduced when the polymer concentration reached 15% because the drug remained within the polymer matrix.

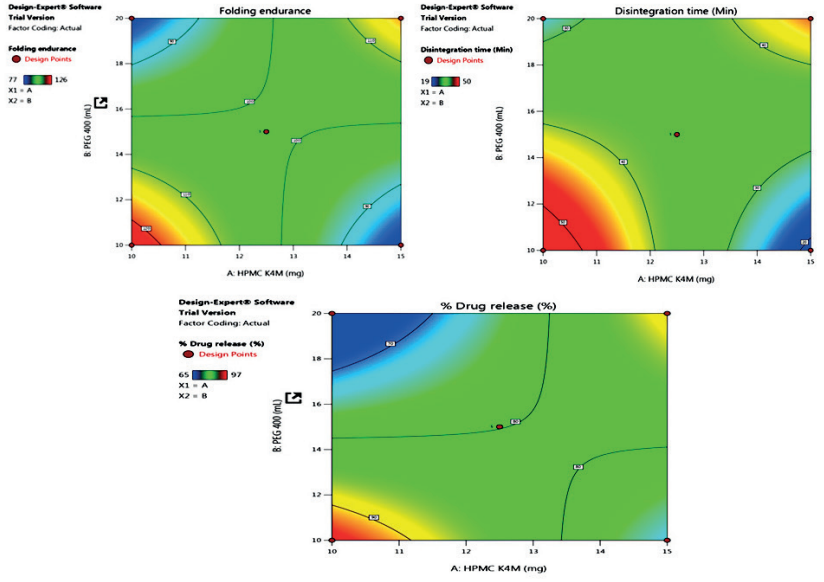

Figure 2. Contour plots showing the effect of HPMC K4M (X_1) and PEG 400 (X_2) on folding endurance (Y_1), Disintegration time (Y_2), and Drug release (Y_3).

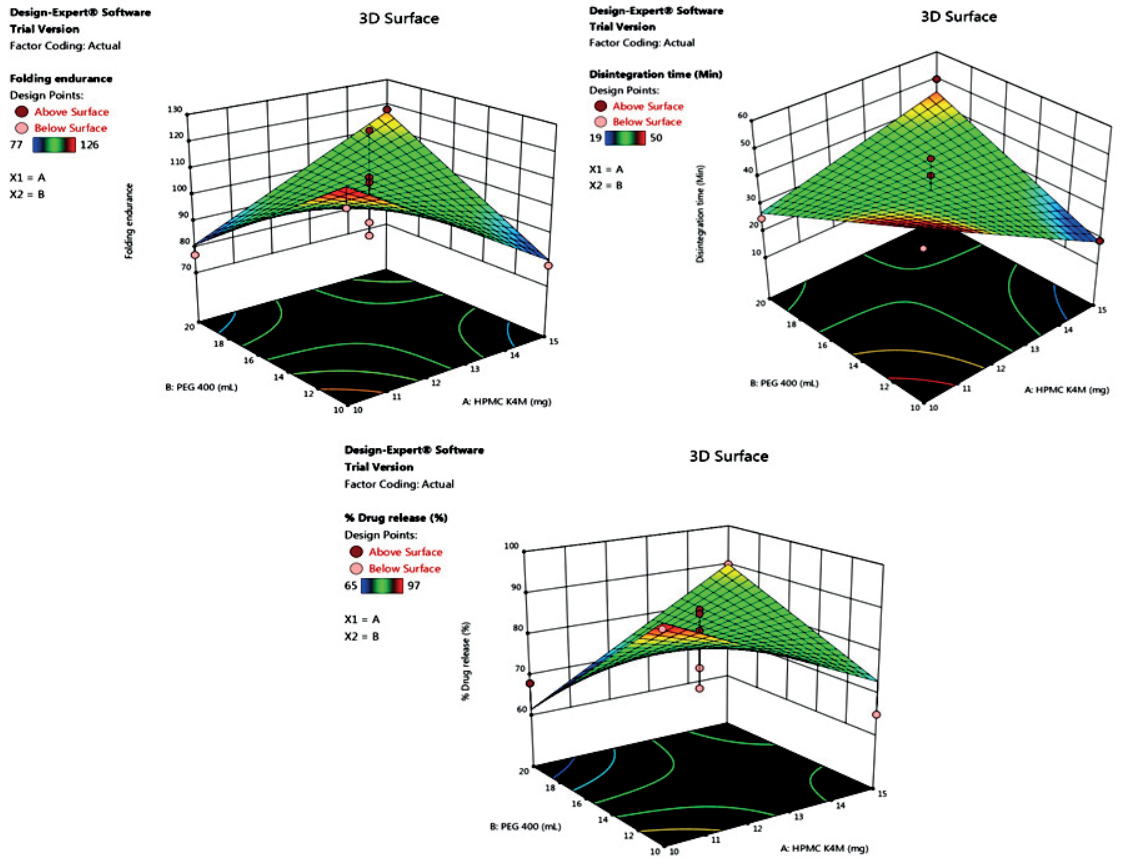

Figure 3. Response surface plots (3D) showing the effect of HPMC K4M (X_1) and PEG 400 (X_2) on Folding endurance (Y_1), Disintegration time (Y_2), and Drug release (Y_3).

Optimization using the desirability functions

There are various methods for optimizing multi-response problems. The desirability feature is one of the most common techniques used for solving multi-response surface problems. The lowest and utmost level must be defined for the apiece parameter employed. Each target can be given a weight to change the shape of its desirability feature. An overall desirability function is created by combining the objectives. Desirability is an objective function with a value of one at the target and zeroes outside of the limits. The software aims to make this role as effective as possible. As a consequence, the foremost intent starts at a random location and progresses up the steepest slope to the highest point. A manifold response means were applied to optimize a combination of two goals (HPMC K4M and PEG 400 concentration). Figure 4 demonstrates the desirability values of HPMC K4M (10-14 mg), and for PEG 400 (10-20 mL) as a "minimum" and "maximum" and within the range to analyze the economically viable optimal condition. At this condition, the model exhibits desirability of 0.999. These optimal values were checked experimentally which resulted in 97.6 %.

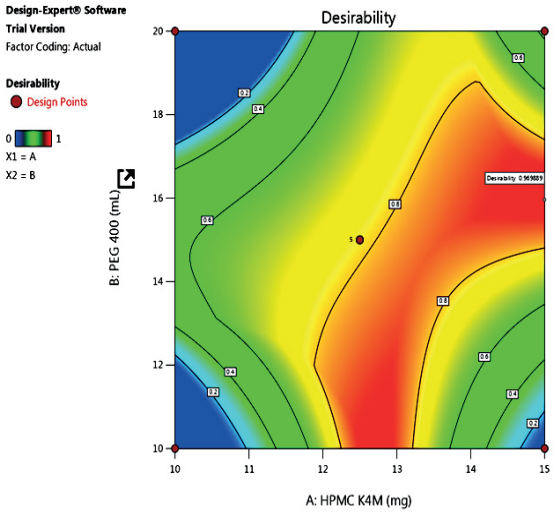

Figure 4. Desirability plot showing the effect of HPMC K4M (X_1) and PEG 400 (X_2).

Evaluation of formulated FDOFs

Appearance

The prepared FDOFs are visually inspected and which is in a whitish transparent appearance.

Thickness

The thicknesses of formulated TDC-loaded FDOFs were in the 0.07 to 0.09 mm range, with a tolerance of 0.01 mm. As shown in Table 3, the mean values were nearly uniform in all F1-F9 formulations. The uniformity in the thickness (due to the low standard deviation obtained) indicated the reproducibility of the method of preparation. According to the findings, increasing film thickness lowers tensile strength while increasing percent elongation. The crystallinity of the film increases as the thickness of the film increases, and the rate of dissolution decreases.

Weight variation test

The percent weight variation of all the formulations is mentioned in Table 3. All the films passed the weight variation test, per the standard Pharmacopoeial limits. The weight of all films was found to be 33.65±1.16 to 39.88±0.95 mg. The weight of the F-4 batch observed is 39.88 ± 0.95 mg.

Determination of surface pH

Table 3 shows the surface pH values of the TDC-loaded film formulations. The surface pH of all of the polymers used in the formulations is neutral. The pH of the surfaces of the film ranged from 6.8 to 7. The neutral surface pH of the films ensured that the mucosal lining of the oral cavity would not be irritated.

Folding endurance

The capacity of a patch to survive a rupture is measured by its folding endurance. The greater the folding endurance, the greater the risk of film rupture, and vice versa. The folding endurance values of all formulations are mentioned in Table 3. The F-4 batch demonstrated the folding endurance of 126±1. The folding endurance of the film increases with increases in the concentration of super disintegrant.

Drug content and content uniformity

The drug content and content uniformity tests were carried out to ensure the uniform distribution of the drug in the film. The % drug content of batch the F-4 is found to be 98.85±1.77. Moreover, the content drug uniformity is observed in all the prepared films.

Percent elongation (%), and tensile strength

The percentage of elongation mainly depends on the tensile strength of the formulated film and which is affected by the nature of polymers used. The % elongation and tensile strength of the F-4 batch are found to be 3.90±0.58%, and 5.58 ± 0.18 respectively.

Disintegration time (DT)

Disintegration time is a very important parameter for OFDFs, to indicate the onset of drug action. The time at which prepared film starts to disintegrate in the solvent is known as DT. The DT of the formulated film was in the range of 19-50 seconds while the F-4 batch exhibited a DT of 19±1 seconds. From the results obtained, it is clear that DT increases with the increased solid contents of the film.

In-vitro drug release study

The simulated saliva was used as a dissolution medium for the dissolution study of TDC fast dissolving film. Amongst, all batches (F-4, F-5, F-8) batch exhibited rapid drug release (Figure 5). The batch F-4 showed significantly more release of TDC (98.55±7.90%) in 5 minutes when compared to the batch F-5 and F-8. This rapid TDC release from all the batches including the F-4 batch may be attributed to the more concentration of PEG 400 and crospovidone which cause augment in the dissolution, and crospovidone (super disintegrating agent). In addition, crospovidone is rapidly wetted into the film by saliva resulting in an expansion of volume and hydrostatic pressure that occurs in rapid disintegration. Moreover, the substantially higher release of TDC from batch 4 could be due to the use of less concentration of HPMC-K4M that yielded thin film formation thereby fast disintegration and dissolution of the film.

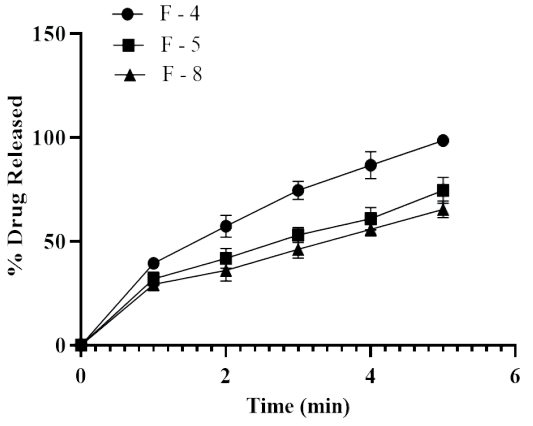

Figure 5. *In-vitro* drug release profile of batch F-4, F-6, and F-8 in simulated saliva (pH 6.8). All the values are expressed as mean ± standard deviation (n=3)

Ex-vivo permeation study

The cumulative percentage of drug permeated through plane drug solution, optimized TDC loaded FDOFs and marketed Quicobal® film was plotted against time as shown in Figure 6. It was found that the slightly increasing concentration of PEG 400 and crospovidone in the film caused a significant increment in the permeation rate. This could be attributed to the concentration-dependent permeation enhancement ability of crospovidone. All the TDC FDOFs showed superior performance *ex-vivo* when compared to plain drug solution. Statistical analysis revealed no significant difference in permeation parameters between optimized film and marketed Quicobal® film. Both the film samples exhibited similar permeation profiles. Moreover, the percent drug permeation was found to be 24.18%, 85.18%, and 85.23% from a plain drug, optimized TDC loaded film and marketed Quicobal® film respectively after 30 minutes.

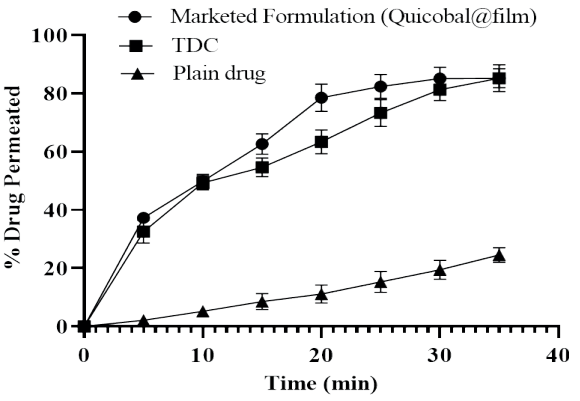

Figure 6. *Ex-vivo* permeation study of plain drug, optimized TDC FDOFs, and marketed Quicobal® film (pH 7.4). All the values are expressed as mean ± standard deviation (n=3)

Table 3. Evaluation of CCD batches of FDOFs

Batch code	Thickness (mm)	Surface pH*	Weight of the film (mg)*	% Elongation	Tensile Strength	Folding endurance	DT (sec)	Drug content per film (2×2 cm)%
F1	0.06±0.008	6.67±0.08	36.68±1.84	1.92±0.82	5.23 ± 0.16	87±0.58	42±1.73	98.79±2.80
F2	0.06±0.007	6.78±0.08	34.55±1.22	1.99±0.67	3.66 ± 0.22	118±1	50±1.73	97.88±2.65
F3	0.08±0.007	6.89±0.08	37.10±1.72	5.94±0.58	5.14 ± 0.20	92±2	25±1.73	98.36±1.89
F4	**0.07±0.008**	**6.97±0.04**	**39.88.±0.95**	**3.90±0.58**	**5.58 ± 0.18**	**126 ±1**	**19±1**	**98.85±1.77**
F5	0.08±0.007	6.90±0.09	38.90±1.14	4.21±0.58	4.37 ± 0.20	118±1.73	24±1	98.73±1.4
F6	0.08±0.008	6.85±0.04	33.65±1.16	1.82±0.58	5.24 ± 0.15	107±1	48±1.7	98.12±1.99
F7	0.08±0.008	6.80±0.08	34.45±1.86	5.34±0.58	4.63 ± 0.25	77±1.73	25±1	97.94±1.92
F8	0.08±0.09	6.86±0.08	37.78±1.84	5.15±0.58	5.11 ± 0.20	118±1.73	24±1	98.79±1.83
F9	0.08±0.009	6.72±0.04	36.78±1.20	2.01±0.58	3.44 ± 0.13	109±1.73	42±1.73	98.18±1.83

*All values are expressed as mean ± S.D. (n=3)

Stability study

The stability of the drug is one of the important parameters considered during the development of a new formulation. During stability studies, the substance is subjected to accelerated temperature and humidity conditions during stability testing. Accelerated stability experiments are those in which a substance is held under high temperatures for a short period. Based on DT, folding endurance, and % cumulative drug release result, batch F-4 is found to be more stable. No significant difference in, the % cumulative drug release, DT, and folding endurance of F-4 batch films were noticed after three months of storage at 40^0±2^0C/, 75 ±5% RH condition (Table 4). Further, the results obtained demonstrated no significant changes observed in the characteristics of the file system.

Table 4. Stability study results of optimized formulation

Formulation (F-4 batch)	Folding endurance	DT	*In-vitro* drug release (%)
Initial	126 ±1	19±1	98.55±1.20
After 1 months	124 ±2.45	21±0.4	96.05±3.50
After 2 months	117 ±0.23	20±0.2	93.78±0.40
After 3 months	109±1.73	24±5.37	93.34±5.02

*All values are expressed as mean ± S.D. (n=3)

CONCLUSION

In this study, novel FDOFs containing the drug TDC were successfully prepared using the solvent casting method. Using a three-level, two-factor (3^2) CCD, the formulations of FDOFs were optimized. Overall, the produced film formulations showed good results in terms of folding endurance, % drug release, and stability. The PEG 400 and crospovidone-driven FDOFs showed immediate disintegration (19 S), improved *in-vitro* dissolution, and faster *ex-vivo* permeation with excellent mechanical properties of TDC from the FDO films. Therefore, these novel FDOFs may provide a potential opportunity for oral delivery of the TDC drug.

ACKNOWLEDGEMENT

We are grateful to our Principal sir, Institute, and Management for their support of this research effort.

CONFLICT OF INTEREST

The authors declare that there is no conflict of interest.

AUTHOR CONTRIBUTION STATEMENT

The investigation, literature research, formulation development, analysis, interpretation of the data, statistics, preparing the study text, and writing the original draft (SSC, MAP, PSK). Developing a hypothesis, reviewing the text, resources, and supervision (ASM, JLD, JID, SAP)

REFERENCES

Ahn, H. (2015). Central Composite Design for the Experiments with Replicate Runs at Factorial and Axial Points. Industrial Engineering, Management Science and Applications, 969-970.

Al-Ani, I. H., Shakya, A. K., Hassan, S. F. (2019). Design, Optimization, and Evaluation of Combined Dosage form of Amoxicillin and Nonsteroidal Anti-inflammatory Agent for Pediatric use using DoE. Asian J of Pharm, 13(2), 125-130.

Al-Mogheraha A. I., Abbas M., Maha I., Hassanb A. (2020). Optimization and evaluation of venlafaxine hydrochloride fast dissolving oral films Saudi Pharmaceutical Journal, 28 (11), 1374-1382. https://doi.org/10.1016/j.jsps.2020.09.001

Balaa, R., & Sharmab, S. (2018). Formulation optimization and evaluation of fast dissolving film of aprepitant by using design of experiment. Bull Fact Pharm Cairo Univ, 56, 159–168.

Bharti K., Mittal P., Mishra B. (2018). Formulation and characterization of fast dissolving oral films containing buspirone hydrochloride nanoparticles using design of experiment, Journal of Drug Delivery Science and Technology, doi: https://doi.org/10.1016/j.jddst.2018.12.013.

Binfeng, X., Zhen, Y., Haiying, Z., Viera, L., Wei, Z., Mikolaj, M and Filippos, K. (2015). Development of a Novel Oral Cavity Compartmental Absorption and Transit Model for Sublingual Administration: Illustration with Zolpidem. AAPS J, 17(3), 631–642.

Bose, A., Wong, T. W., Singh, N. (2013). Formulation development and optimization of sustained release matrix tablet of Itopride HCl by response surface methodology and its evaluation of release kinetics. Saudi Pharm J, 21(2), 201-213.

Chaudhary, H., Gauri, S., Rathee, P., Kumar, V. (2013). Development and optimization of fast dissolving oro-dispersible films of granisetron HCl using Box–Behnken statistical design, Bull Fac Pharm Cairo Univ, 51, 193-201.

Chonkar A.D., Venkat Rao J., Managuli R.S., Mutalik S., Dengale S., Jain P. (2016). Development of Fast Dissolving Oral Films Containing Lercanidipine HCl Nanoparticles in Semicrystalline Polymeric Matrix for Enhanced Dissolution and Ex-Vivo Permeation, European Journal of Pharmaceutics and Biopharmaceutics. Biopharmaceutics, 103, 179-191. doi: http://dx.doi.org/10.1016/j.ejpb.2016.04.001

Dandagi, P., Singh, A., Manvi, F., Belekar, A. (2013). Formulation of trimetazidine matrix tablet using methocel and effect of different parameters on drug release from matrix tablet. Turk J. Pharm Sci, 10 (2), 287-302.

Deswati, S., Izzati, R., Hamzar, S., Zein, R., and Alif, A. (2016). Application of central composite design for optimization the determination of lead using adsorptive cathodic stripping voltammetry. Rasayan J. Chem, 9(1), 8-17.

Dezsi, C. A. (2016). Trimetazidine in Practice: Review of the Clinical and Experimental Evidence. Am J. Ther, 23(3), 871-879.

Habib B. A., Abd El Rehim R. T., Nour S. A. (2014) . Feasibility of optimizing trimetazidine dihydrochloride release from controlled porosity osmotic pump tablets of directly compressed cores. Journal of Advanced Research, 5, (3), 347-356. https://doi.org/10.1016/j.jare.2013.05.005

https://www.fda.gov/media/70877/download

Izhar, S. A., Ahmed, A. M., Arief, M. (2015). Formulation and Characterization of Mucoadhesive Buccal Films of Trimetazidine Dihydrochloride, Lat. Am. J. Pharm, 34 (8), 1585-93.

Karki, S., Kim, H., Jeong, S., Shin, D., Jo, K., Lee, J. (2016). Thin films as an emerging platform for drug delivery, Asian J. Pharm. Sci, 11, 559-574.

Khan, A., Qadir, M. I., Jabeen, F. (2016). Orally disintegrating films: A modern expansion in drug delivery system. Saudi Pharm. J, 24, 537-546.

Khabade, S. S., Chopade, S. S., Gaikwad, E. R., Payghan, S. A. (2017). Potential Screening of Spray Dried Solid Dispersion of Orlistat using Three Dimensional Solubility Parameter. Asian J. of Pharm, (Suppl), 11(4), 760-766.

Kunte, S., & Tandale, P. (2010).Fast dissolving strips: A novel approach for the delivery of verapamil. J. Pharm Bio all. Sci, 4, 325-8.

Logrippo, S., Ricci, G.,Sestili, M., Cespi, M. (2017) Oral drug therapy in elderly with dysphagia: between a rock and a hard place. Clinical Interventions in Aging. 12, 241-251

Maheswari, K. M., Devineni, P. K., Deekonda, S., Shaik, S., Uppala, N. P., and Nalluri B. N. (2014). Development and evaluation of mouth dissolving films of amlodipine besylate for enhanced therapeutic efficacy. J. Pharm (Cairo), 1-10.

Masih A., Kumar A., Singh S., Tiwari A. K., (2017). Fast Dissolving Tablets: A Review. Int J Curr Pharm Res 9, (2) 8-18.

Nair A., Khunt D, Misra M. (2018). Application of quality by design for optimization of spray drying process used in drying of Risperidone nanosuspension. Ptec (2018), doi:10.1016/j.powtec.2018.09.096

Navamanisubramaniana, R., Nerellaa, R., Duraipandianb, C., Seetharamanc, S. (2018). Quality by design approach for optimization of epaglinide buccal tablets using Box-Behnken Design. Future J. of Pharm Sci, 4, 265-272.

Pethe, A. M., & Desai, R. B. (2016). Formulation, Optimization & evaluation of mouth dissolving film of nifedipine by using design of experiment. Asian J. of Pharm Sci, 11, 74-76.

Patel, P., Limbashiya, R., Chavda, M., and Shah, U. (2014). Development and Optimization of Fast Dissolving Orodispersible Film of Baclofen Using 3^2 Central Composite Design. Int J. Pharm Sci, 5(12), 5539-47. http://dx.doi.org/10.13040/IJPSR.0975-8232.5 (12).5539-47

Raza S. N., Kar A. H., Wani T. U. and Khan N. A. (2019). Formulation and evaluation of mouth dissolving films of Losartan potassium using 3^2 factorial design. Int J Pharm Sci & Res, 10(3),1402-11.

Sadhukhan, B., Mondal, N. K., Chattoraj, S. (2016). Optimization using central composite design (CCD) and the desirability function for sorption of methylene blue from aqueous solution onto Lemna major. Karbala International Journal of Modern Science, 2, 145-155.

Semalty, M., Semalty, A., Kumar, G., Juyal, V. (2008). Development of mucoadhesive buccal films of glipizide. Int. J. of Pharm. Sci & Nano, 1(2), 184-190.

Shimoda, H., Taniguchi, K., Nishimura, M., Matsuura, K., Tsukioka, T., Yamashita, H. (2009). Preparation of a fast dissolving oral thin film containing dexamethasone: A possible application to antiemesis during cancer chemotherapy. Euro J. of Pharm. and Biopharm, 73, 361-365.

Singh, B., Dahiya, M., Saharan, V., Ahuja, N. U. (2005). Optimizing drug delivery systems using systematic design of experiments. Part II: retrospect and prospects. Crit. Rev Ther Drug Carrier Syt, 22(3), 215-293.

Suryawanshi D., Wavhule P., Shinde U., Kamble M., Amin P (2021). Development, optimization and *in-vivo* evaluation of cyanocobalamin loaded orodispersible films using hot-melt extrusion technology: A quality by design (QbD) approach. Journal of Drug Delivery Science and Technology 63, 1773-2247. https://doi.org/10.1016/j.jddst.2021.102559

Tomar, A., Sharma, K., Chauhan, N., Mittal, A., Bajaj, U. (2012). Formulation and evaluation of fast dissolving oral film of dicyclomine as potential route of buccal delivery. Int. J Drug Dev & Res, 4(2), 408-417.

Verma U., Rajput R., Naik J.B. (2018). Development and characterization of Fast Dissolving Film of Chitosan embedded Famotidine Using 3^2 Full Factorial Design Approach. Materials Today: Proceedings 5, 408-414.

Wang L., Feng R., Gao J., Xi Y., Huang G. (2016). Generic sustained release tablets of trimetazidine hydrochloride: Preparation and in vitro–in vivo correlation studies. Asian Journal of Pharmaceutical Sciences, 11 (3), 417-426. https://doi.org/10.1016/j.ajps.2015.10.001

Xin, T., Zhao, Y., Jing, H., Zhang, W., Gao, Y., Yang, X. (2014). A time-released osmotic pump fabricated by compression-coated method: Formulation screen, mechanism research and pharmacokinetic study. Asian J. of Pharm Sci, 9, 208-217.

Zayed G.M., Abd-El Rasoul S., Ibrahim M.A., Saddik M.S., Alshora D.H. (2019). In-Vitro and In-Vivo Characterization of Domperidone-Loaded Fast Dissolving Buccal Films, Saudi Pharmaceutical Journal, doi: https://doi.org/10.1016/j.jsps.2020.01.005

FABAD J. Pharm. Sci., 48, 1, 75-90, 2023
Doi: 10.55262/fabadeczacilik.1133276
RESEARCH ARTICLE

Development and Validation of an HPLC Method for Simultaneous Determination of Miconazole Nitrate and Chlorhexidine Digluconate in Chitosan-Based Gel Formulations

Ece TÜRKMEN[*], Selin PARMAKSIZ[**], Mustafa ÇELEBİER[***], Sevda ŞENEL[****°]

Development and Validation of an HPLC Method for Simultaneous Determination of Miconazole Nitrate and Chlorhexidine Digluconate in Chitosan-Based Gel Formulations

SUMMARY

Miconazole nitrate (MN) and chlorhexidine digluconate (CHX) are the commonly used antimicrobials for topical treatment of dermal infections. Combination of antimicrobials has been investigated to enhance the efficacy of the treatment. Gel formulations based on bioadhesive polymers are preferred for delivery of these drugs. Chitosan is a promising bioadhesive polymer due to its penetration enhancing, antimicrobial and tissue healing properties. Yet, most of the gel-based formulations present analytical challenges during testing the drug content. It was aimed to develop an HPLC method for simultaneous determination of MN and CHX in chitosan-based gel formulations. Different solvent combinations were investigated for extraction of drugs from the gels. HPLC conditions such as mobile phase, flow rate, run time, column temperature and wavelength were explored. The method was validated according to ICH guideline Q2(R1). MN and CHX were extracted in solvent composition same with the mobile phase. The method was employed on ACE-C8 column at 40°C by isocratic elution using the mobile phase consisting of methanol:phosphate (75:25 v/v) buffer (containing triethylamine). Flow rate was 1 mL/min. The drugs were detected at 254 nm (CHX) and 230 nm (MN). Linearity was obtained between 5 to 80 µg/mL for both drugs. LOD and LOQ obtained for CHX were 1.61 and 4.87 µg/mL, for MN: 1.06 and 3.21 µg/mL, respectively. A new validated HPLC method was developed for simultaneous determination of CHX and MN in chitosan-based gels, with 98 to 102% recovery, without any interference with the excipients.

Key Words: *HPLC method, simultaneous analysis, miconazole nitrate, chlorhexidine digluconate, chitosan gel, validation*

Kitosan Bazlı Jel Formülasyonlarında Mikonazol Nitrat ve Klorheksidin Diglukonatın Eşzamanlı Tayini için Bir HPLC Yönteminin Geliştirilmesi ve Validasyonu

ÖZ

Mikonazol nitrat (MN) ve klorheksidin diglukonat (CHX), dermal enfeksiyonların topikal tedavisi için yaygın olarak kullanılan antimikrobiyallerdir. Tedavinin etkinliğini arttırmak için antimikrobiyallerin kombinasyonu araştırılmıştır. Bu ilaçların taşınması için biyoadezif polimer bazlı jel formülasyonları tercih edilmektedir. Kitosan, penetrasyon arttırıcı, antimikrobiyal ve doku iyileştirici özellikleri nedeniyle umut verici bir biyoadezif polimerdir. Jel bazlı formülasyonların çoğu, henüz ilaç içeriğinin test edilmesi sırasında analitik zorluklar göstermektedir. Kitosan bazlı jel formülasyonlarında MN ve CHX'in eş zamanlı tayini için bir YBSK yönteminin geliştirilmesi amaçlanmıştır. Jellerden ilaçların ekstraksiyonu için farklı çözücü kombinasyonları incelenmiştir. Mobil faz, akış hızı, çalışma süresi, kolon sıcaklığı ve dalga boyu gibi YBSK koşulları incelenmiştir. Yöntem, ICH kılavuzu Q2(R1)'e göre valide edilmiştir. MN ve CHX, mobil faz ile aynı çözücü bileşiminde ekstrakte edilmiştir. Yöntem, metanol:fosfat (75:25 v/v) tamponundan (trietilamin içeren) oluşan mobil faz kullanılarak izokratik elüsyon ile 40°C'de ACE-C8 kolonunda geliştirilmiştir. Akış hızı 1 mL/dk'dır. İlaçlar 254 nm'de (CHX) ve 230 nm'de (MN) tespit edilmiştir. Her iki ilaç için de 5 ile 80 µg/mL arasında doğrusallık elde edilmiştir. CHX için elde edilen LOD ve LOQ sırasıyla 1.61 ve 4.87 µg/mL, MN için 1.06 ve 3.21 µg/mL'dır. Kitosan bazlı jellerde, yardımcı maddelerle herhangi bir etkileşim olmaksızın %98 - 102 geri kazanım ile CHX ve MN' nin eşzamanlı tayini için yeni bir valide YBSK yöntemi geliştirilmiştir.

Anahtar Kelimeler: *YBSK yöntemi, eşzamanlı analiz, mikonazol nitrat, klorhekzidin diglukonat, kitosan jel, validasyon*

Received: 20.06.2022
Revised: 26.11.2022
Accepted: 01.12.2022

[*] ORCID: 0000-0003-0365-2306, Hacettepe University, Department of Pharmaceutical Technology, Ankara, Turkey
[**] ORCID: 0000-0002-3798-7537, Hacettepe University, Department of Pharmaceutical Technology, Ankara, Turkey
[***] ORCID: 0000-0001-7712-5512, Hacettepe University, Department of Pharmaceutical Technology, Ankara, Turkey
[****] ORCID: 0000-0002-1467-3471, Hacettepe University, Department of Analytical Chemistry, Ankara, Turkey

[°] Corresponding Author; Sevda Şenel
Tel. +90 312 310 12 41, Fax: + 90 312 310 09 06, e.mail: ssenel@hacettepe.edu.tr

INTRODUCTION

Chlorhexidine digluconate (CHX) is a bactericidal biguanide compound with broad-spectrum antibacterial and antifungal activity (Greenstein, 1986; Paulson, 2002; Kampf, 2018) . It is widely used both in human and veterinary medicine as an antimicrobial agent (Guaguère, 1996; Sarkiala-Kessel, 2012; Aronson, 2016; Brookes, 2020). There are currently numerous commercially available preparations of CHX in solution, tablet, aerosol, ointment, cream, lozenge, cloth, sponge and swab forms containing CHX at different concentrations (Silvestri, 2013; "Facts about Chlorhexidine Gluconate," 2017; "What Is Periochip," 2017; Hoang, 2021). CHX is commonly used as topical antiseptic and antimicrobial agent for wound cleansing and wound healing as well as for treatment of oral infections (Bouckaert, 1993; Rawlings, 1998; Şenel, 2000; Main, 2008; Atiyeh, 2009). CHX is positively charged and freely soluble in water (Mohammadi, 2008; Zeng, 2009).

Miconazole nitrate (MN) is an imidazole group drug used against fungal infections and gram-positive bacterial infections (Sawyer, 1975). MN has been widely used in human and veterinary medicine in treatment of super candidiasis and dermal infections, dermatophytosis and pityriasis versicolor through topical (Rochette, 2003; Frymus, 2013), vaginal (Kenechukwu, 2018; Salah, 2018), buccal (Cartagena, 2017; Tejada, 2018), oral (Dimopoulou, 2015) and parenteral (Wade, 1979) administrations. MN is a positively charged compound with 6.7 pKa value and very slightly soluble in water, methanol and alcohol (Al-Badr, 2005; *Martindale: The Complete Drug Reference*, 2009; Qushawy, 2018). The combination of MN with CHX has been shown to exert synergistic effect against numerous bacteria (Perrins, 2003; Mueller, 2008; Nenoff, 2017). Further, presence of the combination of ethylene diamine tetra acetic acid (EDTA) and hydroxymethyl aminomethane (Tris) has been shown to increase the sensitivity of the cell wall of the microbe to microbials (Guardabassi, 2010; Ghibaudo, 2016; Stojanov, 2018). In order to achieve successful topical formulations for delivery of antimicrobial agents, it is important to provide retention of the system on the application site for desired period of time and drug release in a prolonged fashion. Chitosan is a cationic biopolymer which is widely investigated for topical delivery of antimicrobials due to its bioadhesive and penetration enhancing properties as well as for its bioactive properties such as antimicrobial and wound healing (Şenel, 2010; Şenel, 2020). The most preferred form among the developed chitosan-based formulations are gels. However, most of the gel-based formulations present analytical challenges during testing the drug content. These products generally require burdensome extraction and sample preparation procedures. Especially, if there are more than one drug in the formulation the assay becomes more complicated.

Numerous analytical methods such as UV spectrophotometry, high-performance liquid chromatography (HPLC), etc., have been reported for precise quantification of MN (Heneedak, 2012; Belal, 2012; Ei, 2016; Maha Mohamed Abdelrahman, 2017; Eticha, 2018) or CHX (Borissova, 1997; Havlíková, 2007; Abtheen, 2008; Másquio Fiorentino, 2010; Chiapetta, 2011; Maha M. Abdelrahman, 2016; Işık, 2018) in the pharmaceutical dosage forms. However, due to the physico-chemical properties of MN and CHX, when incorporated together in a formulation the analytical methods are affected by interaction between the two drugs. Separation and retention of a polar and a non-polar compound by the same stationary phase can be a useful approach for simultaneous analysis of these compounds. An HPLC method developed for simultaneous determination of chlorhexidine, miconazole, clobetasol and neomycin in a cream formulation was reported by Kumar et al. (Kumar, 2017). In this method, a mixture of 20 mM phosphate buffer (pH 6.6) and acetonitrile at a ratio of 65:35 was used as the mobile phase, at 1 mL/min flow rate. Retention times for chlorhexidine and miconazole in the cream formulation were 4,927 and 5,606 min, respectively.

In this study, we aimed to develop and validate an HPLC method for simultaneous determination of MN and CHX in chitosan-based gel formulation, which we have developed for topical treatment of dermal infections.

MATERIAL AND METHODS

Materials

Miconazole nitrate was generously provided by IE Ulagay-Menarini Group (Turkey). Chitosan was generously provided by Koyo Co., LTD Japan. Chlorhexidine digluconate, Tris base (T6066), EDTA (E-5134) and Tween 80® (Cas no: 9005-65-6) were purchased from Sigma-Aldrich (Germany). Tween 20® was purchased from BDH Laboratory Supplies Poole, England and propylene glycol (Ph. USP Grade) from Merck Millipore (Germany). All other chemical reagents were of analytical grade.

Formulation Development

Chitosan gel was prepared at 3% (w/v) concentration in 2% v/v acetic acid. 2% w/v CHX and 2% w/v MN were incorporated into the gels. Tween 20® and Tween 80® were used as surfactants, propylene glycol and ethanol were used as co-solvents. Tris-EDTA (16:1) was also incorporated into the gels to enhance the antimicrobial activity (Türkmen, 2022).

Instrumental Conditions

HPLC measurements were performed on the Prominence LC-20A Modular HPLC System (Shimadzu, Japan). HPLC sample analysis and data collecting were conducted using LabSolutions software. The HPLC system consisted of a degasser (DGU-20A5), a pump (LC-20AT), an auto sampler (SIL-20A HT), a column oven (CTO-10AS VP). UV detection was performed at SPD-M20A (Photodiode Array Detector-UV-Vis Detector). For simultaneous determination of MN-CHX in chitosan-based gel formulations, different HPLC conditions such as mobile phase, flow rate, run time, column temperature and wavelength were investigated (Table 1). The HPLC conditions at the highest yield were determined as summarized in Table 2.

Table 1. Chromatographic conditions investigated

Mobile phase	Column	Ratio of mobile phase	Elution type	Flow rate (mL/min)	Run time (min)	Wavelength (nm)	
						CHX	MN
Methanol: 20 mM pH 3.0 phosphate buffer (0.1 % triethylamine)	ACE® C18 (250 x 4.6 mm, 5 µm)	80:20	Isocratic	1	30	254	230
Methanol: 20 mM pH 6.9 phosphate buffer (0.2 %TEA)	ACE® C8 (150 × 4.6 mm, 5 µm)	78:22	Isocratic	0.8 and 1	25	210 220 230 240 254 260	210 220 230 240 254 260
		78:22 - 85:15 78:22 - 82:18 78:22 - 80:20 78:22 - 75:25 78:22 - 72:18	Gradient	1	25	254	230
		75:25 78:22 80:20	Isocratic	1 and 1.2	25	254	230

Table 2. HPLC conditions of the developed method

Column	ACE C8 Column (150 mm x 4.6 mm, 5 µm)
Flow rate	1 mL/min
Wavelength	230 nm (MN), 254 nm (CHX)
Temperature	40 °C
Mobile phase	Methanol:20 mM pH 6.9 phosphate buffer (0.2% triethylamine) (75:25)
Injection volume	20 µL

Preparation of mobile phase

3.56 g of sodium phosphate dibasic dihydrate was weighed and dissolved in purified water and completed to 1000 mL. 2 mL of triethylamine (TEA) solution was added to the buffer solution at 0.2% v/v concentration. pH was adjusted to 6.9 by adding 5 M ortho-phosphoric acid. The pH of the mobile phase was measured pH meter (HANNA® Instruments, USA). The final buffer solution was filtered using mixed cellulose (CA-CN) membrane disc (diameter: 47mm; pore size: 0.22 µm) (Lubitech Technologies Ltd, China) and degassed for 30 min prior to use. Mixture of methanol: 20 mM pH 6.9 phosphate buffer (containing 0.2% v/v TEA) solution at different ratios (80:20, 78:22 and 75:25 for isocratic elution; 78:22-85:15, 78:22-82:18, 78:22-80:20, 78:22-75:25 and 78:22-72:18 for gradient elution) was prepared as the mobile phase. Methanol: buffer solution at 50:50 ratio was used for dilution of the gels and standard solutions.

Extraction procedure of the CHX and MN from gels

For extraction of both drugs from the gel, after trying different solvent systems, the most suitable solvent composition was found to be methanol: pH 6.9 phosphate buffer (0.2% TEA) at 75:25 v/v ratio, which is also the mobile phase. The gels were diluted in the extraction solvent and centrifuged at 8500 rpm for 10 min. The supernatant was withdrawn and diluted with mobile phase and injected into HPLC system.

System Suitability Test

System suitability test was performed to show that the system and developed method provides acceptable quality data. For this purpose, % RSD values of retention time and peak area, tailing factor parameters were determined using a standard solution at 80 µg/mL concentration for both drugs.

Method validation

The method was validated according to the International Council for Harmonization (ICH) guideline, ICHQ2(R1) ("Validation of Analytical Procedures: Text and Methodology Q2 (R1)", 1995), determining the parameters such as specificity, selectivity, linearity, limit of detection (LOD), limit of quantitation (LOQ), accuracy, precision and stability.

Specificity

Specificity was evaluated to show the absence of interference with the inactive ingredients used in the formulations (analytical placebo). The placebo solutions were prepared containing Tris: EDTA, Tween 20, Tween 80, propylene glycol and ethanol in chitosan gel. Samples were analyzed in six replicates.

Selectivity

The ability to separate the drugs in the sample was demonstrated by assessing the resolution between the peaks corresponding to CHX and MN. For the selectivity of the method, the standard solution of CHX and MN at the same concentration (80 µg/mL) was prepared as given at 2.3.2 section and injected into HPLC.

Linearity

The linearity of the method was determined using different concentrations (5, 10, 20, 40 and 80.0 µg/mL) of MN and CHX. The linearity was conducted at the same concentration range (5 to 80 µg/mL) for CHX and MN. The calibration curves were obtained by plotting peak area versus concentration. The correlation coefficients were calculated and the linearity was determined by linear regression analysis. The tests were performed in six replicates.

Accuracy

Accuracy was measured as the percent of deviation from the nominal concentration. Standard solutions with accurate concentrations (10 µg/mL, 20 µg/mL and 40 µg/mL) were prepared in six replicates and injected into the system. The recovery percent (recovery %) and the percentage relative standard deviation (RSD %) were calculated for each concentration. Bias % was calculated using Equation 1.

Bias % = [(Measured concentration - theoretical concentration)/ theoretical concentration] x 100 (1)

Precision

To determine the precision of the method, repeatability (same day) and reproducibility (three consecutive days) was evaluated by analyzing the MN and CHX in standard solution prepared at different concentrations (10 µg/mL, 20 µg/mL and 40 µg/mL) with six replicates. RSD % was calculated for each concentration.

Ruggedness

The ruggedness of the developed method was investigated using two different analysts. Standard solutions of CHX and MN (n=5) at 20 µg/ mL concentration were prepared and analyzed separately by two different analysts and the results were compared statistically. The ruggedness was evaluated with two system suitability parameters with the retention time and the peak area.

Robustness

The robustness of the developed method was analyzed at different flow rates and temperatures. Standard solutions of CHX and MN at 20 µg/mL concentration were prepared and analyzed at different flow rates (1 and 1.2 mL/min) and temperatures (39°C and 40°C), and the results were compared, statistically.

Detection and Quantification Limits

LOD and LOQ are defined as the minimum concentration at which the analytes can be detected and quantified, respectively. The LOQ and LOD of the method were determined based on the standard deviation of the response and the slope using Equations 2 and 3. The slope was estimated from the calibration curve.

$$\boldsymbol{LOD} = 3.3 \times \frac{\sigma}{S} \quad (2)$$

$$\boldsymbol{LOQ} = 10 \times \frac{\sigma}{S} \quad (3)$$

σ: standard deviation of the response

S: slope of the calibration curve

Stability

The stability of standards solutions was investigated by reinjection of the samples at 0, 12 and 24 h and measuring recovery % of CHX and MN. Furthermore, the stability of CHX and MN in dissolution medium (pH 5.0 phosphate buffer containing 0.5% Tween 80) was evaluated at 37 °C for 6 h at 0, 3 and 6 h.

Statistical analysis

Statistical analysis of data obtained during method validation was performed to demonstrate validity of the analytical method. Calculation of the mean (or average), standard deviation, relative standard deviation, confidence intervals, and regression analysis was performed using software package, SPSS.

RESULTS AND DISCUSSION

Homogeneous and opaque whitish color gels were prepared with pH of 5.5, which is an appropriate pH for the maintenance of the stability of the drugs, MN and CHX (Türkmen, 2022). CHX solutions have been reported to be stable between the pH range of 5 to 8 and showing the highest antimicrobial activity within this range (Denton, 2001; Paulson, 2002). Similarly, MN is stable in the pH range of 5-8 (Ammara, 2018) and antifungal activity of MN is not changed in this range (Siegel, 1977).

Extraction of CHX and MN from gels

Amongst the different solvents and their combinations used for extraction of MN and CHX from the gels, the highest recovery % was obtained with methanol:20 mM pH 6.9 phosphate buffer (0.2% TEA) (50:50, v/v) which is also the mobile phase (Table 3). The % recovery results of the sample at 20 µg/mL in methanol:20 mM pH 6.9 phosphate buffer (0.2% TEA) (50:50, v/v) extraction solution are shown in Table 4.

Table 3. Extraction of MN and CHX from gels

Extraction Solution	Extraction Recovery % of CHX	Extraction Recovery % of MN
0.1% acetic acid containing 1% w/v sodium lauryl sulfate	27.9 ± 8.3	39.6 ± 2.3
Methanol	65.4 ± 4.5	71.7 ± 2.7
Methanol: water: acetic acid (90:9:1, v/v/v)	75.8 ± 0.9	80.9 ± 1.2
Methanol: 20 mM pH 6.9 phosphate buffer (0.2% TEA) (50:50, v/v)	99.8± 1.1	101.0 ±1.6

Table 4. The results of Recovery % (at 20 µg/mL)

	CHX	MN
Measured concentration (µg/mL)	19.98	19.54
	20.06	20.02
	19.79	19.5
	19.86	19.68
	19.62	19.79
	20.06	19.8
Mean Concentration (µg/mL) ± SD	19.9 ± 0.17	19.7 ± 0.19
Recovery %	99.47	98.6

Method Development

In our preliminary studies for simultaneous quantification of MN and CHX, a UV-spectrophotometric method based on the rule of absorbance additivity was tried; however no satisfactory results were obtained. Hence, it was decided to continue with an HPLC method. Firstly, a suitable column was selected. Uniform peak shapes and better separation were obtained with the C8 (150 mm x 4.6 mm, 5 µm) column. Further the pH condition was investigated and pH 6.9 was decided to be the most suitable pH. The column temperature was kept at 40 °C to obtain a shorter retention time, knowing that both CHX and MN are stable with temperature change ("Final Report on the Safety Assessment of Chlorhexidine/Chlorhexidine Diacetate/Chlorhexidine Dihydrochloride/Chlorhexidine Digluconate", 1993; Sahoo, 2016). Optimization of the mobile phase in HPLC separation is an essential step for the selectivity of the method and the retention time of the substances (Valkó, 1993; Samanidou, 2015). Hence, for mobile phase, the solvents were chosen taking the physico-chemical properties of the drugs, MN (hydrophobic) and CHX (hydrophilic, ionizable) into consideration. Due to the ionizable property of the drug, the pH of mobile phase can be one of the important variables in control of the retention in HPLC separation. The retention time of analyte is known to be affected by the pH changes of the mobile phase (Moldoveanu, 2017). Thus, buffers are widely used for the pH control of mobile phase (Lakka, 2019). Phosphate buffer at different pH (3.0 to 7.4) was investigated as the mobile phase for separation of CHX and MN. pH 6.9 was found to be the most suitable pH avoiding the noise peaks, which is also right pH for the stability of these drugs. TEA at 0.2 % v/v was added to the mobile phase to suppress the tailing of the peaks. Mixtures of methanol:water, methanol:phosphate buffer (pH 6.9), acetonitrile:water, acetonitrile:phosphate buffer (pH 6.9) at different ratios were investigated for separation of MN and CHX in the column at different flow rates to achieve short retention time and high separation efficiency for both CHX and MN (Table 5).

The standard solution prepared from the gel formulation containing CHX and MN was tested at different ratios of mobile phase, wavelengths and flow rates. The standard solution has been analyzed at a wavelength range of 210 to 260 nm with a mixture

of methanol:20 mM pH 6.9 phosphate buffer (0.2 % TEA) (78:22; v/v) as mobile phase and the acceptable system suitability parameters regarding of the chromatograms were obtained at 254 nm for CHX and 230 nm for MN.

The flow rate was changed from 0.8 mL/min to 1 mL/min to improve the column efficiency. Gradient elution with changing concentrations of methanol: buffer solution was analyzed. CHX was not completely eluted from the column with the gradient elution program of the mixture of methanol: 20 mM pH 6.9 phosphate buffer (0.2 % TEA) (78:22 - 85:15 v/v) at the end of the run time. Furthermore, the column efficiency of MN was found to be higher at 230 nm whilst the column efficiency of CHX was found to be low at 254 nm. Column efficiency was found to be >1500 with the gradient elution program of the mixture of methanol:20 mM pH 6.9 phosphate buffer (0.2 % TEA) (78:22 - 72:28 v/v). Further, isocratic elution with constant concentrations of methanol:20 mM pH 6.9 phosphate buffer (0.2 % TEA) was analyzed. 1 mL/min and 1.2 mL/min flow rates were tried to optimize the theoretical plate numbers. The highest theoretical plate numbers were reached in the mobile phase with a ratio of 75:25 v/v at a flow rate of 1 mL/min. A flow rate of 1.2 mL/min was not chosen due to insufficient improvement in the retention times of the peaks and the theoretical plate numbers and undesirable increase in the column back pressure. The well-defined separation of CHX and MN was achieved by isocratic elution at a mobile phase ratio of 75:25 with 1 mL/min flow rate. The retention time of CHX and MN was detected 15.87 min and 3.78 min, respectively (Figure 1 and Figure 2).

Table 5. Chromatographic conditions investigated

Mobile phase	Column	Ratio of mobile phase	Wavelength (nm)		Retention time (min)		Tailing Factor	
			CHX	MN	CHX	MN	CHX	MN
Methanol: 20 mM pH 3.0 phosphate buffer (0.1 % triethylamine)	C18 (250 x 4.6 mm, 5 µm)	80:20	254	230	3.08	17.23	4.71	1.19
Methanol: 20 mM pH 6.9 phosphate buffer (0.2 %TEA)	ACE® C8 (150 × 4.6 mm, 5 µm)	78:22	210		3.21		1.02	
			220		3.21		1.2	
			230		3.21		1.09	
			240		13.69		1.03	
			254		13.68		1.14	
			260		13.67		1.11	
		78:22 (0.8 mL/min)	210		3.906		1.273	
			220		3.906		1.13	
			230		3.906		1.135	
			240		17.573		1.073	
			254		17.565		1.074	
			260		17.579		1.089	
		78:22 - 85:15	254	230	21.58	3.18	1.24	1.18
		78:22 - 82:18			18.7	3.15	1.2	1.21
		78:22 - 80:20			17.53	3.17	1.27	1.22
		78:22 - 75:25			15.42	3.11	1.255	1.26
		78:22 - 72:28			14.64	3.28	1.271	1.22
		75:25	254	230	14.39	3.64	1.314	1.19
		78:22			16.57	3.28	1.33	0.72
		80:20			18.89	2.98	1.22	1.3

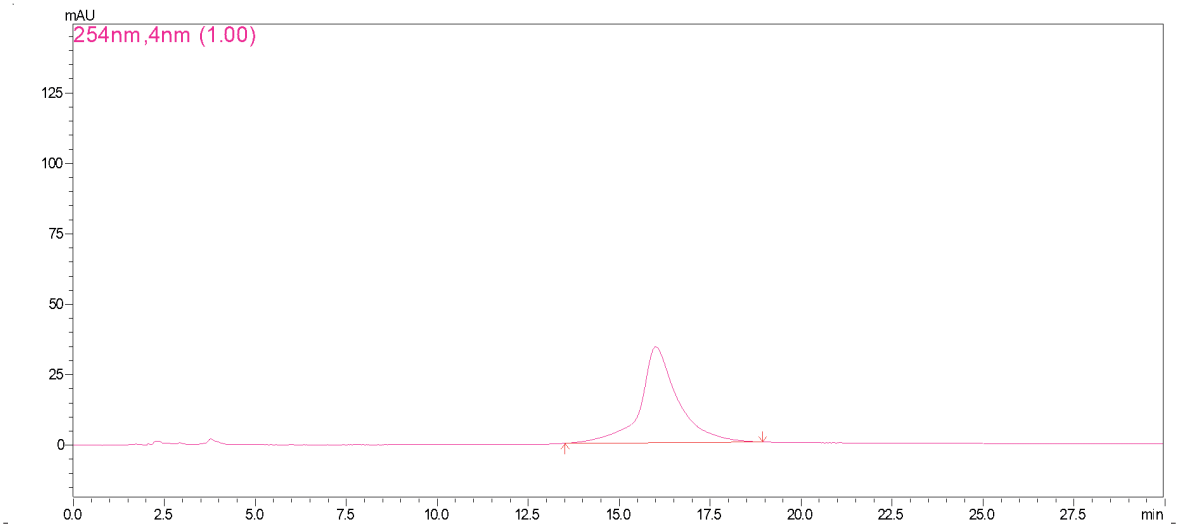

Figure 1. The chromatogram of the mixture of CHX (80 µg/mL) and MN (80 µg/mL) in mobile phase at 254 nm

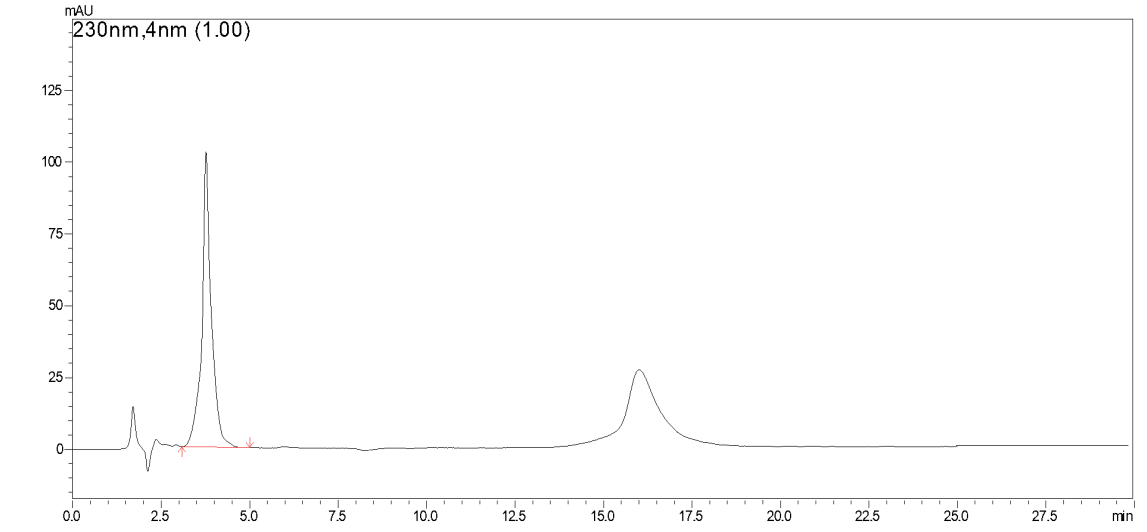

Figure 2. The chromatogram of the mixture of CHX (80 µg/mL) and MN (80 µg/mL) in mobile phase at 230 nm.

In conclusion, it was decided to use methanol:20 mM pH 6.9 phosphate buffer containing 0.2% TEA ratio as 75:25 (v/v) at 40 °C with 1 mL/min as flow rate to perform the analysis. Analysis was performed with wavelength at 254 nm for CHX and 230 nm for MN. The injection volume was chosen as 20 µL for all samples.

System Suitability

The system suitability results are summarized in Table 6. All parameters were shown to be in acceptable limits.

Table 6. System suitability results

Parameter	CHX	MN
% RSD of retention time	0.76	0.21
% RSD of peak area	0.1	0.09
Tailing factor (mean)	1.05	1.04

Method Validation

The developed method was validated in regard to selectivity, linearity range, accuracy, precision, sensitivity (LOD and LOQ) and stability according to the ICH guideline as stated in section 2.4.

Specificity and Selectivity

No interference between the drugs as well as between drugs and the inactive ingredients (Tween 20, Tween80, ethanol, propylene glycol, Tris-EDTA) was observed, indicating the selectivity of the developed method (Figures 3 and 4). Two separate peaks with good resolution and two different retention times were observed for MN and CHX.

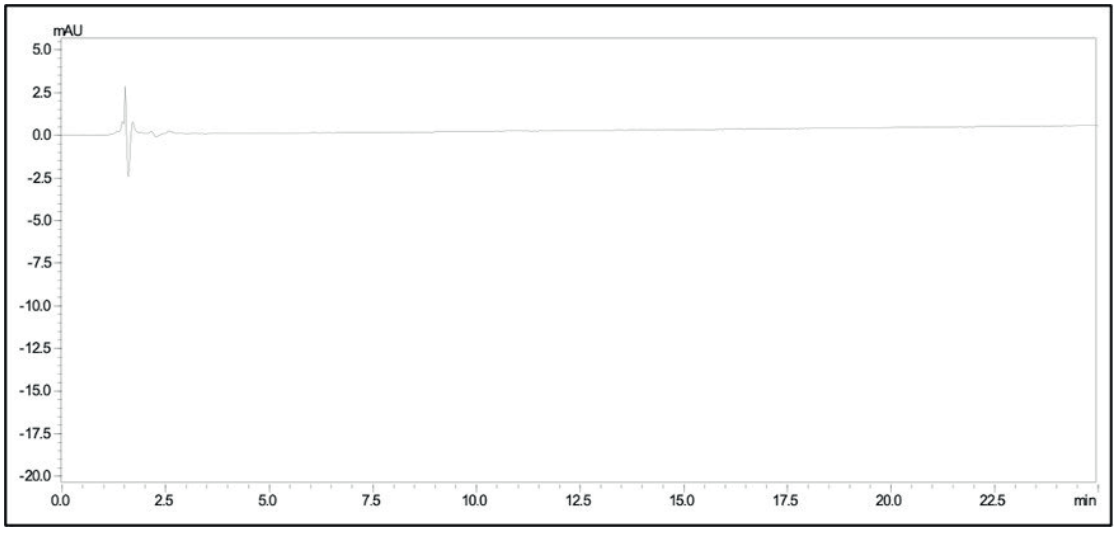

Figure 3. Chromatogram of placebo solution at 254 nm

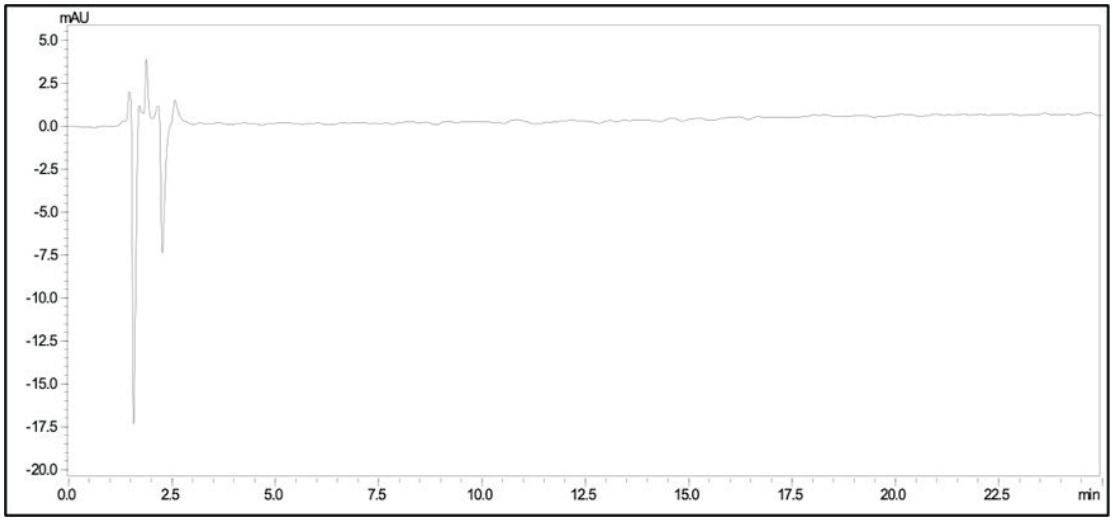

Figure 4. Chromatogram of placebo solution at 230 nm

Linearity

The linearity of the developed method was shown for both CHX and MN in the concentration range of 5 to 80 µg/mL with correlation coefficients of 0.9998 for CHX and 0.9999 for MN (Table 7, Figures 5 and 6).

Table 7. The results of linearity

	CHX	MN
Wavelength	254	230
Regression equation	y = 36394x - 89879	y = 25782x - 18982
Correlation coefficient (R^2)	0.9998	0.9999
Range	5 - 80 µg/mL	5 - 80 µg/mL

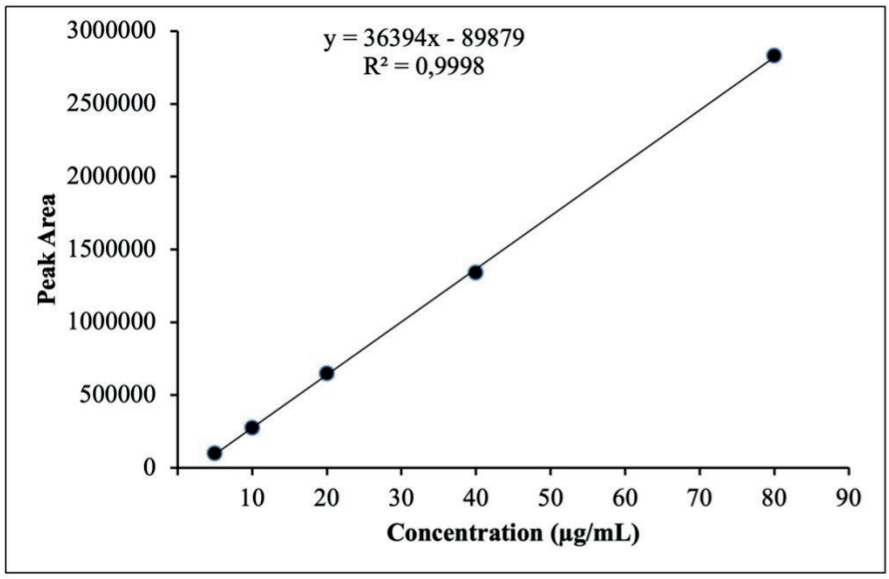

Figure 5. The calibration curve for CHX

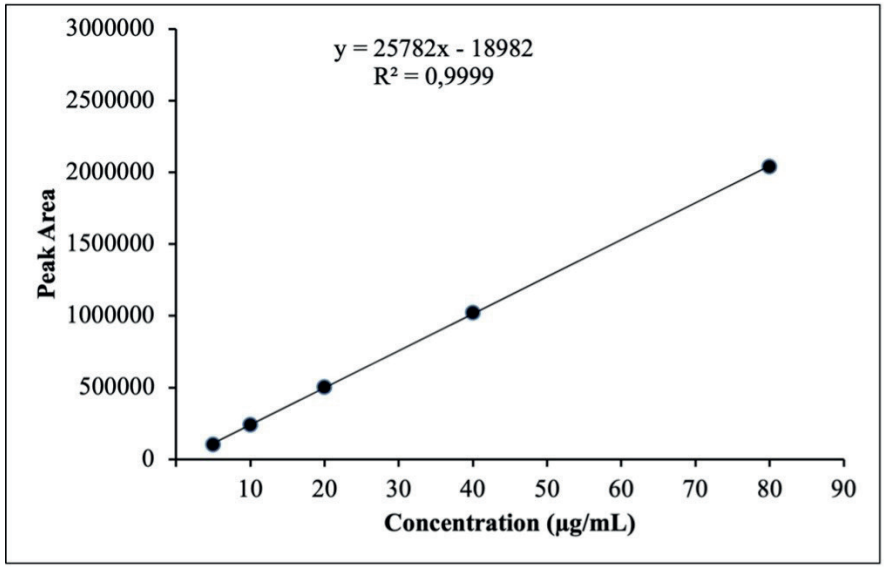

Figure 6. The calibration curve for MN

Accuracy and precision

% RSD values smaller than 1.5, recovery % larger than 98 % with very low % bias values were obtained with both intra- and inter-day analyses, indicating the precision and accuracy of the developed method (Table 8). The p-value for % recovery of CHX was 0.64 ($p>0.05$) and 0.8 ($p>0.05$) for MN according to the t-test results. There was no significant difference between intraday and interday results.

Table 8. Accuracy and precision of the developed method

	Theoretical conc. (µg/mL)	Intra-day				Inter-day (three consecutive days)			
		Measured conc. (µg/mL) ± SD	Precision RSD %	Accuracy Recovery %	Accuracy Bias %	Measured conc. (µg/mL) ± SD	Precision RSD %	Accuracy Recovery %	Accuracy Bias %
CHX	10	9.98±0.09	0.92	99.8	-0.2	10.1±0.1	0.77	100.6	0.6
	20	20.3±0.1	0.21	101.5	1.45	19.91±0.1	0.40	99.6	-0.4
	40	39.33±0.6	1.42	98.2	-1.75	40.81 ±0.11	0.29	102	2
MN	10	10.1±0.1	0.93	100.4	0.4	9.89±0.08	0.82	98.9	-1.1
	20	20.2±0.3	1.29	100.9	0.85	20.2±0.3	1.5	100.9	0.9
	40	40.3 ±0.4	0.96	100.8	0.85	40.7±0.6	1.46	101.7	1.7

Ruggedness

The % recovery results and %RSD of peak area and retention time obtained by two different analysts are given in Table 9 and Table 10. The results obtained were statistically evaluated with the t-test and there was no difference between two analysts (p >0,05). Moreover, % RSD values were found to be smaller than 1.48 indicating the ruggedness of the developed method (Table 10).

Table 9. The results of ruggedness by two different analysts

	CHX		MN	
	Analyst A	Analyst B	Analyst A	Analyst B
Measured concentration (µg/mL)	20.34	20.41	20.43	20.33
	20.26	20.36	20.27	20.26
	20.28	19.95	19.84	20.05
	20.22	20.33	19.88	19.62
	20.33	20.44	20.17	20.25
Mean Concentration (µg/mL) ± SD	20.2±0.05	20.3 ± 0.2	20,12±0,25	20.1±0.3
Recovery %	101.4	101.2	100.6	100.51

Table 10. The system suitability parameters of ruggedness results

	% RSD of retention time		% RSD of peak area	
	Analyst A	Analyst B	Analyst A	Analyst B
CHX	0.38	0.07	0.27	1.13
MN	0.14	0.17	1.29	1.48

Robustness

The robustness of the developed method was evaluated with different column temperatures and flow rates. The %RSD values of retention time at different conditions are given in Table 11. The % RSD values were smaller than 0,72. The robustness of the method has been shown (Table 11). The results obtained were statistically evaluated with the t-test and p >0,5 was obtained.

Table 11. The results of robustness by different chromatographic conditions

Chromatographic conditions	Value	CHX		MN	
		Retention time	% RSD	Retention time	% RSD
Column Temperature (°C)	39	14.49	0.32	3.88	0.04
	40	14.59	0.36	3.89	0.21
Flow rate (mL/min)	1	14.06	0.72	3.87	0.18
	1.2	15.25	0.53	3.77	0.24

Detection and Quantification Limits

LOD obtained for CHX and MN were 1.61 µg/mL and 1.06 µg/mL, respectively. LOQ for CHX and MN were 4.87 µg/mL and 3.21 µg/mL, respectively.

Stability

It was demonstrated that sample solutions were stable in mobile phase for 24h, with RSD% <1.3 and recovery % >98.5 for both MN and CHX. Furthermore, the recovery % was found to be >98 also in the dissolution medium (pH 5.0 phosphate buffer containing 0.5% Tween 80) (Table 12).

Table 12. The stability results (n = 6)

	Mobile Phase					Dissolution Medium				
	Theoretical conc. (µg/mL)	Time (h)	Measured conc. (µg/mL) ± SD	Recovery %	RSD %	Theoretical conc. (µg/mL)	Time (h)	Measured conc. (µg/mL) ± SD	Recovery %	RSD %
CHX	20	0	20.3± 0.1	101.5	0.2	80	0	80.2±0.78	100.3	0.97
	20	12	19.9± 0.2	99.5	0.9	80	3	79.4±0.9	99.2	1.12
	20	24	19.9± 0.2	99.9	0.8	80	6	80.4±0.7	100.5	0.83
MN	20	0	20.2± 0.3	100.9	1.3	80	0	80.9±0.7	101.2	0.88
	20	12	19.7 ± 0.2	98.6	0.9	80	3	80.2±0.5	100.2	0.59
	20	24	19.7 ± 0.1	98.5	0.2	80	6	78.5±0.2	98.1	0.26

The results of the validation showed that the HPLC method possesses significant linearity, specificity, selectivity, accuracy, precision, sensitivity, high efficiency and resolution, and no interference with the excipients used in the formulation.

Sample solutions were shown to be stable during analysis and the developed method was shown to be applicable to the sample solutions taken at dissolution studies without any stability problems.

CONCLUSION

We have successfully developed an HPLC method for simultaneous analysis of CHX and MN with short analysis time and high reproducibility, repeatability and sensitivity. Upto the authors knowledge, this is the first report in the literature for simultaneous analysis of CHX and MN from a chitosan-based gel formulation. Best chromatographic conditions were obtained with ACE® HPLC C8 column of 5 µm particle size (150 × 4.6 mm), with the mobile phase consisting of the mixture of methanol:20 mM pH 6.9 phosphate buffer (0.2 % TEA) (75:25 v/v), providing sufficient selectivity and sensitivity in a short separation time with acceptable peak characteristics, number of theoretical plates and acceptable resolution of MN and CHX, confirming the capability of the developed method. Furthermore, preparation of samples (extraction of MN and CHX from the gels and dilution) was also successful developed allowing recovery % >98. The developed method is suggested for simultaneous analysis of CHX and MN in gel formulations for quality control and in vitro tests to assure the quality and efficacy of the pharmaceutical preparations.

ACKNOWLEDGEMENTS

Authors are thankful to IE Ulagay–Menarini, İstanbul, Turkey for providing Miconazole nitrate and Koyo Company, Japan for providing chitosan as a generous gift. This work was supported by Hacettepe University Scientific Research Coordination Unit, Project number: THD-2020-18516

CONFLICT OF INTEREST

The authors declare that there is no conflict of interest.

AUTHOR CONTRIBUTION STATEMENT

Idea (SŞ), planning the development of HPLC analyses methodology for the active substances (SŞ, MÇ, ET and SP), the manuscript designing and editing (SŞ, MÇ, SP and ET), performing experiments (ET, SP), data interpretation (SŞ, ÇM, SP and ET), literature review (SŞ, ET and SP).

REFERENCES

Abdelrahman, M. M., Naguib, I., Nagieb, H. M., & Zaazaa, H. E. (2017). Different spectrophotometric methods for determination of miconazole nitrate and hydrocortisone in bulk and in topical pharmaceutical preparation without prior separation. *Chem Res J, 2*(2), 56-65.

Abdelrahman, M. M., Naguib, I. A., Elsayed, M. A., & Zaazaa, H. A. (2016). Spectrophotometric Methods for Quantitative Determination of Chlorhexidine Gluconate and its Major Impurity, Metabolite and Degradation Product: Para-chloro-aniline. *Anal Chem Lett, 6*(3), 232-248. https://doi.org/10.1080/22297928.2016.1196148

Abtheen, K. S. S. A., Maheswari, R., Shanmugasundaram, P., & Vijeyaanandhi, M. (2008). Simultaneous estimation of chlorhexidine gluconate, metronidazole, lignocaine hydrochloride and triamcinolone acetonide in combined dosage form by RP-HPLC. *Asian J Chem, 20*(2), 1130-1136.

Al-Badr, A. A. (2005). Miconazole Nitrate: Comprehensive Profile. In H. G. Brittain (Ed.), *Profiles of Drug Substances, Excipients and Related Methodology* (pp. 3-65). Academic Press.

Ammara, S., Syed, H. K., Sajid, A., Muhammad, I., Ikram, u. K., Akhtar, R., Muhammad, I. Q., & Khizar, A. (2018). Miconazole Nitrate Microemulsion: Preparation, Characterization and Evaluation for Enhancement of Antifungal Activity. *Lat Am J Pharm, 37*, 1578-1586.

Aronson, J. K. (2016). Chlorhexidine. In J. K. Aronson (Ed.), *Meyler's Side Effects of Drugs (Sixteenth Edition)* (pp. 239-248). Elsevier.

Atiyeh, B. S., Dibo, S. A., & Hayek, S. N. (2009). Wound cleansing, topical antiseptics and wound healing. *Int Wound J, 6*(6), 420-430. https://doi.org/10.1111/j.1742-481X.2009.00639.x

Belal, T. S., & Haggag, R. S. (2012). Gradient HPLC-DAD stability indicating determination of miconazole nitrate and lidocaine hydrochloride in their combined oral gel dosage form. *J Chromatogr Sci, 50*(5), 401-409. https://doi.org/10.1093/chromsci/bms019

Borissova, R., & Mandjukova, S. (1997). Titrimetric and spectrophotometric determination of chlorhexidine digluconate in tooth pastes. *Fresenius J Anal Chem, 357*(7), 977-980. https://doi.org/10.1007/s002160050285

Bouckaert, S., & Remon, J. P. (1993). In-vitro bioadhesion of a buccal, miconazole slow-release tablet. *J Pharm Pharmacol, 45*(6), 504-507. https://doi.org/10.1111/j.2042-7158.1993.tb05588.x

Brookes, Z. L. S., Bescos, R., Belfield, L. A., Ali, K., & Roberts, A. (2020). Current uses of chlorhexidine for management of oral disease: a narrative review. *J Dent, 103*, 103497. https://doi.org/10.1016/j.jdent.2020.103497

Cartagena, A. F., Lyra, A. M., Kapuchczinski, A. C., Urban, A. M., Esmerino, L. A., Klein, T., Nadal, J. M., Farago, P. V., & Campanha, N. H. (2017). Miconazole Nitrate-loaded Microparticles For Buccal Use: Immediate Drug Release and Antifungal Effect. *Curr Drug Deliv, 14*(8), 1144-1153. https://doi.org/10.2174/1567201813666161006115041

Chiapetta, S., Oliveira, É., Olivier, B., Mercante, L., Henriques, D., & Pereira Netto, A. (2011). Intralaboratory Validation, Comparison and Application of HPLC-UV-DAD Methods for Simultaneous Determination of Benzalkonium Chloride, Chlorexidine Digluconate and Triclosan. *J Braz Chem Soc, 22*, 1913-1920. https://doi.org/10.1590/S0103-50532011001000012

Denton, G. W. (2001). Chapter 15 - Chlorhexidine. In S. S. Block (Ed.), *Disinfection, sterilization, and preservation* (5th ed., pp. 321-333). Lippincott Williams & Wilkins.

Dimopoulou, M., Mourouti, C.-S., Vertzoni, M., Symillides, M., & Reppas, C. (2015). In-vitro evaluation of performance of solid immediate release dosage forms of weak bases in upper gastrointestinal lumen: experience with miconazole and clopidogrel salts. *J Pharm Pharmacol, 68*(5), 579-587. https://doi.org/10.1111/jphp.12406

Ei, Z., Pimthon, J., Vajragupta, O., Leanpolchareanchai, J., & Phechkrajang, C. (2016). Development and validation of high-performance liquid chromatography method for determination of miconazole , triamcinolone , methylparaben and propylparaben in cream. *Mahidol Univ J Pharm Sci, 43*(5), 211-221. https://doi.org/10.14456/mujps.2016.24

Eticha, T., Kahsay, G., Hailu, T., Gebretsadikan, T., Asefa, F., Gebretsadik, H., & Thangabalan, B. (2018). Development and Validation of an Extractive Spectrophotometric Method for Miconazole Nitrate Assay in Pharmaceutical Formulations. *J Anal Methods Chem, 2018*, 1-5. https://doi.org/10.1155/2018/2191072

Facts about Chlorhexidine Gluconate. (2017). FDA. https://www.fda.gov/drugs/drug-safety-and-availability/fda-drug-safety-communication-fda-warns-about-rare-serious-allergic-reactions-skin-antiseptic#:~:text=Facts%20about%20Chlorhexidine%20Gluconate,-Chlorhexidine%20gluconate%20is&text=The%20OTC%20products%20are%20available,Pharmaseal%20Scrub%20Care%2C%20and%20Prevantics. , Access date: 24 August 2022

Final Report on the Safety Assessment of Chlorhexidine/Chlorhexidine Diacetate/Chlorhexidine Dihydrochloride/Chlorhexidine Digluconate (1993). *J Am Coll Toxicol, 12*(3), 201-223. https://doi.org/10.3109/10915819309140642

Frymus, T., Gruffydd-Jones, T., Pennisi, M. G., Addie, D., Belák, S., Boucraut-Baralon, C., Egberink, H., Hartmann, K., Hosie, M. J., Lloret, A., Lutz, H., Marsilio, F., Möstl, K., Radford, A. D., Thiry, E., Truyen, U., & Horzinek, M. C. (2013). Dermatophytosis in Cats: ABCD guidelines on prevention and management. *J Feline Med Surg, 15*(7), 598-604. https://doi.org/10.1177/1098612X13489222

Ghibaudo, G., Santospirito, D., Sala, A., Flisi, S., Taddei, S., Cavirani, S., & Cabassi, C. S. (2016). In vitro antimicrobial activity of a gel containing antimicrobial peptide AMP2041, chlorhexidine digluconate and Tris-EDTA on clinical isolates of Pseudomonas aeruginosa from canine otitis. *Vet Dermatol, 27*(5), 391-e398. https://doi.org/10.1111/vde.12371

Greenstein, G., Berman, C., & Jaffin, R. (1986). Chlorhexidine: An Adjunct to Periodontal Therapy. *J Periodontol, 57*(6), 370-377. https://doi.org/10.1902/jop.1986.57.6.370

Guaguère, E. (1996). Topical treatment of canine and feline pyoderma. *Vet Dermatol, 7*, 145-151. https://doi.org/10.1111/j.1365-3164.1996.tb00239.x

Guardabassi, L., Ghibaudo, G., & Damborg, P. (2010). In vitro antimicrobial activity of a commercial ear antiseptic containing chlorhexidine and Tris-EDTA. *Vet Dermatol, 21*(3), 282-286. https://doi.org/10.1111/j.1365-3164.2009.00812.x

Havlíková, L., Matysová, L., Nováková, L., Hájková, R., & Solich, P. (2007). HPLC determination of chlorhexidine gluconate and p-chloroaniline in topical ointment. *J Pharm Biomed Anal, 43*(3), 1169-1173. https://doi.org/10.1016/j.jpba.2006.09.037

Heneedak, H. M., Salama, I., Mostafa, S., & El-Sadek, M. (2012). HPLC and chemometric methods for the simultaneous determination of miconazole nitrate and nystatin. *J Chromatogr Sci, 50*(10), 855-861. https://doi.org/10.1093/chromsci/bms127

Hoang, T. P. N., Ghori, M. U., & Conway, B. R. (2021). Topical Antiseptic Formulations for Skin and Soft Tissue Infections. *Pharmaceutics, 13*(4), 558. https://doi.org/10.3390/pharmaceutics13040558

Işık, B. D., & Acar, E. T. (2018). Development and Validation of an HPLC Method for the Simultaneous Determination of Flurbiprofen and Chlorhexidine Gluconate. *Chromatographia, 81*(4), 699-706. https://doi.org/10.1007/s10337-018-3485-5

Kampf, G. (2018). Chlorhexidine Digluconate. In G. Kampf (Ed.), *Antiseptic Stewardship: Biocide Resistance and Clinical Implications* (pp. 429-534). Springer International Publishing.

Kenechukwu, F. C., Attama, A. A., Ibezim, E. C., Nnamani, P. O., Umeyor, C. E., Uronnachi, E. M., Gugu, T. H., Momoh, M. A., Ofokansi, K. C., & Akpa, P. A. (2018). Surface-modified mucoadhesive microgels as a controlled release system for miconazole nitrate to improve localized treatment of vulvovaginal candidiasis. *Eur J Pharm Sci, 111*, 358-375. https://doi.org/10.1016/j.ejps.2017.10.002

Kumar, M. S., & P.Shanmugapandiyan. (2017). RP-HPLC-PDA Method For The Simultaneous Determination of Clobetasol, Neomycin, Chlorhexidine And Miconazole In Bulk And Marketed Formulation. *Int J Pharm Technol*, 9(2), 29906 - 29919.

Lakka, N. S., & Kuppan, C. (2019). Principles of Chromatography Method Development. In O.-M. Boldura, C. Baltă, & N. S. Awwad (Eds.), *Biochemical Analysis Tools - Methods for Bio-Molecules Studies*. IntechOpen.

Main, R. C. (2008). Should chlorhexidine gluconate be used in wound cleansing? *J Wound Care, 17*(3), 112-114. https://doi.org/10.12968/jowc.2008.17.3.28668

Martindale: The Complete Drug Reference. (2009). (36th ed.). London: Pharmaceutical Press.

Másquio Fiorentino, F. A., Corrêa, M. A., & Nunes Salgado, H. R. (2010). Analytical Methods for the Determination of Chlorhexidine: A Review. *Crit Rev Anal Chem, 40*(2), 89-101. https://doi.org/10.1080/10408340903232020

Mohammadi, Z. (2008). Chlorhexidine gluconate, its properties and applications in endodontics. *Iran Endod J, 2*(4), 113-125.

Moldoveanu, S. C., & David, V. (2017). Chapter 13 - Solvents, Buffers, and Additives Used in the Mobile Phase. In S. C. Moldoveanu & V. David (Eds.), *Selection of the HPLC Method in Chemical Analysis* (1st ed., pp. 393-450). Elsevier.

Mueller, R. S. (2008). Chapter 24 - Topical dermatological therapy. In J. E. Maddison, S. W. Page, & D. B. Church (Eds.), *Small Animal Clinical Pharmacology* (2nd ed., pp. 546-556). W.B. Saunders.

Nenoff, P., Koch, D., Krüger, C., Drechsel, C., & Mayser, P. (2017). New insights on the antibacterial efficacy of miconazole in vitro. *Mycoses, 60*, 552—557. https://doi.org/10.1111/myc.12620

Paulson, D. S. (2002). Chlorhexidine Gluconate. In D. S. Paulson (Ed.), *Handbook of Topical Antimicrobials* (1st ed., pp. 117-122). CRC Press.

Perrins, N., & Bond, R. (2003). Synergistic inhibition of the growth in vitro of *Microsporum canis* by miconazole and chlorhexidine. *Vet Dermatol, 14*(2), 99-102. https://doi.org/10.1046/j.1365-3164.2003.00325.x

Qushawy, M., Nasr, A., Abd-Alhaseeb, M., & Swidan, S. (2018). Design, Optimization and Characterization of a Transfersomal Gel Using Miconazole Nitrate for the Treatment of Candida Skin Infections. *Pharmaceutics, 10*(1), 26. https://doi.org/10.3390/pharmaceutics10010026

Rawlings, J. M., Gorrel, C., & Markwell, P. J. (1998). Effect on Canine Oral Health of Adding Chlorhexidine to a Dental Hygiene Chew. *J Vet Dent, 15*(3), 129-134. https://doi.org/10.1177/089875649801500303

Rochette, F., Engelen, M., & Vanden Bossche, H. (2003). Antifungal agents of use in animal health--practical applications. *J Vet Pharmacol Ther, 26*(1), 31-53. https://doi.org/10.1046/j.1365-2885.2003.00457.x

Sahoo, D. R., & Jain, S. (2016). A Rapid and Validated RP-HPLC Method for the Simultaneous Quantification of Benzoic Acid, Metronidazole and Miconazole Nitrate in Vaginal Formulations. *J Chromatogr Sci, 54*(9), 1613-1618. https://doi.org/10.1093/chromsci/bmw113

Salah, S., Awad, G. E. A., & Makhlouf, A. I. A. (2018). Improved vaginal retention and enhanced antifungal activity of miconazole microsponges gel: Formulation development and in vivo therapeutic efficacy in rats. *Eur J Pharm Sci, 114*, 255-266. https://doi.org/10.1016/j.ejps.2017.12.023

Samanidou, V. F. (2015). Basic LC Method Development and Optimization. In J. L. Anderson, A. Berthod, V. Pino, & A. Stalcup (Eds.), *Analytical Separation Science* (1st ed., pp. 25-42). Wiley-VCH Verlag GmbH & Co. KGaA.

Sarkiala-Kessel, E. M. (2012). Chapter 3 - Use of antibiotics and antiseptics. In F. J. Verstraete & M. J. Lommer (Eds.), *Oral and Maxillofacial Surgery in Dogs and Cats* (1st ed., pp. 15-21). W.B. Saunders.

Sawyer, P. R., Brogden, R. N., Pinder, R. M., Speight, T. M., & Avery, G. S. (1975). Miconazole: A Review of its Antifungal Activity and Therapeutic Efficacy. *Drugs, 9*(6), 406-423. https://doi.org/10.2165/00003495-197509060-00002

Şenel, S. (2010). Potential applications of chitosan in oral mucosal delivery. *J Drug Deliv Sci Technol, 20*(1), 23-32. https://doi.org/10.1016/S1773-2247(10)50003-0

Şenel, S. (2020). Current status and future of chitosan in drug and vaccine delivery. *React Funct Polym, 147*, 104452. https://doi.org/10.1016/j.reactfunctpolym.2019.104452

Şenel, S., İkinci, G., Kaş, S., Yousefi-Rad, A., Sargon, M. F., & Hıncal, A. A. (2000). Chitosan films and hydrogels of chlorhexidine gluconate for oral mucosal delivery. *Int J Pharm, 193*(2), 197-203. https://doi.org/10.1016/S0378-5173(99)00334-8

Siegel, M. R., Kerkenaar, A., & Sijpesteijn, A. K. (1977). Antifungal activity of the systemic fungicide imazalil. *Neth J PI Path, 83*(1), 121-133. https://doi.org/10.1007/BF03041427

Silvestri, D. L., & McEnery-Stonelake, M. (2013). Chlorhexidine: Uses and Adverse Reactions. *Dermatitis, 24*(3), 112 - 118. https://doi.org/10.1097/DER.0b013e3182905561

Stojanov, I., Milovanovic, A., RuŽIĆ-MusliĆ, D., Ratajac, R., Baloš, M., Maksimovic, N., & Apić, J. (2018). The application of EDTA-Tris and chlorhexidine in the treatment of endometritis as a replacement for antibiotic therapy in cows. *Turk J Vet Anim Sci, 42*, 91-96. https://doi.org/10.3906/vet-1703-74

Tejada, G., Lamas, M. C., Svetaz, L., Salomón, C. J., Alvarez, V. A., & Leonardi, D. (2018). Effect of drug incorporation technique and polymer combination on the performance of biopolymeric antifungal buccal films. *Int J Pharm, 548*(1), 431-442. https://doi.org/10.1016/j.ijpharm.2018.07.023

Türkmen, E., Parmaksız S., Nigiz Ş., Sağıroğlu M., Şenel S. (2022). A safe bioadhesive system for topical delivery of combined antimicrobials in treatment of skin infections in veterinary medicine. *J Drug Deliv Sci Technol (under review)*.

Validation of Analytical Procedures: Text and Methodology Q2 (R1) (1995). International Conference on Harmonization (ICH). https://database.ich.org/sites/default/files/Q2%28R1%29%20Guideline.pdf, Access date: 24 August 2022

Valkó, K., Snyder, L. R., & Glajch, J. L. (1993). Retention in reversed-phase liquid chromatography as a function of mobile-phase composition. *J Chromatogr A, 656*(1), 501-520. https://doi.org/10.1016/0021-9673(93)80816-Q

Velegraki, A., Cafarchia, C., Gaitanis, G., Iatta, R., & Boekhout, T. (2015). Malassezia Infections in Humans and Animals: Pathophysiology, Detection, and Treatment. *PLOS Pathogens, 11*(1), e1004523. 10.1371/journal.ppat.1004523

Wade, T. R., Jones, H. E., & Chanda, J. J. (1979). Intravenous miconazole therapy of mycotic infections. *Arch Intern Med, 139*(7), 784-786. https://doi.org/10.1001/archinte.1979.03630440046016

What Is Periochip. (2017). https://www.periochip.com/what-is-periochip/. Access date: 24 August 2022

Zeng, P., Rao, A., Wiedmann, T. S., & Bowles, W. (2009). Solubility Properties of Chlorhexidine Salts. *Drug Dev Ind Pharm, 35*(2), 172-176. https://doi.org/10.1080/03639040802220318

FABAD J. Pharm. Sci., 48, 1, 91-104, 2023
Doi: 10.55262/fabadeczacilik.1164699
RESEARCH ARTICLE

Caffeine May Improve the Chemotherapeutic Effect of Docetaxel by Inducing Unfolded Protein Response and Autophagy in Breast Cancer Cells

Yalcin ERZURUMLU[*°], Deniz CATAKLI[**], Hatice Kubra DOGAN[***], Esra AYDOGDU[****]

Caffeine may ımprove the chemotherapeutic effect of docetaxel by ınducing unfolded protein response and autophagy in breast cancer cells

SUMMARY

Breast cancer is the most frequently diagnosed cancer type among women. Chemotherapeutic agents are widely used in the treatment of breast cancer, but acquired drug resistance limits their effectiveness. Therefore, there is a continuing need for more effective treatment approaches with fewer side effects. Caffeine is one of the naturally occurring xanthines in coffee beans, caffeine is the most commonly used psychoactive substance worldwide. Numerous studies have highlighted the health benefits of coffee consumption, including reducing the risk of heart disease and certain cancers. Docetaxel is a second-generation antineoplastic agent of the taxane family and is widely used in the treatment of numerous cancers such as breast cancer. Herein, we evaluated the effect of caffeine and its combination with docetaxel on MCF-7 breast cancer cells. To test the effect of caffeine and its combination with docetaxel, we evaluated the autophagy, ubiquitin-proteasome system (UPS), unfolded protein response (UPR) signaling and apoptosis-related protein levels by immunoblotting. Cell viability was measured by WST-1 method. Morphological alterations in cells were evaluated in microscopical examinations. We found that caffeine remarkably induced UPR signaling, accelerated autophagic flux, and UPS-dependent protein turnover. Co-administration of caffeine and docetaxel strongly diminished the viability of MCF-7 cells by expanding the cytotoxic effect of docetaxel through accelerating the UPS-dependent protein turnover, induction of UPR and autophagy and apoptotic protein levels in a dose-dependent manner. Our results suggest that caffeine supplementation with docetaxel may expand the chemotherapeutic efficiency of docetaxel in breast cancer.

Key Words: *Autophagy, Apoptosis, Breast cancer, Caffeine, Unfolded Protein Response, Docetaxel*

Kafein, meme kanseri hücrelerinde katlanmamış protein tepkisini ve otofajiyi indükleyerek dosetakselin kemoterapötik etkisini artırabilir

ÖZ

Meme kanseri, kadınlar arasında en sık teşhis edilen kanser türüdür. Kemoterapötik ajanlar meme kanseri tedavisinde yaygın olarak kullanılmaktadır, ancak kazanılmış ilaç direnci etkinliklerini sınırlamaktadır. Bu nedenle, daha az yan etkiye sahip ve daha etkili tedavi yaklaşımlarına ihtiyaç vardır. Kahve çekirdeklerinde doğal olarak bulunan ksantinlerden biri olan kafein, dünya çapında en yaygın kullanılan psikoaktif maddedir. Çok sayıda çalışma, kalp hastalığı ve bazı kanser risklerinde azalma da dahil olmak üzere kahve tüketiminin sağlığa faydalarına dikkat çekmiştir. Dosetaksel, taksan ailesinden ikinci nesil bir antineoplastik ajandır ve meme kanseri gibi çok sayıda kanserin tedavisinde yaygın olarak kullanılmaktadır. Bu çalışmada kafein ve dosetaksel kombinasyonunun MCF-7 meme kanseri hücreleri üzerindeki etkisini değerlendirdik. Kafeinin dosetaksel ile kombinasyonunun etkisini test etmek için otofaji, ubikitin-proteazom sistemi (UPS), katlanmamış protein yanıtı sinyali (UPR) ve apoptozisle ilgili protein seviyelerini immünoblotlama ile inceledik. Hücre canlılığı WST-1 yöntemi ile ölçüldü. Hücrelerdeki morfolojik değişiklikler mikroskopi ile değerlendirildi. Kafeinin dikkat çekici bir şekilde UPR sinyalini uyardığını, otofajik akışı hızlandırdığını ve UPS'ye bağlı protein dönüşümünü uyardığını belirledik. Kafein ve dosetakselin birlikte uygulanması, dosetakselin sitotoksik etkisini UPS aracılı protein işlenmesini hızlandırarak, UPR ve otofajiyi uyararak ve apoptotik protein seviyelerini doz bağımlı bir şekilde arttırarak MCF-7 hücrelerinin canlılığını güçlü bir şekilde azalttı. Sonuçlarımız, dosetaksel ile kafein takviyesinin meme kanserinde dosetakselin kemoterapötik etkinliğini genişletebileceğini düşündürmektedir.

Anahtar Kelimeler: *Otofaji, Apoptozis, Meme Kanseri, Kafein, Katlanmamış Protein Yanıtı, Dosetaksel*

Received: 20.08.2022
Revised: 29.11.2022
Accepted: 01.12.2022

[*] ORCID: 0000-0001-6835-4436, Suleyman Demirel University, Department of Biochemistry, Faculty of Pharmacy, Isparta, Turkey
[**] ORCID: 0000-0001-7327-5396, Suleyman Demirel University, Department of Pharmacology, Faculty of Medicine, Isparta, Turkey
[***] ORCID: 0000-0002-6061-1300, Suleyman Demirel University, Department of Bioengineering, Institute of Science, Isparta, Turkey
[****] ORCID: 0000-0003-0666-2067, Suleyman Demirel University, Department of Pharmaceutical Research and Development, Institute of Health Sciences, Isparta, Turkey

[°] Corresponding Author; Yalcin ERZURUMLU
Tel. +90 0246 311 0345 / +90 544 88 78 439, e.mail:yalcin.erzurumlu@gmail.com, yalcinerzurumlu@sdu.edu.tr

INTRODUCTION

Breast cancer is described as a heterogeneous neoplasm accumulation around the mammary epithelium. It is divided into different subtypes according to the origin of cancer or receptor expression profiles and incidence, risk factors, prognosis and treatment options show differences between these subtypes. Breast cancer is the most frequently diagnosed cancer type among the women and second most common cause of death from cancer in the United States (Prat et al., 2015; Trayes & Cokenakes, 2021). Although there are different treatment options for breast cancer including radiation, endocrine therapy, immunotherapy, and chemotherapy, the need for novel therapeutic approaches continues (Trayes & Cokenakes, 2021). Acquired drug resistance is the main reason limiting the efficacy of chemotherapeutic agents (Trayes & Cokenakes, 2021). Thus, improving alternative therapeutic options such as natural products or combining these products with existing therapies may offer a good treatment option for breast cancer.

Xanthine is a derivative of purine alkaloids with a wide range of biologically active components (Jacobson et al., 1985). One of the naturally occurring xanthines in coffee beans, caffeine (1,3,7-trimethylxanthine) is the most widely used psychoactive substance around the world. Coffee, tea and beverages such as cola are the main vehicles for caffeine consumption in daily routine (Campa et al., 2005; Mitchell et al., 2015). Numerous studies have shown the health benefits of coffee intake including decrement in the risk of heart disease, endothelial dysfunction, inflammation, diabetes incidence and risk of some cancers (Andersen et al., 2006; Ding et al., 2014; Lopez-Garcia et al., 2006; A. Wang et al., 2016). Anti-cancer effects of caffeine have been studied for a long time. Studies have demonstrated a negative correlation between coffee consumption and the occurrence of various cancer types such as glioma and endometrial cancer (Pranata et al., 2022). Also, it has been reported that using a combination of caffeine and other chemotherapeutic agents such as paclitaxel, cisplatin, 5-fluorouracil and doxorubicin has enhanced antitumor effects in various cancer types such as breast, colorectal, lung and hepatocellular carcinoma (Mhaidat et al., 2014; Tomita & Tsuchiya, 1989; Z. Wang et al., 2019; Yamamoto & Tsuchiya, 2011). However, the effects of caffeine on various cancer types, including breast cancer, are still controversial and have not been achieved consensus. Thus, the possible synergistic effects of the chemotherapeutic agent docetaxel, which is frequently used in clinical applications for many cancer types, with caffeine were investigated in the present study.

Docetaxel also known as Taxotere, is a second-generation antineoplastic agent of the taxane family. It inhibits proliferation and causes cell death by disrupting microtubule functions and leading to cell cycle arrest at the G2/M phase (Jordan & Wilson, 2004). The efficacy of docetaxel has been shown in various types of cancer such as head and neck, gastric, non-small lung, hormone-refractory prostate and breast as well (Lyseng-Williamson & Fenton, 2005). Although it is commonly used in the treatment of breast cancer, adverse effects like unpredictable hypersensitivity reactions, neutropenia, fluid retention, and ocular toxicity limit its usage in advanced and recurrent cancer (Palmeri et al., 2008). Combined treatment of docetaxel with other agents has proven its effectiveness. Also, it is a valuable agent as it is a first-line treatment option for metastatic and aggressive cancer types (Hikita et al., 2021). Therefore, it is important to investigate the combined applications of docetaxel with natural products that do not have side effects that will increase its biochemical action. Herein, we aimed to investigate the possible anti-cancer effects of caffeine and its combined administration with docetaxel on MCF-7 breast cancer cells.

In the present study, we tested the effects of caffeine and its combination with docetaxel on unfolded protein response (UPR) signaling, the ubiquitin-proteasome system (UPS), autophagy and apoptotic cell death in MCF-7 human breast cancer cells. Our

results suggest that caffeine supplementation with docetaxel may expand the chemotherapeutic efficiency of docetaxel in breast cancer cells. However, the potential enhancer effect of caffeine on docetaxel needs to be broadly investigated with advanced experimental models in *in vitro* and *in vivo.*

MATERIAL AND METHODS

Materials

All cell culture reagents including fetal bovine serum (FBS), L-Glutamine and additional cell culture grade growth requirements were purchased from Biological Industries. Dulbecco's Modified Eagle Medium (DMEM) was purchased from LONZA Bioscience. Docetaxel (#9886), Bafilomycin A1 (#54645) and Staurosporine (#9953) were obtained from Cell Signaling Technology, Tunicamycin (sc-3506A) from Santacruz Biotechnology. Rabbit polyclonal antibodies PERK (#24390-1-AP), IRE1α (#27528-1-AP), XBP-1s (#24868-1-AP), ATF4 (#10835-1-AP), ubiquitin (#10201-1-AP), BiP/GRP78 (#11587-1-AP) and PARP1 (#13371-1-AP) were obtained from Proteintech. Rabbit monoclonal antibody against Hrd1 (#14773) and rabbit polyclonal cytochrome-c (#11940), eIF2α (#9722), phospho-eIF2α (Ser51) (#9721), caspase-3 (#9662), Beclin-1 (#3495), Atg5 (#12994), LC3-I/II (#12741), p62/SQSTM1 (#5114) were obtained from Cell Signaling Technology. Mouse monoclonal beta-actin antibody (#A5316) was purchased from Sigma Aldrich. HRP-conjugated goat anti-mouse (#31430) or goat anti-rabbit (#31460) IgG (H+L) was purchased from Pierce. High pure dimethyl sulfoxide (DMSO) was obtained from Genaxxon bioscience. Caffeine (C0750) was obtained from Sigma Aldrich.

Cell Culture

Human epithelial metastatic adenocarcinoma cell line, MCF-7 (HTB-22™) was obtained from American Type Tissue Culture (ATCC). Cells were routinely propagated in DMEM enriched with 10% FBS, 5 mg ml^{-1} penicillin/streptomycin, and 2 mM L-glutamine in a conventional cell culture condition, humidified atmosphere of 5% CO_2 and 95% air at a constant temperature of 37 °C. The absence of mycoplasma contamination was routinely confirmed by using MycoAlert™ Mycoplasma Detection Kit (Lonza).

Docetaxel was dissolved in DMSO (Serva #20385.01) to prepare the stock solution. Caffeine was prepared in cell culture media. The final concentration did not exceed 0.05% of the DMSO application amount. For this purpose, docetaxel was prepared at 2000X concentration. An equal amount of DMSO was applied as a vehicle application.

WST-1 Cell Proliferation Assay

The cell proliferation was measured by WST-1 based cell proliferation assay according to the manufacturer's instructions (Takara). The cells were seeded in 96-well plate (5000 cells/wells). Compound was applied to the cells for 24 or 48 h. To analyze the cell proliferation, 20 µl WST-1 reactive was added per well and cells were incubated for 2 hours under the conventional cell culture conditions. The absorbance was read at 450nm, with 600nm set as the reference wavelength by microplate spectrophotometer (BioTek, Epoch 2). The results were graphed to % fold change.

Microscopic Examination

Morphological changes of cells were performed using a phase-contrast inverted microscope (Sunny SopTop ICX41) and a digital camera system (OD400UHW). All photographs were taken with a 20x lens.

Protein Isolation and Immunoblotting

Cells were lysed in a Radioimmunoprecipitation assay (RIPA) buffer. After the removal of pellet by centrifugation at 14.000 rpm for 20 min at 4°C, total protein concentrations were determined from supernatant by bicinchoninic acid assay (BCA) kit (Takara). Generally, 30 µg of total protein was used for immunoblotting studies. Samples were denatured in 4x Laemmli buffer at 95°C for 5 min and protein samples were separated on 12% - 15% hand-cast polyacrylamide gels. Separated proteins were transferred

to an Immun-blot® polyvinylidene difluoride (PVDF) membrane (Bio-Rad). The membrane was blocked in 5% nonfat dry milk in Phosphate-buffered saline (PBS) containing 0.1% Tween (PBS–Tween) for 1 h which was followed by incubation with the primary antibody in blocking buffer that was waited for 1-2 hours at room temperature. Protein bands were visualized by using clarity western enhanced chemiluminescence (ECL) substrate (Bio-Rad) and ChemiDoc XRS+ system (Bio-Rad).

Statistical Analysis

The results were presented as mean ± standard deviation (SD). The statistical significance of the differences between the groups was determined by the two-tailed equal variance student's t-test with a minimum confidence interval of 95% using GraphPad Prism 7 software. To determine differences among the groups, one-way ANOVA and Tukey's tests were used. The significant level was set at 5% ($p < 0.05$) for all tests.

RESULTS AND DISCUSSION

Caffeine remarkably induces UPR signaling and co-treatment with docetaxel exhibits a stronger effect on UPR in breast cancer cells.

Firstly, we determined the IC_{50} values of caffeine and docetaxel for 24 and 48 hours in MCF-7 cells (Figure 1a, b). We found that IC_{50} values of caffeine were 17.131mM ± 1.13 and 9.813mM ± 1.09 for 24 and 48 hours, respectively (Figure 1a). IC_{50} values for docetaxel were determined as 23.621nM ± 1,84 and 14.207nM ± 1.35 for 24 and 48 hours, respectively (Figure 1b). In further analysis, doses of 15nM for docetaxel and 1, 5 and 10mM for caffeine were used according to the cell viability assay data.

To test the effect of caffeine on UPR signaling, we treated the MCF-7 cells with 1, 5, 10mM caffeine for 24 hours and then tested the inositol-requiring enzyme-1α (IRE1α) and protein kinase R (PKR)-like endoplasmic reticulum kinase (PERK) branches of UPR proteins including total-eukaryotic translation initiation factor 2 (eIF2α), phospho (Ser51)-eIF2α, activating transcription factor 4 (ATF4) and PERK; IRE1α and spliced form of X-box binding protein 1 (XBP-1s) proteins and also ER stress related chaperone binding immunoglobulin protein (BiP)/glucose-regulated protein 78 (GRP78) by immunoblotting. Our data indicated that caffeine treatment gradually increased protein expression level of all tested UPR members in a dose-dependent manner (Figure 1c). Similar to caffeine, docetaxel was determined to stimulate UPR proteins compared to the control group (Figure 1d). Moreover, co-administration of caffeine with docetaxel more strongly induced the expression of all tested proteins in a dose-dependent manner compared to docetaxel alone administration (Figure 1d). These results suggested that caffeine positively regulated UPR signaling and its combined treatment with docetaxel expanded the chemotherapeutic efficiency by synergistically affecting UPR signaling.

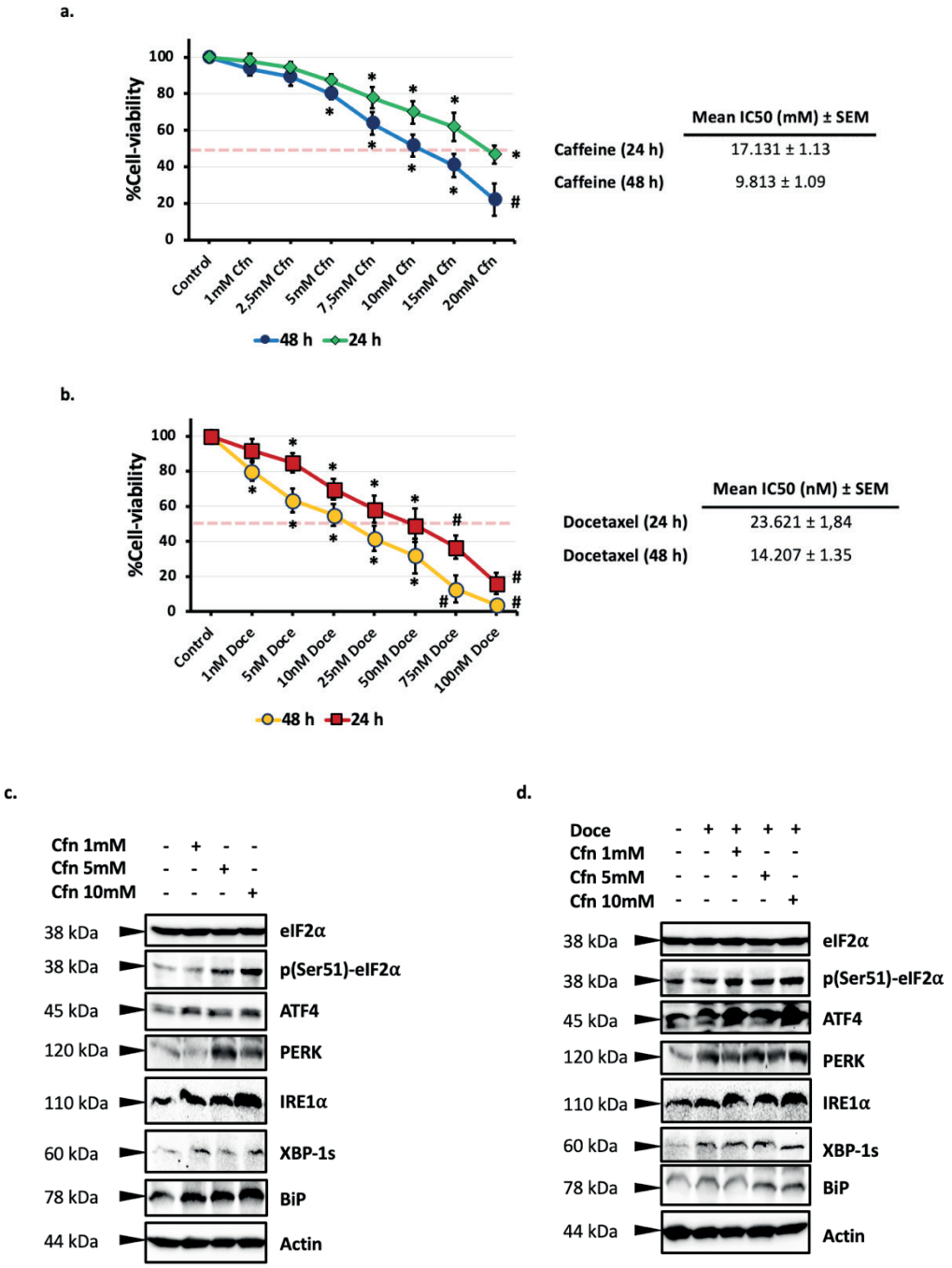

Figure 1. Evaluation of caffeine and its combination with docetaxel on UPR related proteins. (a, b) The effect of caffeine and docetaxel on the cell viability of MCF-7 cells was analyzed using the WST-1 assay. IC_{50} values were calculated using GraphPad Prism 7 Data represented as mean ± SE of three independent experiments made in three replicates. (c) MCF-7 cells were treated with a vehicle or 1, 5 and 10mM for 24 hours and then UPR related protein levels were analyzed by immunoblotting using antibodies raised against them. (d) Combine treatment of caffeine as indicated doses and 15nM docetaxel for 24 hours and then the expression level of UPR proteins was analyzed by immunoblotting. Beta-actin was used as a loading control.

Caffeine dose-dependently decreased the poly-ubiquitination and it exhibits a synergistic effect with docetaxel in breast cancer cells

To evaluate the effect of caffeine on protein turnover, we tested the poly-ubiquitination pattern in MCF-7 cells by immunoblotting. We found that caffeine treatment dose-dependently reduced the poly-ubiquitination levels compared to control group (Figure 2a). Next, we examined the levels of HMG-CoA reductase degradation 1 (Hrd1)/Synoviolin 1 (SYVN1), which is the major E3 ubiquitin ligase enzyme that plays a role in ER-associated degradation (ERAD), we determined that Hrd1 protein levels increased in a dose-dependent manner (Erzurumlu & Ballar, 2017)(Figure 2a). Combined treatment of caffeine with docetaxel more strongly induced Hrd1 protein levels compared to the docetaxel alone group (Figure 2b). Also, the poly-ubiquitination pattern was more robustly decreased by the caffeine-docetaxel group in a dose-dependent manner (Figure 2b).

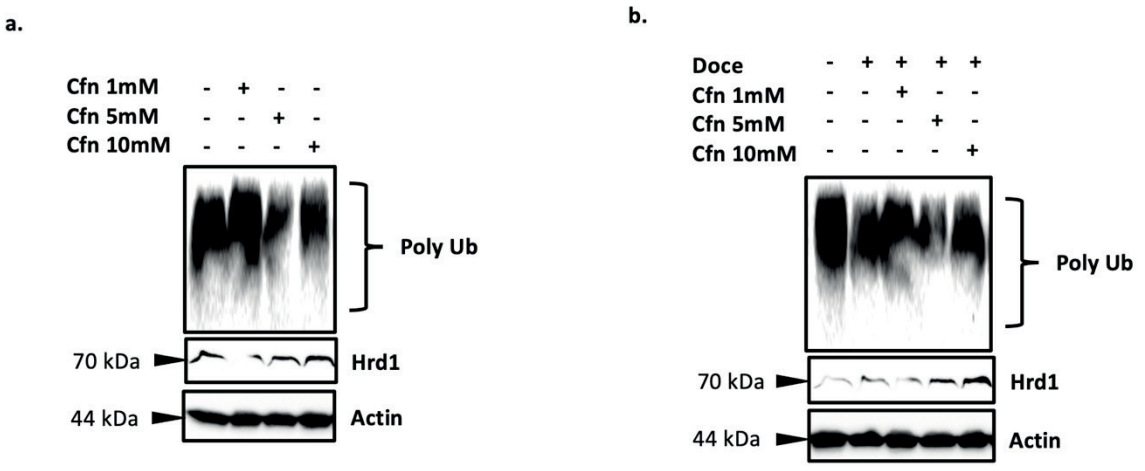

Figure 2. The effect of caffeine and co-treatment with docetaxel on ERAD E3 ligase Hrd1 and poly-ubiquitination pattern. (a) MCF-7 cells were treated with a vehicle or as indicated doses of caffeine for 24 hours and Hrd1 and poly-ubiquitination levels were analyzed by immunoblotting. (b) As indicated doses of caffeine and its combination with docetaxel were applied to the MCF-7 cells for 24 hours and target proteins were analyzed by immunoblotting. Beta-actin was used as a loading control.

Caffeine ameliorates the biochemical effect of docetaxel by autophagic induction

We investigated the effects of caffeine on basal autophagic activity in MCF-7 by testing the Beclin-1, autophagy related 5 (Atg5) protein levels, p62/sequestosome 1 (SQSTM1) turnover and microtubule associated protein 1 light chain 3 (LC3)-I conversion to LC3-II by immunoblotting. Our data indicated that caffeine administration gradually increased Beclin1 levels whereas we did not determine any alteration level of Atg5 at administered all doses of caffeine (Figure 3a). p62/SQSTM1 levels slightly decreased by caffeine treatment in a dose-dependent manner. More strikingly, LC3-I conversion to LC3-II remarkably accelerated with caffeine (Figure 3a).

Next, we evaluated the combined effect of caffeine with docetaxel on autophagy in MCF-7 cells. Docetaxel administration does not affect the Atg5, p62/SQSTM1, LC3-I and LC3-II protein levels whereas Beclin1 expression was decreased (Figure 3b). Co-treatment caffeine with docetaxel remarkably increased Beclin1 and Atg5 protein levels in a dose-dependent manner. Moreover, the turnover of p62/SQSTM1 was accelerated with combined treatment. Additionally, LC3-I to LC3-II conversion was dramatically induced by co-administration compared to the docetaxel-treated group (Figure 3b). In this assay system, BafA1, which is a well-known autophagy inhibitor used as a positive control (Yoshii & Mizushima, 2017). As expected, the steady-state level of LC3-I and LC3-II increased due to the inhibition of the fusion of the autophagosome with the lysosome by 1μM BafA1 treatment (Figure 3b).

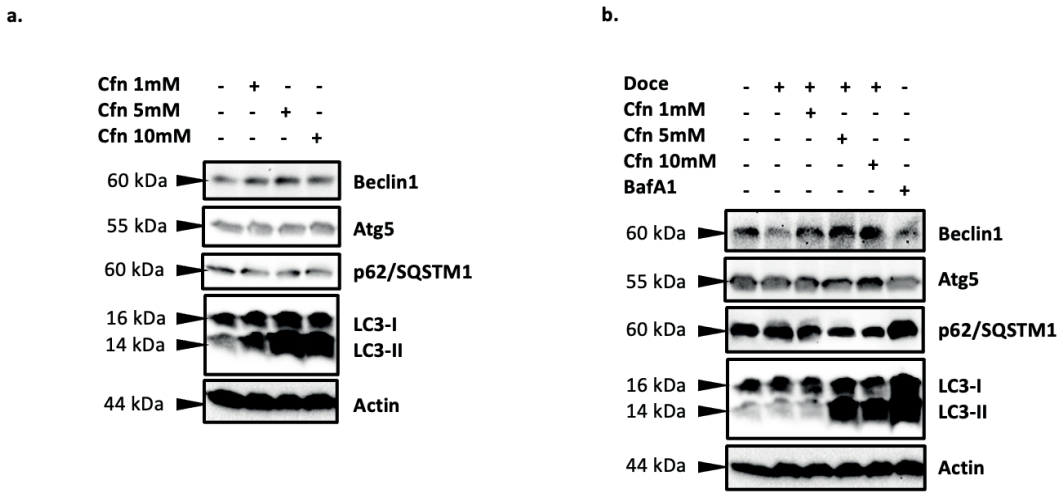

Figure 3. The effect of caffeine and docetaxel on autophagy. (a) Autophagy protein levels including Beclin-1, Atg5, p62/SQSTM1, LC3-I and LC3-II were analyzed by immunoblotting. (b) Autophagy-related protein levels were examined in MCF-7 cells treated with caffeine or co-treatment with docetaxel. Beta-actin was used as a loading control. 1μM BafA1 was used as an autophagic inhibitor control.

Caffeine synergistically enhanced the apoptotic effect of docetaxel

To investigate the cell-death-related effect of caffeine on MCF-7 cells, we tested the Poly(ADP-Ribose) Polymerase 1 (PARP-1) and caspase-3 cleavage, and cytochrome-c levels by immunoblotting. In this assay system, staurosporine, which is a well-characterized apoptotic inducer used as a positive control of apoptotic cell death (Malsy et al., 2019). Our data indicated that caffeine treatment at indicated doses has no apoptotic effect on MCF-7 cells (Figure 4a). Next, we tried its combination with docetaxel, we found that co-treatment of caffeine with docetaxel strongly induced PARP-1 cleavage in a dose-dependent manner compared to docetaxel. We obtained similar results in the caspase-3 cleavage product. (Figure 4b). Moreover, cytochrome-c levels were remarkably up-regulated by combined treatment compared to docetaxel alone administration (Figure 4b). Microscopic examination results showed that combined treatment of docetaxel with caffeine more strongly induced shrinking and the levels of dead cell debris compared to docetaxel group (Figure 4c). Additionally, cell proliferation assay data indicated that co-treatment of docetaxel and caffeine significantly decreased % cell viability (Figure 4d) (Table 1). Collectively these results indicated that caffeine expanded the anti-tumorigenic effect of docetaxel by more efficiently inducing apoptotic cell death. Additionally, we calculated the combination index (CI) value for determining whether the effect of the combined treatment of docetaxel and caffeine synergistically manner. Also, caffeine exhibited a synergistic effect at 5 and 10mM doses with docetaxel on MCF-7 cells (Table 2).

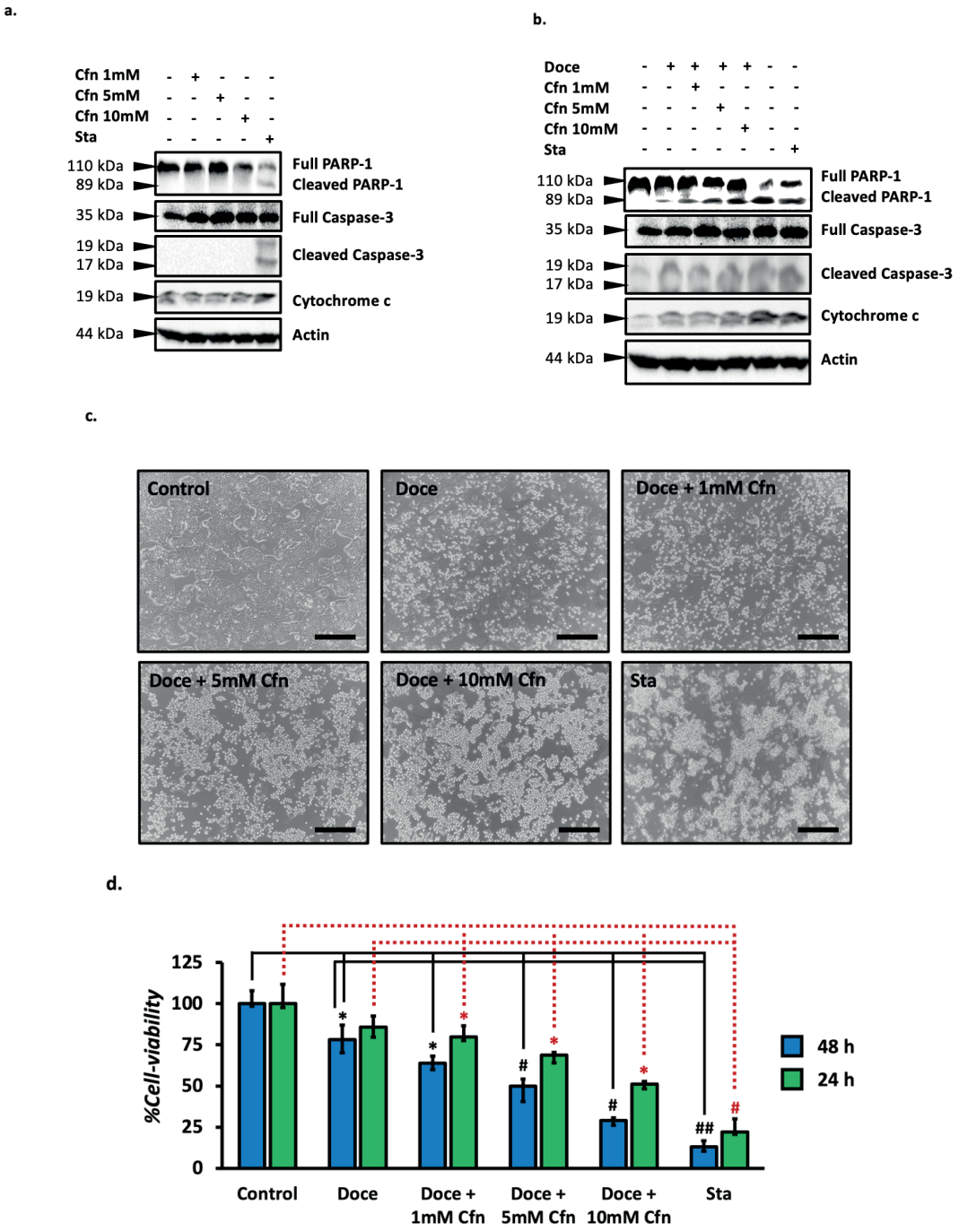

Figure 4. The effects of co-treatment of caffeine with docetaxel on cell-death related proteins. (a) Apoptotic protein levels were analyzed as described Figure 1. Staurosporine (1nM) was used as a positive control of apoptotic cell death. (b) Cells were treated with a vehicle or combined treated with docetaxel and caffeine as indicated doses for 24 hours and target proteins were analyzed by immunoblotting. Beta-actin was used as a loading control. (c) MCF-7 cells were treated with docetaxel and its combination with caffeine and the morphological alterations were visualized in inverted microscope and photographed. Staurosporine was used as a positive control. The scale bar represents 25μm. (d) Cells were treated with vehicle and indicated doses of caffeine or its combination with docetaxel for 24 and 48 hours. % cell viability was analyzed by WST-1 assay. Data represented as mean ± SE of three independent experiments made in three replicates. *$p < 0.05$, #$p < 0.001$, ##$p<0.0001$.

Table 1. The % cell viability values of Docetaxel and its combination with Caffeine.

	% Cell Viability (24h)	% Cell Viability (48h)
Control	100 ± 7.11	100 ± 4.67
Doce	85,723 ± 6.41	78,105 ± 8.37
Doce + 1mM Cfn	79,831 ± 4.46	63,832 ± 4.016
Doce + 5mM Cfn	68,732 ± 3.24	49,921 ± 6.87
Doce + 10mM Cfn	51,084 ± 2.24	28,943 ± 2.24
Sta	22,161 ± 4.71	13,051 ± 3.17

Data represent mean % cell viability value with ± standard deviations.

Table 2. Values of combination index (CI) for docetaxel-caffeine interactions.

	CI value ± SEM	Combine Effect
Docetaxel [15nM] + Caffeine 1mM	1.03 ± 0.03	Additive
Docetaxel [15nM] + Caffeine 5mM	0.83 ± 0.11	Synergistic
Docetaxel [15nM] + Caffeine 10mM	0.65 ± 0.13	Synergistic

CI greater than 1.1 denotes an antagonist effect; CI between 0.99-1.1 indicates an additive effect; CI value less than 0.99 indicate a synergistic effect. Data represent mean CI value with ± standard deviations. Calculations of CI were calculated with GraphPad Prism 7 software.

Caffeine is the most common consumed dietary ingredient around the world. It has various potent biochemical activities such as antioxidant, anti-inflammatory and anti-cancer. Studies demonstrated that it is effective against various diseases such as Alzheimer's disease, Parkinson's disease and cancer in *in vitro* and *in vivo* (Campa et al., 2005; Mitchell et al., 2015; Pranata et al., 2022). Also, it has been shown to give effective results when used as an auxiliary ingredient with traditional drugs and chemotherapeutics (Mhaidat et al., 2014; Tomita & Tsuchiya, 1989; Z. Wang et al., 2019; Yamamoto & Tsuchiya, 2011). In the present study, we evaluated the effect of caffeine and its combination with docetaxel on MCF-7 breast cancer cells. Docetaxel which belongs to the taxane family is one of the commonly used antineoplastic agents in the treatment of breast cancer. It is also effective in the treatment of other cancer types including gastric cancer, head and neck cancer and non-small cell lung cancer. However, long-term usage of docetaxel in treatments causes systemic disturbances, therefore, its therapeutic efficiency is limited clinically (Lyseng-Williamson & Fenton, 2005).

The goal of our study is to test the effects of caffeine on UPS, autophagy and UPR signaling, which are critical mechanisms for breast and other cancer types and they often have increased activity in breast cancer cells. Also, the possible synergistic effects of the use of caffeine together with docetaxel are evaluated through these mechanisms.

Today, it is known that UPS, UPR, and autophagy work together to regulate physiologically cellular homeostasis. UPS is the main proteolytic system that is crucial in the regulation of many cellular processes by promoting protein degradation and homeostasis (Erzurumlu & Ballar, 2017; Mata-Cantero et al., 2015). The endoplasmic reticulum-associated degradation (ERAD) mechanism, which is one of the most effective protein degradation systems in the ER, ubiquitinates the substrate molecules to target 26S proteasome by ubiquitin ligase enzymes (Erzurumlu & Ballar, 2017). Impairment of UPS has been associated with various diseases such as diabetes, Alzheimer's disease, Parkinson's disease, hemophilia, and numerous cancer types (Erzurumlu & Ballar, 2017). The variable factors such as deficiency of nutrients, toxic stimulation and im-

balance of metabolic Ca^{+2} can trigger stressful conditions in ER and these conditions induce called "ER stress" signaling (Madden et al., 2019). Induction of ER stress leads to activation of the UPR mechanism, supporting the restoration of ER homeostasis. UPR is coordinated through the activation of ER-membrane localized three transmembrane proteins, PERK, IRE1α, and activating transcription factor 6 (ATF6) sensor protein and their down-regulators (Madden et al., 2019). To evaluate the effects of caffeine on UPR signaling, we tested effector proteins of UPR, including p(Ser51)-eIF2α, total-eIF2α, ATF4, and PERK and also IRE1α branch, XBP-1s and IRE1α protein levels. Caffeine treatment increased expression of all tested UPR proteins in a dose-dependent manner. Also, to understand the relationship between UPR induction and ER stress, we examined the levels of BiP/GRP78, a well-known stress protein. Our results showed that caffeine administration increased the protein level of BiP/GRP78 in a dose-dependent manner (Figure 1c). These results suggest that caffeine induces ER stress in breast cancer cells and activation of the UPR occurs in this way. In addition, the dose-dependent decrease in the poly-ubiquitination pattern in the cells with caffeine administration and the dose-dependent increase in the levels of Hrd1/SYVN1, one of the major ubiquitin ligase enzymes associated with ERAD, suggests that caffeine decelerates the UPS in breast cancer cells (Figure 2a). Similar results were obtained with the co-administration of caffeine and docetaxel. Co-treatment more strongly decreased the poly-ubiquitination state, whereas increased Hrd1 levels and induced the UPR signaling in MCF-7 cells (Figure 1b, 2b).

Autophagy is a conserved program that is comprised of initiation and membrane nucleation, phagophore formation and expansion, fusion with the lysosomes and degradation (Glick et al., 2010). It controls the level of damaged organelles, long-lived and misfolded proteins (Glick et al., 2010). To investigate effects of caffeine on autophagy, we tested critical regulator proteins Beclin-1 and Atg5, turnover of p62/SQSTM1, which is well known autophagic cargo protein and lipidation of LC3 considered necessary for autophagosome formation.

Our results indicated that caffeine increased Beclin1 levels and did not cause changes in Atg5 levels. Also, it slightly decreased p62/SQSTM1 levels, whereas it remarkably induced LC3-I to LC3-II conversion in a manner dose-dependently (Figure 3a). These results observed that caffeine accelerated the autophagic flux in breast cancer cells. Moreover, co-treatment of caffeine and docetaxel led to an increment level of Beclin1 and Atg5 compared to control or docetaxel alone. More strikingly, the combined treatment of caffeine and docetaxel remarkably accelerated the p62/SQSTM1 turnover and also strongly increased LC3-I to LC3-II conversion. In this assay system, BafA1 was used as an autophagic blocker, which blocks the fusion of autophagosomes with lysosomes, and as expected, it increased p62/SQSTM1 accumulation and LC3-II levels (Figure 3b). Collectively these results suggest that caffeine alone positively regulates autophagic activity, and when combined with docetaxel, it synergistically stimulates autophagic flux in breast cancer cells. Autophagy is also known as the type 2 cell death program, highly increased autophagic activity leads to cell death (Kroemer & Levine, 2008). Consistent with the cell death findings observed in our microscopic results, increased autophagic activity may have led to the death of MCF-7 cells (Figure 4c).

Next, we tested the effect of caffeine and its combination with docetaxel on apoptotic cell death. We observed caffeine administration did not induce any apoptotic cell death-associated protein levels, including PARP-1 and caspase-3 cleavage, cytochrome-c (Figure 4a).

The evaluation of the cleavage forms of caspase-3 and PARP-1 is widely used for understanding apoptotic cell death in *in vitro* and *in vivo* studies (Cohen, 1997; Lazebnik et al., 1994). Also, cytochrome c is a component of the mitochondrial electron transport chain and is an essential parameter for the evaluation of extrin-

sic apoptotic cell death (Liu et al., 1996). Our findings indicated that co-treatment of caffeine with docetaxel strongly induced 89 kDa cleavage fragment of PARP-1, which is one of the main targets of caspase-3 and cleavage form of caspase-3, which is a critical executioner of apoptosis in a dose-dependent manner (Cohen, 1997; Lazebnik et al., 1994). Consistent with these data, co-treatment synergistically increased cytochrome-c levels in MCF-7 cells (Figure 4b).

It is frequently stated as a fact that chemotherapeutic agents trigger cell death through apoptotic mechanisms. However, recent studies indicated that these agents could activate complex cell death modes by affecting different cellular signaling mechanisms, including necrosis, ferroptosis and autophagic cell death (Gao et al., 2022). Herein we tested the possible effects of the natural product caffeine in breast cancer cells and also determined the synergistic effect of its combination with docetaxel. Our results suggest that the concomitant use of caffeine and docetaxel affects breast cancer cells by autophagic induction and intrinsic/extrinsic apoptotic pathway. The mode of action of the combination of caffeine with docetaxel was illustrated in Figure 5.

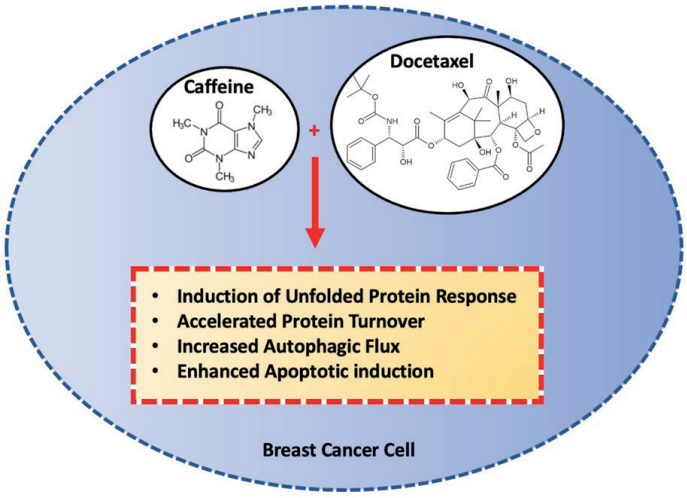

Figure 5: Schematic illustration of the mode of action of caffeine with docetaxel in breast cancer cells.

CONCLUSION

Testing the well-known traditional chemotherapeutics and their combination with natural products is a very valuable effort for increasing their utilization and establishing less toxic treatment protocols. The present study suggests that caffeine, which is frequently consumed in the community as part of the daily diet, may increase the chemotherapeutic efficacy of docetaxel in breast cancer treatment.

ACKNOWLEDGEMENTS

We thank Suleyman Demirel University-Innovative Technologies Application and Research Center. We apologize that we could not perform comprehensive reference representation due to reference limitations. This study was supported by Suleyman Demirel University internal funds (TSG-2021-8302, TAB-2020-8253).

CONFLICT OF INTEREST

Authors declare that there is no conflict of interest.

AUTHOR CONTRIBUTION STATEMENT

Y.E. initiated and directed the project, designed, and conducted the experiments, analyzed, and interpreted the results, and wrote the manuscript. D.C., H.K.D. and E.A. assisted experimental studies. All

correspondence and requests for materials should be addressed to Y.E. All authors have read and approved the final version of the article.

REFERENCES

Andersen, L. F., Jacobs, D. R., Jr, Carlsen, M. H., & Blomhoff, R. (2006). Consumption of coffee is associated with reduced risk of death attributed to inflammatory and cardiovascular diseases in the Iowa Women's Health Study. *The American Journal of Clinical Nutrition*, *83*(5), 1039–1046. https://doi.org/10.1093/ajcn/83.5.1039

Campa, C., Doulbeau, S., Dussert, S., Hamon, S., & Noirot, M. (2005). Qualitative relationship between caffeine and chlorogenic acid contents among wild Coffea species. *Food Chemistry*, *93*(1), 135–139. https://doi.org/10.1016/j.foodchem.2004.10.015

Cohen, G. M. (1997). Caspases: the executioners of apoptosis. *Biochemical Journal*, *326 (Pt 1)*, 1–16. https://doi.org/10.1042/bj3260001

Ding, M., Bhupathiraju, S. N., Chen, M., van Dam, R. M., & Hu, F. B. (2014). Caffeinated and decaffeinated coffee consumption and risk of type 2 diabetes: a systematic review and a dose-response meta-analysis. *Diabetes Care*, *37*(2), 569–586. https://doi.org/10.2337/dc13-1203

Erzurumlu, Y., & Ballar, P. (2017). Androgen Mediated Regulation of Endoplasmic Reticulum-Associated Degradation and its Effects on Prostate Cancer. *Scientific Reports*, *7*, 40719. https://doi.org/10.1038/srep40719

Gao, W., Wang, X., Zhou, Y., Wang, X., & Yu, Y. (2022). Autophagy, ferroptosis, pyroptosis, and necroptosis in tumor immunotherapy. *Signal Transduction and Targeted Therapy*, *7*(1), 196. https://doi.org/10.1038/s41392-022-01046-3

Glick, D., Barth, S., & Macleod, K. F. (2010). Autophagy: cellular and molecular mechanisms. *The Journal of Pathology*, *221*(1), 3–12. https://doi.org/10.1002/path.2697

Hikita, K., Honda, M., Shimizu, R., Teraoka, S., Kawamoto, B., Yumioka, T., Tsounapi, P., Iwamoto, H., Morizane, S., & Takenaka, A. (2021). Efficacy of Combination Chemotherapy With Docetaxel, Estramustine and Carboplatin in Men With Castration-resistant Prostate Cancer. *Cancer Diagnosis & Prognosis*, *1*(5), 451–457. https://doi.org/10.21873/cdp.100607

Jacobson, K. A., Kirk, K. L., Padgett, W. L., & Daly, J. W. (1985). Functionalized congeners of 1,3-dialkylxanthines: preparation of analogues with high affinity for adenosine receptors. *Journal of Medicinal Chemistry*, *28*(9), 1334–1340. https://doi.org/10.1021/jm00147a038

Jordan, M. A., & Wilson, L. (2004). Microtubules as a target for anticancer drugs. *Nature Reviews. Cancer*, *4*(4), 253–265. https://doi.org/10.1038/nrc1317

Kroemer, G., & Levine, B. (2008). Autophagic cell death: the story of a misnomer. *Nature Reviews. Molecular Cell Biology*, *9*(12), 1004–1010. https://doi.org/10.1038/nrm2529

Lazebnik, Y. A., Kaufmann, S. H., Desnoyers, S., Poirier, G. G., & Earnshaw, W. C. (1994). Cleavage of poly(ADP-ribose) polymerase by a proteinase with properties like ICE. *Nature*, *371*(6495), 346–347. https://doi.org/10.1038/371346a0

Liu, X., Kim, C. N., Yang, J., Jemmerson, R., & Wang, X. (1996). Induction of apoptotic program in cell-free extracts: requirement for dATP and cytochrome c. *Cell*, *86*(1), 147–157. https://doi.org/10.1016/s0092-8674(00)80085-9

Lopez-Garcia, E., van Dam, R. M., Willett, W. C., Rimm, E. B., Manson, J. E., Stampfer, M. J., Rexrode, K. M., & Hu, F. B. (2006). Coffee consumption and coronary heart disease in men and women: a prospective cohort study. *Circulation*, *113*(17), 2045–2053. https://doi.org/10.1161/CIRCULATIONAHA.105.598664

Lyseng-Williamson, K. A., & Fenton, C. (2005). Docetaxel: a review of its use in metastatic breast cancer. *Drugs*, *65*(17), 2513–2531. https://doi.org/10.2165/00003495-200565170-00007

Madden, E., Logue, S. E., Healy, S. J., Manie, S., & Samali, A. (2019). The role of the unfolded protein response in cancer progression: From oncogenesis to chemoresistance. *Biology of the Cell / under the Auspices of the European Cell Biology Organization*, *111*(1), 1–17. https://doi.org/10.1111/boc.201800050

Malsy, M., Bitzinger, D., Graf, B., & Bundscherer, A. (2019). Staurosporine induces apoptosis in pancreatic carcinoma cells PaTu 8988t and Panc-1 via the intrinsic signaling pathway. *European Journal of Medical Research*, *24*(1), 5. https://doi.org/10.1186/s40001-019-0365-x

Mata-Cantero, L., Lobato-Gil, S., Aillet, F., Lang, V., & Rodriguez, M. S. (2015). The Ubiquitin-Proteasome System (UPS) as a Cancer Drug Target: Emerging Mechanisms and Therapeutics. In G. T. Wondrak (Ed.), *Stress Response Pathways in Cancer: From Molecular Targets to Novel Therapeutics* (pp. 225–264). Springer Netherlands. https://doi.org/10.1007/978-94-017-9421-3_11

Mhaidat, N. M., Alzoubi, K. H., Al-Azzam, S. I., & Alsaad, A. A. (2014). Caffeine inhibits paclitaxelinduced apoptosis in colorectal cancer cells through the upregulation of Mcl1 levels. *Molecular Medicine Reports*, *9*(1), 243–248. https://doi.org/10.3892/mmr.2013.1763

Mitchell, D. C., Hockenberry, J., Teplansky, R., & Hartman, T. J. (2015). Assessing dietary exposure to caffeine from beverages in the U.S. population using brand-specific versus category-specific caffeine values. *Food and Chemical Toxicology: An International Journal Published for the British Industrial Biological Research Association*, *80*, 247–252. https://doi.org/10.1016/j.fct.2015.03.024

Palmeri, L., Vaglica, M., & Palmeri, S. (2008). Weekly docetaxel in the treatment of metastatic breast cancer. *Therapeutics and Clinical Risk Management*, *4*(5), 1047–1059. https://doi.org/10.2147/tcrm.s3397

Pranata, R., Feraldho, A., Lim, M. A., Henrina, J., Vania, R., Golden, N., & July, J. (2022). Coffee and tea consumption and the risk of glioma: a systematic review and dose-response meta-analysis. *The British Journal of Nutrition*, *127*(1), 78–86. https://doi.org/10.1017/S0007114521000830

Prat, A., Pineda, E., Adamo, B., Galván, P., Fernández, A., Gaba, L., Díez, M., Viladot, M., Arance, A., & Muñoz, M. (2015). Clinical implications of the intrinsic molecular subtypes of breast cancer. *Breast* , *24 Suppl 2*, S26–S35. https://doi.org/10.1016/j.breast.2015.07.008

Tomita, K., & Tsuchiya, H. (1989). Caffeine enhancement of the effect of anticancer agents on human sarcoma cells. *Japanese Journal of Cancer Research: Gann*, *80*(1), 83–88. https://doi.org/10.1111/j.1349-7006.1989.tb02249

Trayes, K. P., & Cokenakes, S. E. H. (2021). Breast Cancer Treatment. *American Family Physician*, *104*(2), 171–178.

Wang, A., Wang, S., Zhu, C., Huang, H., Wu, L., Wan, X., Yang, X., Zhang, H., Miao, R., He, L., Sang, X., & Zhao, H. (2016). Coffee and cancer risk: A meta-analysis of prospective observational studies. *Scientific Reports*, *6*, 33711. https://doi.org/10.1038/srep33711

Wang, Z., Gu, C., Wang, X., Lang, Y., Wu, Y., Wu, X., Zhu, X., Wang, K., & Yang, H. (2019). Caffeine enhances the anti-tumor effect of 5-fluorouracil via increasing the production of reactive oxygen species in hepatocellular carcinoma. *Medical Oncology*, *36*(12), 97. https://doi.org/10.1007/s12032-019-1323-8

Yamamoto, N., & Tsuchiya, H. (2011). Clinical Observations of Caffeine-Potentiated Chemotherapy. *Journal of Caffeine Research*, *1*(3), 163–168. https://doi.org/10.1089/jcr.2011.0007

Yoshii, S. R., & Mizushima, N. (2017). Monitoring and Measuring Autophagy. *International Journal of Molecular Sciences*, *18*(9). https://doi.org/10.3390/ijms18091865

FABAD J. Pharm. Sci., 48, 1, 105-124, 2023
Doi: 10.55262/fabadeczacilik.1126288
RESEARCH ARTICLE

Development and Evaluation of Nanostructured Lipid Carriers for Transdermal Delivery of Ketoprofen

Thulasi SATHYANARAYANANA[*], Preethi SUDHEER[**°], Elsa JACOB[***], Merlin Mary SABU[****]

Development and Evaluation of Nanostructured Lipid Carriers for Transdermal Delivery of Ketoprofen

SUMMARY

Ketoprofen is a nonsteroidal anti-inflammatory drug that displays significant gastrointestinal side effects when administered via the oral route and has a low skin permeation profile. The objective of the present work is to utilise nanostructured lipid carriers (NLCs) as a carrier system for the transdermal delivery of ketoprofen. NLCs were prepared via hot homogenisation technique using beeswax, carnauba wax, glyceryl monostearate (solid lipids), linseed oil (liquid lipid) and poloxamer188 (surfactant) and optimized using custom design via JMP. The responses evaluated were drug entrapment efficiency, particle size and drug release profile. The experimental design was evaluated for model fit with the assistance of variance analysis. The optimum formulations were characterized for particle size, zeta potential, scanning electron microscopy (SEM), differential scanning colorimetry, Fourier transform infrared spectrum (FTIR) and also drug content, entrapment efficiency, in-vitro drug release, and ex-vivo drug release profile was studied. The drug loading efficiency between the formulation ranges between 34±0.03-95.06±0.01%. The drug release from the formulations over a 24 h study was found to be 80%±0.09 to 95%±0.06. The maximum desirability was found to be 0.91. The optimum formulation showed a mean particle size of 425.8nm and a zeta potential of -45mV. SEM results revealed slightly agglomerated particles with uneven surfaces. The ex-vivo skin permeation of NLC optimized patch formulation exhibited a higher flux and permeability coefficient than the pure drug patch formulation, and marketed gel (2.5%w/w) FTIR spectra assured the chemical and physical compatibility. Transdermal delivery of ketoprofen via NLCs would be a promising approach for improving skin permeation.

Key Words: *Ketoprofen, permeation, NLC, skin, oils, optimization, ex-vivo, flux*

Ketoprofen'in Transdermal Uygulanması İçin Nanoyapılı Lipid Taşıyıcıların Geliştirilmesi ve Değerlendirilmesi

ÖZ

Ketoprofen, oral yoldan uygulandığında önemli gastrointestinal yan etkiler gösteren ve düşük deri permeasyon profiline sahip, nonsteroidal antiinflamatuar bir ilaçtır. Mevcut çalışmanın amacı, ketoprofenin transdermal iletimi için taşıyıcı sistem olarak nanoyapılı lipid taşıyıcıları (NLT) kullanmaktır. NLT'ler, balmumu, karnauba mumu, gliserl monostearat (katı lipidler), keten tohumu yağı (sıvı lipid) ve poloksamer188 (yüzey aktif madde) kullanılarak sıcak homojenizasyon tekniği ile hazırlanmıştır ve JMP aracılığıyla özel tasarım kullanılarak optimize edilmiştir. İlaç tutma etkinliği, parçacık boyutu ve ilaç salım profili yanıtları değerlendirilmiştir. Deney tasarımı, varyans analizi yardımıyla model uygunluğu için değerlendirilmiştir. Partikül boyutu, zeta potansiyeli, taramalı elektron mikroskobu (SEM), diferansiyel taramalı kalorimetre, Fourier dönüşümlü kızılötesi (FTIR) için optimum formülasyonlar karakterize edilmiş ve ayrıca ilaç içeriği, tuzak etkinliği, in vitro ilaç salınımı, ex-vivo ilaç salım profili incelenmiştir. Formülasyonlar arasında ilaç yükleme etkinliği 34±0.03-95.06±0.01% aralığındadır. 24 saatlik bir çalışma boyunca formülasyonlardan ilaç salınımının %80±0.09 ila %95±0.06 olduğu bulunmuştur. Maksimum arzu edilirlik 0.91 olarak bulunmuştur. Optimum formülasyon, 425.8 nm'lik bir ortalama parçacık boyutu ve -45mV'lik bir zeta potansiyeli göstermiştir. SEM sonuçları, düzgün olmayan yüzeylere sahip hafif aglomere partiküller ortaya çıkarmıştır. NLC ile optimize edilmiş yama formülasyonunun ex-vivo deri geçirgenliği, saf ilaç yama formülasyonuna kıyasla daha yüksek bir akış ve geçirgenlik katsayısı göstermiştir ve ticari jel (%2,5 a/a) FTIR spektrumları, kimyasal ve fiziksel uyumluluğu desteklemektedir. Ketoprofenin NLC'ler yoluyla transdermal olarak verilmesi, deri geçirgenliğini iyileştirmek için umut verici bir yaklaşım olacaktır.

Anahtar Kelimeler: *Ketoprofen, permeasyon, NLT, Deri, yağlar, optimizasyon, ex-vivo, akım*

Received: 05.06.2022
Revised: 11.11.2022
Accepted: 26.12.2022

[*] ORCID:0000-0002-5126-5813, Department of Pharmaceutics, Krupanidhi College of Pharmacy, Chikka Bellandur, Carmelaram post, Varthur Hobli, Bangalore- 560035, India
[**] ORCID:0000-0002-7041-8993, Department of Pharmaceutics, Krupanidhi College of Pharmacy, Chikka Bellandur, Carmelaram post, Varthur Hobli, Bangalore- 560035, India
[***] ORCID:0000-0003 -4890-6867, Department of Pharmacy practice, Krupanidhi College of Pharmacy, Chikka Bellandur, Carmelaram post, Varthur Hobli, Bangalore- 560035, India
[****] ORCID:0000-0002-4052-4533, Department of Pharmacy practice, Krupanidhi College of Pharmacy, Chikka Bellandur, Carmelaram post, Varthur Hobli, Bangalore- 560035, India

[°] Corresponding Author; Dr. Preethi Sudheer
Email: preetisudheer@gmail.com, Phone: 919449822912

INTRODUCTION

The main aim of novel drug delivery is to provide sustained drug action at a fixed rate or by keeping a relatively constant, adequate level of drug in the body with less or no toxicity or side effects in the affected tissue or organ or to achieve the target drug action employing carriers to deliver the drug to a specific target site (Tamjidi et al., 2013).

Nanotechnology's use is extensive in drug delivery, especially for the transdermal delivery of therapeutic agents. Nanocarriers have been a successful tool for delivering the drug to the target site due to their optimized physicochemical properties. Many nanocarriers are available in the form of dendrimers, polymers, magnetic nanoparticles, silicon, carbon materials, lipid-based systems, etc. (Ghasemiyeh et al., 2018).

Lipid-based systems are more promising over other carriers due to lipids' physiologically safe and biodegradable nature. The lipid-based system has been extended into liposomes, solid lipid nanoparticles (SLN), and nanostructure lipid carriers (NLC). These nanostructures can hold hydrophilic and hydrophobic molecules and exhibit very low toxicity. In addition, they extend the drug action by its sustained drug release property, prolonging the half-life. The carrier surface can be remoulded by a suitable chemical approach, which can overcome sensing by the immune system that helps enhance the drug's permeation across physiological barriers (Jain et al., 2016).

The purpose of developing this first-generation lipid nanocarrier system SLN is to achieve drug delivery by several routes of administration in the medical management of physiological complications. NLCs were introduced by Muller, in which drug incorporated matrix was developed by substituting a fraction of solid lipids with liquid lipids. Due to their biocompatibility and superior formulation properties, NLCs have contemplated potentiality over SLNs. The NLC is a colloidal system class containing biocompatible and regulatory permissible lipids supplied as a liquid and solid carrier material, improving the inserted drug's chemical stability (Chaudhary et al., 2013). The advantages of NLC over liposomes are its high drug loading, low cost of raw materials, and good stability. In addition, they can produce smaller particulates decrease drug leakage problems during storage, amplify the bioavailability, and enable the modulation of the medication, which results in controlled and extended-release properties of the product (Zhou et al., 2018).

Ketoprofen is a propionic acid-based non-steroidal anti-inflammatory medication used to reduce the inflammation, stiffness, and pain involved with osteoarthritis and rheumatoid arthritis. Ketoprofen suppresses the synthesis of prostaglandin and thromboxane precursors by inhibiting the activity of cyclo-oxygenase I and II enzymes. It is absorbed rapidly through the gastrointestinal tract.; peak plasma can occur about 0.5 to 2 hours after a dose. When ketoprofen is given with food, the total bioavailability is altered, and the absorption rate is slowed. The elimination half-life in plasma is about 1-5 to 4 hours. Also, like most nonsteroidal anti-inflammatory drugs, ketoprofen presents gastrointestinal adverse side effects. (Reynolds et al., 1993; Manikkath et al., 2017).

Moreover, the short elimination half-life demands frequent dosing. As a result, it generates an effective transdermal formulation of the therapeutic agent that could assist in the elimination of the drug's oral administration-related side effects while simultaneously enhancing therapeutic efficacy and safety. The challenge in conventional transdermal therapy is that only a tiny amount of ketoprofen is absorbed following topical application. It is applied as 2.5% gel 2 to 4 times daily for seven days for local pain relief.

Therefore, in the present study, NLC has been chosen as a carrier system for increasing transdermal delivery of ketoprofen, and the custom design approach was used for optimization.

MATERIALS AND METHODS

Ketoprofen was an endowment from BEC Chemicals Pvt. Ltd, Mumbai, India. In addition to other chemicals, the lipids were purchased from Sigma Aldrich Mumbai.

Drug: excipient compatibility study by FTIR

A Fourier transform infrared spectrum (FTIR) was used to identify any interaction between ketoprofen and excipients. The sample was analysed by the potassium bromide pellet method using an IR spectrophotometer (Thermo- Nicolet 6700) in the spectral region between 4000-400cm^{-1}(Patwekar et al., 2017).

Preparation of blank formulations

Blank formulations were prepared using liquid lipids linseed oil, solid lipids beeswax, carnauba wax, and glyceryl monostearate alone and in combination with two surfactants, namely tween 80 and poloxamer188. A hot homogenization technique where melted lipids were amalgamated with aqueous surfactant solution under mechanical stirring at 500 rpm to produce coarse oil/water emulsion. This coarse emulsion was further homogenized (Polytron homogenizer) to get a fine emulsion. The resultant emulsion was cooled to room temperature to obtain NLCs. The physical properties of the formulations were observed. Based on physical properties, drug-loaded NLCs were prepared by adding the drug to a melted lipid combination (bee wax, carnauba wax, and glyceryl monostearate), which was further added hot aqueous solution of poloxamer 188, and the same procedure mentioned above was followed (Patwekar et al., 2017).

Utilization of experimental custom design

In pharmaceutical development, quality by design/QbD has improved the resulting formulation integrity by lowering the number of required testing methods, evaluated using various mathematical models. A custom design approach using JMP software version 11 was used to optimize both formulation and processing parameters on the quality attributes. The factors such as phase volume ratio (%), solid lipid: liquid lipid, drug: lipid, stirring speed (rpm), and surfactant (%) were studied on the responses of drug entrapment efficiency (%), particle size(nm) and drug release (%) as given in the (Table 1) and (Table 2). The design generated 12 experimental trials, as given in (Table 3). After experimental trials, responses were collated (Ashwini et al., 2020; Subramanyam et al., 2020).

Table 1. Factors chosen in experimental design

Factors	Levels of factors		
	Low	Medium	High
Phase volume ratio (%)	20		50
Solid lipid: liquid lipid (%)	17		50
Drug: lipid (%)	17		50
Stirring speed (rpm)	10000	12000	15000
Surfactant (%)	0.3		2

Table 2. Responses of experimental design

Responses	Minimum	Maximum
Drug entrapment efficiency (%)	80	90
Particle size(nm)	100	900
Drug release (%)	80	90

Table 3. Experimental runs

Formulation code	Solid lipid: lipid (%)	Drug: Lipid (%)	Phase volume ratio (%)	Surfactant concentration (%)	Stirring speed(rpm)
T1	50	50	50	2	12500
T2	50	50	50	0.3	12500
T3	33.5	33.5	35	1.15	10000
T4	50	50	20	2	10000
T5	17	17	50	2	150000
T6	17	17	20	2	150000
T7	50	50	20	0.3	150000
T8	17	17	50	0.3	10000
T9	33.5	33.5	35	1.15	10000
T10	17	17	20	2	12500
T11	50	50	50	0.3	150000
T12	17	17	20	0.3	12500

Evaluation of NLCs

Drug content and drug entrapment efficiency

For drug content, NLC equivalent to 10 mg of ketoprofen (based on the theoretical drug content) was weighed, transferred into 50 ml of the volumetric flask, and dissolved in (30ml methanol: 20ml ethanol) (stock-I). The 1ml of stock-I preparation was diluted to 10 ml using methanol. The absorbance of 254 nm was measured by UV spectrophotometry. The blank formulation was treated the same way the sample was used as blank (Manikkath et al., 2017). NLC equivalent to 10mg of ketoprofen was weighed and placed in Eppendorf tubes, in 10 ml of methanol, under vigorous vortexing. Centrifugation of the solution was carried out at 5000-10000rpm for 50 min. The resulting supernatant was further diluted with methanol. The absorbance was then measured at 254 nm using methanol as a blank with a UV spectrophotometer (Ramkanth et al., 2018). The entrapment efficiency was calculated by Formula (1) given below (Manikkath et al., 2017).

$$EE = \frac{W - Ws}{W} \times 100, \text{ formula (1),}$$

Where, W = Total drug content, Ws = Free drug content,

Particle size analysis (Horiba SZ-100 particle size analyser):

In nanoparticles, the particle size should not be greater than 1000 nm. The principle involved dynamic light scattering technique <1nm to >1μm. Horiba SZ-100 nanoparticle dynamic light scattering system was used to ascertain the mean particle size, particle size distribution, and zeta potential. All the samples were diluted with double distilled water, and every sample was checked in triplicate at a scattering angle of 90° at 25.2 °C (Fan et al.,2013).

In-vitro release studies for NLC:

Franz diffusion cell assembly was used to perform the *in vitro* studies. About 5mg drug equivalent weight of NLC was put on a cellophane membrane between the donor compartment and receptor compartment of diffusion cell assembly. The donor compartment was moistened by 1ml phosphate buffer of pH 5.5. The receptor compartment is filled with 50 ml of phosphate buffer of pH7.4. Continuous stirring of the receptor compartment at 100-250 rpm employing a magnetic stirrer at a temperature of 35°C. The drug release rate from NLC was carried out by withdrawing 1 ml of receptor fluid every one-hour time interval. The sink condition was maintained by adding an equal volume of phosphate buffer saline (PBS). The spectrophotometric method analyzed the drug concentration after suitable dilution at a λ max of 260 nm (Nair et al., 2015).

Evaluation of experimental study and characterisation of optimum formulations

The responses from the experimental study were substituted into the design and assessed for model fit. The design space was identified from the model, and the desirability function was identified. The surface response curves were obtained. Optimal formulations were prepared and evaluated, and the optimum formula was selected to prepare patches.

Zeta potential determination

Zeta potential is the main characteristic needed for nanoparticles in surface charge estimation. It is a vital factor in the NLC's physical stability. SZ-100 HORIBA Scientific performed the zeta potential measurements. The samples were then diluted with double distilled water, and particles were assessed in triplicate at 90° by electrophoretic light scattering at a temperature of 25°C (Fan et al.,2013).

Scanning Electron microscopy (SEM):

Scanning Electron microscopy model Tescan Vega3 was used to examine the surface morphology of the optimized formulation. NLC dispersion was sputtered with gold and spread on a sample holder. Under argon purging, the figures were acquired at a voltage of 30 kV (Nair et al., 2015).

Differential scanning colorimetry

Differential scanning colorimetry (DSC) analysis was carried out to confirm the thermal behaviour of

pure drugs in the presence of lipids. Approximately 5mg of the sample and drug equivalent formulations were weighed and crimped into non-hermetically sealed aluminum pans. These samples were heated from 0°C to 350°C at 10°C/min. During the measurement, nitrogen was constantly purged at a rate of 40ml/min, and DSC thermograms were documented in Shimadzu DSC-60, Japan (Souto et al., 2005).

Preparation of NLC loaded patch

The transdermal patch used the aluminium-backed adhesive membrane method; A 1.25 % w/v solution (minimum concentration as a film-forming agent) of hydroxypropyl methylcellulose-K100 was dispersed in water, and 1% w/w of polyethylene glycol was added as a plasticizer, followed by the addition of 0.1%w/v of methylparaben. The solution was continuously stirred for 15 min at 1000 pm. Optimized drug-loaded NLC formulations of (0.812g) containing 100mg of the drug were incorporated into the above solution and mixed till a uniform dispersion was obtained. The dispersion was poured over a sheet of an aluminium backing layer covering the area of 67.8cm^2 and dried. A patch formulation of ketoprofen (100mg) was prepared by the same procedure mentioned above for comparison (Patel et al.,2009).

Evaluation of drug loaded patches

Drug content

NLC incorporated patch area of 7 cm^2 containing an equivalent amount of ketoprofen (10mg) was cut, transferred into 50ml of volumetric flask diluted with a mixture of 30ml of methanol and 20 ml warm solution of ethanol (stock-I). 1ml of the stock-I solution was diluted to 10 ml using methanol. UV spectrophotometry measured the absorbance was then measured at 254nm by UV spectrophotometry against the same blank. Note: The pure patch preparation drug content was studied by the same procedure mentioned above (Patel et al.,2009).

Thickness, weight uniformity and folding endurance of patches

Thickness was measured using a screw gauge checking at five different points. 15 -Weight uniformity was measured from five randomly cut (1cmx1cm) patches, and the average weight was calculated (Patel et al., 2009).

A patch strip was cut equally and repeatedly folded at the same spot for folding endurance till it broke (Patel et al., 2009).

Moisture content (%):

Each of the prepared patch was weighed separately and placed in desiccators activated silica for 24h, at room temperature till a constant weight was attained (Patel et al., 2009).

Moisture uptake (%):

The weighed patches were placed in a desiccator with potassium chloride saturated solution at room temperature for 24h at relative humidity (RH) of 84%. After 24 h, the patches were weighed again, and formula (2) determined moisture uptake percentage below (Patel et al.,2009).

$$\%moisture\ uptake = \frac{(Final\ weight - Initial\ weight) * 100}{Initial\ weight}$$

Formula (2)

Ex vivo permeation studies

Preparation of skin samples

The research was performed based on approval for use of wistar rats by Institutional animal ethical committee with ethical approval number (KCP/IAEC/ PCEU/37/2019). *Ex-vivo* permeation studies were performed using the abdominal skin of a healthy male albino Wistar rat. The structural similarities of the rat abdominal skin to human skin are owing to its selection for *ex-vivo* studies. In order to ensure the integrity of the skin, hairs from the abdominal region of the rats were shaved using electronic hair remover without scratching or harming the skin surface. After the sacrifice of the rat, full-thickness skin was excised, of which a specific portion of the skin was excised and washed with distilled water before being used in the permeation study (Phatak et al.,2013; Mennini et al., 2016).

Procedure:

Ex vivo studies were performed by modified Franz diffusion cell assembly. Ketoprofen (5mg) equivalent weight of NLC incorporated patch area of 3.5cm^2 and 6.8cm^2 area of patch formulation containing(5mg) of pure drug and 5mg drug equivalent weight of marketed gel of ketoprofen (2.5%) was separately placed on to the skin sample which was inserted between donor compartment and receptor compartment of diffusion cell assembly. The donor compartment is wetted by 1ml phosphate buffer pH 5.5. The receptor compartment is filled with 50 ml of phosphate buffer pH 7.4. The receptor compartment was constantly stirred using a magnetic stirrer at 100 rpm, maintained at 35°C. The drug release rate from NLC was carried out by withdrawing of 1 ml of receptor fluid every one-hour time interval. The sink condition was preserved by adding an equal amount of PBS. The drug concentration was analysed using a spectrophotometric method after suitable dilution against the blank PBS at a λ max of 260 nm. Drug flux (µg/hr/cm^2) at a steady state was calculated by dividing the slope of the linear portion of the curve by the area of the exposed skin surface, and the permeability coefficient

$$Log\ cd = -\frac{log\, cd\,(0) - PSt}{2.303vd} \qquad \text{Equation (1)}$$

Where Cd = Concentration of donor compartment, Cd (0) = Initial Concentration, P= Permeability coefficient, S=Surface area (Mennini et al., 2016).

FTIR Studies

FTIR studies were carried out for NLC formulation and optimal NLC-loaded ketoprofen patch formulation. Samples were assessed by the potassium bromide pellet method in an IR spectrophotometer (Thermo- Nicolet 6700) in the spectral region between 4000-400cm^{-1} (Zhai et al.,2014).

Stability studies

In the stability studies of NLCs, NLC incorporated patch formula was studied at 25 °**±2**° C/60 % RH ±5% and 40°**±2**° C/75 % RH ±5% for three months. The physical nature, drug content, and entrapment efficiency of formulations were checked during and at the terminal stage of the study period (Patwekar et al., 2018).

RESULTS AND DISCUSSION

Preparation and evaluation of NLCs.

Preliminary trials for the preparation of NLC were carried out by preparing placebo formulations. Liquid lipid linseed oil was used with solid lipids carnauba wax, and beeswax individually and in combination. Blank NLCs were prepared in the presence of surfactants, namely poloxamer 188, and at varying concentrations. NLCs obtained using the surfactant poloxamer were found to be free-flowing. Poloxamer has a high hydrophile-lipophile balance value in comparison to tween 80. So, lipid systems get emulsified with higher efficiency, resulting in o/w emulsion contributing to the free-flowing nature of NLCs. Carnauba wax, beeswax, and glyceryl monostearate were used as solid lipid, linseed oil as liquid lipid, and poloxamer as a surfactant in preparing drug-loaded NLCs. The hot homogenization technique was used in preparing NLCs. The formulations were optimized by a custom design approach using JMP 13. The factors selected were solid lipid to liquid lipid ratio, the drug to lipid ratio, surfactant concentration, phase volume ratio, and the stirring speed. The responses chosen were drug entrapment efficiency (%), drug release (%), and particle size.

Drug content and entrapment efficiency

The drug entrapment was between 34±0.03 to95±0.01% shown in (Table 4). The lowest drug content was observed in T1. The low surfactant is insufficient is insufficient to emulsify the large proportion of the lipids used in the T1 formula. In contrast, formula T5 showed a drug content of 69.92±0.1%. Though the concentration of surfactant used in this formula is high, the liquid lipid concentration is high compared to the solid lipid, and subsequent drug leaking in the absence of a low amount of solid lipids from the system; since NLC consists of NLCs comprised of low and high melting lipids, the coexistence of these two is

required to provide increased loading efficiency.

When the oil is mixed with solid lipid, phase separation results in nano-droplets of fat surrounded by a solid matrix, the presence of lipid matrix on the oil surface prevents leakage of drugs from the interior and thus slows down the drug release and higher entrapment efficiency.

Particle size

The particle size of all formulations ranged from 89-950 nm (Table 4). The characteristics and concentrations of surfactant greatly influence the standard and efficacy of nano lipid carriers. The formula T7 and T9 exhibited the largest particle size. There is a large concentration of lipid phase and a lack of poor emulsification in low surfactant concentration. A higher surfactant-to-lipid ratio may advance the emergence of smaller particles and provide higher stabilization of the nano-system due to the scaling down of interfacial tension between the lipid matrix and the hydrophilic phase. The amphiphilic nature helps the surface-active agents be preferentially located in interfacial regions to lower the interfacial pressure between lipid and aqueous phases. Non-ionic emulsifier, especially poloxamer 188, provides another steric stabilization effect that circumvents the aggregation of fine particles in the colloidal system.

Table 4. Results of particle size, drug content and drug entrapment efficiency

Formulation code	Particle size (nm) + SD	Drug content (%)+ SD	Drug entrapment efficiency (%)+ SD
T1	873.6±0.11	55.2±0.09	34±0.03
T2	280.1±0.39	86.8±0.1	72±0.04
T3	597.1±0.07	76.6±0.009	85±0.05
T4	149.7±0.41	99.8±0.03	74.9±0.008
T5	89.3±0.13	75±0.04	69.92±0.1
T6	506.8±0.24	95.2±0.06	93.2±0.6
T7	104.5±0.18	98.2±1.2	95.06±0.01
T8	957.3±0.42	89±0.3	85.2±0.7
T9	942.8±0.1	85±0.7	75.2±0.03
T10	184.8±0.21	85.2±0.2	75.5±0.07
T11	660.2±0.33	88.9±0.006	85±0.02
T12	198.3±0.27	90±0.1	86.2±0.4

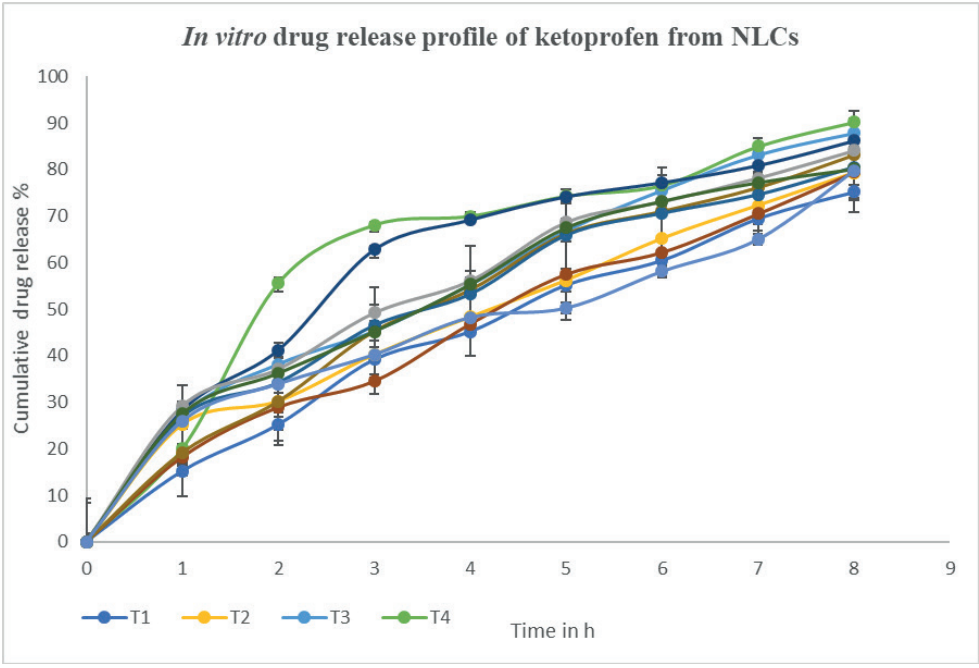

Figure 1. *In vitro* drug release profile of ketoprofen loaded formulations a (T1-T12)

Drug release profile

The formulation drug release over a 24h study was found to be 80%±0.09 to 95%±0.06 shown in (Figure 1). The spatial organization of solid-liquid domains is essential in drug release. The rate at which the drug is released gets affected by the structure of nanoparticles. In typical lipid systems, the uniform distribution of the drug molecules inside the lipid matrix followed by diffusion of these agents through these lipid systems results in drug release. In NLCs, an irregular spatial arrangement of drug molecules, the presence of fluid-natured lipid can cause a rise in the diffusion coefficients of the drugs, thus favouring a faster drug release.

Table 5. Statistical evalution of experimental runs

Sl.No	Source	LogWorth	P value
1	Surfactant (%)(0.3,2)	2.032	0.00928
2	Phase volume ratio(%)(20,50)	1.745	0.01799
3	Solid: Liquid lipid(%)(17,50)	1.655	0.02214
4	Drug: Lipid(%)(17,50)	1.445	0.03592
5	Stirring speed(rpm)	1.364	0.04327

Evaluation of experimental design and summary of the response evaluation

In formulation development, method optimization about the amount of the ingredients and process parameter settings plays an essential role in achieving the required characteristics. Custom design is one of the experimental designs which can tackle a wide range of challenges, all within a framework. So, evaluation of critical formulation variables, the custom design approach was adopted, and a statistical evaluation was carried out. (Table 5).

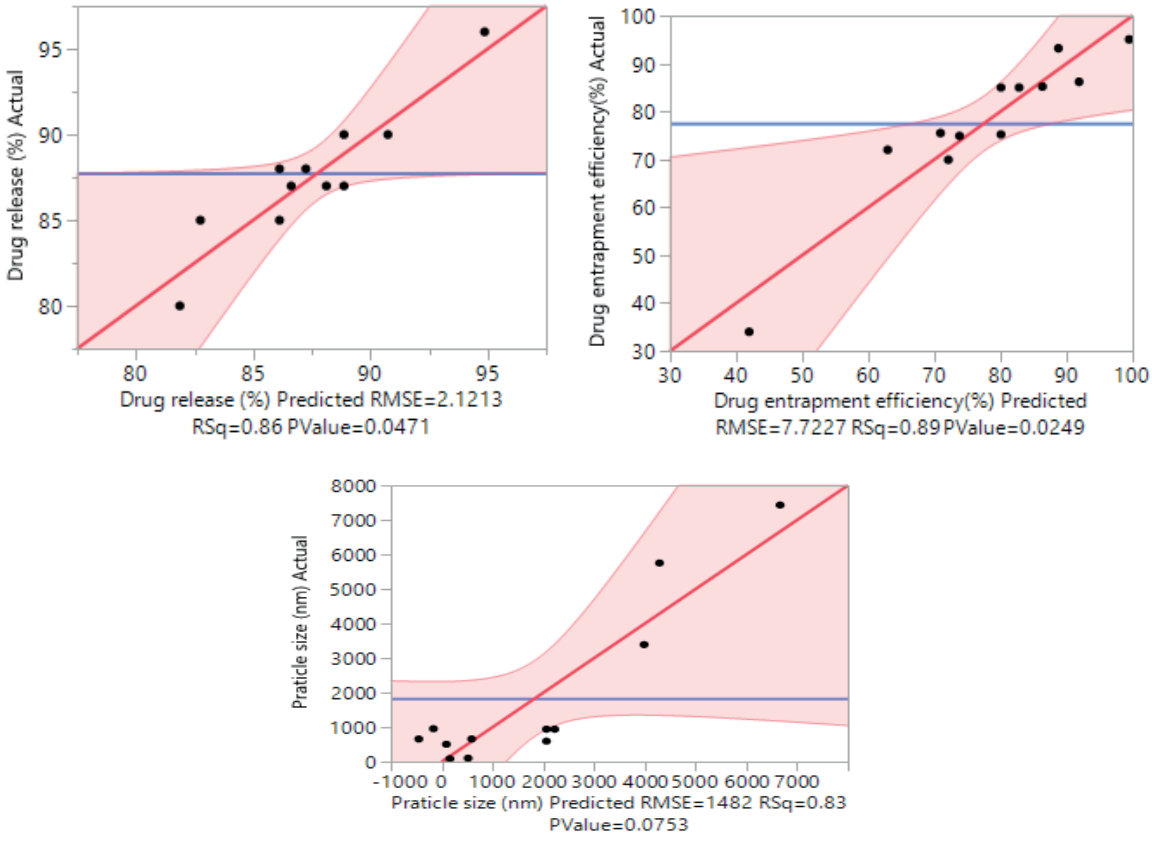

Figure 2. (A) Actual vs Predicted plot of drug release %, (B) drug entrapment efficiency (%) and (C) particle size (nm)

The responses were assessed for their suitability for model fit. P values give the statistical significance of each factor on the selected response. The values ≤ 0.05 indicate that the chosen factors significantly affect overall responses. A highly influencing factor was surfactant concentration, whereas stirring speed did not significantly affect the responses.

The actual vs. predicted plots of the three responses (Figure 2) and the summary of all the factors, level of interactions, and statistical influence is represented in (Table 6,7,8). The desirability function of the model prediction was found to be 0.35 (Figure 3), and the maximum desirability was found to be 0.91. The prediction formula for optimum response is given in equations 2, 3, and 4. Based on the maximum desirability function optimal formula was selected.

Table 6. Response evaluation of entrapment efficiency (%)

Term	Scaled Estimate	Std Error	t Ratio	Prob>|t|
Intercept	77.598333	2.229339	34.81	<.0001*
Solid:liquidlipid (%)(17,50)	-5.13375	2.554029	-2.01	0.1006
Drug:lipid (%)(17,50)	-0.50875	2.554029	-0.20	0.8500
Phase volume ratio(%)(20,50)	-8.84375	2.554029	-3.46	0.0180*
surfacant (%)(0.3,2)	-10.49125	2.554029	-4.11	0.0093*
Stirring speed (rpm)[10000]	2.4766667	3.152762	0.79	0.4677
Stirring speed (rpm)[12500]	-10.67333	3.152762	-3.39	0.0196*
Stirring speed (rpm)[150000]	8.1966667	3.152762	2.60	0.0483*

Table 7. Response evaluation of Particle size(nm)

Term	Scaled Estimate	Std Error	t Ratio	Prob>|t|
Intercept	77.598333	2.229339	34.81	<.0001*
Solid: lipid (%)(17,50)	-5.13375	2.554029	-2.01	0.1006
Drug: lipid (%)(17,50)	-0.50875	2.554029	-0.20	0.8500
Phasevolume ratio(%)(20,50)	-8.84375	2.554029	-3.46	0.0180*
Surfactant (%)(3,6)	-10.49125	2.554029	-4.11	0.0093*
Stirring speed (rpm)[1000]	2.4766667	3.152762	0.79	0.4677
Stirring speed (rpm)[5000]	-10.67333	3.152762	-3.39	0.0196*
Stirring speed (rpm)[10000]	8.1966667	3.152762	2.60	0.0483*

Table 8. Response evaluation of drug release (%)

Term	Scaled Estimate	Std Error	t Ratio	Prob>|t|
Intercept	87.75	0.612372	143.30	<.0001*
Solid:liquid lipid %)(17,50)	0.9375	0.701561	1.34	0.2390
Drug:lipid (%)(17,50)	-1.8125	0.701561	-2.58	0.0492*
Phase volume ratio(%)(20,50)	-1.8125	0.701561	-2.58	0.0492*
Surfactant (%)(0.3,2)	-0.4375	0.701561	-0.62	0.5602
Stirring speed (rpm)[10000]	3	0.866025	3.46	0.0180*
Stirring speed (rpm)[12500]	-2.75	0.866025	-3.18	0.0247*
Stirring speed (rpm)[150000]	-0.25	0.866025	-0.29	0.7844

The desirability approach is a widely used and accepted method for dealing with multiple response processes. It is an objective function that ranges from zero to one. The value depends on how close the upper and lower limits are compared to the optimum. The desirability of the experimental design was found to be 0.35, and the maximum desirability was found to be 0.91. Five factors were chosen for experimental design with low- and high-level values shown in (Table 9).

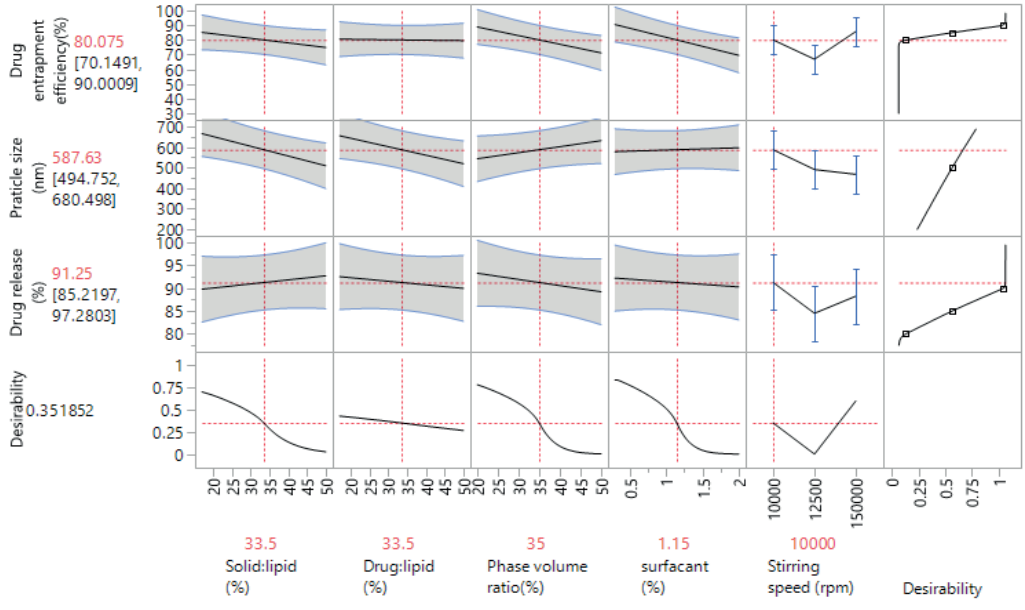

Figure 3. Predication profiler for the experimental runs

Table 9. Prediction formula

	Factors levels	Drug entrapment efficiency (%)	Particle size (nm)	Drug release (%)
Solid: liquid lipid (%)	33.5			
Drug: lipid (%)	33.5			
Phase volume ratio (%)	35			
Surfactant (%)	1.15	80.075	543.06	87.3125
Stirring speed	10000			

Selection of optimal formula and evaluation

Surface response curves and polynormal equations

Surface response curves are a powerful approach for analysing systems and identifying potential trade-offs. Response surface plots such as contour and surface plots are convenient for setting up the required responses and operating conditions. The contour gives the response surface a 2-D view, and the surface plot generally shows a 3-D view. The surface plots indicated first-order effects and no interaction between the responses. Therefore, the curvature effect was found to be minimum. (Figures 4-6).

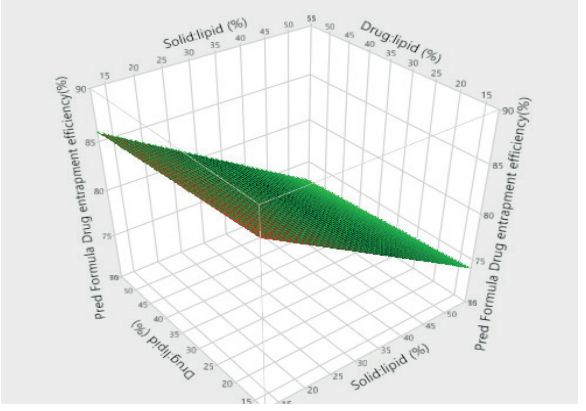

Figure 4. Surface plot of drug entrapment efficiency

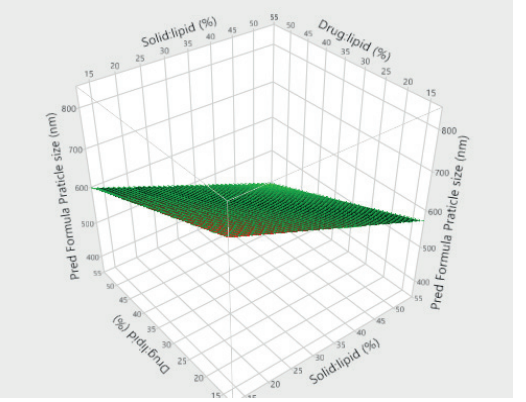

Figure 5. Surface plot of Particle size

80. 07= 77.5983 + -5.13375 * "Solid: liquid lipid (%)" - 33.5) / 16.5) + -0.50875 * ("Drug: lipid (%)") - 33.5) / 16.5) + -8.84375 * (("Phase volume ratio(%)") - 35) / 15) + -10.49125 * ((("surfactant (%)") - 1.15) / 0.85) + ("Stirring speed (rpm)"), "10000", 2.476,"12500", -10.6733,"150000",8.1966- **Equation (2)**

543.06= 515.4583 + -78.203125 * ("Solid: liquid lipid (%)") - 33.5) / 16.5) +-68.053125 * ("Drug: lipid (%)") - 33.5) / 16.5) + 43.996875 * (("Phase volume ratio(%)") - 35) / 15) + 9.52812499999998 * ("surfactant (%)") - 1.15) / 0.85) + ("Stirring speed (rpm)"),"10000", 72.16,"12500", -24.408,"150000", -47.7583- **Equation (3)**

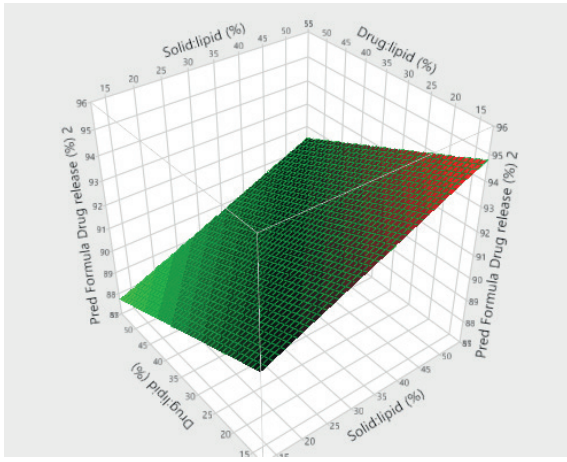

Figure 6: Surface plot of drug release

87.31 = 88 + 1.46875 * ("Solid: liquid lipid (%)") - 33.5) / 16.5) + -1.28125 * ("Drug: lipid (%)") - 33.5) / 16.5) + -2.03125 * ("Phase volume ratio (%)") - 35) / 15) + -0.96875 * ("surfactant (%)") - 1.15) / 0.85) + ("Stirring speed (rpm)"), "10000", 3.25, "12500", -3.5, "150000", 0.25-**Equation (4)**

Evaluation of optimized formula

Particle size distribution and zeta potential

The particle size analysis of optimal formulation showed an average particle size was found to be 425.8nm.

Zeta potential or electrokinetic potential gives an idea about the magnitude of inter electrostatic repulsion in dispersion between the similarly charged adjacent particles**.** The more the zeta potential value, the better the stability of the dispersed system. The zeta potential of the optimal formula was estimated to be -45mV (Figure 7), which indicates the absence of higher-level agglomeration within the system and the stability of NLCs.

Scanning electronic microscopy:

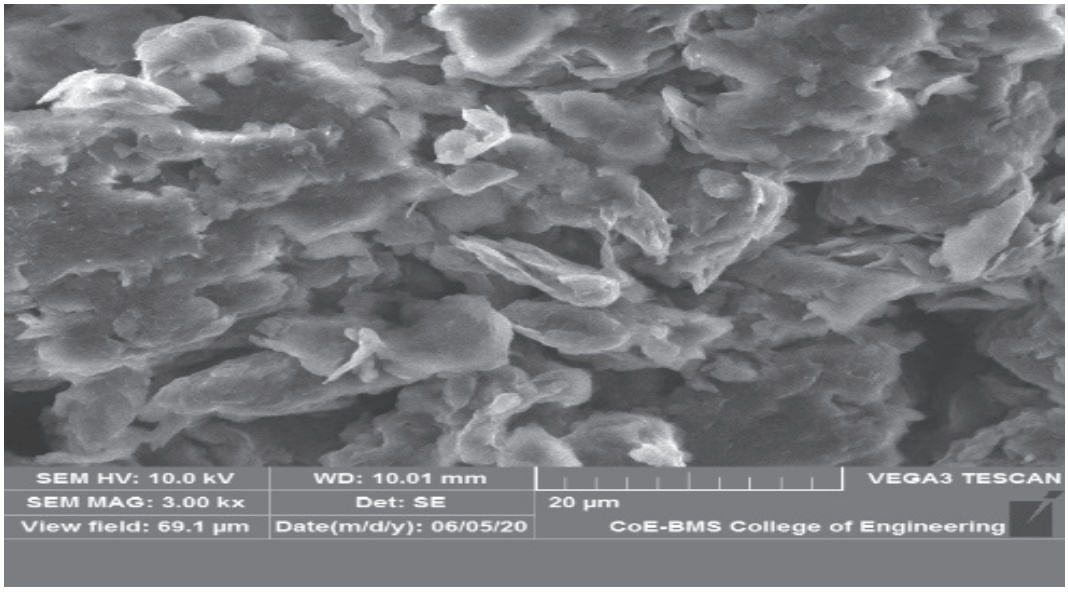

Figure 7: Surface photograph of formulation at different magnification

The surface photograph of the nanoparticles is shown in (Figure 7). The surface picture shows slightly agglomerated particles with uneven surfaces. The effect of high stirring speed disorients the structure of the lipids, which might be one of the contributing factors to the unevenness. At times, the liquid phase containing drug may get ejected during the solidification process, forming an exaggerated version of the liquid phase shell on the solid surface, which might have resulted in such a surface morphology.

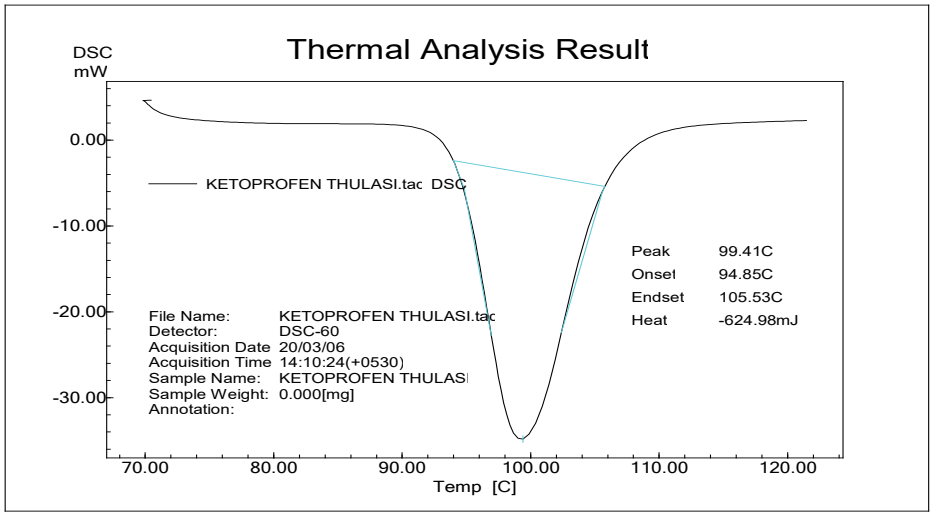

Figure 8. DSC thermogram of a pure drug (Ketoprofen)

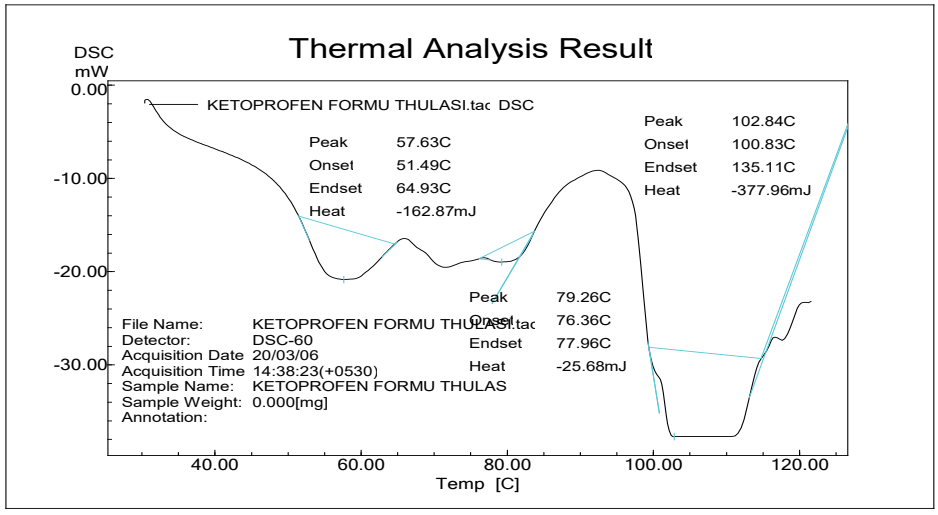

Figure 9. DSC thermogram of NLC formulation

Differential scanning calorimetry

The thermal behaviour of ketoprofen and its NLC were studied using DSC to observe the effect of the lipids on ketoprofen. The DSC thermogram of ketoprofen reveals an endothermic peak at 94.8˚C. In the optimized formulation, the endothermic peak shifted towards lower temperature, i.e., 76.36 ˚C, respectively, shown in (Figure 8) and (Figure 9). This indicates that the lipids (Beeswax, carnauba wax, and linseed oil) and surfactant may have decreased the melting point of NLC of ketoprofen. Thus, this would have resulted in favouring its retention within the matrix of lipids, and on contact with an aqueous medium, it exhibits reversal of effects, thus increasing drug release.

Evaluation of patch formulation

The drug content for the patch formulation was found to be 95.2±0.09, thickness 0.116±0.09, folding endurance 240.2±0.06, weight variation 190±1.2, moisture content 1.3±0. 06. shown in (Table 10).

Table 10. Evaluation of patch

Drug content uniformity (%)±SD	Thickness±SD (mm)	Folding endurance±SD	Weight uniformity (mg)±SD	Moisture content(%)±SD(n=1)
95.2±0.09	0.116±0.09	140.2±0.06	10.5±1.2	1.3±0.06

Preparation of optimum formulation of NLC loaded ketoprofen patch

The optimum formulation from the prediction formula showed 85.4% entrapment efficiency, 425.8nm particle size, and 91.5%± 0.06 of the drug content. The patches were prepared using hydroxypropyl methyl cellulose polymer and polyethylene glycol as a plasticizer.

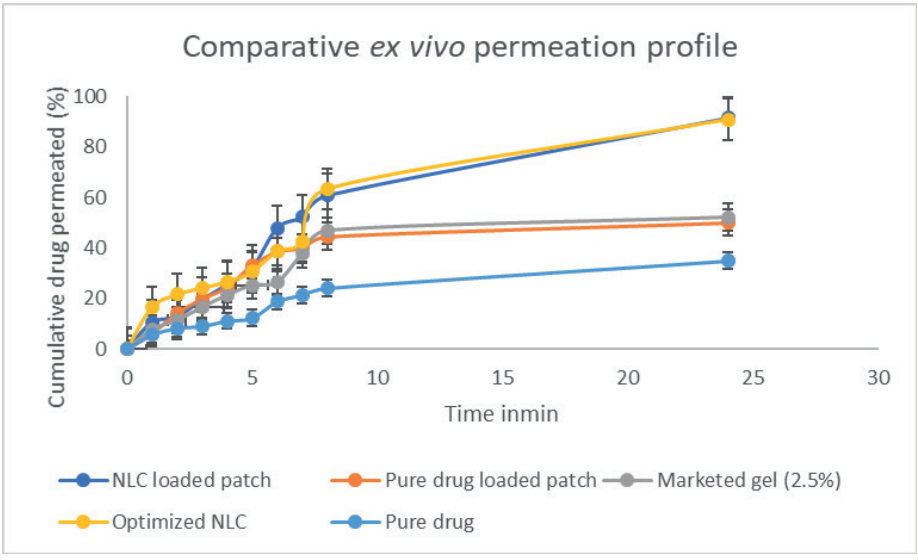

Figure 10. *Ex vivo* permeation profile

Optimized formula from exhibited drug permeation of 90.91±0.98%, whereas pure drug suspension containing the same amount of drug exhibited drug permeation up to 35± 0.14 % in 24 h via the excised rat abdominal skin specimen shown in (Figure 10). NLC's increased skin permeation compared to pure drug patches and marketed formulations is attributed to lipid dynamic behaviour, i.e., the ability of the lipids to get dissolved into the lipid layers of the stratum corneum. Thus, lipid exchange between the stratum corneum and lipid favours ketoprofen's skin delivery. Secondly, as a result of their nano size, these carriers can penetrate the deeper skin layers. Though few particles would endure intact on the surface of the skin, a majority would most likely interact with the stratum corneum, fuse and disrupt the characteristics of the barrier and enhance the drug penetration. Thirdly, the role of poloxamer contributed to the skin permeation of the drug. Surfactants, by virtue of their ability to disrupt the organized stratum corneal layers and their capacity to alter the aqueous fluid content, might have added to the skin permeation.

***Ex vivo* permeation studies of optimal formulation in comparison with ketoprofen loaded patch and marketed gel (2.5%)**

The drug's permeation rate from the NLC patch was 91.5±0.06%, compared to a pure drug, and marketed ketoprofen gel (2.5%) showed a permeation rate of 50.1±0.08% and 52.12±0.06% respectively in 24 h release studies shown in (Table11) and (Figure

11). The NLC formulation showed activity up to 24 h, reaching a maximum at six h, which confirms the prolonged activity of the patch. In contrast, the marketed formulation showed increased activity for the initial eighth. This could be associated with the presence of a significant quantity of alcohol, which is a known skin penetration enhancer. Nevertheless, the marketed formulation exhibited reduced activity at 24 h. In contrast, the pure drug exhibited activity up to 8h. The faster onset of action of the developed NLC patch was confirmed to be comparable to the marketed gel. The sustained action of the NLC patch even at the finish of 24 h could be explained by encapsulation, i.e., when oil is mixed with solid lipid, phase separation takes place, resulting in nanodroplets of oil surrounded by a solid matrix. The lipid matrix on the oil surface prevents drug leakage from the interior and thus slows down the drug release. The *ex vivo* permeation indicated a higher flux and permeability coefficient of NLC patch compared to pure drug incorporated patch and marketed gel of ketoprofen.

Table 11. Comparative steady state flux and permeability coefficient

Time (h)	**Steady state flux Jss (µg/cm²/hr)**		
	NLC loaded patch + SD	**Pure drug loaded patch + SD**	**Marketed gel(2.5%) + SD**
1	0.31±0.02	0.12±0.03	0.22±0.02
2	0.37±0.03	0.17±0.01	0.33±0.03
3	0.56±0.04	0.18±0.06	0.48±0.07
4	0.70±0.05	0.21±0.01	0.62±0.09
5	0.80±0.06	0.25±0.08	0.74±0.01
6	0.94±0.1	0.33±0.9	0.76±0.03
7	1.23±0.04	0.35±0.04	1.05±0.1
8	1.56±0.01	0.39±0.02	1.37±0.01
24	3.05±0.03	0.45±0.05	1.45±0.05

Permeability coefficient Kp ($cmhr^{-1}X10^3$)			
Kp	**NLC loaded patch**	**Pure drug loaded patch**	**Marketed gel (2.5%)**
1	0.75	0.27	0.5

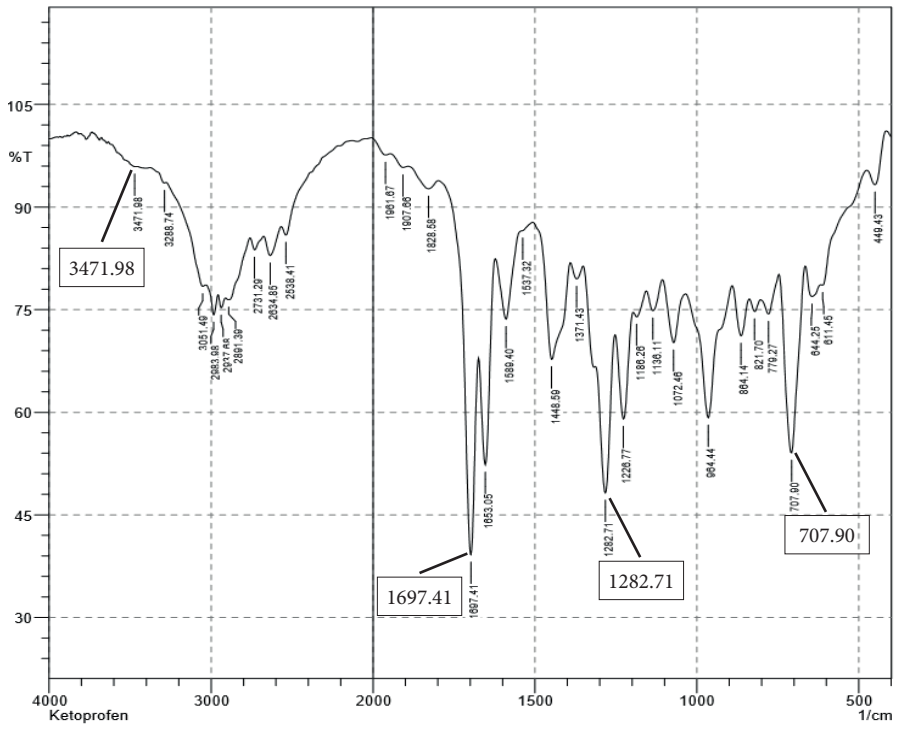

Figure 11: FTIR spectrum of ketoprofen pure drug

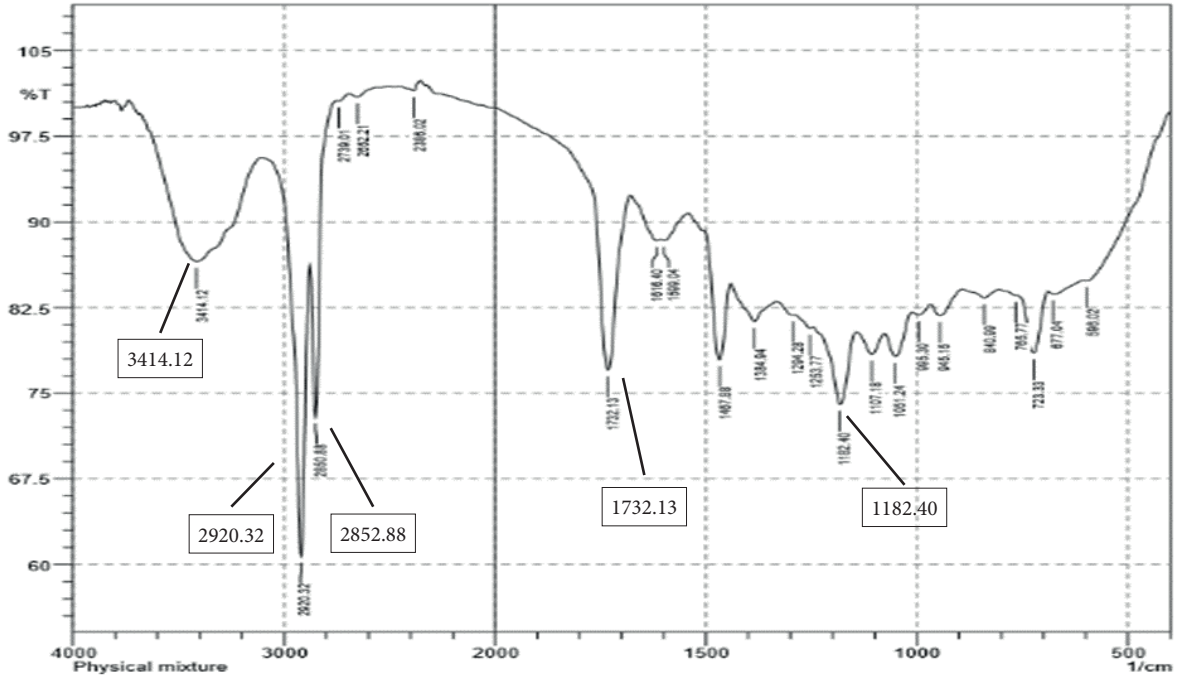

Figure 12: FTIR spectrum of physical mixture

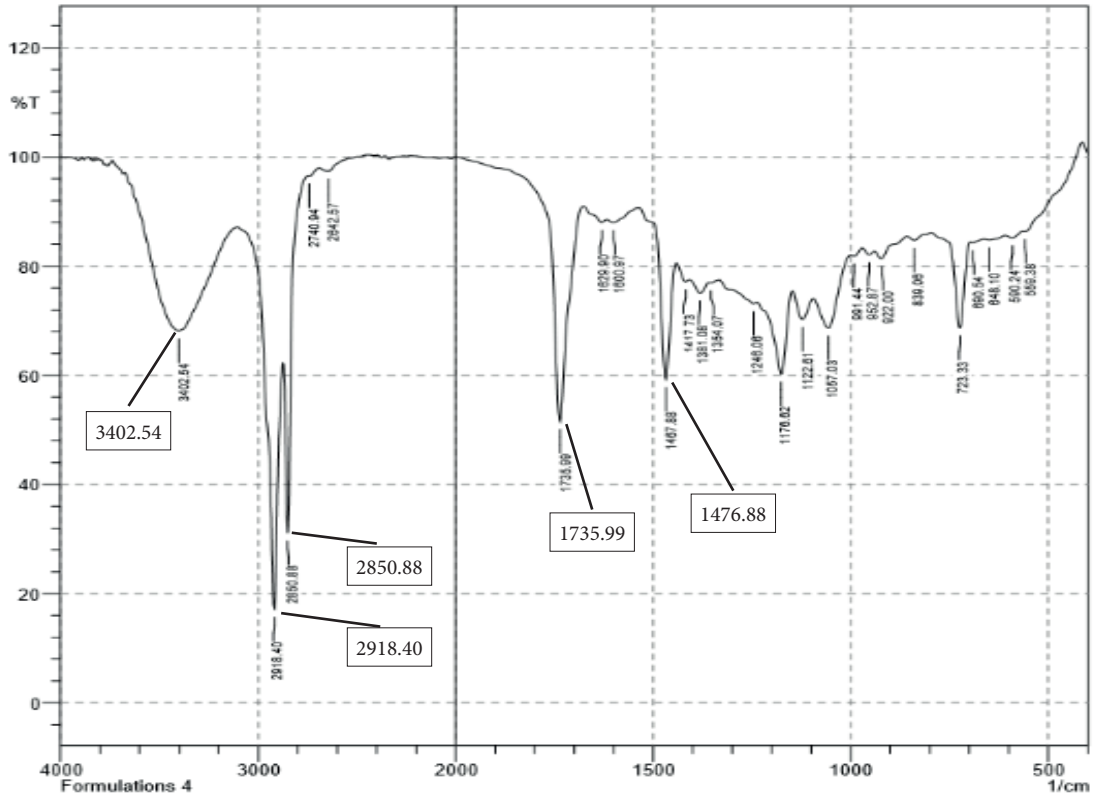

Figure 13: FTIR spectrum of NLC formulation

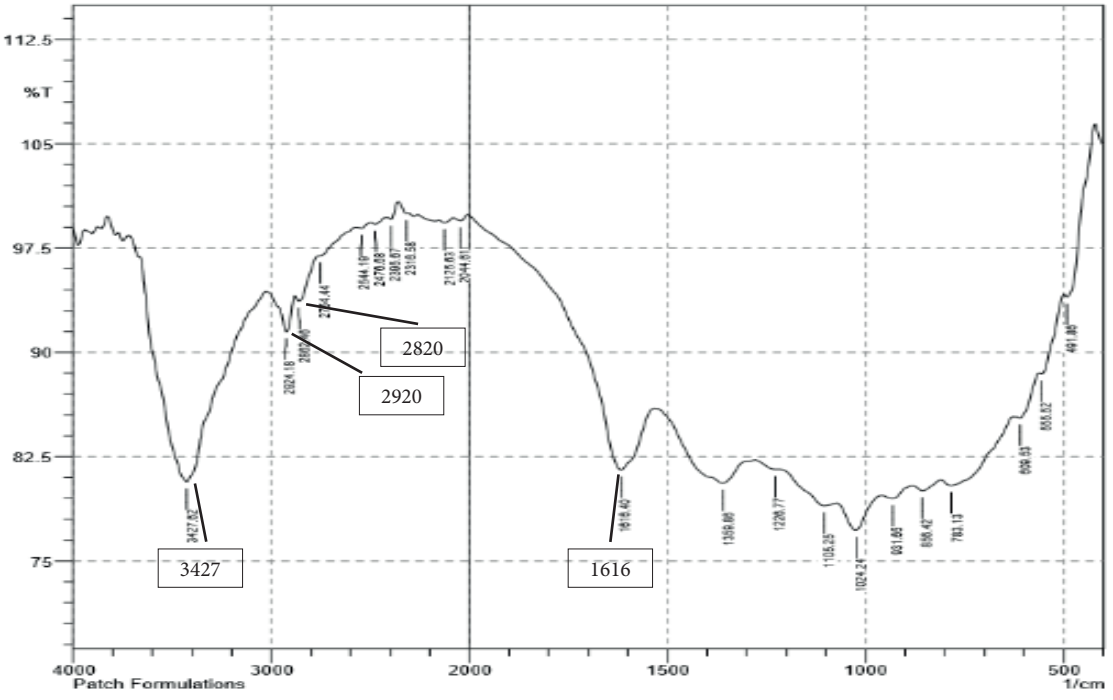

Figure 14: FTIR spectrum of patch formulation

Drug excipients compatibility studies by IR

The compatibility studies by FTIR showed no interaction between the drug and excipients used. The FTIR was performed for drug, drug/excipients and is shown in (Figure 11) and (Figure 12). All the observed ranges were within the stretching range1500-1700 for ketone (C=O),1500-1700 for c carboxylic acid(C=O), and 2000-3000 for aromatic (O-H), 2500-3500 for aromatic (C=C). Both NLC formulation and patch formulation of ketoprofen exhibited the characteristic peaks of ketoprofen as given in (Figure 13) and (Figure 14).

Short term stability studies:

The optimal NLC formula and NLC loaded patch were exposed to short-term stability testing for 90 days at 25°C ± 2°C/ 60% ± 5% RH and 40°C±2°C/75% ±5% RH. The physical appearance result shows no change in the properties at the storage conditions mentioned above (Table 12). It shows that 25°C ± 2°C RH gives better stability conditions than 40°C ± 2°C RH.

Table12. Stability studies

Day	Physical appearance (Optimum NLC formula)		%Drug content ± SD (n=3) (NLC loaded patch)			%Entrapment efficiency ± SD (n=3) (Optimum NLC formula)		
	25±2°C	40±2°C	Initial	25±2°C	40°±2°C	Initial	25±2°C	40°±2°C
0	Free flowing	Free flowing	95.2±0.1	95.2±0.1	95.2±0.1	82.4±0.2	82.4±0.2	82.4±0.2
90	Free flowing	Free flowing	95.01±0.1	94.01±0.8	93.09±0.1	82.2±0.2	82.03±0.1	81.91±0.02

CONCLUSION

NLCs are an effective colloidal drug delivery system for dermal application due to their various beneficial effects on the skin. Considering to be based on non-toxic and non-irritant lipids, they are ideal for inflamed or broken skin. In this present work, ketoprofen-loaded NLC was developed for transdermal application to reduce the systemic adverse effects, escalate the drug's permeation rate and prolong the drug's duration of action.

Ketoprofen was successfully converted to NLCs using natural lipids such as Beeswax, carnauba wax, GMS, and linseed oil as a liquid type of lipid. Poloxamer was an excellent emulsifying agent in this o/w type of system. Hot homogenization was a suitable method to produce NLCs with superior product qualities. The method resulted in free-flowing NLCs with good drug content and entrapment efficiency. The experimental design 'custom design' was suitable for attaining optimum formulations. All the formulations could result in genuinely nanosized particles except one or two higher zeta potentials, an indication of its stability; the zeta potential indicates the excellent stability of the NLCs. The IR studies assure the compatibility of drugs and excipients even after the formulations. The comparative drug release profile assured the improved skin permeation of NLCs to drug-loaded patches and marketed Fastum ® Gel. The nanoparticulate colloidal drug delivery system of ketoprofen using Beeswax, carnauba wax, linseed oil, and poloxamer is anticipated to bestow the clinician with a novel alternative of an economical, reliable, and competent regimen for skin delivery.

ACKNOWLEDGEMENTS

The authors express their gratitude to the management of Krupanidhi College of Pharmacy for their assistance in performing the study and Prof. Prakash V. Mallya for procuring the gift sample of ketoprofen.

CONFLICT OF INTEREST

The authors declare that there is no conflict of interest.

AUTHOR CONTRIBUTION STATEMENT

Experimentation (TS), Hypothesis, mentor, design, (PS), Framing the manuscript (EJ and MMS).

REFERENCES:

Ashwini M, Sudhee P, Sogali B. Custom design perspective in the process parameter optimization of nano lipid carriers. *Int J Appl Pharm. 2020:12*(6), 198–208. https://doi.org/10.22159/ijap.2020v12i6.39565

Chaudhary H, Kohli K, Kumar V. Nano-transfersomes as a novel carrier for transdermal delivery. *Int J Pharm.* 2013; 454(1):367-80.https://doi.org/10.1016/j.ijpharm.2013.07.031

Fan X, Chen J, Shen Q. Docetaxel–nicotinamide complex-loaded nanostructured lipid carriers for transdermal delivery. *Int J Pharm.* 2013;458(2):296-304.https://doi.org/10.1016/j.ijpharm.2013.10.036

Ghasemiyeh P and Mohammadi-Samani S. Solid lipid nanoparticles and nanostructured lipid carriers as novel drug delivery systems: Applications, advantages and disadvantages.*Res Pharm Sci.* 2018; 13(4):288–303. https://doi.org/10.4103/1735-5362.235156

Jain S, Patel N, Shah MK, Khatri P, Vora N. Recent advances in lipid-based vesicles and particulate carriers for topical and transdermal application. *J Pharm Sci.* 2017; 106(2):423-45.https://do.org/10.1016/j.xphs.2016.10.001

Manikkath J, Manikkath A, Shavi GV, Bhat K, Mutalik S. Low frequency ultrasound and PAMAM dendrimer facilitated transdermal delivery of ketoprofen. *J Drug Deliv Sci Technol.* 2017; 41:334-43. https://doi.org/10.1016/j.jddst.2017.07.021

Mennini N, Cirri M, Maestrelli F, Mura P. Comparison of liposomal and NLC (nanostructured lipid carrier) formulations for improving the transdermal delivery of oxaprozin: Effect of cyclodextrin complexation. *Int J Pharm.* 2016; 30;515(1-2):684-91.https://doi.org/10.1016/j.ijpharm.2016.11.013

Nair HA, Soni DM. Optimization of formulation parameters for preparation of docetaxel loaded nanostructured lipid carriers. *Int J Pharm Sci Res.* 2015; 6:2846-57.http://dx.doi.org/10.13040/IJPSR.0975-8232.6(7).

Patel RP, Patel G, Patel H, Baria A. Formulation and evaluation of transdermal patch of aceclofenac. *Res J Pharma Dosage Forms Technol.* 2009;1(2):108-15.http://dx.doi.org/10.5138/ijdd.2009.0975.0215.01005

Patwekar SL, Pedewad SR, Gattani S. Development and evaluation of nanostructured lipid carriers-based gel of isotretinoin. *Part Sci Technol.* 2018; 36(7):832-43.https://doi.org/10.1080/02726351.2017.1305026

Phatak AA, Chaudhari PD. Development and evaluation of nanostructured lipid carrier (NLC) based topical delivery of an anti-inflammatory drug. *J Pharm Res*. 2013;7(8):677-85.http://dx.doi.org/10.1016/j.jopr.2013.08.020

Ramkanth S, Chetty CM, Sudhakar Y, Thiruvengadarajan VS, Anitha P, Gopinath C. Development, characterization and in vivo evaluation of proniosomal based transdermal delivery system of Atenolol. *Future J Pharm Sci*.2018;4(1):80-7.https://doi.org/10.1016/j.fjps.2017.10.003

Reynolds JEF. Martindale The Extra Pharmacopoeia. 30th ed. London: The pharmaceutical Press;21-22, 1993.

Souto EB, Müller RH. SLN and NLC for topical delivery of ketoconazole. *J Microencapsul.* 2005 ;22(5):501-10. https://doi.org/10.1080/02652040500162436

Subramanyam B, Siddiq ZH, Nagoor NH. Optimization of nanostructured lipid carriers: understanding the types, designs, and parameters in the process of formulations. *J Nanoparticle Res.* 22(6): 141doi:10.1007/s11051-020-04848-0

Tamjidi F, Shahedi M, Varshosaz J, Nasirpour A. Nanostructured lipid carriers (NLC): A potential delivery system for bioactive food molecules. *Innov Food Sci Emerging T*. 2013; 19:29-43.http://dx.doi.org/10.1016%2Fj.ifset.2013.03.002

Zhai Y, Yang X, Zhao L, Wang Z, Zhai G. Lipid nanocapsules for transdermal delivery of ropivacaine: in vitro and in vivo evaluation. *Int J Pharm*. 2014;471(1-2):103-11.https://doi.org/10.1016/j.ijpharm.20

Zhou X, Hao Y, Yuan L, Pradha. NS, Shrestha K, Pradhan O, et al. Nano-formulations for transdermal drug delivery: a review. *Chin Chem Lett*. 2018 29;(12):1713-24.https://doi.org/10.1016/j.ijpharm.2013.07.031

FABAD J. Pharm. Sci., 48, 1, 125-138, 2023
Doi: 10.55262/fabadeczacilik.1175781
RESEARCH ARTICLE

Evaluation of Phytochemical Contents and Biological Activities of *Salvia officinalis* and *Salvia triloba* Grown with Organic Farming

Burçin ÖZÜPEK[*], Sultan PEKACAR[**], Didem DELİORMAN ORHAN[***°]

Evaluation of Phytochemical Contents and Biological Activities of Salvia officinalis and Salvia triloba Grown with Organic Farming

SUMMARY

Salvia officinalis L., known as medicinal sage, and Salvia triloba L., known as Anatolian sage, belong to the Lamiaceae family and are species that usually grow in the Mediterranean region. In this study, it was aimed to evaluate the in vitro antidiabetic, antiobesity and antioxidant potentials of the extracts prepared by infusion technique from S. officinalis and S. triloba has grown by organic farming methods. In addition, the effects of the extracts on the pancreatic cholesterol esterase enzyme were also investigated. The Reverse Phase-High Performance Liquid Chromatography (HPLC) technique was used to analyze the phytochemical contents of the extracts. At a concentration of 2 mg/mL, S. officinalis inhibited 64.69% ± 0.23, S. triloba 47.78 ± 2.11% on the α-glucosidase enzyme. Only S. triloba had an inhibitory effect on α-amylase and pancreatic lipase enzyme. On the pancreatic cholesterol esterase enzyme, inhibition values of S. triloba extract at all tested concentrations was found higher than S. officinalis extract. It was observed that the S. officinalis extract had the highest reducing power potential. The metal chelating capacity of both extracts at a concentration of 2 mg/mL was calculated as 100%. It was concluded that the ABTS radical scavenging activity of the extracts increased in a dose-dependently manner. The amounts of rosmarinic acid and hesperidin were found higher in S. officinalis extract than in S. triloba extract by Reverse Phase-HPLC technique. The presence of hesperidin in S. triloba was detected for the first time in this study. These findings considering it was concluded that activity-guided isolation and in vivo activity studies should be performed because these two species grown the organic farming methods have potent α-glucosidase enzyme inhibitory and antioxidant effects.

Keywords: *Antioxidant, enzyme inhibition, phytochemistry, Reverse phase-HPLC, Salvia officinalis, Salvia triloba*

Organik Tarım ile Yetiştirilen Salvia officinalis ve Salvia triloba'nın Fitokimyasal İçeriklerinin ve Biyolojik Aktivitelerinin Değerlendirilmesi

ÖZ

Tıbbi adaçayı olarak bilinen Salvia officinalis L. ve Anadolu adaçayı olarak bilinen Salvia triloba L., Lamiaceae familyasına ait olup, genellikle Akdeniz bölgesinde yetişen türlerdir. Bu çalışmada organik tarım yöntemleri ile yetiştirilmiş S. officinalis ve S. triloba'dan infüzyon tekniği ile hazırlanan ekstrelerinin in vitro antidiyabetik, antiobezite ve antioksidan potansiyellerinin değerlendirilmesi amaçlanmıştır. Bunların yanı sıra ekstrelerin pankreatik kolesterol esteraz enzimi üzerindeki etkileri de incelenmiştir. Ekstrelerin fitokimyasal içeriklerini analiz etmek için Ters Faz-Yüksek Performanslı Sıvı Kromatografisi (YPSK) tekniği kullanılmıştır. α-Glukozidaz enzimi üzerinde 2 mg/mL konsantrasyonda S. officinalis %64.69 ± 0.23, S. triloba ise %47.78 ± 2.11 inhibisyona neden olmuştur. α-Amilaz ve pankreatik lipaz enzimi üzerinde sadece S.triloba inhibitör etki oluşturmuştur. Pankreatik kolesterol esteraz enzimi üzerinde ise S. triloba ekstresinin test edilen tüm konsantrasyonlardaki inhibisyon değerlerinin S. officinalis ekstresinden daha yüksek olduğu tespit edilmiştir. S. officinalis ekstresinin en yüksek indirgeme gücü potansiyeline sahip olduğu gözlemlendi. Her iki ekstrenin 2 mg/mL konsantrasyonda metal bağlama kapasitesi %100 olarak hesaplanmıştır. Ekstrelerin ABTS radikal süpürücü aktivitesinin ise doz bağımlı olarak arttığı sonucuna varılmıştır. Ters Faz-YPSK tekniği ile S. officinalis ekstresinde rosmarinik asit ve hesperidin miktarları S. triloba ekstresine göre daha yüksek bulunmuştur. S. triloba'da hesperidinin varlığı ilk kez bu çalışmada tespit edilmiştir. Tüm bu bulgular göz önüne alındığında, organik tarım yöntemiyle yetiştirilen bu iki türün güçlü α-glukozidaz enzim inhibitör ve antioksidan etkilere sahip olmasından dolayı üzerlerinde aktivite yönlendirmeli izolasyon ve in vivo aktivite çalışmalarının yapılması gerektiği sonucuna varılmıştır.

Anahtar Kelimeler: *Antioksidan, enzim inhibisyonu, fitokimya, ters faz-YPSK, Salvia officinalis, Salvia triloba*

Received: 15.09.2022
Revised: 23.12.2022
Accepted: 26.12.2022

[*] ORCID:0000-0003-2159-9860, Gazi Üniversitesi, Eczacılık Fakültesi, Farmakognozi Ana Bilim Dalı, 06510, Ankara, Türkiye,
[**] ORCID:0000-0002-7782-9832 , Gazi Üniversitesi, Eczacılık Fakültesi, Farmakognozi Ana Bilim Dalı, 06510, Ankara, Türkiye
[***] ORCID:0000-0003-3916-4048, Gazi Üniversitesi, Eczacılık Fakültesi, Farmakognozi Ana Bilim Dalı, 06510, Ankara, Türkiye

[°] Corresponding Author; Didem Deliorman Orhan
Tel. +90 3122023173, Fax: +90 3122023173, e.mail: didem@gazi.edu.tr, didemdeliorman@gmail.com

INTRODUCTION

The genus *Salvia* belongs to the Lamiaceae family, which consists of about 900 species (Lu, 2002). Salvia means "to be healed or to be safe and notharmed" in Latin, referring to the medicinal properties of some species (Kamatou, 2008). *Salvia* genus is widely distributed in three regions of Central-South America, Central Asia-Mediterranean and East Asia (Xu, 2018). Major phytochemical components in *Salvia* species include phenolic acids, diterpenoids, triterpenoids, flavonoids and saccharides. While flavonoids, triterpenoids and monoterpenes are primarily found in the aerial parts of the plant, especially in flowers and leaves; phenolic acids and diterpenoids are mainly found in roots (Xu, 2018). It is reported in the literature that *Salvia* species is used the treatment diabetes mellitus in folk medicine (Eidi, 2009). While the flower, leaf and root extracts of these species are used in wounds, pharyngitis, mouth ulcers and menstrual irregularities in Anatolia, teas prepared from the leaves are used for indigestion, insomnia and pain relief purposes (Sharma, 2019). Some species of *Salvia* genus are used as spices in various countries, while others are utilized in cosmetic formulations, aromatherapy and insecticides (Lu, 2002; Kamatou, 2008).

Diabetes mellitus (DM) is a metabolic disease characterized by hyperglycemia caused by defects in insulin secretion, insulin action, or both (American Diabetes Association, 2005). Globally, the prevalence of type 2 diabetes is increasing rapidly. The global prevalence of diabetes among adults was estimated at 150 million in 1995, projected to increase to 300 million by 2025 (Abubakari, 2008). DM and obesity are strongly and complexly related to each other. Obesity is defined as a risk factor for Type 2 Diabetes (Hussain, 2010). The organism is exposed to oxidative stress resulting in the attack of free radicals (reactive oxygen species (ROS)/ reactive nitrogen species (RNS) formed by the transfer of free unpaired electrons. combat the harmful effects of ROS, the body activates its endogenous antioxidant systems. As another option, the body takes advantage of dietary antioxidants that destroy or detoxify ROS and maintain homeostasis. Oxidative stress, which occurs as a result of increased blood glucose levels, is held responsible for the development of diabetes and its complications (Asmat, 2016). Therefore, in the fight against diabetes, which is a metabolic disorder, there is a need for new drugs of natural or synthetic origin that can both lower blood sugar, reduce oxidative stress caused by diabetes, and play a role in weight control.

The collection of medicinal and aromatic plants from wild sources has been a practice of humanity since ancient times and causes the decline of plant species. 13% of the plants unconsciously collected in the world are under threat, and 22-47% of this percentage has faced extinction (Pitman, 2002). The uncontrolled collection of medicinal and aromatic plants from nature reveals that natural resources will decrease in the future to treat diseases, considering that these plants are used for health purposes. The most significant disadvantage of medicinal plant production using organic farming techniques is the high cost. On the other hand, the benefits of organic agriculture cannot be ignored when the factors such as the healthier and higher quality of the plants grown in this way and the protection of biodiversity are taken into account. For these reasons, the cultivation of medicinal and aromatic plants using organic farming techniques should be encouraged and the phytochemical contents and biological activities of these plants should be investigated. to increase the sustainability of medicinal and aromatic plants, protecting natural resources is one of the most critical applications. For this purpose, it is necessary to cultivate the species or to produce them with organic farming techniques. In this way, it will be possible to protect biodiversity and make healthier and higher-quality products with higher yields.

In this study, which is considered to be a first, the effects of infusions prepared from organic farming-grown *Salvia officinalis* L. and *S. triloba* L. sam-

ples on some enzymes (α-amylase, α-glucosidase, pancreatic lipase, and pancreatic cholesterol esterase enzymes) that play a role in metabolic diseases and their antioxidant potential (2,2-diphenyl-1-picrylhydrazil (DPPH) and 2,2'-azino-bis (3-ethylbenzothiazoline-6 sulfonate) cation ($ABTS^{\bullet+}$) radical scavenging activity, metal chelating, and ferric-reducing power) were evaluated. The total phenolic and total flavonoid contents of the extracts were determined by spectrophotometric methods. Additionally, qualitative and quantitative analysis of the phenolic compounds of the extracts were carried out with by Reverse Phase-HPLC (RP-HPLC) method.

MATERIAL AND METHODS

Plant material

S. officinalis and *S. triloba* has grown with organic farming were provided from Beyşehir Road, 3. km Akyokuş Mevki, Konya, in 2021 (Certificate no: TR-OT-014-İ-197/01, Temmuz Organik Çiftliği). These species were produced by the Organic Agriculture Law and Regulation of the Turkish Republic and have been certified by Nissert and authorized by the Ministry of Agriculture.

Extraction

200 mL of hot water was added to 10 g of powdered aerial parts for extraction. This extract was then filtered and this process was repeated three times. After the resulting filtrates were combined, they were freeze-dried. The yields (w/w %) of the extracts are given in Table 1.

Total phenol content

The extracts were incubated for 5 minutes at room temperature with 10% Folin-Ciocaltaeu reagent. Then sodium carbonate solution was added and the mixture was vortexed. After 30 minutes of incubation in the dark, the absorbance of the extracts was measured at 735 nm with a spectrophotometer (VersaMax ELISA Microplate Reader). Total phenol content was calculated as gallic acid equivalent (GAE) mg/g extract. The calibration equation was $y = 3.7855x + 0.1735$ and $r^2 = 0.9931$ (Zongo, 2010).

Total flavonoid content

Ethanol, sodium acetate and aluminum chloride solutions were added to the extracts, respectively, and the mixture was diluted to 1 mL with distilled water. After 30 minutes incubation at room temperature, the absorbance of the mixture was measured at 415 nm with the ELISA microtiter plate reader. The results were calculated as quercetin equivalent (QE) mg/g extract. Calibration curve equation; $y = 2.8193x - 0.0996$ and $r^2 = 0.9977$ (Kosalec, 2004).

Antioxidant activity

ABTS radical scavenging activity

ABTS (7 mM) was dissolved in distilled water and 2.45 mM potassium persulfate solution. The mixture was incubated for approximately 16 hours at 20°C in the dark. Phosphate buffer with pH 7.4 and ABTS solution was added to the extracts. After the samples were vortexed, their absorbance was read at 734 nm with an ELISA microtiter plate reader. Gallic acid was used as a reference compound (Orhan, 2017).

DPPH radical scavenging effect

After adding 1mM DPPH (2,2-diphenyl-1-picrylhydrazil) solution to 80 µL of extract, it was kept in the dark at room temperature for 30 minutes. The absorbance of the mixture at 520 nm was then measured. Ascorbic acid was used as reference material (Jung, 2011).

Metal chelating capacity

After adding 2 mM $FeCl_2$ solution to the extracts, the mixture was incubated for 5 minutes at room temperature. Then, 5 mM ferrozine solution was added to this mixture and kept at room temperature for 10 minutes, and absorbance was measured at 562 nm with a spectrophotometer. EDTA (Ethylene diaminetetraacetic acid) was used as reference material. Metal chelating capacity was calculated with the formula (%) = $[(A_{Control} - A_{Sample})/A_{Control}] \times 100$ (Dinis, 1994).

Ferric-reducing antioxidant power

After adding 0.1 mol/L sodium phosphate buffer (pH=7.2) to the extracts in various concentrations, 1% potassium ferricyanide solution was added to this

mixture and incubated in an oven at 37°C for 60 minutes. After the incubation period, 10% trichloroacetic acid solution was added and absorbance was measured at 700 nm. At the end of this process, 0.1% $FeCl_3$ solution was added, and the measurement was made again and the difference was taken. The percent ferric reducing power absorbance was calculated according to the following equation: ferric reducing power absorbance = $(B_2-B_1)-(A_2-A_1)$;what is stated here can be expressed : B_1: the first measurement value of the absorbance of the sample, B_2: the second measurement value of the absorbance of the example, A_1: first measurement value of the absorbance of the blank, A_2: the second measurement value of the absorbance of the blank. Quercetin compound was used as a reference substance (Orhan, 2017).

Enzyme assays

***α*-Glucosidase inhibitory activity**

The *α*-Glucosidase type IV enzyme (EC 3.2.1.20, Sigma) was dissolved in 0.5 M phosphate buffer (pH 6.5). Extracts were prepared at concentrations of 2, 1, and 0.5 mg/mL and tested in 3 replicates in 96-well microplates. p-nitrophenyl-*α*-D-glucopyranoside was used as the substrate. After adding the substrate, the plates were incubated at 37°C for 35 minutes. The absorbance of the mixture was then measured at 405 nm. Acarbose was used as a reference substance. The percent inhibition was calculated according to the following equation: Inhibition (%) = (1−(Y−y/X−x)) × 100; what is stated here can be expressed as: x is the negative control without inhibitor, X is the activity without inhibitor, y is the negative control with inhibitor and Y is the activity with inhibitor (Orhan, 2017).

***α*-Amylase enzyme inhibitory activity**

It was dissolved in α-Amylase type VI (EC 3.2.1.1. Sigma) buffer. Potato starch was used, and this substrate was prepared in a phosphate buffer with a pH of 6.9. After the samples were incubated with the enzyme solution at 37°C for 15 minutes, substrate solution was added. Then, incubation was continued with DNS (96 mM 3.5-dinitrosalicylic acid. 5.31 M sodium potassium tartrate) at 80°C for another 40 minutes. Then, distilled cold water was added and absorbance was measured at 540 nm. The amount of maltose produced was calculated using the standard maltose calibration chart (y = 0.6762x - 0.0404) and the net absorbance was obtained. Acarbose was used as a reference substance. The change in absorbance due to maltose formation was read at 540 nm and the calculations were made as follows: A_{Sample} or $_{Control} = A_{Sample} - A_{Blank.}$ Based on the amount of maltose formed, a calibration curve of maltose was formed and percent inhibition was determined. Inhibition (%) = (1−(average of maltose formed in test samples/mean of maltose formed in control)) × 100 (Orhan, 2017).

Pancreatic lipase inhibitory activity

Type II enzyme (EC 3.1.1.3, Sigma) obtained from pig pancreas was added to the extracts, and the pH 6.8 MOPS (morpholinepropanesulfonic acid) buffer and the pH 7.4 Tris HCl buffer wasadded, and the mixture was incubated at 37°C for 15 minutes. 10 mM p-nitrophenylbutyrate was used as substrate. Then the substrate was added and incubated at 37°C for 30 minutes. The absorbance of the samples at 405 nm was measured. Orlistat was used as a reference compound. The percent inhibition was calculated according to the following equation: Inhibition (%) = (1−(Y−y/X−x)) × 100; what is stated here can be expressed as: x is the negative control without inhibitor, X is the activity without inhibitor, y is the negative control with inhibitor and Y is the activity with inhibitor (Lee, 2010).

Cholesterol esterase enzyme inhibitory activity

Cholesterol esterase enzyme (EC3.1.1.13, Sigma) obtained from pork pancreas was dissolved in 100 mM phosphate buffer (pH=7) containing 100 mM NaCl. Phosphate buffer, 12 mM taurocholic acid and substrate solutions were added to the samples, respectively. As a substrate, p-nitrophenylbutyrate was used. After incubation at 25°C for 5 minutes, the enzyme was added and kinetic measurements were made at 405 nm for 15 minutes. Simvastatin was used as a reference compound. The percent inhibition was calculated as follows: Inhibition (%) = $[(A_{Control} - A_{Sample})/A_{Control}] \times 100$ (Ngamukote, 2011).

RP-HPLC analysis

HP Agilent 1260 series LC System and TC-(4.6 mm x 150 mm x 5 µm) column were used in the RP-HPLC system for analysis. The column temperature was kept constant at 25°C throughout the analysis. The following standard compound mixtures were used for the qualitative and quantitative analyzes of the phenolic compounds and flavonoids in the extract. Phenolic compound mixture: Gallic acid, protocatechuic acid, chlorogenic acid, vanillic acid, syringic acid, *p*-coumaric acid, ferulic acid, sinapic acid, *trans*-cinnamic acid, rosmarinic acid, epicatechin, catechin. Flavonoid mixture: Umbelliferone, rutin, naringenin, hesperidin, quercetin-3-*O*-glucoside, apigenin-7-*O*-glucoside, myrcetin, quercetin, luteolin, apigenin. The gradient flow system was started with the mobile phase containing 5% solvent A (acetonitrile: water: formic acid, 50:50:0.5) and 95% solvent B (water: formic acid, 100:0.5). Total analysis time was 58 minutes and the injection volume was 20 µL. This process was carried out at 4 different wavelengths, 260, 280, 320 and 350 nm, using a DAD detector. The extracts were prepared in 25% acetonitrile solution at a concentration of 1 mg/mL. Sample solutions were prepared by filtration through a 0.45 µm membrane filter. A Calibration chart was prepared for hesperidin (Rt= 35.89) and rosmarinic acid (Rt= 37.149 min). from the stock solution of these two standard substances, dilution solutions were prepared at five different concentrations. The concentrations mentioned are 0.5, 10, 20, 50 and 100 ppm. Since the peak area values of these compounds in the extract are in the relevant concentration range, quantification was made by creating a calibration curve based on the ppm values (x) and peak areas (y) (Gök, 2020).

Statistical Analysis

All experiments were done in triplicate. Means of numerical values were calculated and presented in the tables as mean ± standard deviation (SD). Microsoft Excel and GraphPad Instat software programs were used in the calculations and the difference in $p<0.05$ values were evaluated as statistically significant in this study (*$p<0.05$, **$p<0.01$, ***$p<0.001$).

RESULTS AND DISCUSSION

The yields of *S. officinalis* and *S. triloba* extracts prepared by the infusion technique were 27.13% and 16.82% (w/w), respectively. While the total phenol content in *S. officinalis* and *S. triloba* extracts was calculated as 193.50 ± 8.22 and 203.01 ± 7.85 GAE mg/g extract, respectively, the total flavonoid amounts of the extracts were determined as 71.51 ± 1.88 and 78.84 ± 8.76 QE mg/g extract, respectively (Table 1).

Table 1. Yield (w/w), total phenol and total flavonoid contents of *S. officinalis* and *S. triloba* extracts

Extracts	Yield (w/w%)	Total Phenolic Content[a] (Mean ± SD)	Total Flavonoid Content[b] (Mean ± SD)
S. officinalis	27.13	193.50 ± 8.22	71.51 ± 1.88
S. triloba	16.82	203.01 ± 7.85	78.84 ± 8.76

[a]mg GAE/g extract, [b]mg QE/g extract, SD: Standard Deviation

In experiments to evaluate the antioxidant potential of extracts; while the ABTS radical scavenging effect of the extracts of both species increased depending on the dose, on the contrary, the DPPH radical scavenging effect decreased. In the metal chelating activity assay, extracts of both species (100%) displayed higher activity at 2 mg/mL concentrations than EDTA (95.72 ± 0.63%) used as the reference compound. At the ferric reducing power, both species showed the highest absorbance at a concentration of 2 mg/mL, especially the *S. officinalis* extract (3.392 ± 0.01) gave absorbance values almost close to the quercetin (3.538 ±0.02) used as the reference compound (Table 2).

Table 2. ABTS, DPPH radical scavenging activity, metal chelating activity and the ferric-reducing power results of *S. officinalis* and *S. triloba* extracts

Extract	Concentration (mg/mL)	Antioxidant Activity			
		ABTS radical scavenging activity Inhibition% ± SD	DPPH radical scavenging activity Inhibition% ± SD	Metal Chelating Capacity % ± SD	Ferric Reducing Power Absorbance ± SD
S. officinalis	0.5	25.79 ± 0.90**	77.68 ± 0.94***	56.70 ± 3.76***	1.475 ± 0.09***
	1	46.91 ± 0.47***	74.56 ± 0.41***	86.70 ± 1.38***	2.531 ± 0.01***
	2	73.30 ± 0.60***	56.98 ± 6.25***	100***	3.392 ± 0.01***
S. triloba	0.5	31.22 ± 1.41**	79.04 ± 0.58***	-	1.293 ± 0.07**
	1	53.77 ± 0.52***	69.36 ± 2.47***	84.37 ± 5.13***	1.794 ± 0.38***
	2	87.41 ± 0.86***	60.05 ± 2.83***	100***	2.889 ± 0.61***
References	GA/AA/EDTA/QE 0.5	99.54 ± 1.04^{***a}	89.42 ± 3.07^{***b}	99.83 ± 0.39^{***c}	3.253 ± 0.38^{***d}
	GA/AA/EDTA/QE 1	98.94 ± 0.26^{***a}	90.71 ± 0.65^{***b}	99.78 ± 0.26^{***c}	3.560 ± 0.02^{***d}
	GA/AA/EDTA/QE 2	98.10 ± 0.80^{***a}	90.38 ± 0.86^{***b}	95.72 ± 0.63^{***c}	3.538 ±0.02^{***d}

-: No activity, SD: Standard Deviation, ns: Not statistically significant, *p<0.05 **p<0.01 ***p<0.001 GA: [a]Gallic acid, AA: [b]Ascorbic acid, EDTA: [c]Ethylenediamine tetraacetic acid, [d]QE: Quercetin

S. officinalis extract did not inhibit α-amylase and pancreatic lipase enzymes at the concentrations tested. *S. triloba* extract inhibited α-amylase enzyme at rates ranging from 11.33% to 19.48% at all doses tested, in contrast the same extract inhibited pancreatic lipase enzyme at 1 and 2 mg/ml concentrations, 8.84% and 22.79%, respectively. *S. officinalis* extract (64.69 %) inhibited the α-glucosidase enzyme much more potently than *S. triloba* extract (47.78 %) when compared with the reference compound acarbose (99.35 %). The extracts of both species (36.99 ± 2.00% and 38.03 ± 2.59%) at a concentration of 2 mg/mL showed a moderate inhibitory effect against the pancreatic cholesterol esterase enzyme when compared with simvastatin (53.18 ± 3.36%) (Table 3).

Table 3. Inhibitory effects of *S. officinalis* and *S. triloba* extracts on α-glucosidase, α-amylase, pancreatic lipase and pancreatic cholesterol esterase enzyme

Extract	Concentration (mg/mL)	Inhibition %± SD			
		α-Glucosidase	α-Amylase	Pancreatic Lipase	Pancreatic Cholesterol Esterase
S. officinalis	0.5	7.41 ± 0.35^{ns}	-	-	9.85 ± 5.97*
	1	24.28 ± 2.60**	-	-	23.95 ± 2.91**
	2	64.69 ± 0.23***	-	-	36.99 ± 2.00**
S. triloba	0.5	3.01 ± 0.29^{ns}	16.67 ± 1.99*	-	24.60 ± 2.26**
	1	23.73 ± 0.68*	11.33 ± 2.70*	8.84 ± 3.30^{ns}	31.21 ± 0.89**
	2	47.78 ± 2.11***	19.48 ± 2.26**	22.79 ± 4.31**	38.03 ± 2.59**
References	ACA/OR/SIM 0.5	98.88 ± 0.21^{***a}	94.85 ± 0.60^{***a}	52.16 ± 0.00^{***c}	47.88 ± 5.11^{***d}
	ACA/OR/SIM 1	99.47 ± 0.13^{***a}	98.38 ± 0.50^{***a}	69.54 ± 4.19^{***c}	52.21 ± 0.12^{***d}
	ACA/OR/SIM 2	99.35 ± 0.2^{2***}a	95.24 ± 2.60^{***a}	62.55 ± 1.76^{***c}	53.18 ± 3.3^{6***}d

-: No activity, SD: Standard Deviation, ns: Not statistically significant, *p<0.05 **p<0.01 ***p<0.001 ACA: [a] Acarbose, OR: [c]Orlistat, SIM: [d]Simvastatin

RP-HPLC technique was used for the qualitative and quantitative determination of 22 phenolic compounds (gallic acid, protocatechuic acid, chlorogenic acid, vanillic acid, syringic acid, *p*-coumaric acid, ferulic acid, sinapic acid, *trans*-cinnamic acid, rosmarinic acid, epicatechin, catechin, umbelliferone, rutin, naringenin, hesperidin, quercetin-3-*O*-glucoside, apigenin-7-*O*-glucoside, myricetin, quercetin, luteolin, apigenin) in the extracts (Figure 1-3). The amount of rosmarinic acid determined as the main compound in the extracts was found to be approximately two times higher in *S. officinalis* (16.233 ± 0.034 g/100 g extract) than in *S. triloba* (6.975 ± 0.006 g/100 g extract) (Figure 4 and 5). According to the results of the quantitative analysis, the amount of hesperidin in the extracts was determined. The amount of hesperidin was calculated as 0.219 ± 0.002 g/100 g extract in *S. officinalis* and 0.187 ± 0.001 g/100 g extract in *S. triloba* (Figure 6-7).

Table 4. Results of rosmarinic acid and hesperidin (g/100g dry extract) determination of *S. officinalis* and *S. triloba* extracts by Reverse Phase-HPLC

Extract	Compounds	Rt (Minute)	g/100 g dry extract	Calibration Equations	Coefficient of Determination
S. officinalis	Rosmarinic acid	37.149	16.233 ± 0.034	y = 39.256x + 0.2194	r^2 = 1.000
	Hesperidin	35.890	0.219 ± 0.002	y = 46.366x – 5.3259	r^2 = 1.000
S. triloba	Rosmarinic acid	37.149	6.975 ± 0.006	y = 39.256x + 0.2194	r^2 = 1.000
	Hesperidin	35.890	0.187 ± 0.001	y = 46.366x – 5.3259	r^2 = 1.000

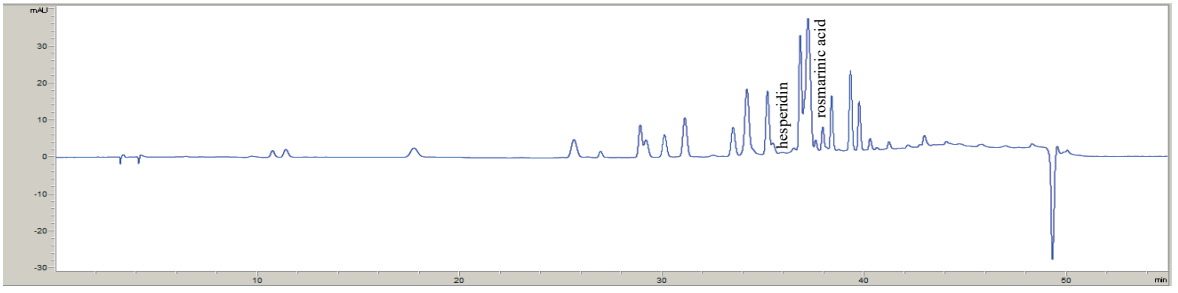

Figure 1. RP-HPLC chromatogram of the mixture standard containing phenolic and flavonoid substances at 280 nm

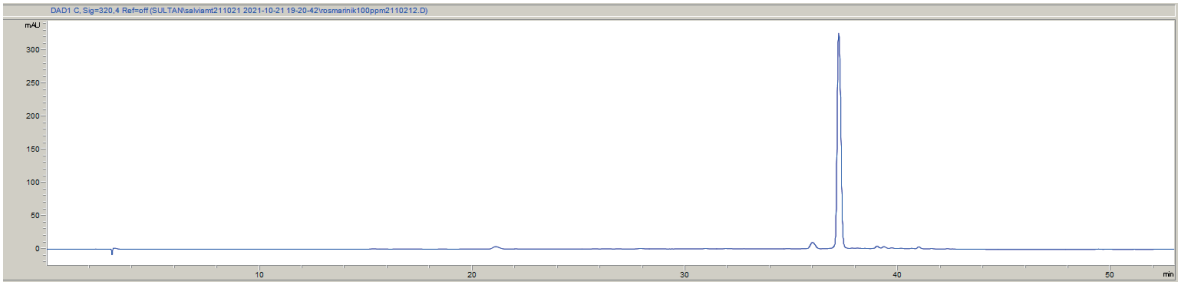

Figure 2. RP-HPLC chromatogram of the standard compound, rosmarinic acid

Figure 3. RP-HPLC chromatogram of the standard compound, hesperidin

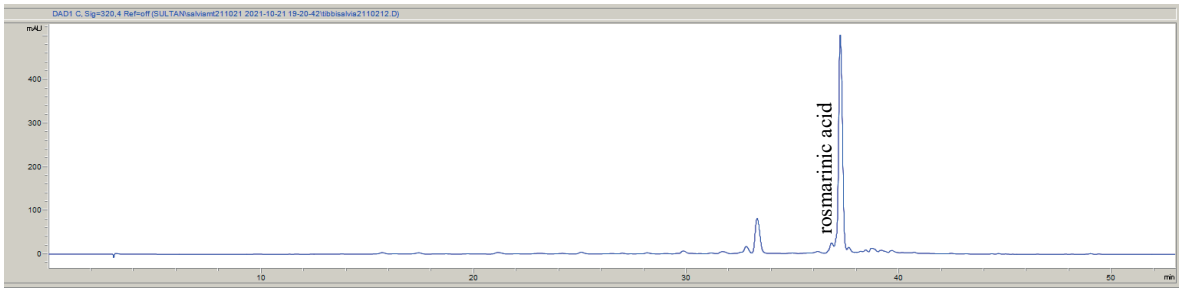

Figure 4. RP-HPLC chromatogram of *S. officinalis* at 320 nm

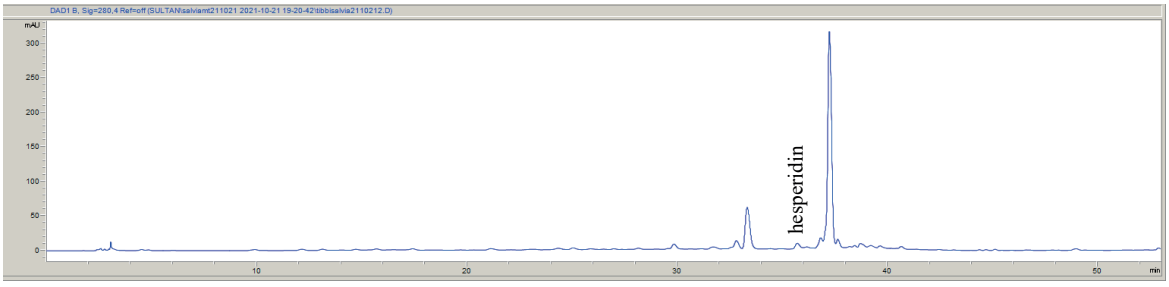

Figure 5. RP-HPLC chromatogram of *S. officinalis* at 280 nm

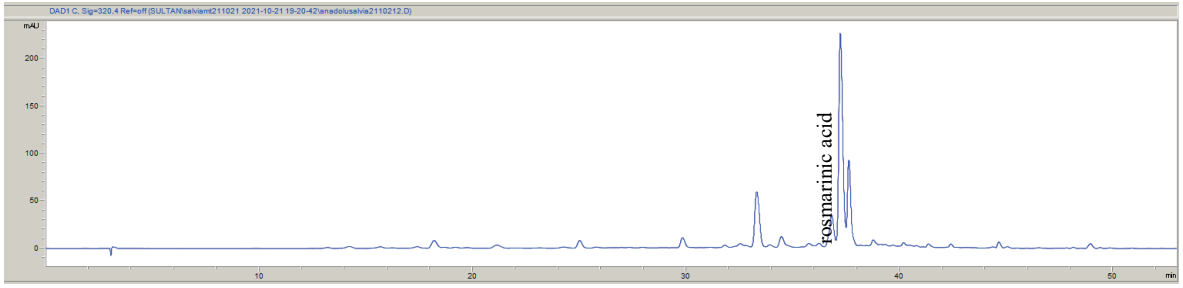

Figure 6. RP-HPLC chromatogram of *S. triloba* at 320 nm

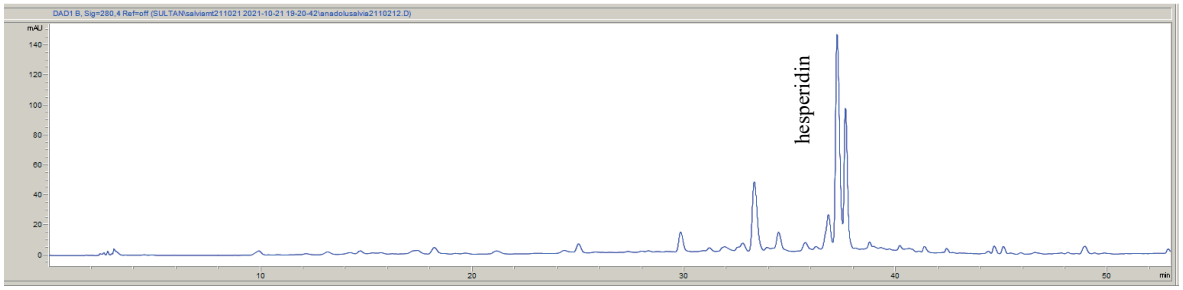

Figure 7. RP-HPLC chromatogram of *S. triloba* at 280 nm

When the activity (antioxidant and enzyme inhibitor activities) and phytochemical analysis studies performed on *S. triloba* and *S. officinalis* to date were examined, it was observed that the samples were generally wild and sometimes cultivated forms. For the first time in this study, activity studies and phytochemical analyzes were carried out on these species grown with the organic farming techniques.

Miliauskas et al. (2004) reported that the total flavonoid amount of *S. officinalis* was 3.5 mg QE/g dried material and the total phenol amount was 22.6 mg GAE/ g dried material (Miliauskas, 2004). Arıduru and Arabacı (2013) found the total phenol content between 11.58-43.55 mg GAE/g dried material of the extracts prepared with solvents of different polarities from *S. officinalis* samples collected from Sakarya (Arıduru, 2013). Hamrouni-Sellam et al. (2013) reported that the total phenol content of the aerial parts of *S. officinalis* samples collected from Tunisia ranged from 0.399 to 2.337 mg GAE/g dried material. Considering the previous studies, it was observed that the total phenol and total flavonoid content of *S. officinalis* samples grown with the organic farming techniques were generally high.

Dinçer et al. (2012) analyzed the total phenol and total flavonoid contents of wild and cultivated *S. triloba* samples in Antalya. The results showed that the total phenol content of the wild sample was 41.58±1.34 mg GAE/g dried material, the total flavonoid content was 35.58 ±0.85 mg QE/g dried material, the total phenol content of the cultivated sample was 44.60±1.21 mg GAE/g dried material and the total flavonoid content was 28.82± 2.53 mg QE/g dried material (Dincer, 2012). Boukhary et al. (2016) determined that the total phenol content of the methanolic extract of *S. triloba* samples collected from Lebanon was 122.67 ± 0.44 mg GAE/g extract (Boukhary, 2016). In a previous study, it was determined by spectrophotometric methods that the total phenol content of 20 *S. triloba* samples collected from the Marmara region varied between 8.47-13.45 mg GAE/g dried material and their total flavonoid contents varied between 5.52-7.63 mg QE/g dried material (Karık, 2018). In our study, it was observed that the total phenol content of *S. triloba* grown using organic farming techniques was higher than that of wild and cultivated samples. The total phenol content of the cultivated sample in the study of Dinçer et al. (2012) was higher than that of the sample grown with the organic farming technique in this study.

Yıldırım et al. (2000) reported that the extracts prepared using hot water from *S. triloba* samples purchased from the market had reducing solid activity. On the other hand, the DPPH radical scavenging effect of the extracts (extract type not specified) prepared from 20 *S. triloba* samples collected from the Marmara region was investigated using the HPLC technique. It was found that the total antioxidant activities of all samples varied between 820.00-876.79 µmol Trolox equivalent/100 g dried material (Karık, 2018). Arıduru and Arabacı (2013) investigated the DPPH radical scavenging effects of extracts prepared with solvents of different polarities (methanol, ethanol, ethyl acetate, and acetone) from *S. officina-*

lis samples collected from Sakarya. The most potent radical scavenging activity was observed in methanol (90.89%) and ethyl acetate (90.48%) extracts, followed by ethanol (86.31%) and acetone (84.78%) extracts. In this study, BHT and Trolox inhibited the DPPH radical by 91.64% and 90.32%, respectively. In a study examining the DPPH radical scavenging activity of extracts of *S. triloba* samples collected from Beirut (Lebanon) during the flowering period, prepared with solvents with different polarities, it was reported that the inhibition % values of the extracts varied between 25.43 and 42.15 (Boukhary, 2016). The EC_{50} values for DPPH radical scavenging activity and reducing power of the decoction prepared from the aerial parts of *S. officinalis* grown by organic farming techniques in Portugal were determined as 3.48±3.30 µg/mL and 40.0±11.2 µg/mL, respectively. Ascorbic acid was used for DPPH radical scavenging activity, BHT was used as a reference compound for reducing power, and their EC_{50} values were determined as 6.69 ±0.70 µg/mL and 16.30±1.50 µg/mL, respectively (Pereria, 2018). Jamous et al. (2018) evaluated the DPPH radical scavenging effect and reducing power of the ethanolic extract of *S. triloba* leaves grown in Palestine. While the IC_{50} value for the DPPH radical scavenging activity of the extract was 0.13±0.00 mg/mL, the EC_{50} value for its reducing power was calculated as 0.32±0.10 mg/mL. In all antioxidant methods tested in our study, both extracts were found to have a moderate to strong effect.

The decoction prepared from the aerial parts of *S. officinalis* grown by organic farming techniques in Portugal showed no inhibitory effect on the α-amylase enzyme but inhibited the α-glucosidase and pancreatic lipase enzymes with an EC_{50} value of 71.2±5.0 µg/mL and an inhibition rate of 4.6±3.6%, respectively. The reference compound acarbose inhibited the α-glucosidase enzyme with an EC_{50} value of 357.8 ±12.3 µg/mL and an inhibition rate of the pancreatic enzyme of 1.8±0.4 % (Pereira, 2018). In our study, the *S. officinalis* sample did not show any activity against pancreatic lipase and α-amylase enzymes. Jamous et al. (2018) reported that the ethanolic extract of the leaves of *S. triloba* grown in Palestine inhibited the pancreatic lipase enzyme by 65.8±2.1% at a concentration of 5 mg/mL (Jamous, 2018). In our study, 5 mg/ml concentration, which is known to be very high, was not used toevaluation of the *in vitro* enzyme inhibitory activities of the extracts. The phosphate-buffered extracts of dried *S. triloba* leaves purchased commercially in İzmir inhibited α-glucosidase, α-amylase and pancreatic lipase enzymes with IC_{50} values of 88.49 ±2.35, 107.65±12.64 and 6.20±0.63, respectively. No reference compound was used in this study to compare results (Ercan, 2018). It was found that the leaves of *S. triloba* and *S. officinalis* collected during the flowering period from different localities of Croatia between May and August 2018 inhibited the α-glucosidase enzyme with IC_{50} values of 5291.51 ± 335.08 µg/mL and 4451.85± 142.22 µg/mL, respectively. The IC_{50} value of acarbose used as the reference compound was calculated as 1104.76 ± 34.80 µg/mL. In fact, when the findings are evaluated, it would not be correct to talk about a strong antioxidant activity for the extracts (Mervić, 2022).

In our study, enzyme inhibitory effects are given as percent inhibition. In the literature presented above, results are expressed regarding IC_{50} and EC_{50} values. Therefore, isn't easy to compare them with our findings. No pancreatic cholesterol esterase enzyme inhibitory activity studies have been performed on either species . It was observed that *S. officinalis* was effective on both glucosidase and pancreatic cholesterol esterase enzyme, while *S. triloba* was effective on pancreatic cholesterol esterase enzyme. For this reason, these species may be the source of further studies for discovering new molecules to inhibit these enzymes. However, since oxidative stress, which occurs as a result of the increased blood sugar levels, is responsible for the development of diabetes and its complications; a relationship can be established between the antioxidant capacity of the extracts and the enzyme activities. In addition to these, it has been stated in the literature

that hesperidin and rosmarinic acid molecules, which were quantitatively analyzed in the extracts, have antidiabetic and obesity potentials, and this information makes us think that the efficacy may be due to these molecules (Ahmet, 2012; Ngo, 2018; Xiong, 2019; Vasileva, 2021)

Pizzale et al. (2002) determined that the methanolic extracts of *S. triloba* and *S. officinalis* samples collected from northern Italy contain rosmarinic acid at varying rates from 21.9 to 81.8 g/kg extract as the major compound. It has been reported that carnosol, carnosic acid and methyl carnosate are also present in the samples besides rosmarinic acid. In a previous study, different amounts of vanillic acid, gallic acid, (+)-catechin, (−)-epicatechin, hesperetin, chlorogenic acid, caffeic acid, *p*-coumaric acid, ferulic acid, apigenin, rutin, morin, luteolin, myricetin, quercetin, and kaempferol were determined in aqueous-methanol extracts of wild and cultivated *S. triloba* samples by HPLC analysis depending on the parameters of storage time, growing conditions and harvest year (Dinçer, 2012). Boukhary et al. (2016) reported that the main components of the methanol extract of *S. triloba* collected from Lebanon were luteolin and rutin by HPLC technique. The amount of carnosic acid was determined as 3.76 ± 0.13 mg/g by HPLC technique in the phosphate-buffered extracts of dried *S. triloba* leaves commercially purchased in İzmir (Ercan, 2018). Başyiğit and Baydar (2017) conducted the qualitative and quantitative analyzes of chlorogenic acid, gallic acid, caffeic acid, ferulic acid, rosmarinic acid, *p*-coumaric acid, quercetin, rutin, naringin, and hesperidin in the methanolic extract of cultivated *S. officinalis* samples provided from Isparta using HPLC technique. Mervic et al. (2022) determined that 70% ethanolic extracts of *S. triloba* and *S. officinalis* samples collected from Serbia contained caffeic acid, chlorogenic acid, rosmarinic acid, *p*-coumaric acid, apigenin, luteolin and luteolin-7-*O*-glucoside by HPLC analysis. The analysis results indicated that rosmarinic acid was the main compound for both extracts. In addition to the compounds mentioned above, it has been reported that *S. triloba* extract contains ferulic acid, and quercetin, while *S. officinalis* extract contains rutin. HPLC analysis findings of our study showed that the amounts of rosmarinic acid were high for both species. In addition, the presence of hesperidin in *S. triloba* was detected for the first time in this study.

CONCLUSION

Phytochemical analyzes and activity studies of *S. triloba* and *S. officinalis* species grown with organic farming techniques were carried out for the first time in this study. As a result of the literature review, it has been seen that the phytochemical analysis and activity studies on *Salvia* species grown with organic agriculture are minimal. It has been determined that these two species, which were grown with organic farming techniques and are widely used as a tea in Anatolia, have high antioxidant activity and especially potential in terms of α-glucosidase inhibitor activity. In this context, the findings obtained from this study showed that these medicinal plants could also be evaluated as pharmaceutical raw materials.

ACKNOWLEDGEMENTS

This work was supported by the TUBITAK 4004 project "I was inspired by nature, I made my raw materials". We would like to thank the Temmuz organic farm for providing organically grown plants.

CONFLICT OF INTEREST

The authors declare that there is no conflict of interest.

AUTHOR CONTRIBUTIONS

Concept: BÖ, SP, DDO; Design: BÖ, SP, DDO; Control: BÖ, SP, DDO; Sources: BÖ, SP, DDO; Materials: BÖ, SP, DDO; Data Collection and/or processing: BÖ, SP, DDO; Analysis and/or interpretation: BÖ, SP, DDO; Literature review: BÖ, SP, DDO; Manuscript writing: BÖ, SP, DDO; Critical review: BÖ, SP, DDO; Other: BÖ, SP, DDO.

REFERENCES

Abubakari, A. R., & Bhopal, R. S. (2008). Systematic review on the prevalence of diabetes, overweight/obesity and physical inactivity in Ghanaians and Nigerians. *Public health*, *122*(2), 173–182. https://doi.org/10.1016/j.puhe.2007.06.012

Adımcılar, V., Kalaycıoğlu, Z., Aydoğdu, N., Dirmenci, T., Kahraman, A., & Erim, F. B. (2019). Rosmarinic and carnosic acid contents and correlated antioxidant and antidiabetic activities of 14 Salvia species from Anatolia. *Journal of Pharmaceutical and Biomedical Analysis*, *175*, 112763. https://doi.org/10.1016/j.jpba.2019.07.011

Ahmed, O. M., Mahmoud, A. M., Abdel-Moneim, A., & Ashour, M. B. (2012). Antidiabetic effects of hesperidin and naringin in type 2 diabetic rats. *Diabetologia Croatica*, *41*(2), 53-67.

American Diabetes Association (2005). Diagnosis and classification of diabetes mellitus. Diabetes care, *28*(1), S37–S42. https://doi.org/10.2337/diacare.28.suppl_1.s37

Arıduru, R., & Arabacı, G. (2013). Ciğertaze otu (*Salvia officinalis*) bitkisinin antioksidan aktivitesinin belirlenmesi. *Sakarya University Journal of Science*, *17*(2), 241-246.

Asmat, U., Abad, K., & Ismail, K. (2016). Diabetes mellitus and oxidative stress-A concise review. *Saudi pharmaceutical journal*, *24*(5), 547–553. https://doi.org/10.1016/j.jsps.2015.03.013

Başyiğit, M., & Baydar, H. (2017). Tıbbi adaçayı (*Salvia officinalis* L.)'nda farklı hasat zamanlarının uçucu yağ ve fenolik bileşikler ile antioksidan aktivite üzerine etkisi. *Süleyman Demirel Üniversitesi Fen Bilimleri Enstitüsü Dergisi*, *21*(1), 131-137. doi: 10.19113/sdufbed.55736

Boukhary, R., Raafat, K., Ghoneim, A. I., Aboul-Ela, M., & El-Lakany, A. (2016). Anti-inflammatory and antioxidant activities of Salvia fruticosa: An HPLC determination of phenolic contents. *Evidence-Based Complementary and Alternative Medicine*, 2016. https://doi.org/10.1155/2016/7178105.

Dincer, C., Topuz, A., Sahin-Nadeem, H., Ozdemir, K. S., Cam, I. B., Tontul, I., ... & Ay, S. T. (2012). A comparative study on phenolic composition, antioxidant activity and essential oil content of wild and cultivated sage (*Salvia fruticosa* Miller) as influenced by storage. *Industrial Crops and Products*, *39*, 170-176. https://doi.org/10.1016/j.indcrop.2012.02.032

Dinis, T. C., Maderia, V. M., & Almeida, L. M. (1994). Action of phenolic derivatives (acetaminophen, salicylate, and 5-aminosalicylate) as inhibitors of membrane lipid peroxidation and as peroxyl radical scavengers. *Archives of Biochemistry and Biophysics*, *315*(1), 161–169. https://doi.org/10.1006/abbi.1994.1485

Eidi A., & Eidi, M. (2009). Antidiabetic effects of sage (*Salvia officinalis* L.) leaves in normal and streptozotocin-induced diabetic rats. *Diabetes & Metabolic Syndrome*: *Clinical Research & Reviews*, *3*(1), 40-44. https://doi.org/10.1016/j.dsx.2008.10.007

Ercan, P., & El, S. N. (2018). Bioaccessibility and inhibitory effects on digestive enzymes of carnosic acid in sage and rosemary. *International Journal of Biological Macromolecules*, *115*, 933-939. https://doi.org/10.1016/j.ijbiomac.2018.04.139

Gök, H. N., Deliorman Orhan, D., Gürbüz, İ., & Aslan, M. (2020). Activity-guided isolation of α-amylase, α-glucosidase, and pancreatic lipase inhibitory compounds from *Rhus coriaria* L. *Journal of Food Science*, *85*(10), 3220-3228. https://doi.org/10.1111/1750-3841.15438

Hamrouni-Sellami, I., Rahali, F. Z., Rebey, I. B., Bourgou, S., Limam, F., & Marzouk, B. (2013). Total phenolics, flavonoids, and antioxidant activity of sage (*Salvia officinalis* L.) plants as affected by different drying methods. *Food and Bioprocess Technology*, *6*(3), 806-817. https://doi.org/10.1007/s11947-012-0877-7

Hussain, A., Hydrie, M. Z. I., Claussen, B., & Asghar, S. (2010). Type 2 Diabetes and obesity: A review. *Journal of Diabetology*, *2*(1), 1-7.

Jamous, R. M., Abu-Zaitoun, S. Y., Akkawi, R. J., & Ali-Shtayeh, M. S. (2018). Antiobesity and antioxidant potentials of selected palestinian medicinal plants. *Evidence-Based Complementary and Alternative Medicine*, 2018. https://doi.org/10.1155/2018/8426752

Jung, H. A., Jin, S. E., Choi, R. J., Manh, H. T., Kim, Y. S., Min, B. S., … Choi, J. S. (2011). Anti-tumorigenic activity of sophoflavescenol against Lewis lung carcinoma *in vitro* and *in vivo*. *Archives of Pharmacal Research*, *34*(12), 2087–2099. https://doi.org/10.1007/s12272-011-1212-y

Kamatou, G. P., Makunga, N. P., Ramogola, W. P., & Viljoen, A. M. (2008). South African Salvia species: a review of biological activities and phytochemistry. *Journal of Ethnopharmacology*, *119*(3), 664–672. https://doi.org/10.1016/j.jep.2008.06.030

Karık, Ü., & Sağlam, A. C. (2018). Marmara Bölgesi'ndeki Anadolu Adaçayı (*Salvia fruticosa* Mill.) populasyonlarının uçucu yağ bileşenleri, toplam antioksidan aktivite, toplam fenolik ve flavonoid madde miktarlarının belirlenmesi. *Anadolu Ege Tarımsal Araştırma Enstitüsü Dergisi*, *28*(2), 37-47.

Kosalec, I., Bakmaz, M., Pepeljnjak, S., & Vladimir-Knezević, S. (2004). Quantitative analysis of the flavonoids in raw propolis from northern Croatia. *Acta Pharmaceutica*, *54*(1), 65–72.

Lee, Y. M., Kim, Y. S., Lee, Y., Kim, J., Sun, H., Kim, J. H., & Kim, J. S. (2012). Inhibitory activities of pancreatic lipase and phosphodiesterase from Korean medicinal plant extracts. *Phytotherapy Research*, *26*(5), 778–782. https://doi.org/10.1002/ptr.3644

Lu, Y., & Foo, L. Y. (2002). Polyphenolics of Salvia--a review. *Phytochemistry*, *59*(2), 117–140. https://doi.org/10.1016/s0031-9422(01)00415-0

Mervić, M., Bival Štefan, M., Kindl, M., Blažeković, B., Marijan, M., & Vladimir-Knežević, S. (2022). Comparative Antioxidant, Anti-Acetylcholinesterase and Anti-α-Glucosidase Activities of Mediterranean Salvia Species. *Plants*, *11*(5), 625. https://doi.org/10.3390/plants11050625

Miliauskas, G., Venskutonis, P.R, Van Beek, T.A. (2004) Screening of radical scavenging activity of some medicinal and aromatic plant extracts. *Food Chemistry*, *85*(2), 231-237. https://doi.org/10.1016/j.foodchem.2003.05.007

Ngamukote, S., Mäkynen, K., Thilawech, T., & Adisakwattana, S. (2011). Cholesterol-lowering activity of the major polyphenols in grape seed. *Molecules*, *16*(6), 5054–5061. https://doi.org/10.3390/molecules16065054

Ngo, Y. L., Lau, C. H., & Chua, L. S. (2018). Review on rosmarinic acid extraction, fractionation and its anti-diabetic potential. *Food and chemical toxicology : an international journal published for the British Industrial Biological Research Association*, *121*, 687–700. https://doi.org/10.1016/j.fct.2018.09.064

Orhan, N., Deliorman Orhan, D., Gökbulut, A., Aslan, M., & Ergun, F. (2017). Comparative analysis of chemical profile, antioxidant, *in-vitro* and *in-vivo* antidiabetic activities of *Juniperus foetidissima* Willd. and *Juniperus sabina* L. *Iranian Journal of Pharmaceutical Research*, *16*, 64–74.

Pereira, O. R., Catarino, M. D., Afonso, A. F., Silva, A., & Cardoso, S. M. (2018). *Salvia elegans*, *Salvia greggii* and *Salvia officinalis* decoctions: antioxidant activities and inhibition of carbohydrate and lipid metabolic enzymes. *Molecules*, *23*(12), 3169. https://doi.org/10.3390/molecules23123169

Pitman, N. C., & Jørgensen, P. M. (2002). Estimating the size of the world's threatened flora. *Science* (New York, N.Y.), *298*(5595), 989. https://doi.org/10.1126/science.298.5595.989

Pizzale, L., Bortolomeazzi, R., Vichi, S., Überegger, E., & Conte, L. S. (2002). Antioxidant activity of sage (*Salvia officinalis* and *S. fruticosa*) and oregano (*Origanum onites* and *O. indercedens*) extracts related to their phenolic compound content. *Journal of the Science of Food and Agriculture*, *82*(14), 1645-1651. https://doi.org/10.1002/jsfa.1240

Sharma, Y., Fagan, J. B., & Schaefer, J. (2019). Ethnobotany, phytochemistry, cultivation and medicinal properties of Garden sage (*Salvia officinalis* L.) *Journal of Pharmacognosy and Phytochemistry*, *8*(3), 3139-3148.

Vasileva, L. V., Savova, M. S., Tews, D., Wabitsch, M., & Georgiev, M. I. (2021). Rosmarinic acid attenuates obesity and obesity-related inflammation in human adipocytes. *Food and Chemical Toxicology: An International Journal Published for the British Industrial Biological Research Association*, *149*, 112002. https://doi.org/10.1016/j.fct.2021.112002

Xiong, H., Wang, J., Ran, Q., Lou, G., Peng, C., Gan, Q., … Huang, Q. (2019). Hesperidin: A therapeutic agent for obesity. *Drug Design, Development and Therapy*, *13*, 3855–3866. https://doi.org/10.2147/DDDT.S227499

Xu, J., Wei, K., Zhang, G., Lei, L., Yang, D., Wang, W., … Li, M. (2018). Ethnopharmacology, phytochemistry, and pharmacology of Chinese Salvia species: A review. *Journal of ethnopharmacology*, *225*, 18–30. https://doi.org/10.1016/j.jep.2018.06.029

Yildirim, A., Mavi, A., Oktay, M., Kara, A. A., Algur, O. F., & Bilaloglu, V. (2000). Comparison of antioxidant and antimicrobial activities of tilia (*Tilia argentea* Desf ex DC), sage (*Salvia triloba* l.L.), and black tea (*Camellia sinensis*) extracts. *Journal of Agricultural and Food Chemistry*, *48*(10), 5030–5034. https://doi.org/10.1021/jf000590k

Zongo, C., Savadogo, A., Ouattara, L., Bassole, I. H. N., Ouattara, C. A. T., Ouattara, A. S., ... Traore, A. S. (2010). Polyphenols content, antioxidant and antimicrobial activities of Ampelocissus grantii (Baker) Planch. (Vitaceae): a medicinal plant from Burkina Faso. *IJP-International Journal of Pharmacology*, *6*(6), 880-887. https://doi.org/10.3923/ijp.2010.880.887

FABAD J. Pharm. Sci., 48, 1, 139-150, 2023
Doi: 10.55262/fabadeczacilik.1214152
RESEARCH ARTICLE

Investigation of Dimethoate Toxicity in Rat Brain and Protective Effect of *Laurocerasus officinalis* Roem. Fruit Extract Against Oxidative Stress, DNA Damage, and Apoptosis

Burcu ÜNLÜ ENDİRLİK[*], Elçin BAKIR[**], Arzu Hanim YAY[***], Fazile CANTÜRK TAN[****], Ayşe BALDEMİR KILIÇ[*****], Ayşe EKEN[******°]

Investigation of Dimethoate Toxicity in Rat Brain and Protective Effect of Laurocerasus officinalis Roem. Fruit Extract Against Oxidative Stress, DNA Damage, and Apoptosis

SUMMARY

Dimethoate is an organophosphate insecticide that is used globally on a wide scale in agriculture. It was associated with numerous negative health effects in many studies. The brain is one of the target organs for dimethoate exposure. The present study aimed to evaluate the sub-chronic (60 days) toxicity of dimethoate (7 mg/kg body weight) by investigating its oxidative stress, DNA damage, apoptosis-inducing effects, and histopathological changes in brain tissue of rats. We also aimed to analyze the protective effects of Laurocerasus officinalis Roem. (cherry laurel) fruit extract. To evaluate oxidative stress, malondialdehyde (MDA) levels, as well as superoxide dismutase (Cu-Zn SOD), glutathione peroxidase (GPx), and catalase (CAT) antioxidant enzymes activities, were calculated. Experimental results demonstrated that dimethoate treatment increased MDA and decreased Cu-Zn SOD, GPx, and CAT enzyme activities, suggesting its potency as an oxidative stress inducer in rat brain tissues. Furthermore, comet and TUNEL assay results showed that dimethoate stimulated DNA damage and apoptosis. Administration of cherry laurel extracts protected against dimethoate-induced oxidative stress, DNA damage, and apoptosis. The findings of the current study are important in terms of demonstrating the beneficial effects of L. officinalis extract against dimethoate toxicity in the brain, considering the sensitivity of this organ to oxidative stress and extensive usage of dimethoate.

Key Words: *Dimethoate, neurotoxicity, Laurocerasus officinalis Roem., in vivo, DNA damage, oxidative stress*

Dimetoat Toksisitesinin Sıçan Beyninde Araştırılması ve Laurocerasus officinalis Roem. Meyve Ekstresinin Oksidatif Stres, DNA Hasarı ve Apoptoza Karşı Koruyucu Etkisi

ÖZ

Dimetoat dünyada tarımda yaygın olarak kullanılan organofosfatlı bir insektisittir. Bir çok çalışmada dimetoatın negatif sağlık etkileriyle ilişkili olduğu belirtilmiştir. Beyin, dimetoat maruziyeti için başlıca hedef organlarından birisidir. Bu çalışmadaki amacımız dimetoatın (7 mg/kg vücut ağırlığı) sub-kronik (60 günlük) toksisitesini, sıçan beyin dokuları üzerindeki oksidatif stres, DNA hasarı ve apoptoz indükleyici etkilerini ve histopatolojik değişiklikleri araştırarak değerlendirmektir. Ayrıca Laurocerasus officinalis Roem. (taflan) meyve ekstresinin koruyucu etkilerinin incelenmesi hedeflenmektedir. Oksidatif stres değerlendirmesi için malondialdehit düzeyleri (MDA) ile birlikte süperoksit dismutaz (Cu-Zn SOD), glutatyon peroksidaz (GPx) ve katalaz (CAT) antioksidan enzim aktiviteleri ölçülmüştür. Deney sonuçları dimetoat muamelesinin MDA'yı arttırdığını ve Cu-Zn SOD, GPx ve CAT enzim aktivitelerini azalttığını göstererek, sıçan beyin dokularında etkin bir oksidatif stres indükleyici olabileceğini ortaya koymaktadır. Ayrıca comet ve TUNEL deney sonuçları da dimetoatın DNA hasarı ve apoptozu arttırdığını göstermiştir. Taflan ekstresi verilmesi, dimetoat tarafından indüklenen oksidatif stres, DNA hasarı ve apoptoza karşı koruyucu etki sağlamıştır. Bu çalışmada elde edilen bulgular, beynin oksidatif strese duyarlılığı ve dimetoatın yaygın kullanımı göz önüne alındığında, L. officinalis ekstresinin dimetoat toksisitesine karşı beyinde faydalı etkilerini göstermesi açısından önem taşımaktadır.

Anahtar Kelimeler: *Dimetoat, nörotoksisite, Laurocerasus officinalis Roem., in vivo, DNA hasarı, oksidatif stres*

Received: 03.12.2022
Revised: 26.12.2022
Accepted: 31.12.2022

[*] ORCID: 0000-0001-5960-1036, Department of Pharmaceutical Toxicology, Faculty of Pharmacy, Erciyes University, Kayseri, Turkey
[**] ORCID: 0000-0001-5333-8273, Department of Pharmaceutical Toxicology, Faculty of Pharmacy, Erciyes University, Kayseri, Turkey
[***] ORCID: 0000-0002-0541-8372, Department of Histology and Embryology, Faculty of Medicine, Erciyes University, Kayseri, Turkey
[****] ORCID: 0000-0002-0747-2209, Department of Biophysics, Faculty of Medicine, Erciyes University, Kayseri, Turkey
[*****] ORCID: 0000-0003-2473-4837, Department of Pharmaceutical Botany, Gülhane Faculty of Pharmacy, University of Health Sciences, Ankara, Turkey
[******] ORCID: 0000-0003-4830-5770, Department of Pharmaceutical Toxicology, Faculty of Pharmacy, Erciyes University, Kayseri, Turkey

[°] Corresponding Author; Ayşe Eken
Phone: 035220766-28325, E-mail: aeken@erciyes.edu.tr

INTRODUCTION

Dimethoate/DMT is an organophosphate insecticide that is widely used in agriculture to protect plants against the harm of insects and mites (Özkara et al., 2016). It acts by inhibiting acetylcholinesterase, an essential enzyme for the normal function of the nervous system (Grue et al., 1997; Eken, 2021). Because of its persistence in soil and plants, widespread usage of dimethoate became a risk for human and animal health (Sharma et al., 2005b; Ahmad et al., 2022), with residues of this pesticide on fruits, vegetables, and drinking water can become chronic exposure sources (Jiang et al., 2022). Previous studies reported that dimethoate had toxicity on various organs and systems, including the liver, lung, kidney, reproductive and immune systems (Bakır et al., 2020; Eken, 2021). Although dimethoate was banned in Europe, it is still being used in several countries (USA, Brazil, etc.) (Ahmad et al., 2022). Recently, the usage of dimethoate was restricted in Turkey (T.C. TOB, 2022).

The brain is considered one of the primary target organs for dimethoate and other organophosphates (Yahia & Ali, 2018). Dimethoate is bioactivated to more neurotoxic omethoate by the cytochrome P450 (CYP 450) enzyme system (Buratti & Testai, 2007; Ahmad et al., 2022). In animal studies, it was shown to cause oxidative stress, inflammation, and mitochondrial function damage in mice and rat brains (Sharma et al., 2005a, 2005b; Astiz et al., 2009b, 2013). The brain is especially susceptible to oxidative damage due to having high levels of polyunsaturated fatty acids (PUFAs) and insufficient free radical scavenging capability (Astiz et al., 2009a).

Interest in studying the preventive effects of natural antioxidants, which are found in several plants, against oxidative stress has increased over recent years (Moure et al., 2001; Ahmadipour et al., 2021). *Laurocerasus officinalis* Roem. (cherry laurel; "taflan, karayemis or laz kirazi" in Turkish) is such a plant native to the Black Sea coast of Turkey (Akkol et al., 2012). Its fruits contain several antioxidant substances, such as phenolics and ascorbic acid (Kolayli et al., 2003; Alasalvar et al., 2005; Karahalil & Şahin, 2011; Orhan & Akkol, 2011). Furthermore, it was previously reported that *L. officinalis* scavenged 2,2-diphenyl-1-picrylhydrazyl (DPPH), hydroxyl and superoxide radicals (Kolayli et al., 2003; Orhan & Akkol, 2011). It is known to have diuretic and anti-diabetic properties, as well as several beneficial effects against several illnesses, including gastrointestinal system problems, bronchitis, eczemas, and hemorrhoids (Kolayli et al., 2003). To the best of our knowledge, the protective effects of this extract against *in vivo* dimethoate toxicity in the brain were not previously investigated.

Considering the above-mentioned information, we aimed to evaluate whether sub-chronic dimethoate exposure affects oxidative stress, apoptosis, DNA damage, and histopathological alterations in brain tissue. Moreover, we investigated for the first time the potential protection of *L. officinalis* (LO) extract in the brain against these toxic effects induced by dimethoate *in vivo*.

MATERIALS AND METHODS

Chemicals

A commercial formulation of dimethoate (Korumagor 40 EC, 40%) was bought from Koruma Tarım (Kocaeli, Turkey). All the other chemicals were obtained from Sigma-Aldrich/Merck KGaA (Darmstadt, Germany) unless indicated otherwise.

Collection of plants and fruit extract preparation

Cherry laurel fruits were collected from the Akçaabat district of Trabzon province. The plant was identified by Dr. Ayşe Baldemir Kılıç. The herbarium specimen of the plant was vouchered in Ankara University Faculty of Pharmacy Herbarium (AEF 26257). Fruit extracts were prepared similarly to the protocol described by Bakır et al. (Bakır et al., 2020). Briefly, after drying, the fruit pulp was cut into small pieces and macerated with methanol at room temperature. After

constant stirring and filtration two times, a vacuum with a rotary evaporator was used for drying filtrates. Following lyophilization, lyophilisates were kept at 4°C until administration to animals in 0.9% NaCl.

Animals and experimental design

Male Wistar albino rats weighing 200-250 g were used in the current study. Animals were housed at 22-24°C with 55-60% relative humidity on a 12 h light/dark cycle in Erciyes University Animal Care Unit. Rats had free access to standard laboratory chow and tap water. This protocol was approved by Erciyes University Animal Ethics Committee (Decision Number: 12/82 and date 15.08.2022). All animal procedures complied with directive 2010/63/EU. Sixty rats were divided into six groups, with ten animals in each. All compounds, freshly dissolved in saline (0.9% NaCl), were administered to animals by oral gavage at indicated doses in 1 ml saline for 60 days. Doses were selected as 7, 100, and 4 mg/kg body weight (b.w) for dimethoate, vitamin C and *L. officinalis* extract, respectively, based on doses used in other studies (Pourmorad et al., 2006; Sayim, 2007; Saafi-Ben Salah et al., 2012). To evaluate its protective effects, LO extract was administered to two groups as either pre- or post-dimethoate treatment. The dimethoate dose used in our study, which is in line with doses in other sub-chronic dimethoate neurotoxicity studies in rats (Sharma et al., 2005b; Astiz et al., 2009a,; Arnal et al., 2019), corresponds to approximately 2% of its LD_{50}, considering LD_{50} value for dimethoate is 310 mg/kg (Eken, 2021).

Experimental groups were determined as follows:

Group 1: Control; administered 1 ml/day saline daily for 60 days, per oral (p.o.)

Group 2: DMT; administered 7 mg/kg/day dimethoate in saline for 60 days, p.o.

Group 3: LO; received 4 mg/kg/day LO fruit extract in saline for 60 days, p.o.

Group 4: LO_{pre} + DMT; administered LO fruit extract 30 min before dimethoate treatment for 60 days, p.o.

Group 5: Vit C + DMT; administered 100 mg/kg/day vitamin C in saline 30 min before dimethoate treatment for 60 days, p.o.

Group 6: DMT + LO_{post}; given dimethoate alone for 30 days, and then, dimethoate 30 min before LO fruit extract for the next 30 days, p.o.

All animals were sacrificed 24 h after the last dose under ketamine-xylazine (75 and 8 mg/kg b.w., respectively) anesthesia. Whole brains were removed and rinsed with ice-cold saline. Small sections of the tissues were fixed in formalin for histopathological examination. For the comet assay, sliced parts of brain tissue were put into cold phosphate buffer saline to get cell suspension immediately. The rest of the tissues were stored at -80 °C until analysis of oxidative stress parameters.

Determination of oxidative stress-related parameters

Brain tissues were homogenized in cold 1.15% KCl with a homogenizer (IKA Ultra-Turrax T10, Germany) to obtain 10% (w/v) whole homogenate. Malondialdehyde (MDA) was determined by studying a portion of the whole homogenate. The remaining part of the homogenate was centrifuged at 20,000 × *g* for 25 minutes at 4 °C, and enzyme activities were determined by using obtained supernatant. Lipid peroxidation was determined spectrophotometrically based on the method of Ohkawa et al. (1979). Thiobarbituric acid-reactive substances level was indicated as MDA nmol/mg protein. To determine superoxide dismutase (Cu-Zn SOD) activities, the method of Arthur and Boyne (1985) was used with slight changes. Glutathione peroxidase (GPx) activity was measured by the method of Pleban et al. (1982), and the method of Aebi (1984) was used for the measurement of catalase (CAT) activity. The determination of protein contents of tissue homogenates and supernatants was made based on the method of Lowry et al. (1951). Enzyme activity results were given as U/mg protein.

Evaluation of DNA damage with the comet assay

The comet assay was conducted in brain samples according to the protocol of Singh et al. (1988) with some modifications. Briefly, the single-cell suspension of brain tissues was embedded in 0.8% low-melting agarose on precoated slides with 0.5% normal-melting agarose. After lysing, unwinding of DNA, and electrophoresis steps, the slides were stained with ethidium bromide. To visualize DNA damage, one hundred cells from two replicate slides were examined under a fluorescent microscope (Olympus, BX51, Japan). To evaluate the images, comet assay software (CASP-1.2.2) was used. Expression of DNA damage was made as DNA percentage in tail (tail intensity).

Evaluation of apoptosis with TUNEL staining

Apoptosis was detected with terminal deoxynucleotidyl transferase dUTP nick end labeling (TUNEL) assay with In situ Cell Death Detection Kit (Roche, UT, USA) following the manufacturer's instructions. Paraffin sections from the tissues were deparaffinized, rehydrated, and washed in phosphate buffer saline. After adding the TUNEL reaction mixture to specimens in a humidified chamber, slides were incubated with converter reagent and then with fast red substrate solution (F4648, Sigma). TUNEL-positive cells were identified and counted in ten randomly chosen visual fields in each slide using Image J software at an original x400 magnification. Examination of slides was made with an Olympus BX51 microscope (Tokyo, Japan).

Histopathologic assessment

Brain tissues were fixed in formalin (10%) and embedded in paraffin. Paraffin portions were sliced into 5 μm thickness and dyed with hematoxylin and eosin. They were observed under a light microscope (Olympus BX-51, Japan) equipped with an Olympus DP-71 (Japan) camera at ×20 magnification for histopathological changes.

Statistical analysis

All results were given as mean ± standard error of the mean (SEM). Analysis of statistical difference was made through one-way ANOVA and Dunnett's or Bonferroni's Multiple Comparison post-hoc test with GraphPad Prism 9 (San Diego, CA). $p<0.05$ was considered significant.

RESULTS AND DISCUSSION

Oxidative stress is the underlying mechanism for several diseases, including neurotoxicity (Rahal et al., 2014). It happens when an imbalance between reactive oxygen species (ROS) production and antioxidant defense capacity occurs in a biological system (Sies, 1997). In the current study, MDA level was used as an indicator of lipid peroxidation, whereas SOD, GPx, and CAT enzyme activities were measured as cellular defense mechanisms. These three enzymes are among the first lines of cellular defenses against oxidative stress (Ighodaro & Akinloye, 2018). As shown in Figure 1, dimethoate exposure led to a 73% increase in MDA level relative to control ($p<0.001$). All three enzyme activities (Cu-Zn SOD, GPx, CAT) decreased by 25% ($p<0.01$), 45% ($p<0.001$), and 31% ($p<0.05$), respectively, after dimethoate treatment. Pre-treatment with both antioxidants ameliorated MDA induction caused by dimethoate by 35% ($p<0.001$). Furthermore, LO post-treatment resulted in a significant 43% reduction in MDA levels ($p<0.001$). In terms of enzymes, all antioxidant treatments rescued Cu-Zn SOD, GPx, and CAT activities disturbed by dimethoate. The range of increases in the enzyme activities was 32-34% for Cu-Zn SOD ($p<0.01$), 57-65% for

GPx (p<0.001), and 45-56% for CAT (p<0.05).

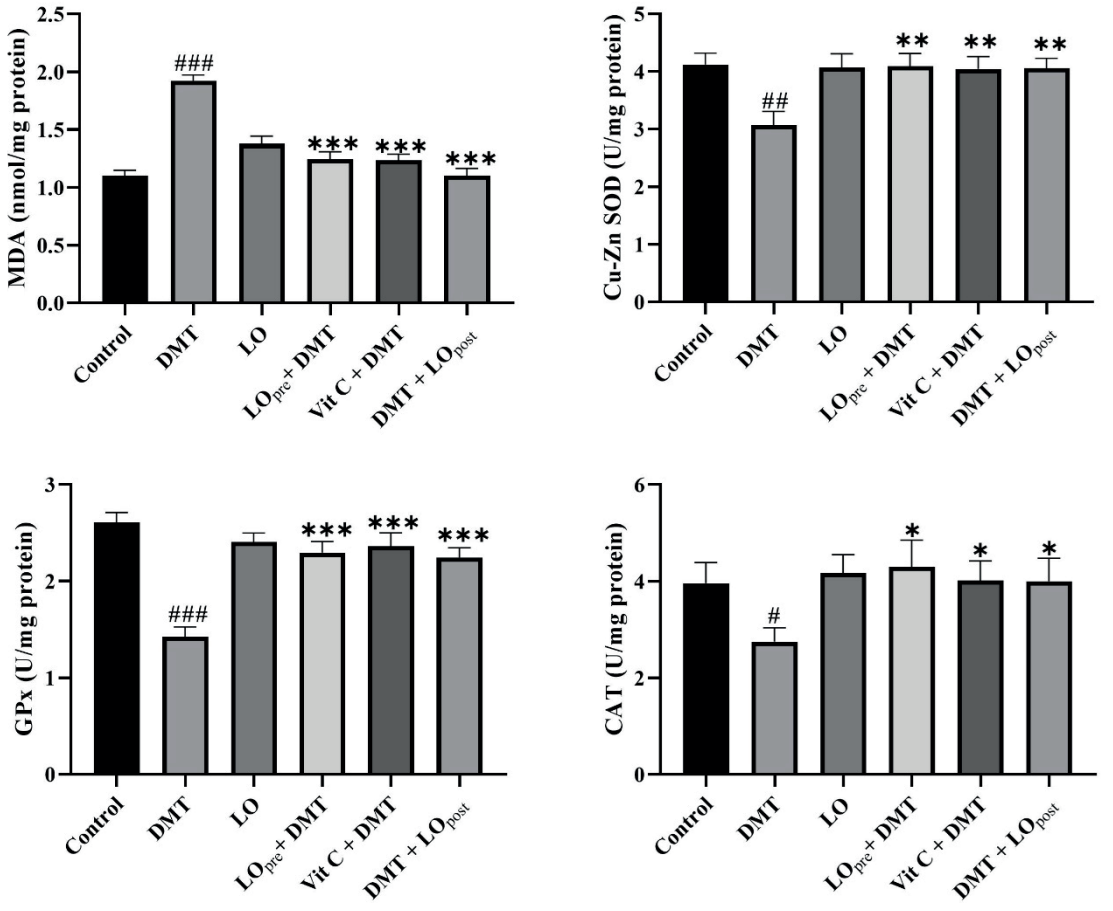

Figure 1. Levels of oxidative stress-related parameters in rat brain tissues given DMT, LO, and Vit C. Data were shown as mean ± SEM. $^{\#}p$<0.05, $^{\#\#}p$<0.01, $^{\#\#\#}p$<0.001 relative to control; *p<0.05, **p<0.01, ***p<0.001

relative to DMT group. DMT: dimethoate, LO: *L. officinalis* fruit extract, Vit C: vitamin C.

As stated before, the nervous system is sensitive to oxidative stress-induced lipid peroxidation because of its containing large amounts of PUFAs and low antioxidant capacity (Astiz et al., 2009a; Endirlik et al., 2022). Dimethoate administration led to increased MDA and depressed SOD, GPx, and CAT, which suggested it had the potency to induce oxidative damage in the brain tissues of rats. Under normal conditions, an equilibrium exists between radical production and antioxidant enzyme activities. When excess ROS are produced in response to chemical exposure, this equilibrium changes, depleting the body's antioxidant defenses (Rahal et al., 2014). Arnal et al. (2019) found that dimethoate exposure elevated MDA levels in rat brains, in agreement with our results. Likewise, in another study with rat brains, dimethoate induced MDA formation, along with reduced SOD activity (Astiz et al., 2009a). In two different studies by Sharma et al. (2005a, 2005b), acute and sub-chronic dimethoate treatment induced lipid peroxidation and histopathological alterations in the brain, whereas SOD, GPx, and CAT activities were found to be augmented, in

contrast to our results. As mentioned before, dimethoate is metabolized by CYP 450 enzymes, and ROS were formed as a by-product of this process (Loida & Sligar, 1993). Moreover, dimethoate was demonstrated to induce CYP 450 isoenzymes, thus leading to further ROS production and subsequent lipid peroxidation (Sharma et al., 2005b).

Oxidative stress and excessive ROS generation might cause oxidative alterations, such as strand breaks, in DNA, (Risom et al., 2005; Kryston et al., 2011). In this study, dimethoate treatment caused a 67% increase in % DNA in tail, relative to the control (p<0.001) (Figure 2). Both antioxidants were shown to protect against dimethoate-induced DNA damage, with LO having more protection than Vit C (38% vs. 24%, relative to the DMT group). Our findings agree with another study where dimethoate exposure caused DNA damage at 48 h in the brain tissue of rats, in addition to MDA induction and GPx decrease (Yahia & Ali, 2018). Previously, Dogan et al. (2011) showed that dimethoate induced DNA damage in *Oncorhynchus mykiss* erythrocytes, which was discussed as being associated with oxidative stress-generating and alkylating properties of this chemical.

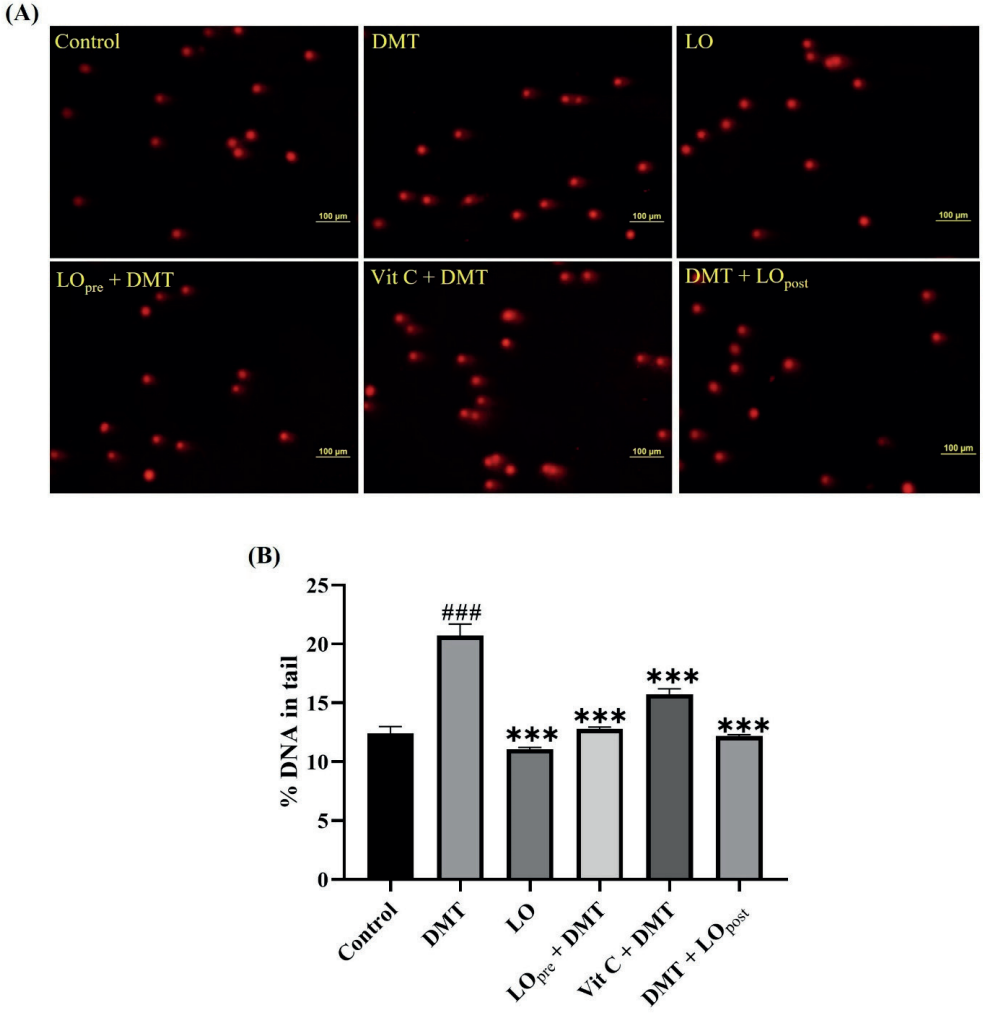

Figure 2. Evaluation of DNA damage in rat brains with comet assay after administration of DMT, LO, and Vit C. (A) Representative images of brain cells stained with ethidium bromide (× 200 magnification). (B) Bar graph data of results obtained from comet assay. Data were shown as mean ± SEM. $^{###}p$<0.001 compared to control; $^{***}p$<0.001 compared to DMT group. DMT: dimethoate, LO: *L. officinalis* fruit extract, Vit C: vitamin C.

Apoptosis is the programmed death of cells, characterized by changes in cellular morphology. The production of ROS and the resulting oxidative stress might play a critical role in regulating apoptosis pathways (Kannan & Jain, 2000). As shown in Figure 3, our results indicated that the TUNEL+ cell percentage increased 3.75-fold after single dimethoate treatment relative to control (p<0.001). Pre-treatments with vitamin C and *L. officinalis* rescued some of the TUNEL+ cell percentage caused by dimethoate by 46% and 53%, respectively (p<0.05), whereas post-treatment of *L. officinalis* was not found to have any significant protective effect. In a study with rat brains, dimethoate exposure for 5 weeks (15 mg/kg b.w.) was also shown to activate intrinsic apoptotic pathways (Arnal et al., 2019). Regarding histopathological results, the cerebrum of brain tissues showed normal histologic architecture with the cell bodies of nerves in all the groups except the DMT group (Figure 4). In this group, nuclear pyknosis was observed in cerebrum neurons. In another study made with rats, sub-chronic dimethoate (30 mg/kg) exposure resulted in mild ischemic changes (Sharma et al., 2005b). The higher dimethoate concentration used in this study might have caused the difference from our research.

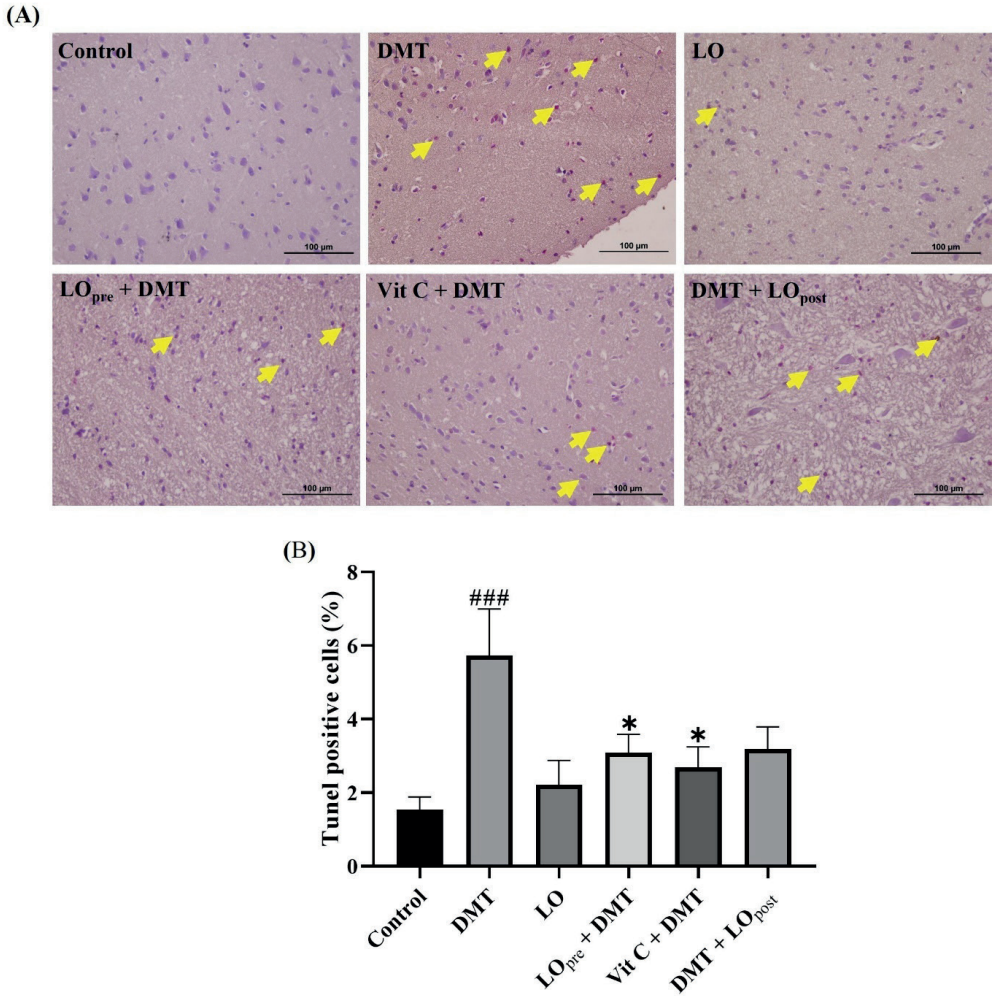

Figure 3. Apoptosis evaluation in brain tissue after administration of DMT, LO, and Vit C (A) Representative images of TUNEL assay (× 400 magnification). Yellow arrows denote TUNEL + cells. (B) Semi-quantitative analysis of TUNEL + cells. Data were shown mean ± SEM. $^{###}p$<0.001 compared to control; $^{*}p$<0.05 compared to DMT group. DMT: dimethoate, LO: *L. officinalis* fruit extract, Vit C: vitamin C.

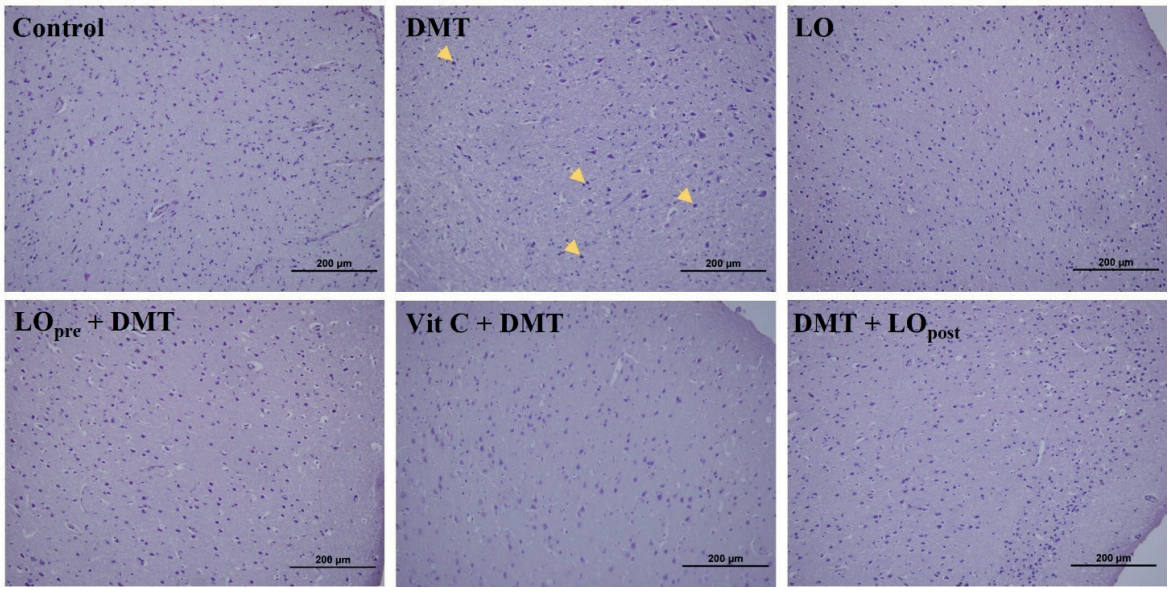

Figure 4. Histopathological examination of brain tissue in rats given DMT, LO, and Vit C. Yellow arrows indicate nuclear pyknosis (× 20 magnification). DMT: dimethoate, LO: *L. officinalis* fruit extract, Vit C: vitamin C.

L. officinalis fruit extract was observed to provide significant protection against lipid peroxidation, DNA damage, and apoptosis, in addition to the restoration of antioxidant enzyme activities close to control levels. These results might be attributed to the antioxidant characteristics of LO extracts. Previously, we demonstrated fruit extract of this plant has DPPH radical scavenging activity and high content of phenolic compounds, which points to its antioxidant property (Eken et al., 2017). Additionally, we used vitamin C as a positive control (Bendich et al., 1986) in our experiments which also demonstrated protection against the harmful effects of dimethoate.

CONCLUSION

In conclusion, we demonstrated lipid peroxidation, DNA damage, apoptosis, and depletion of antioxidant enzymes caused by dimethoate in the brain tissue of rats. Results obtained in the present study are significant, considering the sensitivity of the nervous system to organophosphate insecticide dimethoate exposure and the widespread usage of this chemical in agriculture, especially for occupationally exposed populations. To the best of our knowledge, the antioxidant effects of *L. officinalis* fruit extract against dimethoate-induced neurotoxicity were shown for the first time *in vivo*. However, further studies are required to confirm our findings, with a detailed analysis of the role of components in the beneficial effects associated with this plant extract.

ACKNOWLEDGEMENTS

This research was funded by the Erciyes University Scientific Research Project Unit (Grant No: TCD-2013-4127)

CONFLICT OF INTEREST

The authors declare that there is no conflict of interest.

AUTHOR CONTRIBUTION STATEMENT

Concept and Design (A.E.), Supervision (A.E.), Funding Acquisition (A.E.), Materials (B.Ü.E., E.B., A.H.Y., F.C.T., A.B.K.), Data Collection and/or Processing (B.Ü.E., E.B., A.H.Y., F.C.T., A.B.K., A.E.), Analysis and/or Interpretation (B.Ü.E., E.B., A.H.Y., F.C.T., A.B.K., A.E.), Literature Review (B.Ü.E., A.E.) Writing Manuscript (B.Ü.E., A.H.Y., F.C.T., A.B.K., A.E.); Review and Editing (B.Ü.E., E.B., A.H.Y., F.C.T., A.B.K., A.E).

REFERENCES

Aebi, H. (1984). Catalase in vitro. *Methods in Enzymology*, *105,* 121-126. https://doi.org/10.1016/S0076-6879(84)05016-3

Ahmad, S., Pinto, A. P., Hai, F. I., Badawy, M. E.T. I., Vazquez, R. R., Naqvi, T. A., Munis, F. H., Mahmood, T., & Chaudhary, H. J. (2022). Dimethoate residues in Pakistan and mitigation strategies through microbial degradation: a review. *Environmental Science and Pollution Research*, *29*, 51367–51383. https://doi.org/10.1007/s11356-022-20933-4

Ahmadipour, A., Sharififar, F., Anani, H., & Karami-Mohajeri, S. (2021). Protective Effects of Ferulic Acid Against Isoniazid-Induced Hepatotoxicity in Rats. *FABAD Journal of Pharmaceutical Sciences*, *46*(2), 119-128.

Akkol, E. K., Kırmızıbekmez, H., Küçükboyacı, N., Gören, A. C., & Yesilada, E. (2012). Isolation of active constituents from cherry laurel (Laurocerasus officinalis Roem.) leaves through bioassay-guided procedures. *Journal of Ethnopharmacology*, *139*(2), 527-532. https://doi.org/10.1016/j.jep.2011.11.043

Alasalvar, C., Al-Farsi, M., & Shahidi, F. (2005). Compositional characteristics and antioxidant components of cherry laurel varieties and pekmez. *Journal of Food Science*, *70*(1), S47-S52. https://doi.org/10.1111/j.1365-2621.2005.tb09064.x

Arnal, N., Morel, G., Marra, C. A., & Astiz, M. (2019). Pro-apoptotic effects of low doses of dimethoate in rat brain. *Toxicology and Applied Pharmacology*, *363,* 57-63. https://doi.org/10.1016/j.taap.2018.11.013

Arthur, J., & Boyne, R. (1985). Superoxide dismutase and glutathione peroxidase activities in neutrophils from selenium deficient and copper deficient cattle. *Life Sciences, 36*(16), 1569-1575. https://doi.org/10.1016/0024-3205(85)90381-9

Astiz, M., de Alaniz, M. J., & Marra, C. A. (2009a). Antioxidant defense system in rats simultaneously intoxicated with agrochemicals. *Environmental Toxicology and Pharmacology*, *28*(3), 465-473. https://doi.org/10.1016/j.etap.2009.07.009

Astiz, M., de Alaniz, M. J., & Marra, C. A. (2009b). Effect of pesticides on cell survival in liver and brain rat tissues. *Ecotoxicology and Environmental Safety*, *72*(7), 2025-2032. https://doi.org/10.1016/j.ecoenv.2009.05.001

Astiz, M., Diz-Chaves, Y., & Garcia-Segura, L. M. (2013). Sub-chronic exposure to the insecticide dimethoate induces a proinflammatory status and enhances the neuroinflammatory response to bacterial lypopolysaccharide in the hippocampus and striatum of male mice. *Toxicology and Applied Pharmacology*, *272*(2), 263-271. https://doi.org/10.1016/j.taap.2013.07.008

Bakır, E., Sarıözkan, S., Endirlik, B. Ü., Kılıç, A. B., Yay, A. H., Tan, F. C., Eken, A., & Türk, G. (2020). Cherry laurel fruit extract counters dimethoate-induced reproductive impairment and testicular apoptosis. *Archives of Industrial Hygiene and Toxicology*, *71*(4), 329-338. https://doi.org/10.2478/aiht-2020-71-3412

Bendich, A., Machlin, L., Scandurra, O., Burton, G., & Wayner, D. (1986). The antioxidant role of vitamin C. *Advances in Free Radical Biology & Medicine*, *2*(2), 419-444. https://doi.org/10.1016/S8755-9668(86)80021-7

Buratti, F. M., & Testai, E. (2007). Evidences for CYP3A4 autoactivation in the desulfuration of dimethoate by the human liver. *Toxicology*, *241*(1-2), 33-46. https://doi.org/10.1016/j.tox.2007.08.081

Dogan, D., Can, C., Kocyigit, A., Dikilitas, M., Taskin, A., & Bilinc, H. (2011). Dimethoate-induced oxidative stress and DNA damage in Oncorhynchus mykiss. *Chemosphere, 84*(1), 39-46. https://doi.org/10.1016/j.chemosphere.2011.02.087

Eken, A. (2021). *Dimethoate organophosphate insecticide toxicity and the role of oxidative stress. Toxicology: Oxidative Stress and Dietary Antioxidants.* U.K., Academic Press. https://doi.org/10.1016/B978-0-12-819092-0.00007-8

Eken, A., Endirlik, B., Bakir, E., Baldemir, A., YAY, A., & Canturk, F. (2017). Effect of Laurocerasus officinalis Roem.(cherry laurel) fruit on dimethoate induced hepatotoxicity in rats. *Kafkas Universitesi Veteriner Fakultesi Dergisi*, *23*(5), 779-787. https://doi.org/10.9775/kvfd.2017.17748

Endirlik, B. Ü., Eken, A., Canpınar, H., Öztürk, F., & Gürbay, A. (2022). Perfluorooctanoic acid affects mouse brain and liver tissue through oxidative stress. *Archives of Industrial Hygiene and Toxicology*, *73*(2), 148-156. https://doi.org/10.2478/aiht-2022-73-3629

Grue, C. E., Gibert, P. L., & Seeley, M. E. (1997). Neurophysiological and behavioral changes in non-target wildlife exposed to organophosphate and carbamate pesticides: thermoregulation, food consumption, and reproduction. *American Zoologist*, *37*(4), 369-388. https://doi.org/10.1093/icb/37.4.369

Ighodaro, O., & Akinloye, O. (2018). First line defence antioxidants-superoxide dismutase (SOD), catalase (CAT) and glutathione peroxidase (GPX): Their fundamental role in the entire antioxidant defence grid. *Alexandria Journal of Medicine*, *54*(4), 287-293. https://doi.org/10.1016/j.ajme.2017.09.001

Jiang, Q., Qi, X., Ding, C., Liu, X., Lei, Y., Li, S., & Cao, Z. (2022). Melatonin Rescues Dimethoate Exposure-Induced Meiotic and Developmental Defects of Porcine Oocytes. *Animals*, *12*(7), 832. https://doi.org/10.3390/ani12070832

Kannan, K., & Jain, S. K. (2000). Oxidative stress and apoptosis. *Pathophysiology*, *7*(3), 153-163. https://doi.org/10.1016/S0928-4680(00)00053-5

Karahalil, F. Y., & Şahin, H. (2011). Phenolic composition and antioxidant capacity of cherry laurel (Laurocerasus officinalis Roem.) sampled from Trabzon region, Turkey. *African Journal of Biotechnology*, *10*(72), 16293-16299. https://doi.org/10.5897/AJB11.1929

Kolayli, S., Küçük, M., Duran, C., Candan, F., & Dinçer, B. (2003). Chemical and antioxidant properties of Laurocerasus officinalis Roem.(cherry laurel) fruit grown in the Black Sea region. *Journal of Agricultural and Food Chemistry*, *51*(25), 7489-7494. https://doi.org/10.1021/jf0344486

Kryston, T. B., Georgiev, A. B., Pissis, P., & Georgakilas, A. G. (2011). Role of oxidative stress and DNA damage in human carcinogenesis. *Mutation Research/Fundamental and Molecular Mechanisms of Mutagenesis*, *711*(1-2), 193-201. https://doi.org/10.1016/j.mrfmmm.2010.12.016

Loida, P. J., & Sligar, S. G. (1993). Molecular recognition in cytochrome P-450: mechanism for the control of uncoupling reactions. *Biochemistry*, *32*(43), 11530-11538. https://doi.org/10.1021/bi00094a009

Lowry, O. H. (1951). Protein measurement with the Folin phenol reagent. *Journal of Biological Chemistry*, *193*, 265-275. https://doi.org/10.1016/S0021-9258(19)52451-6

Moure, A., Cruz, J. M., Franco, D., Domínguez, J. M., Sineiro, J., Domínguez, H., Núñez, M. a. J., & Parajó, J. C. (2001). Natural antioxidants from residual sources. *Food Chemistry, 72*(2), 145-171. https://doi.org/10.1016/S0308-8146(00)00223-5

Ohkawa, H., Ohishi, N., & Yagi, K. (1979). Assay for lipid peroxides in animal tissues by thiobarbituric acid reaction. *Analytical Biochemistry*, *95*(2), 351-358. https://doi.org/10.1016/0003-2697(79)90738-3

Orhan, I. E., & Akkol, E. K. (2011). Estimation of neuroprotective effects of Laurocerasus officinalis Roem.(cherry laurel) by in vitro methods. *Food Research International*, *44*(3), 818-822. https://doi.org/10.1016/j.foodres.2011.01.037

Özkara, A., Akyıl, D., & Konuk, M. (2016). *Pesticides, environmental pollution, and health. Environmental Health Risk-Hazardous Factors to Living Species*. Crotia, IntechOpen. https://doi.org/10.5772/63094

Pleban, P. A., Munyani, A., & Beachum, J. (1982). Determination of selenium concentration and glutathione peroxidase activity in plasma and erythrocytes. *Clinical Chemistry*, *28*(2), 311-316. https://doi.org/10.1093/clinchem/28.2.311

Pourmorad, F., Hosseinimehr, S., & Shahabimajd, N. (2006). Antioxidant activity, phenol and flavonoid contents of some selected Iranian medicinal plants. *African Journal of Biotechnology*, *5*(11), 1142-1145.

Rahal, A., Kumar, A., Singh, V., Yadav, B., Tiwari, R., Chakraborty, S., & Dhama, K. (2014). Oxidative stress, prooxidants, and antioxidants: the interplay. *BioMed Research International*, *2014,* 1-19. https://doi.org/10.1155/2014/761264

Risom, L., Møller, P., & Loft, S. (2005). Oxidative stress-induced DNA damage by particulate air pollution. *Mutation Research/Fundamental and Molecular Mechanisms of Mutagenesis*, *592*(1-2), 119-137. https://doi.org/10.1016/j.mrfmmm.2005.06.012

Saafi-Ben Salah, E. B., El Arem, A., Louedi, M., Saoudi, M., Elfeki, A., Zakhama, A., Najjar, M. F., Hammami, M., & Achour, L. (2012). Antioxidant-rich date palm fruit extract inhibits oxidative stress and nephrotoxicity induced by dimethoate in rat. *Journal of Physiology and Biochemistry*, *68*(1), 47-58. https://doi.org/10.1007/s13105-011-0118-y

Sayim, F. (2007). Dimethoate-induced biochemical and histopathological changes in the liver of rats. *Experimental and Toxicologic Pathology*, *59*(3-4), 237-243. https://doi.org/10.1016/j.etp.2007.05.008

Sharma, Y., Bashir, S., Irshad, M., Gupta, S. D., & Dogra, T. D. (2005a). Effects of acute dimethoate administration on antioxidant status of liver and brain of experimental rats. *Toxicology*, *206*(1), 49-57. https://doi.org/10.1016/j.tox.2004.06.062

Sharma, Y., Bashir, S., Irshad, M., Nag, T., & Dogra, T. (2005b). Dimethoate-induced effects on antioxidant status of liver and brain of rats following subchronic exposure. *Toxicology*, *215*(3), 173-181. https://doi.org/10.1016/j.tox.2005.06.029

Sies, H. (1997). Oxidative stress: oxidants and antioxidants. *Experimental Physiology: Translation and Integration*, *82*(2), 291-295. https://doi.org/10.1113/expphysiol.1997.sp004024

Singh, N. P., McCoy, M. T., Tice, R. R., & Schneider, E. L. (1988). A simple technique for quantitation of low levels of DNA damage in individual cells. *Experimental Cell Research*, *175*(1), 184-191. https://doi.org/10.1016/0014-4827(88)90265-0

T.C. TOB. (2022). Türkiye Cumhuriyeti Tarım ve Orman Bakanlığı, Gıda ve Kontrol Genel Müdürlüğü, Aktif Madde Kısıtlama ve Yasaklamaları (Chloridazon, Desmedipham, Dimethoate, Ethoprophos ve Linuron). Retrieved 1.12.2022 from https://bku.tarimorman.gov.tr/Duyuru/DuyuruDetay/81?csrt=5577822346345255811

Yahia, D., & Ali, M. F. (2018). Assessment of neuro-hepatic DNA damage in male Sprague–Dawley rats exposed to organophosphates and pyrethroid insecticides. *Environmental Science and Pollution Research*, *25*(16), 15616-15629. https://doi.org/10.1007/s11356-018-1776-x

FABAD J. Pharm. Sci., 48, 1, 151-164, 2023
Doi: 10.55262/fabadeczacilik.1228030
RESEARCH ARTICLE

Investigation of Age-Related Alterations in Brain and Serum Samples in a Healthy Aging Rat Model

Eda ÖZTURAN ÖZER*°

Investigation of Age-Related Alterations in Brain and Serum Samples in a Healthy Aging Rat Model

SUMMARY

Male albino rats of Wistar strain (n=24) were assigned to three groups 2-month-old (GRP I), 9-month-old (GRP II) and 15-month-old (GRP III), (n=8 in each) to investigate age-related changes in serum and brain samples. Malondialdehyde (MDA), reduced glutathione (GSH), acetylcholinesterase (AChE) and paraoxonase (PON) enzyme activities, soluble and aggregated amyloid β1-42 (Aβ1-42) levels were analyzed in brain tissues. Tissues were also stained with Congo-red dye to observe fibrillation. Serum total cholesterol, uric acid, and triglyceride levels, and PON activities were investigated. Serum uric acid levels were significantly decreased ($p<0.05$) whereas total cholesterol and triglyceride levels were increased ($p<0.01$) in GRP III rats. Brain tissue MDA and GSH concentrations did not change significantly among the groups. Both Free Aβ1-42 concentrations and fibrillation levels were significantly increased in brain tissues in GRP III ($p<0.05$). Tissue AChE activities were reduced significantly ($p<0.05$) and PON activities did not change among groups. Our serum results indicated age-related systemic oxidative stress. Brain results did not show oxidative stress in terms of lipid peroxidation but the decreased AChE activities and, unaltered PON activities accompanied with increased amyloidogenesis are accepted as an early response of neurodegeneration in older rats.

Key Words: *Aging, oxidative stress, acetylcholinesterase, paraoxonase, amyloid-β-peptide*

Sağlıklı Yaşlanma Sıçan Modelinde Beyin ve Serum Örneklerinde Yaşa Bağlı Değişikliklerin Araştırılması

ÖZ

Çalışmada 24 adet Wistar albino cinsi sıçan, serum ve beyin örneklerinde yaş-ilişkili değişiklikleri değerlendirmek için kullanılmıştır. Sıçanlar her grupta sekiz adet olacak şekilde GRP I (2 aylık), GRP II (9 aylık)ve GRP (III) (15 aylık) olarak ayrılmıştır. Beyin dokularında ise malondialdehit (MDA), indirgenmiş glutatyon (GSH) derişimleri, asetilkolinesteraz (AChE) ve paraoksonaz (PON) aktiviteleri ile serbest ve fibriler amiloid-β-1-42 peptid düzeyleri belirlenmiştir. Dokularda ayrıca kongo kırmızı boyaması ile fibrilasyon görüntülenmiştir. Serum trigliserit, kolesterol ve asit ile PON enzim aktiviteleri analiz edilmiştir. Serum örneklerinde GRP III sonuçlarında azalan ürik asit derişimleri ($p<0.01$) ile değişen lipid içerikleri ($p<0.05$) yaşa bağlı gelişen sistemik bir oksidatif stres varlığını işaret etmiştir.Beyin dokularında MDA ve GSH derişimlerinde gruplar arası anlamlı bir farklılık gözlenmemiştir. Serbest ve fibrile amiloid-β-1-42 seviyeleri ise GRP III beyin dokularında diğer gruplara önemli derecede artış göstermiştir ($p<0.05$). Doku AChE aktiviteleri yaş ile azalırken PON aktiveleri değişmemiştir. Sonuçlarımız yaşlanma ile birlikte sistemik oksidatif stres gelişimini kanıtlamıştır. Beyin dokularında lipid peroksidasyonu bağlamında gruplar arası bir bir değişiklik gözlenmemiş ancak azalan AChE aktiviteleri,değişmeyen PON düzeyleri ile birlikte artan amiloid-β-1-42 derişimleri beyin dokusunda yaşlanmaya bağlı nörodejenerasyonunun erken bir yanıtı olarak değerlendirilmiştir.

Anahtar Kelimeler: *Yaşlanma, oksidatif stres, asetilkolinesteraz, paraoksonaz, amiloid-β-peptit*

Received: 01.01.2023
Revised: 27.01.2023
Accepted: 31.01.2023

* ORCID: 0000-0001-6543-4043, Department of Biochemistry, Faculty of Medicine, Başkent University, 06530 Ankara, Turkey

° Corresponding Author; Eda Özturan Özer
eozer@baskent.edu.tr, Tel: 0.312.246 66 66/1561 Fax: 0.312.246 66 89

INTRODUCTION

Aging is an irreversible multifactorial incident that has molecular and cellular phases leading to decrements in various organ functions (Aliabbas, 2021). Especially central nervous system (CNS) and brain may be considered the main targets of aging. Several factors such as oxidative stress, inflammation and mitochondrial dysfunction are known to contribute to the molecular mechanism of brain aging. Progression of neurodegenerative diseases mainly are related to brain aging and so investigating the alterations of cellular protein levels and enzyme activities has a pivotal role in understanding and clarifying the exact mechanisms (Aliabbas, 2021).

Considering healthy individuals, aging is accepted as the single most important risk factor for Alzheimer's Disease (AD) genesis. Amyloid beta (Ab) peptides and their oligomerization products are the basic hallmarks of AD, dementia, and other related disorders whereas their monomeric forms may behave as antioxidants depending on the concentration (Salazar,2019). Studies have indicated that the accumulation of amyloid peptides is attributed not only to increased synthesis but also decreased brain efflux by age resulting in the elevated accumulation of peptides under normal physiological conditions. Several previous studies report the contribution of amyloid deposition to cognitive impairment in aged rat models (Chiu, 2012; Peng, 2021). The increment of Ab is also known to activate inflammation exacerbating cognitive dysfunction (Xu, 2021).

Cholinergic neurons play a key role in AD, dementia, or normal aging. It is well-established that AD is caused by synaptic dysfunction and amyloidogenesis may result in the death of cholinergic neurons (Schliebs, 2011). Aging-related cholinergic dysfunctions are reported as the important factor in neurological disorders in aging.

Oxidative stress may simply be described as the generation of an imbalance between prooxidants and antioxidants in cells. Reactive oxygen molecules (ROM) are the main contributors to this condition which are highly reactive and has ability to damage many biological macromolecules especially proteins and lipids (Tian, 1998). It is mainly reported that oxidative stress is increased in aging at any stage due to the increased reactive oxygen species (ROS) production (Starke-Reed, 1989; Smith, 1991), and the age-related enhancement of prooxidant production may be the cause of membrane damage in senescent cells. The brain may be considered as a primary target to oxidative damage due to its structural and functional composition with high rate of oxygen utilization (Drivera, 2000; Youdim, 2000). Besides the given, also, neuroinflammation is an important factor in aging and investigated in several reports (Salazar, 2019).

The paraoxonases are ubiquitous Ca-dependent hydrolyses having antioxidant, antiatherogenic, antiinflamatory and, also scavenging properties with broad substrate specificities. Three isozymes, paraoxonase 1 (PON1) and 3 are mainly expressed in the liver and secreted to circulation (Reichert, 2021). Enzymes derive their nomenclature from their ability to hydrolyze paraoxon, whereas PON1 has two activities; paroxonase and arylesterase. Enzyme (PON1) also has known to hydrolyze organophosphates such as chlorpyrifos, diazinon, and also nerve toxins such as sarin, soman having detoxificant activity (Mota, 2019). PON1 is found mainly in high density lipoproteins (HDL) and its main physiological role is to hydrolyse oxidized lipids. It is known that PON1 is transferred via HDL to extrahepatic tissues and suggested that the main antioxidant capacity of HDL comes from its PON1 content (Morris, 2021).

The following study is aimed to investigate the age-related alterations in acetylcholinesterase (AChE), paraoxonase enzyme activities, and Ab peptide levels in a healthy aging rat model considering the possible contribution of oxidative stress.

MATERIALS and METHODS

Chemicals

All chemicals used were obtained from Sigma-Aldrich (St Louis, MO, USA), and Merck (Darmstadt, Germany). Aβ1- 42 ELISA kit was purchased from SunRed-Bio (Shangai, China).

Animals

Wistar albino male rats (*n*=24) were assigned to three groups eight in each group as 2-month-old (GRP I), 9-month-old (GRP II) and 15-month-old (GRP III). All experimental procedures involving animals approved by the Başkent University Institutional Review Board and Ethics Committee, Ankara, Turkey with project number DA11/12. Sacrification was performed by an intracardiac puncture after rats were anesthetized i.p. with ketamine (50 mg/kg) /xylazine (10 mg/kg). After sacrification, brain tissues and serum samples were stored at -86°C for biochemical analysis. All biochemical studies were performed in duplicate by using the left hemisphere of the brain.

Analysis of serum biochemical parameters

Serum uric acid, total cholesterol, and triglyceride concentrations were analyzed autoanalyzer system (Roche Hitachi modular system, Mannheim, Germany) using Roche Diagnostic reagents.

Determination of Tissue Malondialdehyde (MDA) and Reduced Glutathione (GSH) Concentrations

Brain homogenates were prepared in ice-cold 0.15 M KCl (10%, w/v) using an all-glass homogenizer.

Buege and Aust's method was used to determining MDA levels (Buege, 1978). Homogenate samples were incubated with thiobarbituric acid reagent at 100 °C in a water bath for 15 min. After cooling, samples were centrifugated at 1000x g for 10 min and the absorbance of the supernatant was measured spectrophotometrically (Shimadzu UV-1601, Japan) at λ: 535 nm. Concentrations were quantified by using the molar extinction coefficient of 1.56×10^5 $M^{-1}cm^{-1}$. The results were expressed as nmol MDA/g tissue. GSH levels were assayed in tissue homogenates according to the method of Ellman (Ellman,1959). Samples were deproteinized and supernatants were used for analysis. Ellman color reagent was added into the supernatants and then the absorbance of the generated color complex was measured immediately at 412 nm against a reagent blank with a spectrophotometer (Shimadzu UV-1601, Japan). Concentrations were calculated by using GSH standard curve and were expressed as μmol GSH/g tissue.

Determination of serum and tissue PON Arylesterase Activity

Tissue homogenates were prepared in Tris-HCl buffer (50 mM), pH 8.0+ 2 mM $CaCl_2$ using an all-glass homogenizer. Homogenates were centrifuged at 15000xg for 10 min and supernatants were used as enzyme sources. PON arylesterase activities of serum and tissue homogenates were analyzed according to the method of Jerzy Beltwoski (Beltwoski,2004). The method is based on the determination of the hydrolysis rate of phenylacetate spectrophotometrically at 270 nm (Shimadzu UV-1601, Japan). Quantitation was performed by using the molar extinction coefficient ($\mathfrak{E}$=1310 $M^{-1}cm^{-1}$). Results were expressed as U/g and U/ml and one unit is defined as the one ml of the enzyme that hydrolyzes 1 mmol of phenylacetate per minute.

Determination of Tissue Acetylcholinesterase Activity

Brain homogenates were prepared in 0.1 M potassium phosphate buffer pH 7.4 with glass homogenizer and supernatants that are obtained after centrifugation at 10000xg were used as enzyme sources. AChE activity was determined by the method of Ellman method (Ellman,1961) with a spectrophotometer (Shimadzu UV-1601, Japan). Assays were carried out at 25^0 C in a mixture containing 84 mM potassium phosphate buffer pH 7.4, 0.1 mM *5,5'-dithiobis-2-nitrobenzoic acid*, and 0.84 ml of enzyme source. The reaction was initiated by the addition of substrate acetylthiocholine. Activity was defined as μmol acetylthiocholine utilized /min/gram tissue (U/g).

Determination of Tissue Aβ1-42 Levels

Tissue Ab1-42 levels were determined by using an ELISA kit (SunRed-Bio, Cat No: 201-11-0094, Shangai, China). Brain homogenates were prepared according to the instructions in the kit. Standards and samples were pipetted onto monoclonal antibody-coated wells of microtiter strips and the assay was carried out as indicated in the instructions of the

manufacturer. The optical densities were measured at 450 nm by a microplate reader (Bio-Tek Instruments, INC.ELX 800, USA). Quantitation was carried out by a standard curve and expressed as ng/g tissue.

Thioflavin T Analysis

Thioflavin T (ThT) is a dye that binds to various peptides, polypeptides, and proteins, and especially the cross-sheet structure, found in most amyloid proteins is a specific binding target of ThT (Khurna, 2005; Biancalana, 2010). ThT fluorescence measurement is generally accepted as an indication of amyloid fibril formation (fibrillation) (Nilsson, 2004; Griffin, 2020). Tissues were homogenized gently in 100 mM sodium phosphate buffer, pH 7.4, using a glass-glass homogenizer (10%, w/v) and the ThT fluorescences of supernatants were determined using 8 μM ThT in 100 mM sodium phosphate buffer, pH 7.4, using a spectrofluorimeter (Shimadzu RF-5301, Japan) at excitation and emission wavelengths 442 and 482 nm respectively. Fluorescence intensities were recorded and expressed as arbitrary units (A.U.).

Congo red staining

Congo-red staining is the traditional qualitative method used for the identification of amyloids. Formalin-fixed and paraffin-embedded brain tissues were used for the histopathological evaluation of cerebral amyloidosis. Hematoxylin and eosin (H&E) followed by Congo-red staining was performed to evaluate the neuronal architecture and amyloid fibrils in brain semi-thin sections. The images were captured using a Leica microscope (Leica DM 400; Wetzlar, Germany) (Puchtler, 1962; Bancroft, 2008).

Statistical Analysis

Data were evaluated with SPSS, Version 17.0 Software. Univariate analysis of variance (ANOVA) coupled with Duncan's posthoc test was performed. Data were expressed as means ± Standard error of the mean (SEM) and *p*-values less than 0.05 were considered statistically significant.

RESULTS AND DISCUSSION

Serum parameters

In the following study, serum biochemical parameters were evaluated to investigate the response of the organism in a healthy aging process considering the progression of a probable oxidative stress, and results are given in Table 1. As shown in the table, serum uric acid levels were significantly decreased in GRP III when compared to GRP I ($p<0.05$). Triglyceride and total cholesterol concentrations are significantly elevated in GRP III compared to GRP I and GRP II ($p<0.001$). Uric acid, the end product of purine metabolism, is known to behave as a neuroprotective molecule having roles in neuronal activity, brain development, and cognitive functions due to its antioxidant properties (Tang, 2002; Kuzuya, 2002; Liu,2002; Qiao,2021). A previously reported study of Khan et al. indicated a positive relationship between serum uric acid levels with the prevention of onset of a probable dementia and cognitive impairment (Khan,2016). In our experimental model, serum uric acid levels were evaluated as the marker of the total antioxidant status of rats. Our results indicated a significant decrease in aged rats compared to the young group indicating a decrement of the antioxidant capacity of the organisms with aging (Table 1). It is well established that aging is commonly associated with metabolic disorders characterized by serious complications such as the co-existence of dyslipidemia and especially triglyceride levels may be accepted as a biomarker of a healthy aging (Liu, 2015; Deleen, 2016; Abo-Elsoud, 2022). In our experimental model triglyceride and cholesterol levels were significantly increased in aged group (Table 1) similar to the previous reports, and accepted as the response of lipid metabolism to age (Bey, 2001; Ghezzi, 2012; Johnson, 2019).

Table 1. Serum parameters. GRP I (2 months), GRP II (9 months), and GRP III (15 months). Values are mean ± SEM. The sample size of each group is 8. * p<0.05 GRP III vs GRP I; ** p<0.01 GRP III vs GRP I and GRP I

	GRP I	GRP II	GRP III
Uric acid (mg/dl)	1.8 ± 0.27	1.14 ± 0.24	0.9 ± 0.08*
Cholesterol (mg/dl)	59.9 ± 3.61	58.6 ± 4.13	81.1 ± 3.63**
Triglyceride (mg/dl)	36.5 ± 2.17	47.6 ± 4.26	58.8 ± 8.63**

Tissue MDA and GSH concentrations

Tissue MDA and GSH concentrations were analyzed to determine age-related alterations of oxidative stress in brain tissues. Brain MDA concentrations were investigated as the lipid peroxidation index in each group. As shown in Table 2 there was not significant change in MDA concentrations concerning to age in each group. Also, GSH concentrations, determined as the index of the redox status of the cell, did not change significantly among different aged goups.

Aging is a progressive deterioration and is known to enhance susceptibility to free radical reactions (Doğru-Abbasoğlu, 1977). Normal processes of cells, such as mitochondrial respiration, may lead to the formation of free radicals, but the increased rate of these cellular activities in maturing /aging brain may show an enhancement (Drivera, 2000). Considering healthy aging for cells, it is established that oxidative stress is an inevitable cellular modification due to altered cellular metabolism and damaged membrane blood-brain permeability, especially during senescent brain cells (Enciu,2013; Freitas,2022). Several studies have shown the existence of oxidative stress in aging rat models in terms of increased lipid peroxidation (MDA levels) and also decreased GSH concentrations (Cand,1989). Whereas lipid peroxidation index, in terms of MDA levels, is a commonly used marker to investigate oxidative damage, several reports suggest that this may not be the most sensitive method, and direct measurement of basal ROS production and oxidative protein damage must be investigated (Drivera, 2000) to determine the intrinsic age-related differences in the potential to produce free radicals. In our model, brain tissue MDA levels did not change significantly (Table 2) between groups compatible with some previous reports (Doğru-Abbasoğlu, 1977; Cand,1989; Matsuo, 1992). It is reported that, normally, oxidatively modified proteins are major targets of proteolytic system instead of native proteins that are proposed as a secondary free radical defense system (Tian, 1998). Presumably, the mechanism is also valid for the damaged lipids making them as a candidate for rapid degradation and explaining the stable MDA levels among groups, and unaltered oxidative stress in terms of lipid peroxidation (Holmes, 1992).

Thiol redox status (TRS) is accepted as a marker of the antioxidant defence capacity of cells. TRS includes the reduced and oxidized forms of several thiols (protein/non-protein). The most abundant non-protein thiol, GSH has two roles in the antioxidant system. It either behaves as an antioxidant itself or has a role as a substrate in enzymatic antioxidant defense mechanisms. Recent studies highlight the redox status as a marker of aging and neurodegeneration and the reduced form of GSH is generally determined to investigate the antioxidant status of the cell (Grintazalis, 2022; Chen,2022). However many several studies report the decline in GSH levels in aging brain tissues (Zhua,2006), our results did not show a significant difference among groups compatible with the findings of Schultz et al. in the human brain and rat brain (Schulz,2000, Chen,2022).

Table 2. Tissue MDA and GSH concentrations. GRP I (2 months), GRP II (9 months), and GRP III (15 months). Values are mean ± SEM. The sample size of each group is 8.

	MDA (nmol/g)	GSH (mmol/g)
GRP I	22.25 ± 1.83	2.19 ± 0.31
GRP II	24.01 ± 4.28	1.83 ± 0.11
GRP III	20.51 ± 3.14	2.03 ± 0.28

Tissue amyloidogenesis

In monomeric forms, Ab peptides are known to have antioxidant roles depending on their local concentration (Kontush, 2001) but at high concentrations (mM) they exhibit toxic properties linked to methionine-35 mediated radical generation and also their tendency to aggregate (Sehar, 2022). By having these two-faced functions, it is mainly suggested that Ab behaves as a stress-related protein. In the present study, Ab1-42 monomeric levels and also accompanied aggregate formation, due to the predisposition of Ab1-42's to aggregate, are significantly increased indicating cellular stress in the aged group as an acute phase response of organism (Table 3) (Kontush, 2001; Butterfield, 2001; Cheignona, 2018; Özturan-Özer, 2020; Salazar, 2022;). The accumulation of beta peptides is caused by not only increased synthesis but also depends on the decreased removal. The efflux of Ab peptides is mediated by blood-brain barrier associated p-glycoprotein and it is mainly reported that the concentration and expression of this protein is decreased with age. Also, it is reported that the expression of beta-secretase enzymes, which are responsible for the production of pathological amyloid peptides, is increased during aging. So, we may conclude that the inevitable increment of Ab formation and also aggregation during the aging process is caused by the imbalance between synthesis and removal mechanisms in the brain (Chiu, 2012). The unaltered GSH levels were considered as a compensatory mechanism due to the generated cellular stress resulting from elevated amyloid plague formation in the aging process (Hussain, 1995; Mandal, 2022).

Table 3. Tissue Ab1-42 concentrations and fibrillation levels. Values are mean ± SEM. The sample size of each group is 8. * p< 0.05; GRP III vs GRP I and GRP II

	Ab1-42 (pg/g)	Fluorescence intensity (A.U.)
GRP I	365 ± 29.5	3 ± 1.6
GRP II	384 ± 48,1	14 ± 4.2
GRP III	453 ± 33.4*	39 ± 6.4*

Histopathological analysis, Congo-red staining

Our biochemical findings about amyloidogenesis were confirmed by the histological ultrastructural studies (Figure 1). The Congo red stained semi-thin brain sections showed the aggregates of amyloid plaques as brick-red cloudy materials in brain tissues (Figure 1C) (Setti,2021; Addi,2022) also accumulation in arterial vessels. This accumulation forms cerebral amyloid angiopathy due to impaired clearence of Ab peptides mostly through perivascular drainage pathways with age (Figure 1D) in older rats (Tanner, 2022).

AChE activities

The alterations of AChE activities with age are given in Figure 2. As shown in the figure, brain AChE activities were significantly decreased in aged rats. GRP I activities were significantly higher than GRP II and GRP III enzyme activities (665 ± 62.3; 404 ± 65.4; 511 ± 59.1 respectively).

Whereas oxidative stress and related pathologies are accepted as the main hallmarks of aging, cholinergic dysfunction is also seriously important. These alterations generally are associated with cognitive decline, neurobehavioral deficits, and susceptibility to immune disorders (Benfante, 2021). In progressive aging, the decrease of acetylcholine levels whether caused by decreased enzyme activity or damage of cholinergic neurons is a well-known phenomenon. This decrease is reported to be associated with the construction and maintenance of learning memory in the brain with aging (Schliebs, 2011). Several reports emphasize the importance of AChE activities for nervous systems and mostly it is reported that an decrease in AChE activity can be accepted as an indicator of neurodegeneration (Haider, 2014). In our study, the decreased AChE levels in GRP II and GRP III with age were consistent with the previous studies (Liu,2022). It is abundantly evident that Abs trigger cholinergic dysfunction in several ways: affecting a-7 nicotinic acetylcholine receptors, affecting nerve growth factor signaling, and also interacting with the peripheral an-

ionic site of acetylcholinesterase (Sultzer, 2022). In the following study, it is clear that the decreased AChE levels in the GRP III group are also accompanied by the enhanced levels of Ab1-42, which is much more prone to aggregate and displays higher neurotoxicity *in vivo* (Haider,2014).

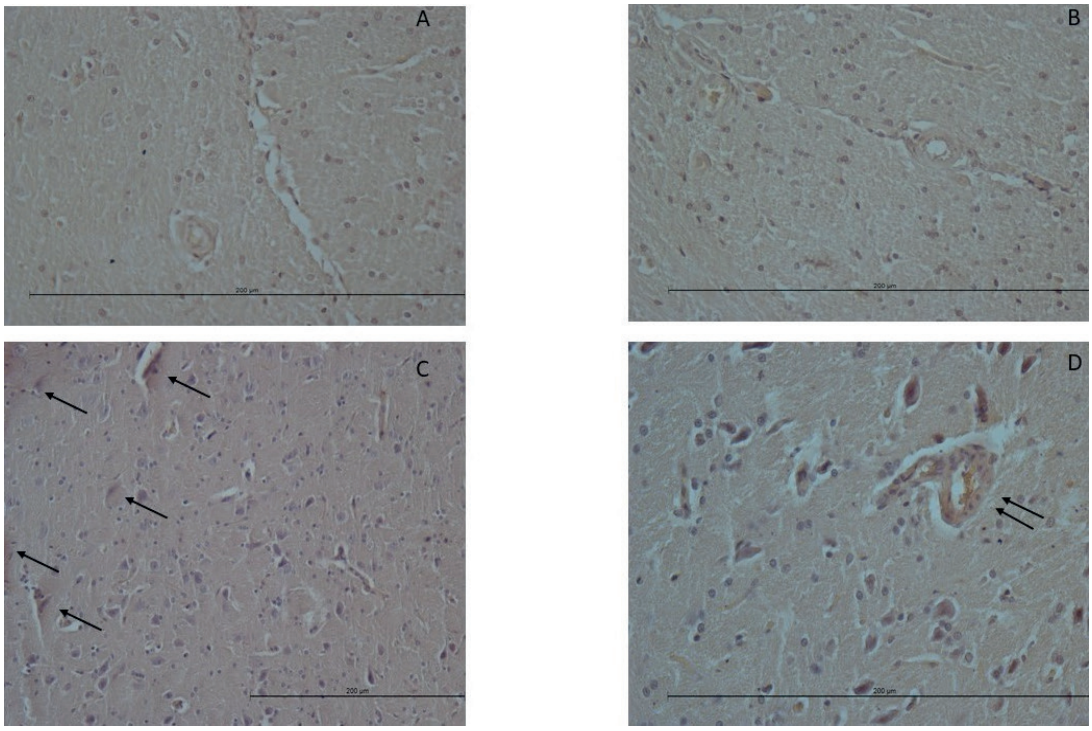

Figure 1. Histopathology of rat cerebral sections. Microscopic image of Congo red staining of **of 2 month(A),** 9 month (B) and 15 months (C and D) age of rate brain sections. **B**. 9 month **C and D**. 15 months age of rat brain sections. Sections were counterstained with H&E. All the pictures were taken at magnification x 40. Scale bars, 200 mM. Black single arrows indicate aggregated Ab plaques and double arrows indicate the Ab deposition in vessel walls (Addi, 2002; Tanner, 2022).

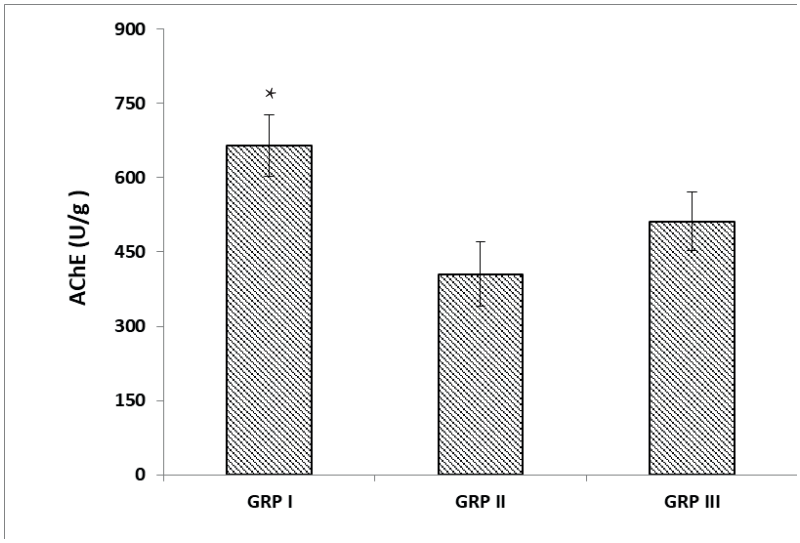

Figure 2. Tissue AChE activities Values are mean ± SEM. The sample size of each group is 8.

* p< 0.05; GRPI vs GRP II and GRP III

PON activities

Serum and brain PON activities are shown in Figure 3. As seen in the Figure 3A, there was no significant variation in brain PON activities among groups whereas Figure 3B shows that serum PON activities were significantly higher in the aged group with respect to other two groups ($p<0.01$) (92.3 ± 6.44; 78.14± 2.29; 118.7 ± 8.86 respectively).

PON enzymes, especially PON arylesterase are defined to be a critical defense system against lipid peroxidation, and a decrease in activity is a marker of increased systemic oxidative stress (Menini, 2014; Bassu, 2022; Ayada, 2022; Wang, 2022). Many clinical and experimental studies report a significant decrease in serum PON arylesterase activity in several pathological conditions such as dementia (Menini, 2014), rheumatoid arthritis (Erre, 2022), coronary artery diseases (Sofflai, 2022), cancer (Elseadya, 2002; Jasinski, 2022; Thompson, 2022), COVID-19 (Gabaldo,2022) and also in a rat model (Dube, 2022). On the contrary, in our healthy aging model, serum PON levels were significantly increased in older rats accompanied by a decrement in uric acid levels. In general, it is known that aging triggers elevated levels of cholesterol, and triacylglycerols that are associated with cardiac and vascular diseases (Sofflai, 2022). In the following study, the increased paraoxonase arylesterase activities were accepted as a response of the organisms against to generated systemic oxidative stress (decrement of uric levels) and also a protection mechanism. Also, this increase was found to be positively correlated with serum cholesterol levels ($r=0.593$). This association was regarded as a prevention mechanism by paraoxonase enzyme against the oxidation of lipoproteins (Mackness, 2021).

PON family members are lactonases with broad substrate specificity and tissue distribution. PON1 and PON 3 are expressed in the liver and their protein product can be found in circulation. Among the three ones, PON-2 is the only one expressed in nervous tissues. Although it is believed there is no PON1 and PON3 gene expression in the brain; studies report the existence of these enzymes in brain's regions indicating a possible role in modulating the brain oxidative stress. Also, Salazar et al reported the abundant expression of PON1 and PON 3 surrounding Ab plaques (Salazar, 2021). Another study showed the existence of PON1 in the brain suggesting and supporting the idea of transfer of PON enzymes from blood circulation to the central nervous system whenever needed (Levy, 2019; Salazar, 2021). It is known that the cellular modifications in neurodegeneration in the brain, such as Ab deposition, lead to the production of ROS by activated astrocytes, oligodendrocytes, and microglia resulting in generating oxidative stress. In our model, there was no increase in PON activity and also MDA and GSH levels with age suggesting no alteration of apperant oxidative stress.

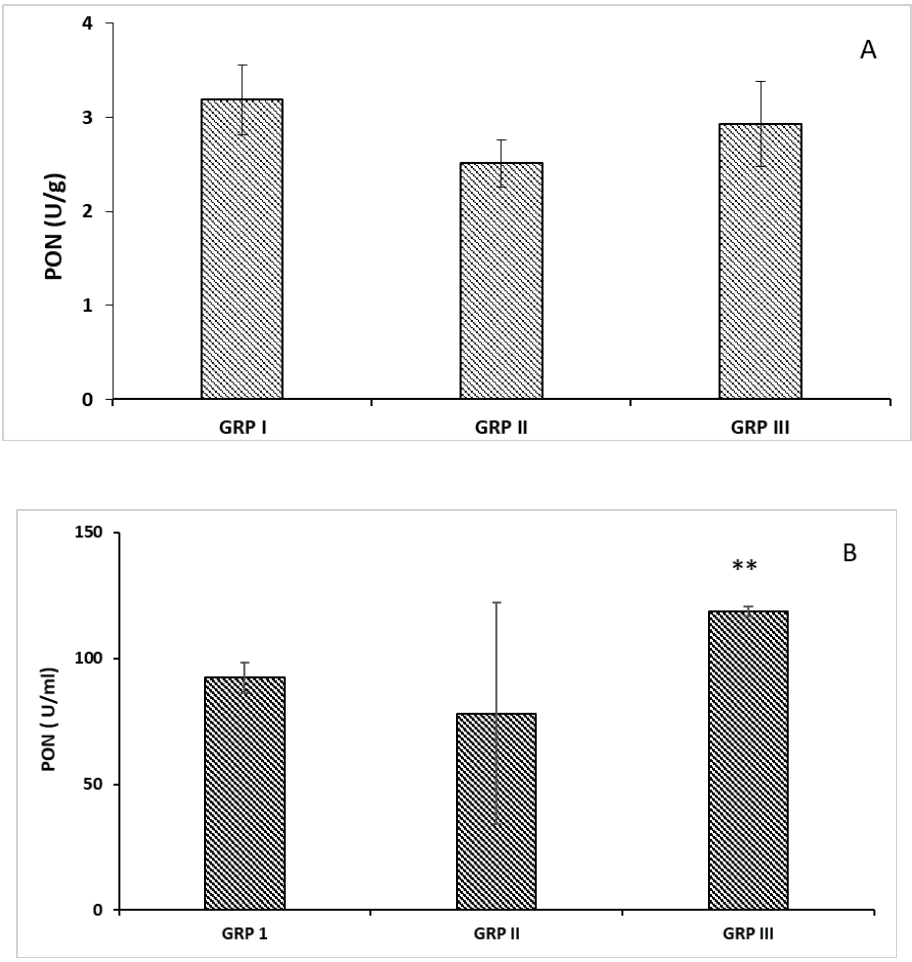

Figure 3. (A) Brain (B) Serum PON activities. GRP I (2 months), GRP II (9 months),and GRP III (15 months). Values are mean ± SEM. The sample size of each group is 8.

**p<0.01 GRP III vs GRP I and GRP II

CONCLUSIONS

Aging causes complex and irreversible cellular modifications. Senescent cells mainly suffer from mitochondrial dysfunction and also oxidative stress (Zhang, 2022). In our study, the systemic antioxidant status of aged group rats; uric acid; was significantly decreased with age as expectedly. Also, the generated dyslipidemia with age was consistent with the situation indicating a systemic oxidative damage. The brain results were confusing as there was no alteration of tissue markers in terms of lipid peroxidation and PON activities. But also, the decrease in AChE levels during aging indicated neurodegeneration in the brain. This decrease accompanied by the increased amyloid levels suggested that the cholinergic system is the first target of brain aging. However, the increased levels of amyloid plaque formation may contribute cellular stress in our model, we may suggest that amyloid monomers have shown a two-faced role as antioxidants preventing probable oxidative stress and, but not properly effective considering the decreased AChE levels. So we may conclude that the brain has its protection mechanisms against systemic oxidative stress and Ab peptide levels must be strictly evaluated to determine probable stress in brain tissue.

ACKNOWLEDGEMENT

The author acknowledges Prof.Dr.Suna Türkoğlu for her support and help on the data evaluation, and also Dr. Fatma Helvacıoğlu and Ece Lakşe for their contribution to histological analysis.

CONFLICTS OF INTEREST

The authors declare no conflict of interest.

AUTHOR CONTRIBUTION STATEMENT

EO: %100.

REFERENCES

Abo-Elsoud, R.AA., Elfakhrany, A.T., Shaban, A. MH. &Gaafar, A. MM. (2022). Effect of fenofibrate on biochemical & vascular reactivity changes in aged rats. *Bulletin of Egypt Society of Physiological Sciences, 42*(3), 294-302. https://doi.org/10.21608/besps.2022.120408.1118

Addi, U.R., Jakhotia, S., Reddy, S.S., Reddy, G.B. (2022). Age-related neuronal damage by advanced glycation end products through altered proteostasis. *Chemico-Biological Interactions*, *355*, 109840-109850. https://doi.org/10.1016/j.cbi.2022.10984

Aliabbas, Z., PourbagherShahri, A.M., Farkhondeh, T., &Samarghandia S. (2021). Molecular and cellular pathways contributing to brain aging. *Behavioral Brain Function*, *17*, 6-30. https://doi.org/10.1186/s12993-021-00179-9

Ayada, C., Umran Toru Erbay, U.T., Korkut, Y., Guleken, Z., Öner, Z. (2022). Evaluation of oxidative system parameters in Alzheimer's disease before medical treatment. *International Journal of Geron*tology, *16*, 395-399. https://doi.org/10.6890/IJGE.202210_16(4).0016

Bancroft, J.D. & Gamber, M. (2008). Theory & practice of histological techniques. 6th edition., Churchill Livingstone Elsevier, Nottingham UK & North Hollywood USA, 270-272.

Bassu, S., Mangoni, A.A., Satta, R., Argiolas, D., Carru C. (2022). Paraoxonase and arylesterase activity of serum PON-1 enzyme in psoriatic patients: a systematic review and metaanalysis. *Clinical and Experimental Medicine*, *21*, 11-22. https://doi.org/10.1007/s10238-022-00818-z

Bełtowski, J., Wójcicka, G., & Jamroz, A. (2004). Effect of *3-hydroxy-3-methylglutarylcoenzyme* A reductase inhibitors (Statins) on tissue paraoxonase 1 and plasma platelet activating factor acetylhydrolase activities. *Journal of Cardiovascular Pharmacology*, *43*(1), 121-127.

Benfante, R., Di Lascio, S., Cardani, S., Fornasari, D. (2021). Acetylcholinesterase inhibitors targeting the cholinergic antiinflammatory pathway: a new therapeutic perspective in agingrelated disorders. *Aging Clinical and Experimental Research, 33*, 823–834. https://doi.org/10.1007/s40520-019-01359-4

Bey, L., Areiqat, E., Sano,A., Hamiton, M.T. (2001). Reduced lipoprotein lipase activity in postural skeletal muscle during aging. *Journal of Applied Physiology*, *91*, 687-692. https://doi.org/10.1152/jappl.2001.91.2.687

Biancalana, M., & Koide, S. (2010). Molecular mechanism of thioflavin-T binding to amyloid fibrils. *Biochimica and Biophysica Acta*, *1804*, 1405-1412. https://doi.org/10.1016/j.bbapap.2010.04.001

Buege, J.A., & Aust, AD. (1978). Microsomal lipid peroxidation. *Methods in Enzymology*, *302-310*.

Butterfield, D.A., Drake, J., Pocernich, C. & Castegna, A. (2001). Evidence of oxidative damage in Alzheimer's disease brain: central role for amyloid b-peptide. *Trends in Molecular Med*icine, *7*(12), 548-554. https://doi.org/10.1016/S1471-4914(01)02173-6

Cand, F., &Verdetti J. (1989). Superoxide dismutase, glutathione peroxidase, catalase and, lipid peroxidation in the major organs of the aging rat. *Free Radical Biology and* Medicine, *7*, 59–63. https://doi.org/10.1016/0891-5849(89)90101-9.

Cheignona, C., Tomas, A.M., Bonnefont-Rousselotc, D., Fallerf, P., Hureaua, C., &Collina F. (2018). Oxidative stress and the amyloid beta peptide in Alzheimer's disease. *Redox Biology*, *14*, 450–464. https://doi.org/10.1016/j.redox.2017.10.014

Chen, J.J., Thiyagarajah, M., Song, J., Chen, C., Herrmann, N., &Lanctot, K.L.(2022). Altered central and blood glutathione in Alzheimer's disease and

mild cognitive impairment: a meta-analysis. *Alzheimer's Research and Therapy, 14*, 23-40. https://doi.org/10.1186/s13195-022-00961-5

Chiu, C., Miller, M.C., Caralopoulos I.N., Worden, M.S., Brinker, T., & Silverberg, G.D. (2012). Temporal course of cerebrospinal fluid dynamics & amyloid accumulation in the aging rat brain from three to thirty months. *Fluids & Barriers of the CNS, 9*, 3-11. https://doi.org/10.1186/2045-8118-9-3

Deleen, J., van Der Akker, E.B., Trompet, S., van Heemst, D.,_Mooijaart, S.P. & Beekman, M. (2016). Employing biomarkers of healthy aging for leveraging genetic studies into human longevity. *Experimenal Gerontology*, *82*, 166–174. https://doi.org/10.1016/j.exger.2016.06.013

Dogru-Abbasoglu, S., Tamer-Toptani, S., Ugurnal, B, Koçak-Toker, N., Aykac-Toker, G., Uysal, M. (1977). Lipid peroxidation & antioxidant enzymes in livers and, brains of aged rats. *Mechanism of Age Development, 98*, 177–180. https://doi.org/10.1016/S0047-6374(97)00082-1

Drivera, A.S., Rao, P. Kodavantib, S., &Mundyb, W.R. Age-related changes in reactive oxygen species production in rat brain homogenates. (2000). *Neurotoxicology and Teratol*, *22*(2), 175–181. https://doi.org/10.1016/S0892-0362(99)00069-0

Dube, P., Khalaf, F.K., DeRiso, A., Mohammed, C.J., Connolly J.A., &Kennedy, D.J. (2022). Cardioprotective role for paraoxonase 1 in chronic kidney disease. *Biomedicines*, *10*, 2301-2312. https://doi.org/10.3390/biomedicines10092301

Ellman, G.L., Courtney, K.D., Andres, V., Feather-Stone, R.M. A new and, rapid colorimetric determination of acetylcholinesterase activity. (1961). *Biochemical Pharmacology*, *7*, 88-90. https://doi.org/10.1016/0006-2952(61)90145-9

Ellmann, GL. (1959). Tissue sulphydryl groups. *Archives of Biochemistry and Biophysics*, *82*, *70-77*.

Elseadya, S.S., Sharsharb, R. S., Abdelnabyc, A.Y., Abdella, A.M. (2022). Study of the diagnostic utility of paraoxonase enzyme in serum & bronchoalveolar lavage in patients with lung cancer. The *Egypt Journal of Chest Diseases and Tuberc*ulosis, *71*, 485-490. DOI: 10.4103/ecdt.ecdt_11_22

Enciu, A.M., Gherghiceanu, M., & Popescu ,B.O. (2013). Triggers & effectors of oxidative stress at blood-brain barrier level: relevance for brain aging and neurodegeneration. *Oxidative Medicine and Cellular Longevity, 2013*, 297512-297525. http://dx.doi.org/10.1155/2013/297512

Erre, G.L., Bassu, S., Giordo, R., Mangon,i A.A., Carru, C. (2022). Association between Paraoxonase/arylesterase activity of serum PON-1 enzyme & rheumatoid arthritis. A systematic review & meta-Analysis. *Antioxidants*, *1*, 2317-2328. https://doi.org/10.3390/antiox11122317

Freitas, H.R., Ferreira, G.D., Trevenzoli, I.H., Oliveira, K.D., & Melo, R.A. (2017). Fatty Acids antioxidants & physical Activity in Brain Aging. *Nutrients*, *9*, 1263-1286. doi:10.3390/nu9111263

Gabaldó, X., Juanpere, M, Castañé, H., Rodríguez-Tomàs., E, López-Azcona A.F., &Joven, J. (2022). Usefulness of the measurement of serum paraoxonase-1 arylesterase activity in the diagnoses of COVID-19. *Biomolecules*, *12*, 879-888. https://doi.org/10.3390/biom12070879.

Ghezzi, A.C., Cambri, L.T., Botezelli, J.D., Ribeiro, C., Dalia R.A. &DeMello, MAR. (2012). Metabolic syndrome markers in Wistar rats of different ages. *Diabetology and Metabolic Syndrome*. *4*, 16-23. https://doi.org/10.1186/1758-5996-4-16

Griffin, M.D., Wilson, L.M., Mok, Y., Januszewski, A.S., Wilson, A.M., &Howlett, G.J. (2010). Thioflavin T fluorescence in human serum: Correlations with vascular health & cardiovascular risk factors. *Clinical Biochemistry, 43*, 278-86. https://doi.org/10.1016/j.clinbiochem.2009.10.010

Grintzalis, K., Patsoukis, N., Papapostolo, I., Zervoudakis, G., Kalaitzopoulou, E., &Panagopoulos N.T. (2022). Alterations in thiol redox state & lipid peroxidation in the brain areas of male mice during aging. *Advances in Redox Research*, *6*, 100043-100049. https://doi.org/10.1016/j.arres.2022.100043

Haider, S., Saleem, S., Perveen, T., Tabassum, S., Batool, Z.,&Madiha, S. (2014). Age-related learning & memory deficits in rats: role of altered brain neurotransmitters, acetylcholinesterase activity & changes in antioxidant defense system. *Age, 36*, 1291–1302. 10.1007/s11357-014-9653-0

Holmes, G.E., Bernstein, C., Bernstein, H. (1992). Oxidative & other DNA damages as the basis of aging: A review. *Mutational Research, 75*, 305–315. https://doi.org/10.1016/0921-8734(92)90034-M

Hussain, S., Slikker, JRW., &Ali S.F. (1995). Age-related changes in antioxidant enzymes, superoxide dismutase, catalase, glutathione peroxidase & glutathione in different regions of mouse brain. *International Journal of Developmental Neuroscience, 13*(8), 811-817. https://doi.org/10.1016/0736-5748(95)00071-2

Jasinski, M., Olszewska-Slonina, D. (2022). Serum Paraoxonase-1 Activity & the Risk of Prostate Cancer Recurrence in Patients Treated with Radiotherapy. *Antioxidants*, *11*, 346-356. https://doi.org/10.3390/antiox11020346

Johnson, A.A., Stolzing, A. (2019). The role of lipid metabolism in aging, lifespan regulation, & age-related disease. *Aging Cell*, *18*(6), e13048-e1304864. DOI: 10.1111/acel.13048

Khan, A.A., Quinn, T.J., Hewitt, J., Fan, Y., Dawson, J. (2016). Serum uric acid level & association with cognitive impairment & dementia: systematic review&meta-analysis. *Age*, *38*, 16-24. DOI 10.1007/s11357-016-9871-8

Khurana, R., Coleman, C., Ionescu-Zanetti, C., Carter, S.A., Krishna,V., &Sing, S. (2005). Mechanism of thioflavin T binding to amyloid fibrils. *Journal of Structural Biology*, *151*, 229-38. https://doi.org/10.1016/j.jsb.2005.06.006

Kontush, A. (2001). Amyloid-beta: an antioxidant that becomes prooxidant & critically contributes to Alzheimer's disease. *Free Radical Biology and Medicine, 31*(9), 1120–1131. https://doi.org/10.1016/S0891-5849(01)00688-8

Kuzuya, M., Ando, F., Iguchi A., &Shimokata, H. (2002). Effect of aging on serum uric acid levels: Longitudinal changes in a large Japanese population group. *Journal of Gerontology, 57A*(10), M660–M664. https://doi.org/10.1093/gerona/57.10.M660

Levy, D., Reichert, C.O. &Bydlowski, S.P. (2019). Paraoxonases Activities & Polymorphisms in Elderly & Old-Age Diseases: An Overview. *Antioxidants, 8,* 118-142. doi:10.3390/antiox8050118.

Liu, D., Yun, Y., Yang, D., Hu, X., Dong, X., & Dua,W. (2019). What Is the Biological Function of Uric Acid? An Antioxidant for Neural Protection or a Biomarker for Cell Death. *Disease Marker, 2019*, 4081962-4081972. https://doi.org/10.1155/2019/4081962

Liu, H.H., Li, J.J. (2015). Aging & dyslipidemia: A review of potential mechanisms. *Aging. Reserach Reviews*, *19*, 43–52. https://doi.org/10.1016/j.arr.2014.12.001

Liu, W., Li, I., Yang, M., Ke X., Dai Y., &Tao,J. (2022). Chemical genetic activation of the cholinergic basal forebrain hippocampal circuit rescues memory loss in Alzheimer's Disease. *Alzheimer Research and Therapy, 14*, 53-64. https://doi.org/10.1186/s13195-022-00994-w

Mackness, M. &Sozmen E.Y. (2021). A critical review on human serum paraoxonase-1 in the literature: truths & misconceptions. *Turkish Journal of Biochemistry*, *46*(1), 3–10. https://doi.org/10.1515/tjb-2020-0186

Mandal, P.K., Roy, G.H., & Samkaria A. (2022). Oxidative Stress: glutathione & its potential to protect methionine-35 of Aβ peptide from oxidation. *ACS Omega*, *7*, 27052−27061. https://doi.org/10.1021/acsomega.2c02760

Matsuo, M., F. Gomi, F., Dooley, M.M. (1992). Age-related alterations in antioxidant capacity & lipid peroxidation in brain, liver, & lung homogenates of normal & vitamin E-deficient rats. *Mechanism of Aging and Development, 64,* 273–292. https://doi.org/10.1016/0047-6374(92)90084-Q.

Menini, T., Gugliucci, A. (2014). Paraoxonase 1 in neurological disorders. *Redox Reports*, *19*(2), 49-59. https://doi.org/10.1179/1351000213Y.0000000071.

Morris, G., Puri ,K.B., Bortolasci, C.C., Carvalho, A., Berk, M. &Maes, M. (2021). The role of high-density lipoprotein cholesterol, apolipoprotein A and, paraoxonase-1 in the pathophysiology of neuro progressive disorders. *Neuroscience and Biobehavioral Reviews*, *125*, 244–263. https://doi.org/10.1016/j.neubiorev.2021.02.037

Mota, A., Hemati-dinarvand, M., Taheraghdam, A.A., Nejabati, H.R., Ahmadi, R., Valilo, M., (2019). Association of paraoxonse1 (PON1) genotypes with the activity of PON1 in patients with Parkinson's Disease. *Acta Neurologica Taiwan*, *28*, 66-74.

Nilsson, M.R. (2004). Techniques to study amyloid fibril formation in vitro. *Methods*, *34*, 151-60. https://doi.org/10.1016/j.ymeth.2004.03.012

Özturan-Özer, E., Türkoğlu, S. (2020). Contribution of amyloid β-Peptides to acrylamide-induced toxicity in rat brain tissue. *Advances in Animal and Veterinary Sciences*, *8*(1), 54-60. http://dx.doi.org/10.17582/journal.aavs/2020/8.1.54.60.

Peng, H.B., Bukuroshi, P., Durk, M.R., Grootendorst, P., Yan, X., &Pang K.S. (2021). Impact of age, hypercholesterolemia and the vitamin D receptor (VDR) on brain endogenous β-amyloid peptide accumulation in mice. *Biopharmaceuticals and drug disposition, 42*(8), 349-398. https://doi.org/10.1002/bdd.2297

Puchtler, H., Sweat, F., Levine, M. (1962). On the binding of Congo red by amyloid. *Journal of Histochemistry and Cytochemistry*, *10*(3), 1-15. https://doi.org/10.1177/10.3.355

Qiao, M., Chen, C., Liang, Y., Luo Y., & Wu W. (2021). The influence of serum uric acid level on Alzheimer's Disease: A narrative review. *Biomedical Research International, 2021*, 5525710-5525718. https://doi.org/10.1155/2021/5525710

Reichert, C.O., Levy, D. &Bydlowski, S.P. (2021). Paraoxonase role in human neurodegenerative diseases. *Antioxidants, 10*, 11-37. https://dx.doi.org/10.3390/antiox10010011

Salazar, S.V., O.Cox, T.O., Lee S., Brody, A.H., Chyung, A.S., &Strittmatter, S.M. (2019). Alzheimer's disease risk factor Pyk2 mediates amyloid-β induced synaptic dysfunction and loss. *J. Neuroscience*, *39*(4), 758-772. Doi: 10.1523/JNEUROSCI.1873-18.2018

Salazar, J., Joana Poejo, J., Mata, A.M., Samhan-Arias, A., &Carlos Gutierrez-Merino, C. (2022). Design and experimental evaluation of a peptide antagonist against amyloid-b-(1-42) interactions with calmodulin and calbindin-D28k. *International Journal of Molecular Sciences*, *23*(4), 2289-2311. https://doi.org/10.3390/ijms23042289

Salazar, J.G., Marsillach, J., Revert, I., Mackness, B., Mackness, M., &Colomina, M.T. (2021). Paraoxonase-1 and-3 protein expression in the brain of the Tg2576 mouse model of Alzheimer's Disease. *Antioxidants*, *10*, 339-350. https://doi.org/10.3390/antiox10030339

Schliebs, R., &Arendt, T. (2011). The cholinergic system in aging & neuronal degeneration. *Behavioural Brain Research, 221,* 555–563. https://doi.org/10.1016/j.bbr.2010.11.058

Schulz, J.B., Lindenau, J., Seyfried, J., Dichgans, J. (2000). Glutathione, oxidative stress and neurodegeneration. *European Journal of Biochemistry*, *267*, 4904-4911. https://doi.org/10.1046/j.1432-1327.2000.01595.x

Sehar, U., Rawat, P., Reddy, A.B., Kopel, J., Reddy, H.P. (2022). Amyloid beta in aging and Alzheimer's Disease. *International Journal of Molecular Sciences*, *23*, 12924-12949. https://doi.org/10.3390/ijms232112924

Setti S.E., Raymick J., Hanig J., Sarkar S. (2021). In vivo demonstration of Congo Red labeled amyloid plaques via perfusion in the Alzheimer disease rat mode. *J. Neurosci Methods*, *353*, 109082-109091. https://doi.org/10.1016/j.jneumeth.2021.109082

Smith, C.D., Carney, J.M. Starke-Reed, P.E., Oliver, C.N., Stadtman, E.R. &Markesbery, W.R. (1991). Excess brain protein oxidation & enzyme dysfunction in normal aging in Alzheimer's disease. *Proceedings of the National Academy of Science, 88*, 10540–10543. https://doi.org/10.1073/pnas.88.23.10540

Sofflai, SS., Baktashian, M., Moghaddam, K.H., Karimian, M.S., Kosari N. (2022). Association of paraoxonase-1 genotype and phenotype with angiogram positive coronary artery disease. *Arquiovos Brasileiros Cardiologia, 119*(4), 593-601. https://doi.org/10.36660/abc.20210422

Starke-Reed, P.E., Oliver C.N. (1989). Protein oxidation & proteolysis during aging & oxidative stress. *Archives of Biochemistry and Biophysics, 275*, 559–567. https://doi.org/10.1016/0003-9861(89)90402-5.

Sultzer, D.L., Lim, A.C., Gordon,H.L., &Melrose, R.J. (2022). Cholinergic receptor binding in unimpaired older adults, mild cognitive impairment and Alzheimer's disease dementia. *Alzheimer Research and Therapy*, *14*, 25-36. https://doi.org/10.1186/s13195-021-00954-w

Tang, X., Song, Z.H., Cardoso, M.A., Zhou, J.B., Simó, R. (2022). The relationship between uric acid and brain health from observational studies. *Metabolic Brain Disorders, 37*, 1989-2003 https://doi.org/10.1007/s11011-022-01016-2

Tanner, J.A., Richie, M.B., Cadwell, C.R., Eliaz, A., Kim, S., &Guterman, E.L. (2022). Amyloidβ related angiitis presenting as eosinophilic meningitis: a case report. *BMC Neurology, 22,* 116-123. https://doi.org/10.1186/s12883-022-02638-w

Thompson, E.W., Demissei, B.G., Smit, A.M., Brahmbhatt, P., Wang J. (2022). Paraoxonase-1 activity in breast cancer patients treated with doxorubicin with or without trastuzumab. *Journal of American College of Cardiology, 7*(1), 1-10. https://doi.org/10.1016/j.jacbts.2021.10.010

Tian, L., Cai, Q., &Wei H. (1998). Alterations of antioxidant enzymes and oxidative damage to macromolecules in different organs of rats during aging. *Free Radical Biology and Medicine, 24*(9): 1477–1484. https://doi.org/10.1016/S0891-5849(98)00025-2

Wang, Q., Lu, M., Zhu, X., Gu, X., Zhang, T., & Zhou, M. (2022). Brain mitochondrial dysfunction: A possible mechanism links early life anxiety to Alzheimer's Disease in later life. *Aging. Disease*, *13*(4), 1127-1145. http://dx.doi.org/10.14336/AD.2022.0221 2022

Xu, Y., Dong, Y., Wang, C., Jiang, Q., Chu H., & Yue Tian. (2021). Lovastatin attenuates sevoflurane-induced cognitive disorder in aged rats via reducing Aβ accumulation. *Neurochemistry International, 148,* 105078-105088. https://doi.org/10.1016/j.neuint.2021.105078

Youdim, K.A &Deans, S.G. (2000). Effect of thyme oil & thymol dietary supplementation on the antioxidant status & fatty acid composition of the aging rat brain. *British Journal of Nutrition, 83*(1), 87–93. https://doi.org/10.1017/S000711450000012X

Zhang, L., Pitcher, L.E., Yousefzadeh, M.J., Niedernhofer, L.J., Robbins P.D., &Zhu, Y. (2022). Cellular senescence: a key therapeutic target in aging & diseases. *The Journal of the Clinical Investigation*, *132*(15), e158450-e158463. https://doi.org/10.1172/JCI158450

Zhua, Y., Carveya, P.M., Linga, Z. (2006). Age-related changes in glutathione & glutathione-related enzymes in rat brain. *Brain Research*, *1090*(1), 35-44. https://doi.org/10.1016/j.brainres.2006.03.063

FABAD J. Pharm. Sci., 48, 1, 165-182, 2023
Doi: 10.55262/fabadeczacilik.1172020
REVIEW ARTICLE

Monoclonal Antibodies and Immuno-PET Imaging: An Overview

Elif Tugce SARCAN[*], Asuman Yekta ÖZER[**°]

Monoclonal Antibodies and Immuno-PET Imaging: An Overview

SUMMARY

Radiopharmaceuticals are radioactive medicines used for imaging and/or therapeutic purposes, consisting of radionuclidic and pharmaceutical parts. While Positron Emission Tomography (PET) and Single Photon Emission Computed Tomography (SPECT) methods are commonly used for imaging purposes, the immuno-PET imaging method has gained popularity recently. Immuno-PET imaging method is a combination of PET radionuclides and biomolecules, especially monoclonal antibodies (mAb), proteins, peptides, which are frequently used for the imaging of different types of cancer. Radionuclides with long half-lives are generally used in immuno-PET imaging. Long biological half-lives of mAbs are the most important reason to be preferred for immuno-PET imaging. Today, Zirconium-89 (Zr-89), Iodine-124 (I-124) with long half-lives and Copper-64 (Cu-64) and Yttrium-86 (Y-86) radionuclides with relatively long half-lives are preferred in immuno-PET imaging. In this article, preclinical and clinical studies of Zr-89, Cu-64, I-124 and Y-86-labeled mAbs with a long half-lives were reviewed. Also, these 4 radionuclides, which are frequently used in the labelling of biomolecules (particularly mAbs) are compared.

Key Words: *Immuno-PET, zirconium-89, copper-64, yttrium-86, iodine-124, monoclonal antibodies, imaging.*

Monoklonal Antikorlar ve Immuno-PET Görüntülenmesi: Genel Bakış

ÖZ

Radyofarmasötikler, radyonüklidik ve farmasötik kısımlardan oluşan görüntüleme ve/veya tedavi amaçlı kullanılan radyoaktif ilaçlardır. Görüntüleme amaçlı pozitron emisyon tomografisi (PET) ve tek foton emisyon tomografisi (SPECT) yöntemleri kullanılırken, son zamanlarda immuno-PET görüntüleme yöntemi de popülerlik kazanmıştır. PET radyonüklidleri ve biyomoleküllerin, özellikle monoklonal antikor (mAb), protein, peptit kombinasyonları olan immuno-PET görüntüleme ajanları ve yöntemi özellikle farklı kanser türlerinin görüntülenmesinde sıklıkla kullanılmaktadır. İmmuno-PET görüntülenmesinde sıklıkla uzun yarılanma ömrüne sahip radyonüklidlerden yararlanılmaktadır. Bunun en önemli nedeni ise uzun biyolojik yarılanma ömrüne sahip mAb'ların immuno-PET görüntülenmesinde sıklıkla tercih edilmeleridir. Günümüzde uzun yarılanma ömrüne sahip Zirkonyum-89 (Zr-89), Iyot-124 (I-124) ve nispeten uzun yarılanma ömrüne sahip Bakır-64 (Cu-64) ile İtriyum-86 (Y-86) radyonüklitleri tercih edilmektedir. Bu çalışmada, kullanımı ve popüleritesi giderek artan mAb'ların immuno-PET görüntülenmesinde kullanımları ve uzun yarılanma ömrüne sahip klinik ve preklinik çalışmaları süren Zr-89, Cu-64, I-124 ve Y-86 ile işaretli mAb'ların çalışmaları derlenmiştir, özellikle mAb'ların, işaretlenmesinde sıklıkla kullanılan bu 4 radyonüklidin karşılaştırılmasına yer verilmiştir.

Anahtar Kelimeler: *İmmuno-PET, zirkonyum-89, bakır-64, itriyum-86, iyot-124, monoklonal antikor, görüntüleme*

Received: 07.09.2022
Revised: 19.12.2022
Accepted: 18.01.2023

[*] ORCID: 0000-0002-7323-6044, Hacettepe University, Faculty of Pharmacy, Department of Radiopharmacy, 06100-Ankara, Turkey.
[**] ORCID: 0000-0001-6707-247X, Hacettepe University, Faculty of Pharmacy, Department of Radiopharmacy, 06100-Ankara, Turkey.

° Corresponding Author; Asuman Yekta Ozer
E-mail: ayozer@hacettepe.edu.tr, Phone: 0312 310 2152

INTRODUCTION

Monoclonal antibodies (mAb) have been used for imaging and therapy for more than three decades. Hybridoma technology, discovered by Köhler and Milstein, is a milestone for mAb production and broke fresh ground for using mAbs (Wong et al., 2011). The use of mAbs and mAb-linked products have gradually increased since the first mAb was approved in 1986. Besides their use for therapeutic purposes, they can also be benefited from targeting due to their specificity for the target (Ecker, Jones, & Levine, 2015).

Radiolabelled mAbs have been used for diagnosis and/or therapy for many years. Immuno-imaging was done in the '90s with immuno-Single Photon Emission Computed Tomography (SPECT) (Sarcan & Özer, 2021). SPECT requires radiopharmaceutical radiolabelled with gamma-emitting radionuclides with an ideal gamma energy of 100-250 keV (Wadas, Wong, Weisman, & Anderson, 2010) .

Positron Emission Tomography (PET) is based on positron travels after emission and being annihilated with an electron. After the annihilation of the positron and electron, 2 gamma rays with 511 keV energy are launched. PET imaging methods show better sensitivity, specificity, and higher resolution than SPECT imaging methods (Kaur et al., 2012; Sarcan, Silindir-Gunay, Ozer, & Hartman, 2021). F-18, N-13, O-15, and C-11 are conventional PET radionuclides with short half-lives. In addition to these conventional radionuclides, new PET radionuclides with long half-lives show increasing popularity, such as Zr-89, Cu-64, Y-86, and I-124 in preclinical and clinical stages (Holland, Williamson, & Lewis, 2010; Wadas et al., 2010). These long-lived radionuclides are used in immuno-PET because their half-lives are similar to biomolecules such as mAbs, proteins, etc. (Reddy & Robinson, 2010). Biomolecules can circulate in the body for a long time, and when they are labelled with long half-life radionuclides, monitoring of mAbs can be possible (van Dongen, Visser, Lub-de Hooge, de Vries, & Perk, 2007).

Immuno-PET is based on the "magic bullet" concept, and the idea explains the utilization of radionuclides to biomolecules. Beyond the diagnosis purposes of immuno-PET with Zr-89, Cu-64, Y-86, and I-124 radionuclides, it can also be used for tracking mAbs behavior and monitoring therapy (Sarcan et al., 2021; Van Dongen et al., 2015).

Many papers have been published about preclinical and clinical studies of immuno-PET for different aims. In this article, radiolabelled mAbs for immuno-PET are reviewed and discussed comparatively for the advantages and disadvantages of Zr-89, Cu-64, Y-86, and I-124 radionuclides for mAb labelling.

MONOCLONAL ANTIBODIES

MAb production studies started after Köhler and Milstein discovered hybridoma technology in 1975. Briefly, hybridomas are formed by combining B cells of mice immunized with antigen and myeloma cancer cells (Figure 1) (Barbaros & Dikmen, 2015; Templar Smith, 2012). mAbs have an average molecular weight of 150 kDa, containing 2 heavy and 2 light chains, and these chains stay together with disulfide bonds (Figure 2) (Breedveld, 2000a). Murine, chimeric, humanized, and fully human mAbs have been produced with developing Technologies (Breedveld, 2000a). Murine mAbs faced several problems in clinical use because of their immunogenicity of murine mAbs (van Dongen & Vosjan, 2010).

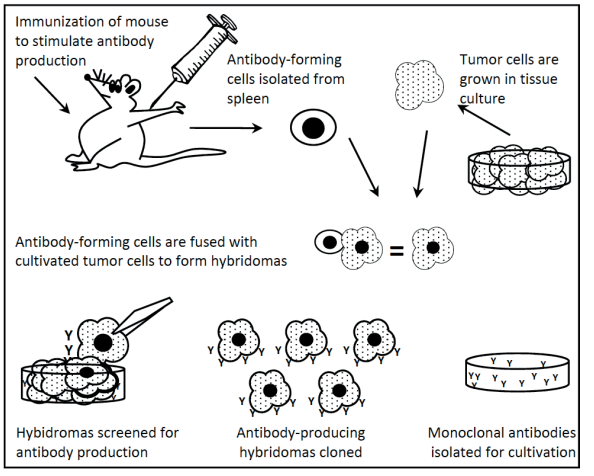

Figure 1. Monoclonal antibody production with hybridoma technology (Templar Smith, 2012).

MAbs consists of 4 regions, i.e., 2 heavy and 2 light chains of Fab and Fc fragments (Figure 2). Fab fragment is the antigen-binding site, while the Fc fragment defines the antibody functions (Breedveld, 2000b). Intact antibodies show slow clearance, high tumor uptake, and background signal while showing nonspecific accumulation (Kobayashi, Choyke, & Ogawa, 2016). Unlike intact antibodies, antibody fragments show rapid renal clearance and high tumor penetration (Kenanova & Wu, 2006).

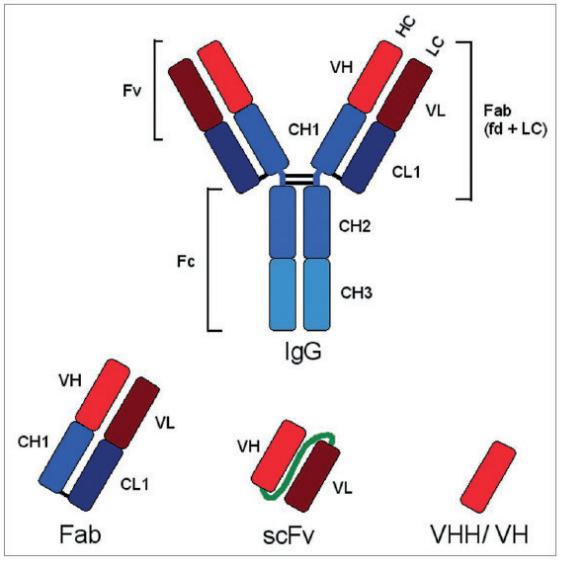

Figure 2. mAb fragments (Nelson, 2010).

MAbs have been used for therapy, diagnosis, etc., with the contribution of hybridoma technology, although the clinical use of mAbs took several decades after the discovery of hybridoma technology by Köhler and Milstein (Breedveld, 2000b; Templar Smith, 2012).

Many mAbs, mAb-drug conjugates, radionuclide labelled mAbs, etc., have been approved by Food and Drug Administration (FDA). Also, many of them are used in clinics as much as in clinical trials (Hollinger & Hudson, 2005). FDA first approved Muromonab-CD3 with the generic name Orthoclone OKT3 in 1986 for kidney transplant rejection (Lu et al., 2020). After that, the approved mAb for cancer treatment was Rituximab with Rituxan generic name in 1997 for B-cell Non-Hodgkin's Lymphoma (NHL) therapy (Dillman, 2006; Schrama, Reisfeld, & Becker, 2006). Trastuzumab (Herceptin) for breast cancer; Alemtuzumab (Campath) for chronic lymphocytic leukemia; Bevacizumab (Avastin) for colorectal cancer were approved by FDA between 1998-2004 (Schrama et al., 2006). 24 antibody-drug conjugates were approved by FDA for cancer therapy until 2016 (McKnight & Viola-Villegas, 2018).

In radiopharmaceutical science, many antibodies have been radiolabelled with various radionuclides, and many are under preclinical and clinical trials. Paul Ehrlich developed the concept of how biomolecules, especially mAbs, affect as a targeting part to transfer the radionuclides called "magic bullet," and radiolabelled biomolecules investigation started with this concept (Cutler, Hennkens, Sisay, Huclier-Markai, & Jurisson, 2013). The high specificity and accumulation on the target area of mAbs make them attractive and suitable for molecular imaging (Kobayashi et al., 2016).

RADIOPHARMACEUTICALS

Radionuclides such as gamma and positron emitters (Table 1) are used for the therapy, diagnosis, and monitoring diseases with SPECT and PET (Drude, Tienken, & Mottaghy, 2017). Multiple cameras of SPECT rotate around the patients to give three-dimensional information about the radioactivity uptake in the body. Radionuclides should emit gamma radiation within the 100-300 keV range to be detected by SPECT camera.

Table 1. Gamma and positron emitting radionuclides.

Radionuclides	Half-life	Main Energy (kEv)	Imaging Method
Tc-99m	6.06 h	140.51 (gamma)	SPECT
In-111	67.9 h	245 (gamma)	SPECT
I-123	100.8 h	159 (gamma)	SPECT
I-124	4.2. day	2149 (β^+)	PET
Ga-68	68 min	1,899 (β^+)	PET
F-18	110 min	633 (β^+)	PET
Zr-89	78.4 h	395 (β^+)	PET
Y-86	14.7 h	1248 (β^+)	PET
Cu-64	12.7 h	653 (β^+)	PET

SPECT imaging with different types of collimators and detectors provides individualization of diagnosis and therapy of patients with other biomarkers (Figure 3) (Wallberg & Stahl, 2013). PET imaging provides higher resolution and sensitivity with lower radiotracer than SPECT imaging. PET imaging method is based on the positron-emitting radionuclides, and the positron produces two gamma-photons with 511 keV while traveling in the body. These two photons are directed in 180° opposite direction, and annihilation is placed (Cutler et al., 2013; Wallberg & Stahl, 2013).

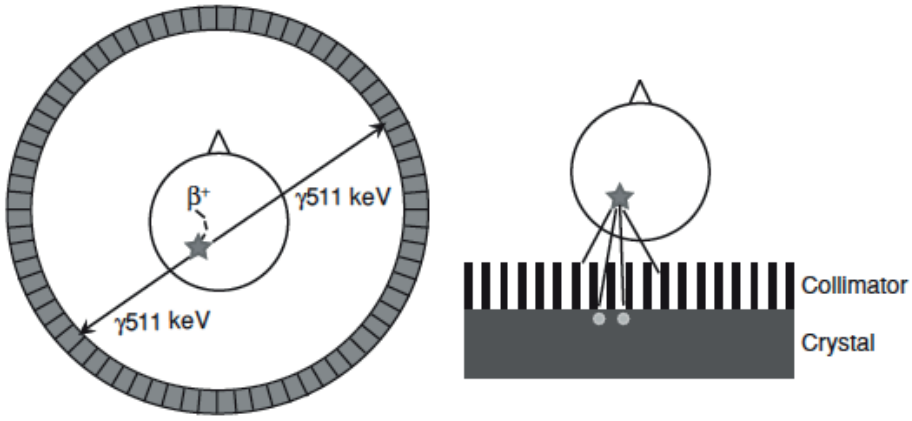

Figure 3. PET (left) and SPECT (right) schema (Wallberg & Stahl, 2013).

Radiometals have some advantages, such as simple labelling procedures and half-life, which are more suitable for antibody labelling, circulation, and accumulation studies in tumor tissue rather than non-radiometal tracers (Morais & Ma, 2018). Germanium-67/Gallium-68 (^{67}Ge/^{68}Ga) is one of the most widely used generators of PET radionuclides which is evaluated as a better alternative to some of the other radionuclides like ^{18}F, ^{124}I, ^{64}Cu, ^{89}Zr due to easy accessibility in radiopharmacy labs (Drude et al., 2017). However, considering the half-life of radionuclides, ^{89}Zr, ^{64}Cu, ^{86}Y, and ^{124}I are more suitable radiotracers for mAb radiolabelling instead of ^{68}Ga, ^{18}F (Morais & Ma, 2018).

^{89}Zr, a radiometal with a 78.4 h half-life, is generally produced by ^{89}Y(p,n)^{89}Zr reaction in cyclotrons. ^{89}Zr is widely used in mAb radiolabelling due to its long half-life (Aluicio-Sarduy et al., 2018). ^{89}Zr also helps to understand the tumor targeting properties and pharmacokinetics of mAbs (Heskamp et al., 2017). The high resolution, sensitivity, and accurate image quantification are more frequently used properties for the labelling of mAbs. Also, the residualized

features of ^{89}Zr provide improved tumor retention and tumor/normal tissue ratios due to internalization (Verel et al., 2003).

^{64}Cu, another commonly used radiotracer for radiolabelling of mAbs and proteins, has a 12.7 h half-life and is generally used by ^{64}N(p,n)^{64}Cu reaction (Avila-Rodriguez, Nye, & Nickles, 2007). ^{64}Cu has been used for radiolabelling of many mAbs (anti-Epidermal growth factor receptor (EGFR), anti-CD20 mAbs, etc.), but most of them are limited in preclinical studies due to the half-life (12.7 h) of ^{64}Cu; intermediate half-life limits the clinical imaging studies (Aluicio-Sarduy et al., 2018; Ferreira et al., 2008; Sihver et al., 2014).

^{86}Y is another promising radionuclide as an immuno-PET radiotracer. ^{86}Y can be produced by ^{86}Sr(p,n)^{86}Y reaction in a small cyclotron with high radionuclidic purity. It has a 14.7 h half-life. However, due to the decay properties of ^{86}Y, production rates of ^{86}Y are lower than ^{89}Zr and ^{64}Cu (Lubberink & Herzog, 2011; Wadas et al., 2010).

^{124}I is a radionuclide with a long half-life (4.18 days) used for imaging and therapy. ^{124}I radiolabelled mAbs show high potential as an immuno-PET imaging agent (Crisan et al., 2022).

Many radiolabelled mAbs with ^{64}Cu, ^{89}Zr, ^{124}I, and ^{86}Y have been investigated for many years in both preclinical and clinical studies. Researches on ^{86}Y and ^{64}Cu radiolabelled mAbs are limited due to the relatively short half-lives of ^{86}Y and ^{64}Cu compared with the mAbs' biological half-life. ^{89}Zr has a long half-life, making it a suitable radionuclide for mAbs radiolabelling; hence, it has been successfully used in clinical and preclinical studies. ^{124}I shows lower residualized features compared with ^{89}Zr, which means ^{124}I shows lower liver uptake (Carrasquillo et al., 2018).

In addition to these long-lived PET radionuclides, several radiolabelled mAbs have been approved by FDA and European Medicine Agency (EMA) (Table 2): ^{111}In radiolabelled Capromab Pendetide (ProntaScint); ^{90}Y radiolabelled Ibritumomab Tiuxetan (Zevalin); ^{99m}Tc radiolabelled Sulesomab (LeukoScan); ^{111}In radiolabelled Satumomab Pendetide (OncoScint); ^{131}I radiolabelled Tositumomab (Bexxar) for different purposes. ^{111}In-ProstaScint was approved in 1996 for prostate cancer diagnosis; ^{90}Y-Zevalin was the first radioimmunoconjugate approved as an anticancer agent in 2002 (Dilworth & Pascu, 2018).

Table 2. Some of the FDA and EMA approved radiolabelled mAbs.

Commercial Name	Radiolabelled-mAb	Year
OctreoScan	^{111}In-Octreotide	1994
ProntaScint	^{111}In-Capromab Pendetide	1996
	^{99m}Tc-Apcitide	1997
LeukoScan	^{99m}Tc-Sulesomab	1997
OncoScint	^{111}In-Satumomab Pendetide	1998
Zevalin	^{90}Y-Ibritumomab Tiuxetan	2002
Bexxar	^{131}I-Tositumomab	2003
Scintimun	^{99m}Tc-Besilesomab	2010

IMMUNO-PET with RADIOLABELLED MONOCLONAL ANTIBODIES

Immuno-imaging studies were started at the beginning of the '90s with SPECT with radiolabelled antibodies or fragments (Knowles & Wu, 2012). Although SPECT is a very sensitive imaging method, PET provides better quantification and higher sensitivity. Also, it is possible to determine the pharmacokinetics and biodistribution of pharmaceuticals with immuno-PET (Kumar & Ghosh, 2021). Radiopharmaceuticals of Immuno-PET development have several principles: appropriate radionuclide and chelator selection, suitable biological and chemical properties of mAbs, and the stability between mAbs, chelators,

and radionuclides (McKnight & Viola-Villegas, 2018).

PET radionuclides (radiometals and non-radiometals) are frequently used in preclinical and clinical stages. Especially, long-lived PET radionuclides are commonly utilized for immuno-imaging due to their several advantages. ^{89}Zr, ^{64}Cu, and ^{124}I PET radionuclides show appropriate half-lives to antibodies and/or proteins/peptides (Knowles & Wu, 2012). The similarity of physical and biological half-lives of mAbs and PET radionuclides provides proper accumulation in the tumor before radioactive decay and also provides enough clearance from normal tissues (McKnight & Viola-Villegas, 2018). Although long biological and physical half-lives ensure these advantages, long waiting times for imaging can be considered as a disadvantage (Kaur et al., 2012). In this part, ^{89}Zr, ^{64}Cu, ^{86}Y and ^{124}I radiolabelled mAb studies have been reviewed (Table 3).

Table 3. Summary of the studies on radiolabelled mAbs mentioned in this article.

Radionuclide	Compared Radionuclide	mAb	References
Zr-89		U36	(Borjesson et al., 2006; Börjesson et al., 2009)
	In-111	Trastuzumab	(E. Dijkers et al., 2007; E. C. Dijkers et al., 2009)
		MMOT0530A	(Lamberts et al., 2016)
		J591	(J. P. Holland, Divilov, et al., 2010)
		anti-PD-L1 mAb	(Kikuchi et al., 2017)
Cu-64		Cetuximab Abegrin	(Achmad et al., 2012; T. P. Nayak & Brechbiel, 2009; Zeng et al., 2014)
		Trastuzumab	(Parakh, Lee, Gan, & Scott, 2022; Tamura et al., 2013)
		Trastuzumab	(Kurihara et al., 2015; Tamura et al., 2013)
		3/F11 mAbs	(Maier et al., 2019)
		Rituximab	(Xie et al., 2017)
		PSMA-617	(Grubmuller et al., 2016)
Y-86	In-111	hu3S193	(Lövqvist et al., 2001)
	In-111	Trastuzumab	(Palm et al., 2003)
		Bevacizumab	(T. K. Nayak, Garmestani, Baidoo, Milenic, & Brechbiel, 2011)
I-124		Codrituzumab	(Carrasquillo et al., 2018)
		U36	(Verel et al., 2004)
		uA33	(Carrasquillo et al., 2011)
		mu1G8	(Olafsen et al., 2007)
		cG250	(Divgi et al., 2007; Povoski et al., 2013)

REGULATIONS

The preparation and use of radiopharmaceuticals are regulated by directives, regulations and rules in European Union (EU) (Gillings et al., 2021) and United States (U.S.) and many other countries. Radiopharmaceuticals are regulated by the Center for Drug Evaluation and Research (CDER) under the FDA in the USA; by European Medicine Agency in European Union; by The Australian Radiation Protection and Nuclear Safety Agency (ARPANSA) and Radiation Health Committee in Australia; by Health Product and Food Branch (HPFB) in Canada; by Atomic Energy Regulatory Board (AERB) in India (Saharma, Baldi, Singh, & Sharma, 2018).

Regulations of radiopharmaceuticals are associated with radiopharmaceutical monographs in pharmacopeias such as United States Pharmacopeias, European Pharmacopeias. The guidelines on cGMPs and current Good Radiopharmacy Practice (cGRPP) are the main guidelines for radiopharmaceuticals from development to release. In addition, the requirements are specified in the relevant monographs of the phar-

macopeias (USP, EP, JP, etc.) and in the general information section. For example, USP general chapter indicates the regulations about PET radiopharmaceuticals and how they should produce, prepare and the information given in USP meets the cGMP regulations ((CDER), 2011; Gillings et al., 2021; U.S.Pharmacopoeia, 2009). In the EU, adoptions and interpretations of regulations and directives may differ depending on the countries and these differences may occur only if the members provide the general scope and limits of directives (Gillings et al., 2021).

Immuno-PET radiopharmaceuticals, like other radiopharmaceuticals, should be produced according to the guidelines. Gillings and co-workers (2021), prepared the *"Guideline on cGRPP for Small-Scale Preparation Radiopharmaceuticals"* in the 3 sections: general aspects; radiopharmaceutical preparations with licensed generators and kits; and radiopharmaceutical preparations with non-licenced materials (Gillings et al., 2021). Some of the immune-PET radiopharmaceuticals can be evaluated under Section 2 and Section 3. However, all processes should meet the cGRRP rules.

Quality Control

Radiolabelled mAb formulations quality control tests are done right after radiolabelling procedures (purification, formulation preparation). Radiochemical purity, antigen binding, internalization and stability tests should be performed as clinical and preclinical quality control tests of radiolabelled mAbs. Radiochemical purities are mostly analyzed by Radio-High Pressure Liquid Chromatography (RHPLC); however, Radio-Thin Layer Chromatography (RTLC) and spin filter are also used as radiochemical purity analysis based on the molecular weight separation. Immuno-reactivity tests and/or binding assays are performed for the determination of antigen binding (Parakh et al., 2022). More quality control tests should be done for clinical applications. All formulations and radiolabelling steps should be performed under cGMP (current Good Manufacture Practise) rules and cGMP grade requires: 1) radiochemical purity 2) appearance 3) immunoreactivity and/or binding assay and/or ELISA 4) apyrogenicity 5) sterility 6) stability (Vugts, Visser, & van Dongen, 2013).

Radiochemical purity: Any analytical method can be mentioned in monographs depending on the radiopharmaceuticals. These methods may be paper chromatography, TLC, ITLC, size exclusion chromatography, liquid and gas chromatography with radioactivity detector. Bacterial endotoxin/pyrogen test are done after product release for radiopharmaceuticals with a short half-life. Recently, a kinetic LAL test taking 20 mins and provides the opportunity complete pyrogen tests before releasing for the radiopharmaceuticals with a longer half-life than 30 mins. Limits of bacterial endotoxins are mentioned in each monograph. Sterility tests are carried out according to the general methods. Also, radiopharmaceuticals can be released for patient use before the results of sterility tests are available ("Guideline on Radiopharmaceuticals, CHMP, EMEA/CHMP/QWP/306970/2007 (draft released for consultation)," 2007; WHO, 2017).

^{89}Zr Radiolabelled Monoclonal Antibodies

Many preclinical and clinical trials started after Immuno-PET technology with ^{89}Zr (Table 2) (E.T. Sarcan & Özer, 2021; van Dongen & Vosjan, 2010). In 2006, the first clinical ^{89}Zr radiolabelled mAb, ^{89}Zr-U36, was investigated for primary head and neck squamous cell carcinomas (HNSCC), especially lymph nodes, as reported by Börjesson and co-workers in 2006 (Borjesson et al., 2006). 20 patients with HNSCC have been included in this study, and 74 MBq ^{89}Zr-U36 was applied as a safe dose and no adverse reactions were observed. All primary tumor lesions were detected by ^{89}Zr-U36 immuno-PET. These results could prove that ^{89}Zr-U36 is a suitable agent which can be used for tumor detection, although it did not show any significant improvement compared to the traditional agent, ^{18}F-fluorodeoxyglucose (FDG) (Jauw et al., 2016). Biodistribution study was performed by Borjesson et al. in 2009, as a following

study. After injection, the uptake increased gradually in tumor while the uptake in blood pool, lungs, liver, kidneys and spleen decreased (Börjesson et al., 2009).

Before the clinical study of ^{89}Zr-trastuzumab, several preclinical studies showed that ^{89}Zr-trastuzumab could be a promising agent for HER2 overexpressed breast cancer imaging and therapy (Dijkers et al., 2009). Dijkers et al. (2009), radiolabelled trastuzumab with ^{89}Zr and ^{111}In (for comparison), and animal PET/CT imaging and biodistribution studies were performed. ^{89}Zr labelling procedures were performed with Verel et al. (2003) method (Verel et al., 2003) and quality control tests showed that trastuzumab was labelled with ^{89}Zr with high chemical purity and specific activity. In-vivo studies were performed for 6 days in 15 mice. In this stage, the optimal amount of trastuzumab was also calculated and 100 μg of trastuzumab was evaluated as optimal. During the *in vivo* studies between day 1 and 6, tumor uptake was significantly increased while blood-pool uptake decreased. But the liver and spleen radioactivity uptakes were found slightly higher than expected. When comparing to the ^{89}Zr-trastuzumab uptake of HER2/neu positive and negative groups, tumor uptakes were not different on day 1. However, significantly different tumor uptake was found on day 6. As a result of this study, ^{89}Zr-trastuzumab can be considered for clinical testing due to labelling with high chemical purity, high stability, and appropriate tumor uptake with high Tumor to Normal Tissue ratios. Also, biodistribution studies showed similarity to ^{111}In-trastuzumab used in clinical breast cancer studies (Dijkers et al., 2009).

Dijkers and co-workers reported a study of ^{89}Zr radiolabelled trastuzumab in 14 patients who have HER2-positive metastatic breast cancer (Dijkers et al., 2007). This study showed trastuzumab dose-dependent relation with imaging dose and biodistribution (Dijkers et al., 2007). ^{64}Cu-trastuzumab was also successfully labelled and found to be a comparable agent with ^{89}Zr-trastuzumab due to tumor/tissue ratios and the ability to identify primary and metastatic tumors with low uptake (Parakh et al., 2022; Tamura et al., 2013).

Many researchers have been carried out on EGFR, HER2, PSMA, CD20 and VEGF-A, PSMA, and PD-L1 antigens (Heskamp et al., 2017; Holland, Sheh, Smith-Jones, & Lewis, 2009). ^{89}Zr-cetuximab, ^{89}Zr-pertuzumab, ^{89}Zr ibritumomab tiuxetan, ^{89}Zr huJ591, ^{89}Zr-bevacizumab, ^{89}Zr-nimotuzumab, ^{89}Zr-pembrolizumab have also been investigated for various cancer diagnosis (Table 4).

Lamberts and co-workers (2016) used ^{89}Zr radiolabelled MMOT0530A (mesothelin antibody) to follow DMOT4039A (antibody-drug conjugate) treatment of pancreatic and ovarian cancer lesions in Phase 1 studies. The main purpose of ^{89}Zr-MMOT0530A used was to understand the mesothelin expression, antibody tumor uptake and distribution, relation between the uptake and treatment response (Lamberts et al., 2016). This was the first-in-human study for anti-mesothelin antibody tumor uptake and body distribution. ^{89}Zr- MMOT0530A provided the visualization of antibody distribution and provided the imaging of pancreatic and ovarian cancer lesions. Researchers mentioned that this immuno-PET imaging technique with ^{89}Zr- MMOT0530A can potentially guide the treatment (Lamberts et al., 2016).

In 1997, J451, J533, J591, and E99 mAbs, specific to epitopes on PSMA, were produced by Liu et al. (Liu et al., 1997; Liu et al., 1998). J591 was found to be a promising one for diagnostic and therapeutic immuno-conjugates for PSMA targeting among of these 4 PSMA targeting mAbs. After this finding, preclinical and clinical studies started and have been reported for radiolabelled J591 with various radionuclides for treatment and diagnostic purposes (Holland, Divilov, et al., 2010).

Holland et al. (2010) studied the production of ^{89}Zr-J591 and evaluated the in vitro studies and preclinical data of ^{89}Zr-J591 in prostate-specific membrane antigen (PSMA) (+) tumor (LNCaP cells). In this study, researchers completed the radiochemistry

part with a high yield of radiolabelling (77%) and very high radiochemical purity (99%). In vivo studies proved that ^{89}Zr-J591 shows a high tumor/background tissue ratio. All results in radiochemistry for in vitro and preclinical studies showed that ^{89}Zr-J591 is a promising radiopharmaceutical for clinical studies in PSMA (+) tumor types (Holland, Divilov, et al., 2010).

Kikuchi and co-workers (2017) studied PD-L1-based radiotherapy and mAb therapy and measured PD-L1 expression with ^{89}Zr radiolabelled anti-PD-L1 mAb. Because of the difficulties in monitoring the radiotherapy with mAbs, ^{89}Zr radiolabelled anti-PD-L1 mAb was planned to overcome this difficulty. In this study, researchers investigated the treatment of head and neck squamous cell carcinoma (HNSCC). In the end, PET/CT images with ^{89}Zr-anti PD-L1 mAbs showed therapeutic efficiency and proved increased uptake in irradiated tumors, although it could not be monitored non-invasively. This report is the first data indicating that ^{89}Zr-radiolabelled anti-PD-L1 can be employed to monitor of radiotherapy in PD-L1 positive tumors (Kikuchi et al., 2017).

Table 4. ^{89}Zr radiolabelled mAbs and their clinical trial situation (McKnight & Viola-Villegas, 2018).

mAb	Types	Target	Cancer Type	Clinical Trial Status	Responsible Party
Rituximab	**Chimeric**				
Trastuzumab	**Humanized**	HER 2	Breast Cancer	Completed, 2017	Dr. Géraldine Gebhart et. al.
Pertuzumab	**Humanized**	HER 2	HER 2 (+) malignancy	Completed, 2018	Memorial Sloan Kettering Cancer Center
U36	**Chimeric**	CD 44	Head and neck cancer	Completed	
Ibritumomab Tiuxetan	**Mouse**	CD 20	NHL	Completed	
huJ591	**Humanized**	PSMA	Prostate cancer	Completed, 2020	Weill Medical Colloge of Cornell University
Bevacizumab	**Humanized**	VEGF	Breast cancer	Completed, 2019	Heather A. Jacene
Cetuximab	**Chimeric**	EGFR	Colorectal cancer	Completed, 2020	C. Menke- van der Houven van Oordt
Pembrolizumab	**Humanized**	PD-1	Non small cell lung cancer	Phase 2	E. F. Smith

^{64}Cu Radiolabelled Monoclonal Antibodies

Various ^{64}Cu radiolabelled mAbs have been reported for immuno-imaging and radioimmunotherapy. Cetuximab and Abegrin (FDA-approved mAbs) have been radiolabelled and studied in preclinical models (Nayak & Brechbiel, 2009; Zeng et al., 2014).

Cai et al. reported the quantitative PET imaging of EGFR expression with ^{64}Cu-cetuximab in mice. In this study, biodistribution results of ^{64}Cu-cetuximab in various EGFR overexpressed tumor models were given. The study showed that the highest tumor uptake was found at 48th h after radiopharmaceutical injection (Battal & Özer, 2021; Cai et al., 2007).

Ping Li and co-workers (2008) reported ^{64}Cu radiolabelled cetuximab for PET/CT imaging of EGFR overexpressed tumor types and evaluated the ^{64}Cu-cetuximab formulations for EGFR overexpressed tumors. Researchers studied receptor binding of ^{64}Cu-cetuximab to EGFR through in vitro and in vivo studies. In vivo studies were performed in A431 and MDA-MB-435 tumor-bearing mice. The uptake in A431 tumors was increased until 48 h after the administration and significant differences were found between EGFR-positive tumor uptake and blocked

uptake at 24 h. Micro PET/CT imaging was performed at 20 and 48 h after injection of ^{64}Cu-cetuximab in A431 and MDA-MB-435 tumor-bearing mice. Overall, ^{64}Cu-cetuximab was found as a promising agent for tumor imaging and also has excellent potential for predicting the cetuximab therapy response and helping the dose calculation in tumors (Anderson & Ferdani, 2009; Ping Li, Meyer, Capretto, Sherman, & Anderson, 2008).

Achmad et al. (2012) studied the ^{64}Cu-cetuximab for predicting cetuximab accumulation in Kirsten rat sarcoma viral oncogene homolog (KRAD) mutant colorectal cancer. In vivo study results were found promising in the end with radioimmunoimaging with ^{64}Cu-cetuximab (Achmad et al., 2012).

Tamura et al. (2012) studied the safety, distribution, and dosimetry of ^{64}Cu-trastuzumab in human HER2 (+) breast cancer. This study was performed on 6 patients with primary or metastatic breast cancer. 130 MBq doses of ^{64}Cu-trastuzumab were injected in 6 patients, and after 1, 24, and 48 h, PET images were taken. Results showed that the best imaging time was 48 h after the administration time of ^{64}Cu-trastuzumab. Also, brain metastases were imaged by PET in 2 patients. Results indicated that ^{64}Cu-trastuzumab is a suitable agent for diagnosing of HER2 (+) breast cancer and likely brain metastases the HER2 (+) breast cancer. Also, researchers mentioned dosimetry and pharmacologic safety results were within acceptable limits (Tamura et al., 2013). After this study, researchers also investigated the same agent (^{64}Cu-trastuzumab) for metastatic brain lesions of HER2(+) breast cancer.

Kurihara and co-workers (2015) studied ^{64}Cu-trastuzumab for metastatic brain cancer imaging and its specificity on HER2. PET studies were performed at 1, 24, and 48 hs after 500 MBq ^{64}Cu-trastuzumab injection on 5 patients suffering metastatic brain cancer from HER2 (+) breast cancer. As a result, researchers found that ^{64}Cu-trastuzumab could visualize metastatic brain cancer in all 5 patients. Overall, researchers indicated that ^{64}Cu-trastuzumab PET imaging is a safe technique and could be used to visualize metastatic brain lesions in HER2(+) breast cancer patients (Kurihara et al., 2015).

Zaheer and co-workers (2019) used ^{64}Cu radiolabelled trastuzumab to investigate the optimal therapeutic administration and micro distribution of mAb in radioimmunotherapy imaging. ^{64}Cu-trastuzumab was found an effective agent in the gastric cancer mouse model for diagnosis (Zaheer, Kim, Lee, Lim, & Kim, 2019).

In another study, immuno-PET and immuno-Cerenkov luminescence imaging (immuno-CLI) were compared for PSMA (+) tumor detection in mice by using ^{64}Cu radiolabelled 3/F11 mAbs. Immuno-CLI was found cheaper and showed fast acquisition times as advantage. However; the overall, sensitivity was lower than PET imaging, and also tissue penetration depth was found lower. In the end, PET imaging with ^{64}Cu-3/F11 was found as a better technique that is already used in clinical and preclinical use. In addition, this new method could be promising in vivo imaging tool (Maier et al., 2019).

Xie and co-workers studied ^{64}Cu radionuclides from production to the imaging process. In this study, rituximab was radiolabelled with ^{64}Cu, and an in-vivo study was performed on Ramos cells (lymphoma). In the end, the production of ^{64}Cu and radiolabelling processes were completed with high radiochemical and radionuclidic purity, and immuno-PET was successfully done (Xie et al., 2017).

Grubmüller et al. (2016) investigated the diagnostic potential of ^{64}Cu radiolabelled PSMA-617 in patients with PSMA (+) prostate cancer. This study was carried out at 2 different centers with 29 patients. The whole body PET images were taken in 1 h after injection and pelvis PET images were taken in 2 h post-injection. Primary prostate lesions were detected in 23 patients out of 29. Even with low prostate specific antigen levels in some patients, lesions were detected with high contrast after 1 h of injection. This study proved that ^{64}Cu radiolabelled mAbs could be

used in patients in centers where ^{68}Ga radionuclide is not available. ^{64}Cu-PSMA-617 showed high imaging quality and contrast (Grubmuller et al., 2016).

^{86}Y Radiolabelled Monoclonal Antibodies

^{86}Y has been used for imaging and monitoring therapy with ^{90}Y and getting more attraction for imaging and investing in ^{90}Y studies due to its relatively long half-life (Mikolajczak, van der Meulen, & Lapi, 2019; Nayak & Brechbiel, 2009). Also, the chelate-bioconjugate reaction could be easier than ^{89}Zr because ^{86}Y and ^{90}Y show the same chemistry (Ramogida & Orvig, 2013). However, ^{86}Y faced some limitations, one of which is the availability of ^{86}Y (Herrero Alvarez, Bauer, Hernandez-Gil, & Lewis, 2021).

Lövqvist et al. (2001) studied the ^{86}Y radiolabelled hu3S193 mAb and compared it with ^{111}In radiolabelled hu3S193 mAb to provide a better understanding of ^{86}Y radiolabelled mAbs for ^{90}Y radioimmunotherapy. 2 days after injections of ^{111}In-hu3S193 and ^{86}Y- hu3S193, uptakes of them were found similar at many tissues and organs, however, after 4 days, uptake and activity of ^{86}Y- hu3S193 were found higher than ^{111}In-hu3S193 in many tissues, tumors and bones. As a result, ^{86}Y- hu3S193 was as a better alternative for observing ^{90}Y biodistribution and therapy (Lövqvist et al., 2001).

Palm and co-workers (2003) studied ^{86}Y radiolabelled trastuzumab for estimating ^{90}Y radiolabelled trastuzumab biodistribution and dosimetry. Before ^{86}Y studies, ^{111}In has been used; however, several differences were detected between ^{111}In and ^{90}Y. ^{86}Y has been investigated due to very similar chemistry with ^{90}Y. ^{86}Y-trastuzumab PET images were confirmed by Magnetic Resonance (MR) images (Palm et al., 2003).

Nayak et al. (2011) investigated ^{86}Y-bevacizumab as a potential immuno-PET imaging agent and also the agent for a surrogate marker of ^{90}Y radioimmunotherapy in metastatic colorectal carcinoma. Results showed that ^{86}Y-bevacizumab has great potential as an immuno-PET agent to determine bevacizumab uptake and localization. Additionally, ^{86}Y-bevacizumab also can used as a marker for ^{90}Y-bevacizumab immunotherapy (Nayak et al., 2011).

^{124}I Radiolabelled Monoclonal Antibodies

Carrasquillo and co-workers (2018) performed PET imaging research and biodistribution of ^{124}I-codrituzumab in 14 patients with hepatocellular carcinoma. Different immunotherapy processes were also applied in some patients before and after immuno-PET. In the end, tumor localization was found in 13 patients, and tumor uptake of ^{124}I-codrituzumab in patients undergoing immunotherapy was found to decrease. In conclusion, ^{124}I-codrituzumab successfully detected tumor localization in most patients' suffering from hepatocellular carcinoma (Carrasquillo et al., 2018).

Verel et al. (2004) studied ^{124}I-U36 mAb from the labelling process to PET imaging before ^{131}I-radioimmunotherapy. Radiolabelling was successfully done with more than 95% radiochemical purity, and PET imaging was performed in nude mice. The main focus of this study was the scouting with PET imaging before radioimmunotherapy. Because ^{124}I was thought as an ideal radionuclide for the scouting procedure. In the end, tumor uptake was detected with ^{124}I-U36 mAb, and ^{124}I radiolabelled mAbs were found to be a suitable agent for PET imaging (Verel et al., 2004).

Carrasquillo et al. (2011) studied on huA33 mAbs and radiolabelled with ^{124}I to understand better targeting, biodistribution and safety for patients with colorectal cancer. The study was performed on 25 patients with primary or metastatic colorectal cancer and 19 patients who had surgical exploration and injected with 343 MBq ^{124}I-huA33 solution. Results showed good localization without any toxicity in patients. ^{124}I-huA33 mAbs showed high uptake in tumors and adequate tumor imaging in all patients (Carrasquillo et al., 2011). In another clinical study in 2011, huA33 was radiolabelled with ^{124}I and applied in 15 patients with colorectal cancer by O'Donoghue et al. This study results also supported Carrasquillo and co-workers' study (O'Donoghue et al., 2011).

Olafsen and co-workers (2007) radiolabelled mu1G8 mAbs with ^{124}I to determine the specific activity and tumor uptake in prostate cancer xenografts. Specific tumor targeting was observed by ^{124}I-mu1G8 mAbs in PET imaging (Olafsen et al., 2007).

Povoski et al. (2013) explained the new multimodal imaging and detection methods with ^{124}I radiolabelled cG250 mAbs to confirm preoperative and intraoperative localization for open surgical resection of renal cell carcinoma (Povoski et al., 2013). Divgi and co-workers reported a phase 1 trial of ^{124}I-cG250 mAb administration to assess preoperative PET localization in patients in 2007 (Divgi et al., 2007).

CONCLUSION

PET imaging shows several advantages, especially for deep tissues, such as sensitivity, and contrast resolution compared with SPECT imaging. These advantages provide significant superiority for radioimmunoimaging (Holland, Divilov, et al., 2010).

MAbs have been used for therapy and imaging for several decades because of their selectivity to specific targets (Wong et al., 2011). Radiolabelled mAbs have been shown increasing popularity for many years, and immuno-PET, which combines mAbs and PET radiometals, has great advantages due to the sensitivity of PET radionuclides and the specificity of mAbs. Radiolabelled mAbs are commonly used in applications: diagnose and imaging of diseases, monitoring of tumor response during therapy, metastatic lesion detection, therapy and dosimetric calculations (Wong et al., 2011). Moreover, immune-PET can also be used the determine antigen expression, antibody biodistribution, and organ pharmacokinetics. However, this approach is not yet used as much as immuno-PET is used for disease diagnosis and imaging, and it is seen as a deficiency in many phase 1 studies. (Lamberts et al., 2016).

The PET radionuclides, ^{89}Zr, ^{64}Cu, ^{124}I and ^{86}Y, are the most common radionuclides used for mAb radiolabelling; however, each radionuclide has advantages and disadvantages compared with each others. ^{89}Zr is the most suitable radionuclide for mAb radiolabelling, and it has already been used in clinical studies. Long half-life and half-life compatibility with mAbs's body clearance are the advantages of ^{89}Zr used for mAb radiolabelling, although its high positron energy and residualized features cause disadvantages. ^{124}I, which also has a long half-life, is also a promising radionuclide for mAb radiolabelling and shows lower residualized features when compared with ^{89}Zr. It makes ^{124}I also suitable and promising radionuclides for immuno-PET. ^{64}Cu and ^{86}Y have relatively short half-lives compared with ^{89}Zr and ^{124}I, and their short half-lives limit the studies for mAb radiolabelling.

Besides all these advantages, mAbs show relatively poor tumor uptake. Therefore, labelling of mAb fragments and obtaining immuno-PET images with mAb fragments are also getting popular recently. Fab fragments can also provide several advantages such as reducing non-specific distribution, different blood clearance and tumor localization, faster clearance and better penetration and may be reducing immunogenicity (Wong et al., 2011).

In conclusion, immuno-PET, combined with mAbs and these radionuclides which are relatively long half-life, show great potential for diagnosing diseases, monitoring therapies, and monitoring the mAbs behavior in the body, but various challenges should be overcome before clinical stages.

ACKNOWLEDGEMENTS

This work is not funded by any organization.

CONFLICT OF INTEREST

The authors declare that there is no conflict of interest.

AUTHOR CONTRIBUTION STATEMENT

Determination of the Subject (AYO; ETS), Literature Review, Preparation of the Text (ETS), Evaluation of the Text (AYO)

REFERENCES

(CDER), U. S. D. o. H. a. H. S. F. a. D. A. C. f. D. E. a. R. (2011). *PET Drugs- Current Good Manufacturing Practice (cGMP)- Small Entity Compliance Guide*. Retrieved from

Achmad, A., Hanaoka, H., Yoshioka, H., Yamamoto, S., Tominaga, H., Araki, T., . . . Endo, K. (2012). Predicting cetuximab accumulation in KRAS wild-type and KRAS mutant colorectal cancer using 64Cu-labeled cetuximab positron emission tomography. *Cancer Sci, 103*(3), 600-605. doi:10.1111/j.1349-7006.2011.02166.x

Aluicio-Sarduy, E., Ellison, P. A., Barnhart, T. E., Cai, W., Nickles, R. J., & Engle, J. W. (2018). PET radiometals for antibody labeling. *J Labelled Comp Radiopharm, 61*(9), 636-651. doi:10.1002/jlcr.3607

Anderson, C. J., & Ferdani, R. (2009). Cooper-64 Radiopharmaceuticals for PET Imaging of Cancer: Advances in Preclinical and Clinical Research. *Cancer Biother Radiopharm, 24*, 379-394. doi:10.1089=cbr.2009.0674

Avila-Rodriguez, M. A., Nye, J. A., & Nickles, R. J. (2007). Simultaneous production of high specific activity 64Cu and 61Co with 11.4 MeV protons on enriched 64Ni nuclei. *Appl Radiat Isot, 65*(10), 1115-1120. doi:10.1016/j.apradiso.2007.05.012

Barbaros, B., & Dikmen, M. (2015). Cancer Immunotherapy. *Erciyes University Journal of the Institute of Science and Technology, 31*(4), 177-181.

Battal, H., & Özer, A. Y. (2021). Copper-64 Radiopharmaceuticals-An Overview. In A. Y. Özer (Ed.), *New Trensd in Radiopharmaceuticals* (pp. 9-15). Ankara: Türkiye Klinikleri.

Borjesson, P. K., Jauw, Y. W., Boellaard, R., de Bree, R., Comans, E. F., Roos, J. C., . . . van Dongen, G. A. (2006). Performance of immuno-positron emission tomography with zirconium-89-labeled chimeric monoclonal antibody U36 in the detection of lymph node metastases in head and neck cancer patients. *Clin Cancer Res, 12*(7 Pt 1), 2133-2140. doi:10.1158/1078-0432.CCR-05-2137

Börjesson, P. K., Jauw, Y. W., de Bree, R., Roos, J. C., Castelijns, J. A., Leemans, C. R., . . . Boellaard, R. (2009). Radiation dosimetry of 89Zr-labeled chimeric monoclonal antibody U36 as used for immuno-PET in head and neck cancer patients. *Journal of Nuclear Medicine, 50*(11), 1828-1836.

Breedveld, F. C. (2000a). Therapeutic monoclonal antibodies. *Lancet, 355*(9205), 735-740. doi:10.1016/s0140-6736(00)01034-5

Breedveld, F. C. (2000b). Therapeutic monoclonal antibodies. *The Lancet, 355*(9205), 735-740. doi:10.1016/s0140-6736(00)01034-5

Cai, W., Chen, K., He, L., Cao, Q., Koong, A., & Chen, X. (2007). Quantitative PET of EGFR expression in xenograft-bearing mice using 64Cu-labeled cetuximab, a chimeric anti-EGFR monoclonal antibody. *Eur J Nucl Med Mol Imaging, 34*(6), 850-858. doi:10.1007/s00259-006-0361-6

Carrasquillo, J. A., O'Donoghue, J. A., Beylergil, V., Ruan, S., Pandit-Taskar, N., Larson, S. M., . . . Abou-Alfa, G. K. (2018). I-124 codrituzumab imaging and biodistribution in patients with hepatocellular carcinoma. *EJNMMI Res, 8*(1), 20. doi:10.1186/s13550-018-0374-8

Carrasquillo, J. A., Pandit-Taskar, N., O'Donoghue, J. A., Humm, J. L., Zanzonico, P., Smith-Jones, P. M., . . . Larson, S. M. (2011). (124)I-huA33 antibody PET of colorectal cancer. *J Nucl Med, 52*(8), 1173-1180. doi:10.2967/jnumed.110.086165

Crisan, G., Moldovean-Cioroianu, N. S., Timaru, D. G., Andries, G., Cainap, C., & Chis, V. (2022). Radiopharmaceuticals for PET and SPECT Imaging: A Literature Review over the Last Decade. *Int J Mol Sci, 23*(9). doi:10.3390/ijms23095023

Cutler, C. S., Hennkens, H. M., Sisay, N., Huclier-Markai, S., & Jurisson, S. S. (2013). Radiometals for combined imaging and therapy. *Chem Rev, 113*(2), 858-883. doi:10.1021/cr3003104

Dijkers, E., Hooge, M. N. L.-d., Kosterink, J. G., Jager, P. L., Brouwers, A. H., Perk, L. R., . . . Vries, E. G. d. (2007). Characterization of 89Zr-trastuzumab for clinical HER2 immunoPET imaging. *Journal of Clinical Oncology, 25*(18_suppl), 3508-3508. doi:10.1200/jco.2007.25.18_suppl.3508

Dijkers, E. C., Kosterink, J. G., Rademaker, A. P., Perk, L. R., van Dongen, G. A., Bart, J., . . . Lub-de Hooge, M. N. (2009). Development and characterization of clinical-grade 89Zr-trastuzumab for HER2/neu immunoPET imaging. *J Nucl Med, 50*(6), 974-981. doi:10.2967/jnumed.108.060392

Dillman, R. O. (2006). Radioimmunotherapy of B-cell lymphoma with radiolabelled anti-CD20 monoclonal antibodies. *Clin Exp Med, 6*(1), 1-12. doi:10.1007/s10238-006-0087-6

Dilworth, J. R., & Pascu, S. I. (2018). The chemistry of PET imaging with zirconium-89. *Chem Soc Rev, 47*(8), 2554-2571. doi:10.1039/c7cs00014f

Divgi, C. R., Pandit-Taskar, N., Jungbluth, A. A., Reuter, V. E., Gönen, M., Ruan, S., . . . Russo, P. (2007). Preoperative characterisation of clear-cell renal carcinoma using iodine-124-labelled antibody chimeric G250 (124I-cG250) and PET in patients with renal masses: a phase I trial. *Lancet Oncol, 8*(4), 304-310. doi:10.1016/s1470-2045(07)70044-x

Drude, N., Tienken, L., & Mottaghy, F. M. (2017). Theranostic and nanotheranostic probes in nuclear medicine. *Methods, 130*, 14-22. doi:10.1016/j.ymeth.2017.07.004

Ecker, D. M., Jones, S. D., & Levine, H. L. (2015). The therapeutic monoclonal antibody market. *MAbs, 7*(1), 9-14. doi:10.4161/19420862.2015.989042

Ferreira, C. L., Yapp, D. T., Lamsa, E., Gleave, M., Bensimon, C., Jurek, P., & Kiefer, G. E. (2008). Evaluation of novel bifunctional chelates for the development of Cu-64-based radiopharmaceuticals. *Nucl Med Biol, 35*(8), 875-882. doi:10.1016/j.nucmedbio.2008.09.001

Gillings, N., Hjelstuen, O., Ballinger, J., Behe, M., Decristoforo, C., Elsinga, P., . . . Todde, S. (2021). Guideline on current good radiopharmacy practice (cGRPP) for the small-scale preparation of radiopharmaceuticals. *EJNMMI Radiopharm Chem, 6*(1), 8. doi:10.1186/s41181-021-00123-2

Grubmuller, B., Baum, R. P., Capasso, E., Singh, A., Ahmadi, Y., Knoll, P., . . . Mirzaei, S. (2016). (64) Cu-PSMA-617 PET/CT Imaging of Prostate Adenocarcinoma: First In-Human Studies. *Cancer Biother Radiopharm, 31*(8), 277-286. doi:10.1089/cbr.2015.1964

Guideline on Radiopharmaceuticals, CHMP, EMEA/CHMP/QWP/306970/2007 (draft released for consultation). (2007). Retrieved from https://www.gmp-compliance.org/files/guidemgr/EMA_WC500003538_radio.pdf

Herrero Alvarez, N., Bauer, D., Hernandez-Gil, J., & Lewis, J. S. (2021). Recent Advances in Radiometals for Combined Imaging and Therapy in Cancer. *ChemMedChem, 16*(19), 2909-2941. doi:10.1002/cmdc.202100135

Heskamp, S., Raave, R., Boerman, O., Rijpkema, M., Goncalves, V., & Denat, F. (2017). (89)Zr-Immuno-Positron Emission Tomography in Oncology: State-of-the-Art (89)Zr Radiochemistry. *Bioconjug Chem, 28*(9), 2211-2223. doi:10.1021/acs.bioconjchem.7b00325

Holland, J., Sheh, Y., Smith-Jones, P., & Lewis, J. (2009). Zr-89 radiolabeling of monoclonal antibodies for immunoPET. *Journal of Nuclear Medicine, 50*(supplement 2), 497-497.

Holland, J. P., Divilov, V., Bander, N. H., Smith-Jones, P. M., Larson, S. M., & Lewis, J. S. (2010). 89Zr-DFO-J591 for immunoPET of prostate-specific membrane antigen expression in vivo. *J Nucl Med, 51*(8), 1293-1300. doi:10.2967/jnumed.110.076174

Holland, J. P., Williamson, M. J., & Lewis, J. S. (2010). Unconventional nuclides for radiopharmaceuticals. *Mol Imaging, 9*(1), 1-20.

Holliger, P., & Hudson, P. J. (2005). Engineered antibody fragments and the rise of single domains. *Nature Biotechnology, 23*(9), 1126-1136. doi:10.1038/nbt1142

Jauw, Y. W., Menke-van der Houven van Oordt, C. W., Hoekstra, O. S., Hendrikse, N. H., Vugts, D. J., Zijlstra, J. M., . . . van Dongen, G. A. (2016). Immuno-Positron Emission Tomography with Zirconium-89-Labeled Monoclonal Antibodies in Oncology: What Can We Learn from Initial Clinical Trials? *Front Pharmacol, 7*, 131. doi:10.3389/fphar.2016.00131

Kaur, S., Venktaraman, G., Jain, M., Senapati, S., Garg, P. K., & Batra, S. K. (2012). Recent trends in antibody-based oncologic imaging. *Cancer Lett, 315*(2), 97-111. doi:10.1016/j.canlet.2011.10.017

Kenanova, V., & Wu, A. M. (2006). Tailoring Antibodies for Radionuclide Delivery. *Expert Opinion on Drug Delivery, 3*(1), 53-70. doi:https://doi.org/10.1517/17425247.3.1.53

Kikuchi, M., Clump, D. A., Srivastava, R. M., Sun, L., Zeng, D., Diaz-Perez, J. A., . . . Ferris, R. L. (2017). Preclinical immunoPET/CT imaging using Zr-89-labeled anti-PD-L1 monoclonal antibody for assessing radiation-induced PD-L1 upregulation in head and neck cancer and melanoma. *Oncoimmunology, 6*(7), e1329071. doi:10.1080/2162402X.2017.1329071

Knowles, S. M., & Wu, A. M. (2012). Advances in immuno-positron emission tomography: antibodies for molecular imaging in oncology. *J Clin Oncol, 30*(31), 3884-3892. doi:10.1200/JCO.2012.42.4887

Kobayashi, H., Choyke, P. L., & Ogawa, M. (2016). Monoclonal antibody-based optical molecular imaging probes; considerations and caveats in chemistry, biology and pharmacology. *Curr Opin Chem Biol, 33*, 32-38. doi:10.1016/j.cbpa.2016.05.015

Kumar, K., & Ghosh, A. (2021). Radiochemistry, Production Processes, Labeling Methods, and ImmunoPET Imaging Pharmaceuticals of Iodine-124. *Molecules, 26*(2). doi:10.3390/molecules26020414

Kurihara, H., Hamada, A., Yoshida, M., Shimma, S., Hashimoto, J., Yonemori, K., . . . Tamura, K. (2015). (64)Cu-DOTA-trastuzumab PET imaging and HER2 specificity of brain metastases in HER2-positive breast cancer patients. *EJNMMI Res, 5*, 8. doi:10.1186/s13550-015-0082-6

Lamberts, L. E., Menke-van der Houven van Oordt, C. W., ter Weele, E. J., Bensch, F., Smeenk, M. M., Voortman, J., . . . de Vries, E. G. (2016). ImmunoPET with Anti-Mesothelin Antibody in Patients with Pancreatic and Ovarian Cancer before Anti-Mesothelin Antibody-Drug Conjugate Treatment. *Clin Cancer Res, 22*(7), 1642-1652. doi:10.1158/1078-0432.CCR-15-1272

Liu, H., Moy, P., Kim, S., Xia, Y., Rajasekaran, A., Navarro, V., . . . Bander, N. H. (1997). Monoclonal antibodies to the extracellular domain of prostate-specific membrane antigen also react with tumor vascular endothelium. *Cancer Res, 57*(17), 3629-3634.

Liu, H., Rajasekaran, A. K., Moy, P., Xia, Y., Kim, S., Navarro, V., . . . Bander, N. H. (1998). Constitutive and antibody-induced internalization of prostate-specific membrane antigen. *Cancer Res, 58*(18), 4055-4060.

Lövqvist, A., Humm, J., Sheikh, A., Finn, R., Koziorowski, J., Ruan, S., . . . Larson, S. M. (2001). PET Imaging of 86Y-Labeled Anti-Lewis Y Monoclonal Antibodies in a Nude Mouse Model: Comparison Between 86Y and 111In Radiolabels. *J Nucl Med, 42*, 1281-1287.

Lu, R.-M., Hwang, Y.-C., Liu, I. J., Lee, C.-C., Tsai, H.-Z., Li, H.-J., & Wu, H.-C. (2020). Development of therapeutic antibodies for the treatment of diseases. *Journal of Biomedical Science, 27*(1), 1. doi:10.1186/s12929-019-0592-z

Lubberink, M., & Herzog, H. (2011). Quantitative imaging of 124I and 86Y with PET. *Eur J Nucl Med Mol Imaging, 38 Suppl 1*(Suppl 1), S10-18. doi:10.1007/s00259-011-1768-2

Maier, F. C., Wild, A. M., Kirchen, N., Holm, F., Fuchs, K., Schwenck, J., . . . Wiehr, S. (2019). Comparative immuno-Cerenkov luminescence and -PET imaging enables detection of PSMA(+) tumors in mice using (64)Cu-radiolabeled monoclonal antibodies. *Appl Radiat Isot, 143*, 149-155. doi:10.1016/j.apradiso.2018.09.006

McKnight, B. N., & Viola-Villegas, N. T. (2018). (89) Zr-ImmunoPET companion diagnostics and their impact in clinical drug development. *J Labelled Comp Radiopharm, 61*(9), 727-738. doi:10.1002/jlcr.3605

Mikolajczak, R., van der Meulen, N. P., & Lapi, S. E. (2019). Radiometals for imaging and theranostics, current production, and future perspectives. *J Labelled Comp Radiopharm, 62*(10), 615-634. doi:10.1002/jlcr.3770

Morais, M., & Ma, M. T. (2018). Site-specific chelator-antibody conjugation for PET and SPECT imaging with radiometals. *Drug Discov Today Technol, 30*, 91-104. doi:10.1016/j.ddtec.2018.10.002

Nayak, T. K., Garmestani, K., Baidoo, K. E., Milenic, D. E., & Brechbiel, M. W. (2011). PET imaging of tumor angiogenesis in mice with VEGF-A-targeted (86)Y-CHX-A"-DTPA-bevacizumab. *Int J Cancer, 128*(4), 920-926. doi:10.1002/ijc.25409

Nayak, T. P., & Brechbiel, M. W. (2009). Radioimmunoimaging with Longer-Lived Positron-Emitting Radionuclides: Potentials and Challenges. *Bioconjug Chem, 20*, 825-841. doi:10.1021/bc800299f

Nelson, A. L. (2010). Antibody fragments: hope and hype. *MAbs, 2*(1), 77-83. doi:10.4161/mabs.2.1.10786

O'Donoghue, J. A., Smith-Jones, P. M., Humm, J. L., Ruan, S., Pryma, D. A., Jungbluth, A. A., . . . Larson, S. M. (2011). 124I-huA33 antibody uptake is driven by A33 antigen concentration in tissues from colorectal cancer patients imaged by immuno-PET. *J Nucl Med, 52*(12), 1878-1885. doi:10.2967/jnumed.111.095596

Olafsen, T., Gu, Z., Sherman, M. A., Leyton, J. V., Witkosky, M. E., Shively, J. E., . . . Reiter, R. E. (2007). Targeting, Imaging, and Therapy Using a Humanized Antiprostate Stem Cell Antigen (PSCA) Antibody. *J Immunother, 30*, 396-405.

Palm, S., Enmon, R. M., Matei, C., Kolbert, K. S., Xu, S., Zanzonico, P. B., . . . Sgouros, G. (2003). Pharmacokinetics and Biodistribution of 86Y-Trastuzumab for 90Y Dosimetry in an Ovarian Carcinoma Model: Correlative MicroPET and MRI. *J Nucl Med, 44*, 1148-1155.

Parakh, S., Lee, S. T., Gan, H. K., & Scott, A. M. (2022). Radiolabeled Antibodies for Cancer Imaging and Therapy. *Cancers (Basel), 14*(6). doi:10.3390/cancers14061454

Ping Li, W., Meyer, L. A., Capretto, D. A., Sherman, C. D., & Anderson, C. J. (2008). Receptor-binding, biodistribution, and metabolism studies of 64Cu-DOTA-cetuximab, a PET-imaging agent for epidermal growth-factor receptor-positive tumors. *Cancer Biother Radiopharm, 23*(2), 158-171. doi:10.1089/cbr.2007.0444

Povoski, S. P., Hall, N. C., Murrey, D. A., Jr., Sharp, D. S., Hitchcock, C. L., Mojzisik, C. M., . . . Bahnson, R. R. (2013). Multimodal imaging and detection strategy with 124 I-labeled chimeric monoclonal antibody cG250 for accurate localization and confirmation of extent of disease during laparoscopic and open surgical resection of clear cell renal cell carcinoma. *Surg Innov, 20*(1), 59-69. doi:10.1177/1553350612438416

Ramogida, C. F., & Orvig, C. (2013). Tumour targeting with radiometals for diagnosis and therapy. *Chem Commun (Camb), 49*(42), 4720-4739. doi:10.1039/c3cc41554f

Reddy, S., & Robinson, M. K. (2010). Immuno-positron emission tomography in cancer models. *Semin Nucl Med, 40*(3), 182-189. doi:10.1053/j.semnuclmed.2009.12.004

Saharma, S., Baldi, A., Singh, R. K., & Sharma, R. K. (2018). Regulatory Framework of Radiopharmaceuticals: Current Status and Future Recommendations. *Research Journal of Life Sciences, Bioinformatics, Pharmaceutical and Chemical Sciences, 4*(3). doi:10.26479/2018.0403.25

Sarcan, E. T., & Özer, A. Y. (2021). Zirconium-89 radiopharmaceuticals: Current status and future. In A. Y. Özer (Ed.), *New Trends in Radiopharmaceuticals.* (pp. 16-22). Ankara: Türkiye Klinikleri.

Sarcan, E. T., Silindir-Gunay, M., Ozer, A. Y., & Hartman, N. (2021). 89Zr as a promising radionuclide and it's applications for effective cancer imaging. *Journal of Radioanalytical and Nuclear Chemistry, 330*(1), 15-28. doi:10.1007/s10967-021-07928-0

Schrama, D., Reisfeld, R. A., & Becker, J. C. (2006). Antibody targeted drugs as cancer therapeutics. *Nat Rev Drug Discov, 5*(2), 147-159. doi:10.1038/nrd1957

Sihver, W., Pietzsch, J., Krause, M., Baumann, M., Steinbach, J., & Pietzsch, H. J. (2014). Radiolabeled Cetuximab Conjugates for EGFR Targeted Cancer Diagnostics and Therapy. *Pharmaceuticals (Basel), 7*(3), 311-338. doi:10.3390/ph7030311

Tamura, K., Kurihara, H., Yonemori, K., Tsuda, H., Suzuki, J., Kono, Y., . . . Fujiwara, Y. (2013). 64Cu-DOTA-Trastuzumab PET Imaging in Patients with HER2-Positive Breast Cancer. *Journal of Nuclear Medicine, 54*(11), 1869-1875. doi:10.2967/jnumed.112.118612

Templar Smith, B. (2012). Polyclonal and Monoclonal Antibodies. In J. Norenbergh (Ed.), *Introduction to Diagnostic and Therapeutic Monoclonal Antibodies* (Vol. 17): University of New Mexico Health Science Center and Pharmacy Continuing Education.

U.S.Pharmacopoeia. (2009). Radiopharmaceuticals for Positron Emission Tomography —Compounding. *USP 32*.

Van Dongen, G. A., Huisman, M. C., Boellaard, R., Harry Hendrikse, N., Windhorst, A. D., Visser, G. W., . . . Vugts, D. J. (2015). 89Zr-immuno-PET for imaging of long circulating drugs and disease targets: why, how and when to be applied? *Q J Nucl Med Mol Imaging, 59*(1), 18-38.

van Dongen, G. A., Visser, G. W., Lub-de Hooge, M. N., de Vries, E. G., & Perk, L. R. (2007). Immuno-PET: a navigator in monoclonal antibody development and applications. *Oncologist, 12*(12), 1379-1389. doi:10.1634/theoncologist.12-12-1379

van Dongen, G. A., & Vosjan, M. J. (2010). Immuno-positron emission tomography: shedding light on clinical antibody therapy. *Cancer Biother Radiopharm, 25*(4), 375-385. doi:10.1089/cbr.2010.0812

Verel, I., Visser, G. W., Boerman, O. C., van Eerd, J. E., Finn, R., Boellaard, R., . . . van Dongen, G. A. (2003). Long-lived positron emitters zirconium-89 and iodine-124 for scouting of therapeutic radioimmunoconjugates with PET. *Cancer Biother Radiopharm, 18*(4), 655-661. doi:10.1089/108497803322287745

Verel, I., Visser, G. W., Vosjan, M. J., Finn, R., Boellaard, R., & van Dongen, G. A. (2004). High-quality 124I-labelled monoclonal antibodies for use as PET scouting agents prior to 131I-radioimmunotherapy. *Eur J Nucl Med Mol Imaging, 31*(12), 1645-1652. doi:10.1007/s00259-004-1632-8

Vugts, D. J., Visser, G. W., & van Dongen, G. A. (2013). 89Zr-PET radiochemistry in the development and application of therapeutic monoclonal antibodies and other biologicals. *Curr Top Med Chem, 13*(4), 446-457. doi:10.2174/1568026611313040005

Wadas, T. J., Wong, E. H., Weisman, G. R., & Anderson, C. J. (2010). Coordinating Radiometals of Copper, Gallium, Indium, Yttrium, and Zirconium for PET and SPECT Imaging of Disease. *Chem Rev, 110*, 2858-2902.

Wallberg, H., & Stahl, S. (2013). Design and evaluation of radiolabeled tracers for tumor imaging. *Biotechnol Appl Biochem, 60*(4), 365-383. doi:10.1002/bab.1111

WHO. (2017). The International Pharmacopoeia Radiopharmaceuticals: General Monograph. Retrieved from https://www.who.int/docs/default-source/medicines/norms-and-standards/current-projects/qas13-542rev2-general-chapter-radiopharmaceuticals.pdf?sfvrsn=516dbf81_2

Wong, K. J., Baidoo, K. E., Nayak, T. K., Garmestani, K., Brechbiel, M. W., & Milenic, D. E. (2011). In vitro and in vivo pre-clinical analysis of a F(ab')2 fragment of panitumumab for molecular imaging and therapy of HER1-positive cancers. *EJNMMI Research, 1*(1), 1. doi:10.1186/2191-219X-1-1

Wong, K. J., Baidoo, K. E., Nayak, T. K., Garmestani, K., Brechbiel, M. W., & Milenic, D. E. (2011). In vitro and in vivo pre-clinical analysis of a F(ab')2 fragment of panitumumab for molecular imaging and therapy of HER1-positive cancers. *EJNMMI Res, 1*.

Xie, Q., Zhu, H., Wang, F., Meng, X., Ren, Q., Xia, C., & Yang, Z. (2017). Establishing Reliable Cu-64 Production Process: From Target Plating to Molecular Specific Tumor Micro-PET Imaging. *Molecules, 22*(4). doi:10.3390/molecules22040641

Zaheer, J., Kim, H., Lee, Y. J., Lim, S. M., & Kim, J. S. (2019). Comparison between Fractionated Dose and Single Dose of Cu-64 Trastuzumab Therapy in the NCI-N87 Gastric Cancer Mouse Model. *Int J Mol Sci, 20*(19). doi:10.3390/ijms20194708

Zeng, D., Guo, Y., White, A. G., Cai, Z., Modi, J., Ferdani, R., & Anderson, C. J. (2014). Comparison of conjugation strategies of cross-bridged macrocyclic chelators with cetuximab for copper-64 radiolabeling and PET imaging of EGFR in colorectal tumor-bearing mice. *Mol Pharm, 11*(11), 3980-3987. doi:10.1021/mp500004m